

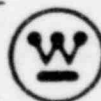
# Clinch River Breeder Reactor Plant

## FUEL ASSEMBLY STRUCTURAL ANALYSIS IN SUPPORT OF THE FINAL DESIGN REVIEW

JANUARY, 1978

Prepared for the United States Department of Energy under contracts DE-ACIS-76CL02395 and EW-76-C-15-0003.

Any Further Distribution by any Holder of this Document or of the Data Therein to Third Parties Representing Foreign Interest, Foreign Governments, Foreign Companies and Foreign Subsidiaries or Foreign Divisions of U.S. Companies Should be Coordinated with the Director, Division of Reactor Research and Technology, United States Department of Energy.



**Westinghouse Electric Corporation**

ADVANCED REACTORS DIVISION

BOX 158

MADISON, PENNSYLVANIA 15663

8009020017\*

## **INFORMATION CONCERNING USE OF THIS DOCUMENT**

### **PRELIMINARY DOCUMENT**

This document contains information of a preliminary nature prepared in the course of work for the U.S. Department of Energy. This information is subject to correction or modification upon the collection and evaluation of additional data.

### **NOTICE**

This document was prepared as an account of work sponsored by the United States Government. Neither the U.S. Department of Energy, nor any of their employees, nor any of their contractors, subcontractors, or their employees, makes any warranty, express or implied, or assumes any legal liability or responsibility for the accuracy, completeness or usefulness of any information, apparatus, product or process disclosed, or represents that its use would not infringe privately owned rights.

---

---

WESTINGHOUSE ELECTRIC CORPORATION  
ADVANCED REACTORS DIVISION  
BOX 158  
MADISON, PENNSYLVANIA 15663



CRBRP FUEL ASSEMBLY STRUCTURAL ANALYSIS  
IN SUPPORT OF THE  
FINAL DESIGN REVIEW

January 1978

Prepared by: T. V. Prevenslik  
T. V. Prevenslik

Contributors: A. D. Sane  
D. V. Swenson  
M. A. Todd

Approved by: J. L. Bitner  
J. L. Bitner, Manager  
Structural Analysis

WESTINGHOUSE ELECTRIC CORPORATION  
Advanced Reactors Division  
P.O. Box 158  
Madison, Pennsylvania 15663

## TABLE OF CONTENTS

	<u>page</u>
1.0 INTRODUCTION . . . . .	1
1.1 Purpose . . . . .	1
1.2 Scope . . . . .	1
1.3 Applicability . . . . .	1
1.4 Summary . . . . .	2
2.0 DESCRIPTION AND APPROACH . . . . .	3
2.1 Shield Block . . . . .	6
2.2 CMP Hex Duct . . . . .	6
2.3 ACLP Hex Duct . . . . .	7
2.4 TLP Outlet Nozzle . . . . .	8
2.5 Attachment Assembly . . . . .	8
2.6 Orifice Plate . . . . .	9
3.0 CRITERIA . . . . .	10
3.1 Background and Rationale . . . . .	13
3.1.1 ASME Section III Code . . . . .	13
3.1.2 Code Case 1592 . . . . .	14
3.1.3 RDT Draft Criteria for Breeder Reactor Core Components . . . . .	15
3.1.4 CRBRP F/A Core Components . . . . .	17
3.1.4.1 Crack Initiation . . . . .	19
3.1.4.1.1 Local Ductile Rupture . . . . .	19
3.1.4.1.2 Creep-Fatigue Damage . . . . .	21
3.1.4.2 Excessive Deformations . . . . .	23
3.2 Application . . . . .	24
3.2.1 Crack Initiation . . . . .	25
3.2.1.1 Local Ductile Rupture . . . . .	25
3.2.1.2 Creep-Fatigue Damage . . . . .	26
3.2.2 Excessive Deformation . . . . .	28
4.0 SHIELD BLOCK ANALYSIS AND EVALUATION . . . . .	29
4.1 Loading Analysis . . . . .	29
4.1.1 Mechanical . . . . .	29
4.1.2 Thermal . . . . .	30
4.1.2.1 Model and Geometry . . . . .	34

4.1.2.2	Properties . . . . .	36
4.1.2.3	Boundary Conditions and Wetted Surfaces.	36
4.1.2.4	Heat Generation Rates . . . . .	38
4.1.2.5	Analysis and Results . . . . .	38
4.1.3	Worst Case Duty Cycle . . . . .	45
4.2	Structural Analysis. . . . .	47
4.2.1	Model, Geometry, and Boundary Conditions . . . .	47
4.2.2	Properties . . . . .	49
4.2.2.1	Linear . . . . .	50
4.2.2.2	Non-linear . . . . .	50
4.2.2.2.1	Stress-Strain Curves . . . .	50
4.2.2.2.2	Thermal Creep Equations . . .	53
4.2.3	Worst Case Duty Cycle Response . . . . .	53
4.2.3.1	Constraints and Reference Temperature Selections . . . . .	54
4.2.3.2	Analysis and Results . . . . .	56
4.2.3.2.1	Time Independent . . . . .	56
4.2.3.2.2	Time Dependent . . . . .	63
4.3	Structural Evaluation. . . . .	66
4.3.1	Crack Initiation . . . . .	67
4.3.1.1	Local Ductile Rupture . . . . .	67
4.3.1.1.1	Allowable Uniaxial Strains .	67
4.3.1.1.1.1	Uniform Elongation	68
4.3.1.1.1.2	Fracture . . . .	68
4.3.1.1.2	Comparison with Criterion . .	69
4.3.1.2	Creep-Fatigue Damage . . . . .	70
4.3.1.2.1	Allowable Limits . . . . .	70
4.3.1.2.1.1	Fatigue Life . .	71
4.3.1.2.1.2	Creep-Rupture Time	75
4.3.1.2.2	Comparison with Criterion . .	79
4.3.2	Excessive Deformation . . . . .	80
4.3.2.1	Peak Plus Accumulated Deformations . . .	80
4.3.2.2	Residual Deformations . . . . .	81
4.3.3	Summary . . . . .	81

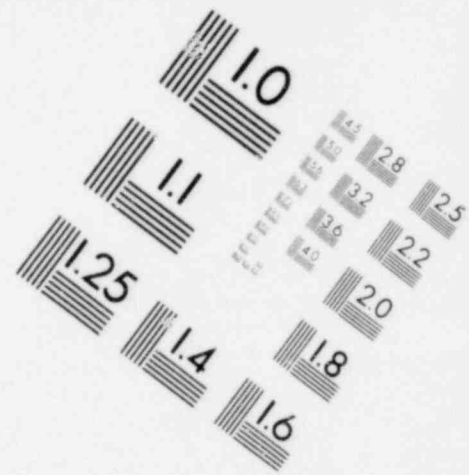
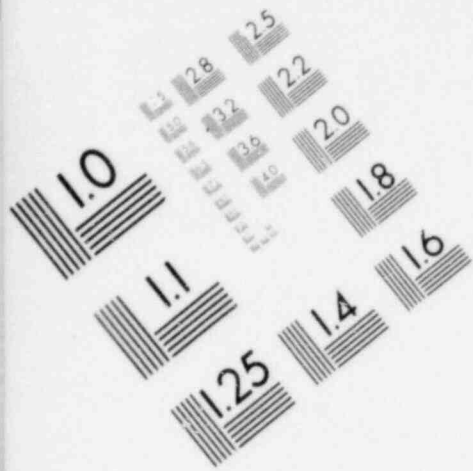
5.0	CMP HEX DUCT ANALYSIS AND EVALUATION . . . . .	83
5.1	Loading Analysis. . . . .	83
5.1.1	Mechanical . . . . .	83
5.1.1.1	Beam Bending . . . . .	84
5.1.2	Thermal. . . . .	87
5.1.2.1	Model and Geometry . . . . .	92
5.1.2.2	Properties . . . . .	94
5.1.2.3	Boundary Conditions and Wetted Surfaces .	94
5.1.2.4	Heat Generation Rates . . . . .	96
5.1.2.5	Analysis and Results . . . . .	97
5.1.3	Worst Case Duty Cycle . . . . .	102
5.2	Structural Analysis . . . . .	104
5.2.1	Model, Geometry and Boundary Conditions . . . . .	104
5.2.2	Properties . . . . .	106
5.2.2.1	Linear . . . . .	106
5.2.2.2	Non-linear . . . . .	106
5.2.2.2.1	Stress-Strain Curves . . . . .	106
5.2.2.2.2	Thermal Creep Equations . . . . .	108
5.2.3	Worst Case Duty Cycle Response . . . . .	109
5.2.3.1	Constraints and Reference Temperature Selections. . . . .	109
5.2.3.2	Analysis and Results . . . . .	110
5.2.3.2.1	Time Independent . . . . .	111
5.2.3.2.2	Time Dependent . . . . .	115
5.3	Structural Evaluations. . . . .	116
5.3.1	Crack Initiation . . . . .	117
5.3.1.1	Local Ductile Rupture . . . . .	117
5.3.1.1.1	Allowable Uniaxial Strains . . . . .	118
5.3.1.1.1.1	Uniform Elongation . . . . .	118
5.3.1.1.1.2	Fracture . . . . .	119
5.3.1.1.2	Comparison with Criterion . . . . .	119
5.3.1.2	Creep-Fatigue Damage . . . . .	120
5.3.1.2.1	Allowable Limits . . . . .	120
5.3.1.2.1.1	Fatigue Life . . . . .	121
5.3.1.2.1.2	Creep Rupture Time . . . . .	125
5.3.1.2.2	Comparison and Criterion . . . . .	128

5.3.2	Excessive Deformation . . . . .	129
5.3.2.1	Peak Plus Accumulated Deformations . . . . .	129
5.3.2.2	Residual Deformations . . . . .	130
5.3.3	Summary . . . . .	130
6.0	ACLP HEX DUCT ANALYSIS AND EVALUATION . . . . .	131
6.1	Loading Analysis . . . . .	131
6.1.1	Mechanical . . . . .	131
6.1.1.1	Beam Bending . . . . .	132
6.1.1.2	Local Contact . . . . .	135
6.1.1.2.1	OBE and SSE Seismic . . . . .	136
6.1.1.2.2	Steady State and Transient Core Restraint . . . . .	141
6.1.2	Thermal . . . . .	147
6.1.2.1	Model and Geometry . . . . .	154
6.1.2.2	Properties . . . . .	156
6.1.2.3	Boundary Conditions and Wetted Surfaces . . . . .	156
6.1.2.4	Heat Generation Rates . . . . .	158
6.1.2.5	Analysis and Results . . . . .	159
6.1.3	Worst Case Duty Cycle . . . . .	164
6.2	Structural Analysis . . . . .	167
6.2.1	Model, Geometry and Boundary Conditions . . . . .	167
6.2.2	Properties . . . . .	169
6.2.2.1	Linear . . . . .	169
6.2.2.2	Non-Linear . . . . .	169
6.2.2.2.1	Stress Strain Curves . . . . .	169
6.2.2.2.2	Thermal Creep Equations . . . . .	174
6.2.2.2.3	Irradiation Creep and Swelling Equations . . . . .	177
6.2.3	Worst Case Duty Cycle Response . . . . .	178
6.2.3.1	Constraints and Reference Temperature Selection . . . . .	178
6.2.3.2	Analysis and Results . . . . .	179
6.2.3.2.1	First Cycle - Time Independent . . . . .	179
6.2.3.2.2	First Cycle - Time Dependent . . . . .	185
6.2.3.2.3	Second Cycle - Time Independent . . . . .	189
6.2.3.2.4	Second Cycle - Time Dependent . . . . .	192

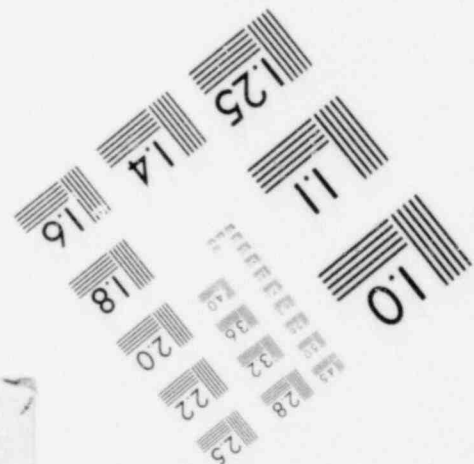
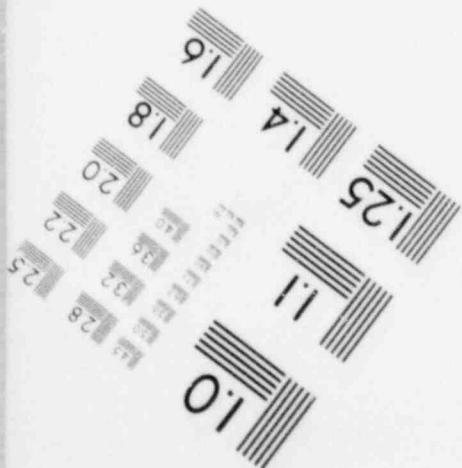
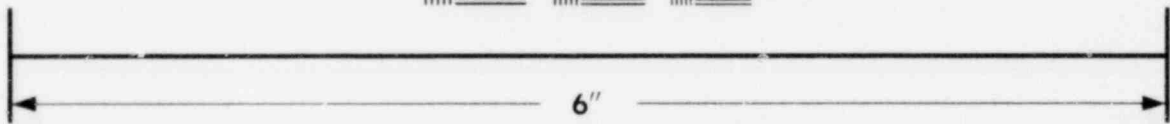
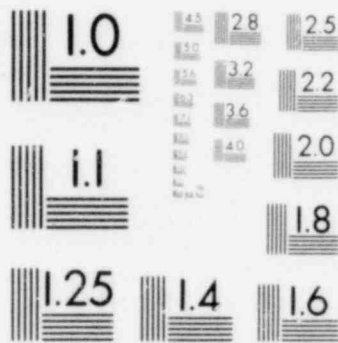
6.3	Structural Evaluation . . . . .	195
6.3.1	Crack Initiation . . . . .	195
6.3.1.1	Local Ductile Rupture . . . . .	195
6.3.1.1.1	Allowable Uniaxial Strains . . . . .	196
6.3.1.1.2	Comparison with Criterion . . . . .	196
6.3.1.2	Creep-Fatigue Damage . . . . .	199
6.3.1.2.1	Allowable Limits . . . . .	199
6.3.1.2.2	Comparison with Criterion . . . . .	202
6.3.2	Excessive Deformation . . . . .	204
6.3.2.1	Peak Plus Accumulated Deformations . . . . .	204
6.3.2.2	Residual Deformations . . . . .	205
6.3.3	Summary . . . . .	206
7.0	TLP OUTLET NOZZLE ANALYSIS AND EVALUATION. . . . .	207
7.1	Loading Analysis . . . . .	207
7.1.1	Mechanical . . . . .	207
7.1.2	Thermal . . . . .	208
7.1.2.1	Model and Geometry . . . . .	213
7.1.2.2	Properties. . . . .	215
7.1.2.3	Boundary Conditions and Wetted Surfaces . . . . .	215
7.1.2.4	Heat Generation Rates . . . . .	217
7.1.2.5	Analysis and Results . . . . .	218
7.1.3	Worst Case Duty Cycle . . . . .	223
7.2	Structural Analysis . . . . .	224
7.2.1	Model, Geometry, and Boundary Conditions . . . . .	224
7.2.2	Properties . . . . .	226
7.2.2.1	Linear . . . . .	226
7.2.2.2	Non-Linear . . . . .	226
7.2.2.2.1	Stress-Strain Curves . . . . .	226
7.2.2.2.2	Thermal Creep Equations . . . . .	227
7.2.3	Worst Case Duty Cycle Response . . . . .	230
7.2.3.1	Constraints and Reference Temperature Selection . . . . .	230
7.2.3.2	Analysis and Results . . . . .	232
7.2.3.2.1	Time Independent . . . . .	233
7.2.3.2.2	Time Dependent . . . . .	239

7.3	Structural Evaluation . . . . .	243
7.3.1	Crack Initiation . . . . .	243
7.3.1.1	Local Ductile Rupture . . . . .	243
7.3.1.1.1	Allowable Uniaxial Strains . . . . .	244
7.3.1.1.2	Comparison with Criterion. . . . .	244
7.3.1.2	Creep-Fatigue Damage. . . . .	245
7.3.1.2.1	Allowable Limits . . . . .	245
7.3.1.2.2	Comparison with Criterion. . . . .	248
7.3.2	Excessive Deformation. . . . .	249
7.3.2.1	Peak Plus Accumulated Deformations. . . . .	249
7.3.2.2	Residual Deformation. . . . .	250
7.3.3	Summary. . . . .	250
8.0	ATTACHMENT ASSEMBLY ANALYSIS AND EVALUATION. . . . .	252
8.1	Loading Analysis. . . . .	252
8.1.1	Mechanical . . . . .	252
8.1.1.1	Deadweight. . . . .	253
8.1.1.2	Pressure Drop . . . . .	256
8.1.1.3	Seismic . . . . .	259
8.1.1.3.1	Horizontal . . . . .	261
8.1.1.3.2	Vertical . . . . .	264
8.1.1.4	Summary . . . . .	266
8.1.2	Thermal. . . . .	268
8.1.2.1	Dimensional Extent and Finite Element Detail. . . . .	269
8.1.2.2	Thermal Analysis. . . . .	273
8.1.2.2.1	Model, Boundary Conditions, and Wetted Surfaces. . . . .	273
8.1.2.2.2	Properties . . . . .	275
8.1.2.2.3	Results. . . . .	275
8.1.2.3	Structural Analysis . . . . .	276
8.1.2.3.1	Model and Boundary Conditions . . . . .	276
8.1.2.3.2	Properties . . . . .	278
8.1.2.3.3	Results. . . . .	278
8.1.2.4	Conclusions . . . . .	280
8.1.3	Worst Case Duty Cycle. . . . .	281





**IMAGE EVALUATION  
TEST TARGET (MT-3)**



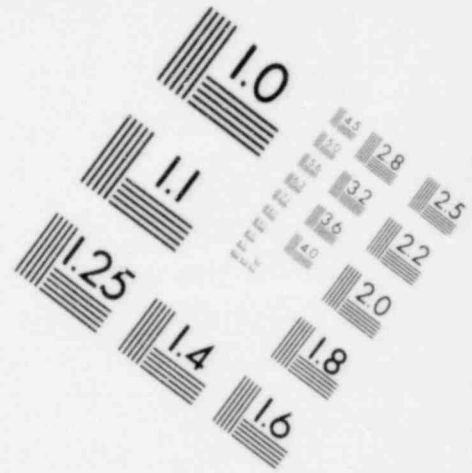
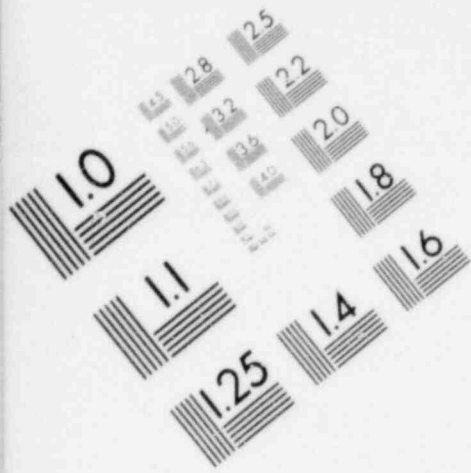
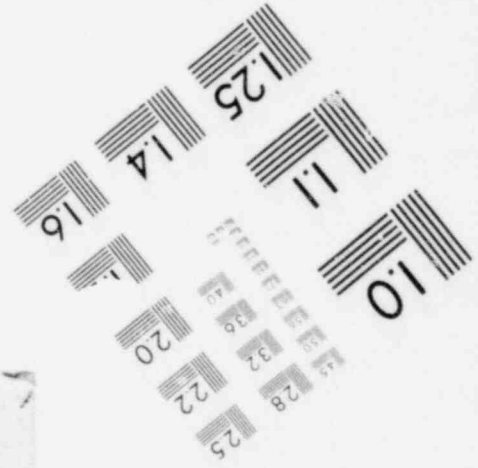
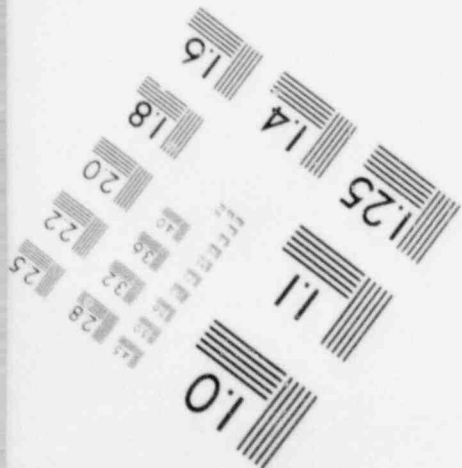
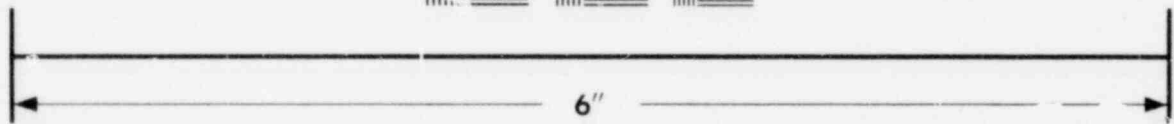
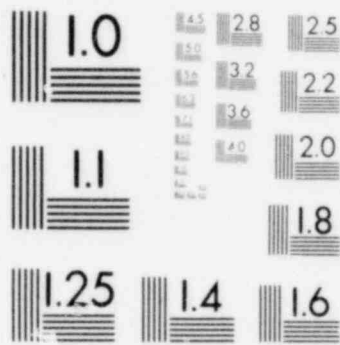


**IMAGE EVALUATION  
TEST TARGET (MT-3)**



8.2	Structural Analysis . . . . .	285
8.2.1	Model and Geometry . . . . .	285
8.2.2	Boundary Conditions and Loading Application. . .	287
8.2.3	Properties . . . . .	289
8.2.3.1	Linear. . . . .	289
8.2.3.2	Non-Linear. . . . .	289
8.2.3.2.1	Stress-Strain Curves . . . .	289
8.2.3.2.2	Thermal Creep Equasions. . .	291
8.2.4	Worst Case Duty Cycle Response . . . . .	291
8.2.4.1	Analysis and Results. . . . .	292
8.3	Structural Evaluation . . . . .	301
8.3.1	Crack Initiation . . . . .	301
8.3.1.1	Local Ductile Rupture . . . . .	301
8.3.1.1.1	Allowable Uniaxial Strains .	302
8.3.1.1.2	Comparison with Criterion. .	302
8.3.1.2	Creep Fatigue Damage. . . . .	303
8.3.1.2.1	Allowable Limits . . . . .	304
8.3.1.2.2	Comparison with Criterion. .	304
8.3.2	Excessive Deformation. . . . .	305
8.3.2.1	Peak Plus Accumulated Deformation . . .	305
8.3.2.2	Residual Deformations . . . . .	306
8.3.3	Summary. . . . .	307
9.0	OFFICE PLATE ANALYSIS AND EVALUATION . . . . .	309
9.1	Loading Analysis. . . . .	309
9.1.1	Mechanical . . . . .	309
9.1.2	Thermal. . . . .	312
9.1.3	Worst Case Duty Cycle. . . . .	315
9.2	Structural Analysis . . . . .	316
9.2.1	Model and Geometry . . . . .	316
9.2.2	Properties . . . . .	318
9.2.2.1	Linear. . . . .	318
9.2.2.2	Non-Linear. . . . .	318
9.2.2.2.1	Stress-Strain Curves . . . .	318
9.2.2.2.2	Thermal Creep Equations. . .	319

9.2.3	Elastic Response . . . . .	321
9.2.3.1	Pressure Drop . . . . .	321
9.2.3.1.1	Model and Boundary Conditions . . . . .	321
9.2.3.1.2	Analysis and Results . . . . .	323
9.2.3.2	Radial Interference . . . . .	325
9.2.3.2.1	Model and Boundary Conditions . . . . .	325
9.2.3.2.2	Analysis and Results . . . . .	327
9.2.3.3	Conclusions . . . . .	327
9.2.4	Worst Case Duty Cycle Response . . . . .	329
9.2.4.1	First Cycle - Time Independent. . . . .	329
9.2.4.2	First Cycle - Time Dependent. . . . .	333
9.2.4.3	Second Cycle - Time Independent . . . . .	333
9.2.4.4	Second Cycle - Time Dependent . . . . .	334
9.3	Structural Evaluation . . . . .	337
9.3.1	Crack Initiation . . . . .	337
9.3.1.1	Local Ductile Rupture . . . . .	338
9.3.1.1.1	Allowable Uniaxial Strains . . . . .	338
9.3.1.1.2	Comparison with Criterion. . . . .	338
9.3.1.2	Creep-Fatigue Damage. . . . .	340
9.3.1.2.1	Allowable Limits . . . . .	340
9.3.1.2.2	Comparison with Criterion. . . . .	341
9.3.2	Excessive Deformation. . . . .	342
9.3.2.1	Peak Plus Accumulated Deformations. . . . .	342
9.3.2.2	Residual Deformations . . . . .	343
9.3.3	Summary. . . . .	343
10.0	REFERENCES . . . . .	345
11.0	ACKNOWLEDGEMENTS . . . . .	349
	APPENDIX A - DAMAGE PROCESSOR . . . . .	A-1

LIST OF TABLES

1.0-1	F/A Margin of Safety Summary . . . . .	2
3.0-1	CRBRP F/A Inelastic Criteria and Limits . . . . .	12
4.1-1	Worst Case F/A Shield Block Duty Cycle ANSYS Input Data . . . . .	39
4.2-1	F/A Shield Block True Minimum Mean of BOL and EOL Stress-Strain Data SA-316-SS . . . . .	53
4.2-2	F/A Shield Block Reference Temperatures . . . . .	55
4.2-3	F/A Shield Block Time Independent Analysis Summary Initial Steady State Conditions . . . . .	57
4.2-4	F/A Shield Block Time Independent Analysis Summary E-4a Transient and Return to Final Steady State Conditions . . . . .	58
4.2-5	F/A Shield Block Time Dependent Analysis Summary 10-day Hold-Time and Unloading . . . . .	63
4.3-1	F/A Shield Block Fractional Reduction Rupture Strength SA-316-SS . . . . .	76
4.3-2	F/A Shield Block Structural Evaluation Summary . . . . .	82
5.1-1	F/A CMP Hex Duct OBE and SSE Seismic, and Core Restraint Bending Moments, Stresses, and Strains . . . . .	86
5.1-2	Worst Case F/A CMP Hex Duct Duty Cycle ANSYS Input Data . . . . .	97
5.2-1	F/A CMP Hex Duct Minimum Yield and Proportional Elastic Limit Stress First Core 20% CW-316-SS . . . . .	107
5.2-2	F/A CMP Hex Duct Reference Temperatures . . . . .	110
5.2-3	F/A CMP Hex Duct Time Independent Analysis Summary Initial Steady State, E-16 Transient, and Final Steady State . . . . .	111
5.3-1	F/A CMP Hex Duct Structural Evaluation Summary . . . . .	130
6.1-1	F/A ACLB Hex Duct OBE and SSE Seismic and Core Restraint Bending Moments, Stresses, and Strains . . . . .	134
6.1-2	F/A ACLP Hex Duct Average 1g 90° Sector Loads . . . . .	140
6.1-3	F/A ACLP Hex Duct Average Steady State Core Restraint 90° Sector Loads . . . . .	145
6.1-4	Worst Case F/A ACLP Hex Duct Duty Cycle ANSYS Input Data . . . . .	159
6.2-1	F/A ACLP Hex Duct True Minimum Mean of BOL and EOL Stress-Strain Data . . . . .	172
6.2-2	F/A ACLP Hex Duct Reference Temperatures . . . . .	178
6.2-3	F/A ACLP Hex Duct First Cycle Time Independent Analysis Summary Initial Steady State, E-16 Transient/Mechanical Loads, and Final Steady State . . . . .	180

6.2-4	F/A ACLP Hex Duct First Cycle Time Dependent Analysis Summary 10-day Hold-Time and Unloading . . . . .	185
6.2-5	F/A ACLP Hex Duct Second Cycle Time Independent Analysis Summary Initial Steady State, E-16 Transient, and Final Steady State . . . . .	189
6.2-6	F/A ACLP Hex Duct Second Cycle Time Dependent Analysis Summary 10-day Hold-Time and Unloading . . . . .	192
6.3-1	F/A ACLP Hex Duct Structural Evaluation Summary . . . . .	206
7.1-1	Worst Case F/A Outlet Nozzle Duty Cycle ANSYS Input Data . .	218
7.2-1	F/A Outlet Nozzle True Minimum BOL and EOL Stress Strain Data SA-316-SS . . . . .	227
7.2-2	F/A Outlet Nozzle Reference Temperatures . . . . .	232
7.2-3	F/A Outlet Nozzle Time Independent Analysis Summary Initial Steady State, E-16 Transient, and Final Steady State . . . .	234
7.2-4	F/A Outlet Nozzle Time Dependent Analysis Summary 10-day Hold-Time and Unloading . . . . .	239
7.3-1	F/A Outlet Nozzle Structural Evaluation Summary . . . . .	251
8.1-1	F/A Attachment Assembly Support Bar, Deadweight Distribution by Rows. . . . .	255
8.1-2	F/A Attachment Assembly Support Bar, Pressure Drop Distribution by Rows . . . . .	259
8.1-3	F/A Attachment Assembly, Horizontal OBE and SSE Seismic Load, Distribution by Rows . . . . .	263
8.1-4	F/A Attachment Assembly Support Bar, Vertical OBE and SSE Seismic Loads, Distribution by Rows. . . . .	266
8.1-5	F/A Attachment Assembly Support Bar, Mechanical Load Summary, Distribution by Rows. . . . .	267
8.1-6	F/A Attachment Assembly Support Bar, E-4a Transient, Ansys Input Data . . . . .	275
8.2-1	F/A Attachment Assembly Support Bar, First Duty Cycle, Time Independent and Dependent Analysis Summary. . . . .	293
8.3-1	F/A Attachment Assembly Support Bar, Structural Evaluation Summary . . . . .	308
9.1-1	F/A Orifice Plate, Average Steady State Pressure Drops . . .	310
9.2-1	F/A Orifice Plate, True Minimum BOL and EOL Stress-Strain Data, SA-316-SS. . . . .	319
9.2-2	F/A Orifice Plate, First Cycle-Time Independent Analysis Summary . . . . .	330
9.2-3	F/A Orifice Plate, Second Cycle-Time Independent Analysis Summary . . . . .	333
9.3-1	F/A Orifice Plate, Structural Evaluation Summary . . . . .	344

A.1	Damage Processor Typical Output for One Element. . . . .	A-4
A.2	Damage Processor Maximum Damage Factors Typical Output . . .	A-6
A.3	Damage Processor Source Deck Listing . . . . .	A-7



LIST OF FIGURES

2.0-1	CRBRP Core Arrangement Sector A Designation Scheme . . . . .	4
2.0-2	CRBRP F/A Design Layout Drawing. . . . .	5
3.1-1	Combined Creep-Damage Factor . . . . .	21
4.1-1	F/A Shield Block E-4a Transient . . . . .	32
4.1-2	F/A Shield Block Worst Case Duty Cycle . . . . .	33
4.1-3	F/A Shield Block Thermal Model Dimensional Extent and Finite Element Detail . . . . .	35
4.1-4	F/A Shield Block Boundary Conditions and Wetted Surfaces . . .	37
4.1-5	F/A Shield Block E-4a Transient Load Steps . . . . .	40
4.1-6	F/A Shield Block E-4a Transient Temperature Difference vs. Cumulative Iteration . . . . .	42
4.1-7	F/A Shield Block E-4a Transient Cumulative Iterations 2 and 36 Temperature Distributions . . . . .	43
4.1-8	F/A Shield Block E-4a Transient Cumulative Iteration 63 Temperature Distribution . . . . .	44
4.2-1	F/A Shield Block Structural Model, geometry, and Boundary Conditions . . . . .	48
4.2-2	F/A Shield Block SA-316SS Stress-Strain Curves Minimum Mean of BOL and EOL . . . . .	52
4.2-3	F/A Shield Block Initial and Final Steady State Time Independent Equivalent Stress . . . . .	60
4.2-4	F/A Shield Block Cumulative Iteration 36 and 63 Time Independent Equivalent Stress . . . . .	61
4.2-5	F/A Shield Block Non-Uniform Deformation Time Independent . .	62
4.2-6	F/A Shield Block Non-Uniform Deformation Time Dependent . . .	65
4.3-1	F/A Shield Block SA-316-SS Fatigue Life EOL Fluence ( $E > 0.1$ Mev, $\phi t = 0.31 \times 10^{22}$ n/cm <sup>2</sup> ) Temperature $\sim 800^\circ\text{F}$ . . . . .	74
4.3-2	F/A Shield Block SA-316-SS Creep Rupture Time EOL Fluence ( $E > 0.1$ Mev, $\phi t = 0.31 \times 10^{22}$ n/cm <sup>2</sup> ) Temperature $\sim 800^\circ\text{F}$ . . .	78
5.1-1	F/A CMP Hex Duct E-16 Transient. . . . .	90
5.1-2	F/A CMP Hex Duct Worst Case Duty Cycle . . . . .	91
5.1-3	F/A CMP Hex Duct Thermal Model Dimensional Extent and Finite Element Detail. . . . .	93
5.1-4	F/A CMP Hex Duct Boundary Conditions and Wetted Surfaces . . .	95
5.1-5	F/A CMP Hex Duct E-16 Transient Load Steps . . . . .	98
5.1-6	F/A CMP Hex Duct E-16 Transient Temperature Difference vs. Cumulative Iteration . . . . .	100

5.1-7	F/A CMP Hex Duct E-16 Transient Cumulative Iterations 2 and 27 Temperature Distributions . . . . .	101
5.2-1	F/A CMP Hex Duct Structural Model, Geometry, and Boundary Conditions . . . . .	105
5.2-2	F/A CMP Hex Duct Steady State and Cumulative Iteration 27 Equivalent Stress Time Independent . . . . .	113
5.2-3	F/A CMP Hex Duct Steady State and Cumulative Iteration 27 Non-Uniform Deformations Time Independent . . . . .	114
5.3-1	F/A CMP Hex Duct First Core 20% CW-316-SS Fatigue Life . . .	124
5.3-2	F/A CMP Hex Duct First Core 20% CW-316-SS Creep Rupture Time	127
6.1-1	F/A ACLP Hex Duct PCM 1g Static Load Locations . . . . .	138
6.1-2	F/A ACLP Hex Duct Method of Selecting Static 1g Loads . . .	139
6.1-3	F/A ACLP Hex Duct CRM Core Restraint Load Locations . . . .	143
6.1-4	F/A ACLP Hex Duct Method of Selecting Core Restrain Loads .	144
6.1-5	F/A ACLP Hex Duct E-16 Transient . . . . .	150
6.1-6	F/A ACLP Hex Duct E-16 Transient Largest Sustained S.S. Temp.	152
6.1-7	F/A ACLP Hex Duct Worst Case Duty Cycle . . . . .	153
6.1-8	F/A ACLP Hex Duct Dimensional Extent and Finite Element Detail	155
6.1-9	F/A ACLP Hex Duct Boundary Conditions and Wetted Surfaces .	157
6.1-10	F/A ACLP Hex Duct E-16 Transient Largest Sustained S.S. Temperatures Load Steps. . . . .	160
6.1-11	F/A ACLP Hex Duct E-16 Transient Temperature Difference vs. Cumulative Iteration . . . . .	162
6.1-12	F/A ACLP Hex Duct E-16 Transient Cumulative Iteration 2 and 32 Temperature Distributions . . . . .	163
6.2-1	F/A ACLP Hex Duct Structural Model, Geometry, and Boundary Conditions . . . . .	168
6.2-2	F/A ACLP Hex Duct First Core 20% CW-316-SS Stress-Strain Curves Minimum Mean of BOL and EOL at 1000°F . . . . .	173
6.2-3	F/A ACLP Hex Duct First Cycle Time Independent Initial Steady State Equivalent Stress and Peak Non-Uniform Deformation . . . . .	182
6.2-4	F/A ACLP Hex Duct First Cycle Time Independent Core Restraint and SSE Loads with Cumulative Iteration 32 Temperature Distribution Equivalent Stress and Peak Non-Uniform Deformation . . . . .	183
6.2-5	F/A ACLP Hex Duct First Cycle - Time Independent Final Steady State Equivalent Stress and Peak Non-Uniform Deformation . . .	184

6.2-6	F/A ACLP Hex Duct First Cycle - Time Dependent Final Steady State Equivalent Stress and Non-Uniform Deformation . . . . .	187
6.2-7	F/A ACLP Hex Duct First Cycle - Time Dependent Unloading for Residuals Equivalent Stress and Non-Uniform Deformation .	188
6.2-8	F/A ACLP Hex Duct Second Cycle - Time Independent Cumulative Iteration 32 Temperature Distribution Equivalent Stress and Peak Non-Uniform Deformation . . . . .	190
6.2-9	F/A ACLP Hex Duct Second Cycle - Time Independent Final Steady State Equivalent Stress and Non-Uniform Deformation .	191
6.2-10	F/A ACLP Hex Duct Second Cycle Time Dependent Final Steady State Equivalent Stress and Non-Uniform Deformation . . . . .	193
6.2-11	F/A ACLP Hex Duct Second Cycle - Time Dependent Unloading for Residuals Equivalent Stress and Non-Uniform Deformation .	194
6.3-1	F/A ACLP Hex Duct First Core 20% CW-316-SS Fatigue Life . . .	200
6.3-2	F/A ACLP Hex Duct First Core 20% CW-316-SS Creep Rupture Time	201
7.1-1	F/A Outlet Nozzle E-16 Transient. . . . .	211
7.1-2	F/A Outlet Nozzle Worst Case Duty Cycle . . . . .	212
7.1-3	F/A Outlet Nozzle Thermal Model Dimensional Element and Finite Element Detail . . . . .	214
7.1-4	F/A Outlet Nozzle Boundary Conditions and Wetted Surfaces . .	216
7.1-5	F/A Outlet Nozzle E-16 Transient Load Steps . . . . .	219
7.1-6	F/A Outlet Nozzle E-16 Transient Temperature Difference vs. Cumulative Iterations . . . . .	221
7.1-7	F/A Outlet Nozzle E-16 Transient Cumulative Iteration 3, 16, and 31 Temperature Distributions . . . . .	222
7.2-1	F/A Outlet Nozzle Structural Model, Geometry, and Boundary Conditions . . . . .	225
7.2-2	F/A Outlet Nozzle SA-316-SS True Minimum BOL and EOL Stress-Strain Curves . . . . .	228
7.2-3	F/A Outlet Nozzle Solution SA-316-SS Secondary Creep Rate at 1000°F and 1200°F . . . . .	231
7.2-4	F/A Outlet Nozzle Initial and Final Steady State Equivalent Stress Time Independent . . . . .	236
7.2-5	F/A Outlet Nozzle E-16 Transient Cumulative Iteration 31 Equivalent Stress Time Independent . . . . .	237
7.2-6	F/A Outlet Nozzle Initial Steady State and E-16 Transient Cumulative Iteration 31 Non-Uniform Deformation Time Independent . . . . .	238
7.2-7	F/A Outlet Nozzle Final Steady State Equivalent Stress and Non-Uniform Deformation Time Dependent . . . . .	241

7.2-8	F/A Outlet Nozzle Residual Deformation . . . . .	242
7.3-1	F/A Outlet Nozzle SA-316-SS Fatigue Life EOL Fluence ( $E > 0.1$ Mev, $\phi t = 0.31 \times 10^{22}$ n/cm <sup>2</sup> ) Temperature $\sim 1250^{\circ}\text{F}$ . . . . .	246
7.3-2	F/A Outlet Nozzle Creep Rupture Time EOL Fluence ( $E > 0.1$ Mev, $\phi t = 0.07 \times 10^{22}$ n/cm <sup>2</sup> ) Temperature $\sim 1100^{\circ}\text{F}$ . . . . .	247
8.1-1	F/A Attachment Assembly, Deadweight Load Distribution. . . . .	254
8.1-2	F/A Attachment Assembly, Pressure Drop Load Distribution . . . . .	258
8.1-3	F/A Attachment Assembly, Seismic Load Distribution . . . . .	260
8.1-4	F/A Attachment Assembly Support Bar, Thermal Load Model, Dimensional Extent and Finite Element Detail . . . . .	270
8.1-5	F/A Attachment Assembly Support Bar, Thermal Load Model, Heat Transfer Boundary Conditions and Wetted Surfaces. . . . .	274
8.1-6	F/A Attachment Assembly Support Bar, Thermal Load Model, Structural Boundary Conditions . . . . .	277
8.1-7	F/A Attachment Assembly Support Bar, E-4a Thermal Loads, Relative Displacements . . . . .	279
8.2-1	F/A Attachment Assembly Support Bar, Dimensional Extent and Finite Element Detail. . . . .	286
8.2-2	F/A Attachment Assembly Support Bar, Boundary Conditions and Load Applications. . . . .	288
8.2-3	F/A Attachment Assembly Support Bar, First Cycle - Time Independent Initial Steady State, Deadweight + Pressure Drop, Equivalent Stress Deformations . . . . .	295
8.2-4	F/A Attachment Assembly Support Bar, First Cycle - Time Independent, First SSE Seismic Loading, Pressure Drop + Up Vertical + Left Horizontal, Equivalent Stress and Deformations . . . . .	296
8.2-5	F/A Attachment Assembly Support Bar, First Cycle - Time Independent, Second SSE Seismic Loading, Deadweight + Down Vertical + Right Horizontal, Equivalent Stress and Deformations . . . . .	297
8.2-6	F/A Attachment Assembly Support Bar, First Cycle - Time Independent, First E-4a Thermal Loading, Deadweight + Inward Base Motion, Equivalent Stress and Deformations . . . . .	298
8.2-7	F/A Attachment Assembly Support Bar, First Cycle - Time Independent, Second E-4a Thermal Loading, Deadweight + Outward Base Motion, Equivalent Stress and Deformations. . . . .	299
8.2-8	F/A Attachment Assembly Support Bar, First Cycle - Time Independent, Final Steady State, Deadweight + Pressure Drop, Equivalent Stress and Deformations . . . . .	300

9.2-1	F/A Orifice Plate, Dimensional Extent and Finite Elemental Detail. . . . .	317
9.2-2	F/A Orifice Plate, SA-316SS, True Minimum BOL and EOL Stress - Strain Curves. . . . .	320
9.2-3	F/A Orifice Plate, Pressure Drop Structural Model . . . . .	322
9.2-4	F/A Orifice Plate, Pressure Drop Elastic Response, Equivalent Stress and Perpendicular Displacements . . . . .	324
9.2-5	F/A Orifice Plate, Radial Interference Structural Model . . . . .	326
9.2-6	F/A Orifice Plate, Radial Interference Elastic Response, Equivalent Stress and In-Plane Deformations . . . . .	328
9.2-7	F/A Orifice Plate, First Cycle - Time Independency, Peak E-4a Radial Interference, Equivalent Stress and Non-Uniform Deformation . . . . .	331
9.2-8	F/A Orifice Plate, First Cycle - Time Independent, Final Steady State, Equivalent Stress and Non-Uniform Deformation . . . . .	332
9.2-9	F/A Orifice Plate, Second Cycle - Time Independent, Peak E-4a Radial Interference, Equivalent Stress and Non-Uniform Deformation . . . . .	335
9.2-10	F/A Orifice Plate, Second Cycle - Time Independent, Final Steady State, Equivalent Stress and Non-Uniform Deformation . . . . .	336
A-1	Damage Assessment Flow Chart. . . . .	A-3

## 1.0 INTRODUCTION

The Clinch River Breeder Reactor Plant (CRBRP) core is comprised of Control (C/A), Fuel (F/A), Blanket (B/A), and Removable Radial Shield (RRS/A) assemblies arranged in a hexagonal pattern within the core barrel. The core assemblies are exposed to nuclear irradiation at elevated temperature in direct contact with liquid sodium and are subjected to mechanical and thermal loads. Owing to the severity of the environment and loadings over the replacement schedules planned for the C/A, F/A, B/A, and RRS/A, it is important that attendant structural damage does not impair the intended function of the core components in the overall CRBRP system.

### 1.1 Purpose

The purpose of this report is to present a structural evaluation of the CRBRP F/A in support of the Final Design Review so as to assure that structural damage does not impair intended F/A function in the CRBRP system in accordance with the requirements of the Equipment Specification for the First Core Fuel Assembly [1].

### 1.2 Scope

The scope of the Structural evaluation is applicable to all F/A in the CRBRP core and all F/A components, excluding the fuel rods. The scope of F/A structural evaluation was reduced by evaluating only worst case F/A locations. Further, only worst case F/A regions were evaluated, which included the shield block, Core Mid-Plane (CMP) hex duct, Above Core Load Plane (ACLPL) hex duct, Top Load Plane (TLP) outlet nozzle, attachment assembly, and orifice plate. Other F/A locations and component regions were bracketed within the worst case approach.

### 1.3 Applicability

Prior F/A structural evaluations in support of Preliminary Design Reviews were applicable to the homogeneous CRBRP core arrangement and respective thermal and nuclear performance. The F/A structural evaluation presented in this report is based on June 1977 thermal and nuclear performance of the CRBRP Heterogeneous core over the first and second cycles of 100 and 200 full power-days respectively, for a total of 328 full-power days.



#### 1.4 Summary

The F/A structural evaluation was performed in accordance with the criteria identified in the First Core Fuel Assembly Equipment Specification [1] which assure the intended function of the F/A in the CRBRP core is not impaired over the first and second reactor cycles comprising a total of 328 full power days. The F/A criteria protect against the crack initiation failure modes of local ductile rupture and combined creep-fatigue damage. In addition, the excessive deformation failure modes of peak plus accumulated and residual deformation are protected against by the F/A criteria. The F/A structural evaluation based on the June 1977 loads and currently available materials data showed that the F/A design comprising the shield block, TLP outlet nozzle, CMP and ACLP hex ducts, attachment assembly, and orifice plate are not expected to experience crack initiation and excessive deformation failure over the first and second reactor cycles. A summary of the margins of safety for the F/A regions structurally evaluated is presented in Table 1.0-1.

TABLE 1.0-1  
F/A MARGIN OF SAFETY SUMMARY

F/A Region	Margin of Safety*			
	Crack Initiation		Excessive Deformation	
	Local Ductile Rupture	Combined Creep-Fatigue Damage	Peak plus Accumulated	Residual
Shield Block	2.80	61.62	4.75	2.13
CMP Hex Duct	12.76	191.3	37.4	∞
ACLP Hex Duct	10.49	91.68	4.65	1.58
TLP Outlet Nozzle	0.37	0.29	3.0	1.86
Attachment Assembly	82.33	925,925	10.11	∞
Orifice Plate	4.03	291,544	0.43	1.52

\*Margin of Safety =  $\frac{\text{Allowable Value}}{\text{Calculated Value}} - 1$



## 2.0 DESCRIPTION AND APPROACH

The heterogeneous core plan places F/A adjacent to C/A, B/A, or other F/A. A total of 156 F/A, 15 C/A, 208 B/A, 306 RRS/A and 6 assemblies which can be either F/A or B/A are provided. The full 360° plan view arrangement is subdivided into 60° sectors designated by A, B, C, D, E, and F. The core map for Sector A including the individual assembly designation scheme is presented in Figure 2.0-1.

The F/A structural evaluation presented in this report addresses the shield block, CMP and ACLP hex ducts, TLP outlet nozzle, attachment assembly and orifice plate. The F/A design at all locations in the core is identical in terms of materials of construction, dimensions, and tolerances. The F/A design layout is presented in Figure 2.0-2.

The F/A structural evaluation approach adopted for the shield block, CMP and ACLP hex ducts, TLP outlet nozzle, attachment assembly, and orifice plate was to construct analytical models for the respective F/A regions in relation to prominent design features and loading conditions which would provide worst case structural damage. The ANSYS Computer Program [2] was used extensively in the analytical approach adopted for the F/A structural evaluation. In the following, the F/A regions selected for structural evaluation are described in terms of prominent design features and worst case loadings from which the ANSYS analytical models were formulated.



# DOCUMENT/ PAGE PULLED

ANO. 8009020017

NO. OF PAGES 1

## REASON

PAGE ILLEGIBLE

HARD COPY FILED AT: PDR CF

OTHER \_\_\_\_\_

BETTER COPY REQUESTED ON 1-1-1

PAGE TOO LARGE TO FILM.

HARD COPY FILED AT: PDR CF

OTHER \_\_\_\_\_

FILMED ON APERTURE CARD NO. 8009020017

## 2.1 Shield Block

The F/A shield block, located between the hex duct and inlet nozzle, functions to limit the irradiation of the core support plate. The shield block is a near solid SA-316-SS hexagonal bar with nominal flat-to-flat dimensions of 4.695 in. x 12 in. long. In order to permit sodium to pass from the inlet nozzle through the F/A, the shield block is provided with a pattern of 7 flow holes, nominally 0.75 in. diameter, comprising a central hole and 6 symmetrically spaced holes on a nominal 2.750 in. diameter circle. The shield block region is identified adjacent to Section E-12 in the F/A design layout presented in Figure 2.0-2.

The shield block region represents the worst case location for structural damage for the F/A inlet hardware. Thermal loads caused by steady state and inlet sodium transients control structural damage as mechanical core restraint and seismic loads are relatively insignificant throughout the inlet nozzle region. The thermal loads cause the worst damage in the shield block because the inlet sodium transients in the flow hole passages are restrained by the relatively thick-walled shield block body. Other prominent F/A inlet locations include the nozzle, nozzle to shield block weld, and hex duct to shield block weld. However, the latter locations are relatively thin-walled with welds on exterior surfaces exposed to the stagnant sodium interstice and not to the inlet sodium transients. As such, the structural damage caused by thermal loads in the F/A inlet hardware would be worst case in the shield block, or alternately the structural damages of the F/A inlet nozzle, and nozzle and hex duct to shield block welds is considered to be conservatively bounded by the structural damage of the shield block.

## 2.2 CMP Hex Duct

The F/A CMP hex duct is the region of the hex duct body at the core mid-plane. The CMP hex duct is constructed from 20%-CW-316 SS with nominal outside dimensions of 4.575 in. flat to flat x 0.120 in. wall thickness. The CMP hex duct construction is identical to the hex duct body above and below the ACLP as depicted in Section E-16 of the F/A design layout presented in Figure 2.0-2.

The CMP hex duct region represents the worst case location for structural damage in the F/A hex duct body above and below the ACLP. The CMP region is exposed to the worst case fluence levels over the life of the F/A. As such, the available ductility of the F/A hex duct material which can be safely exhausted during thermal and mechanical loadings in damage evaluations is a worst case minimum at the CMP.

### 2.3 ACLP Hex Duct

The F/A ACLP hex duct is the thickened region of the hex duct body at the above core load plane which functions to transfer inter-duct loads between adjacent assemblies to the ACLP core former. The ACLP hex duct is constructed from 20%-CW-316-SS with nominal outside dimensions of 4.745 in. flat to flat x 0.205 in. wall thickness over a 4 in. axial extent. Minimum ACLP wall thickness is 0.190 in. The ACLP hex duct construction as depicted by Section E-14 of the F/A design layout is presented in Figure 2.0-2.

The ACLP hex duct region represents the worst case location for structural damage of the F/A under lateral mechanical core restraint and seismic inter-duct loadings as a hollow thin walled construction is required to accommodate the fuel rod bundle. Other F/A locations which transfer lateral mechanical loads are the inlet and TLP outlet nozzles, however, these locations are not critical as relatively thick walled construction is permitted. The failure mode of interest at the ACLP hex duct is duct crushing initiated by instability or rupture related to the ductility at fluence and temperature.

### 2.4 TLP Outlet Nozzle

The F/A TLP outlet nozzle, located at the top of the F/A, functions to channel the sodium coolant into the outlet plenum while providing lateral support of adjacent assemblies in transferring lateral mechanical core restraint and seismic loads to the TLP core former. The TLP outlet nozzle is constructed from SA-316-SS with nominal outside hex dimensions of 4.745 in. flat to flat. The outside nozzle surface at one end is provided with a shoulder to accommodate the hex duct weld while the other end is formed to permit handling during installation and removal. The inside nozzle surface is

generally circular with the exception of a fluted region which prevents fuel rod and bundle damage in the event that a RB/A is inadvertently inserted in an occupied F/A position. The TLP outlet nozzle region is identified in Section E-16 of the F/A design layout presented in Figure 2.0-2.

The TLP outlet nozzle region constitutes the worst case location for structural damage in the F/A outlet nozzle hardware. Thermal loads caused by steady state and outlet sodium transients control structural damage. Mechanical core restraint and seismic loads are not significant in contributing to structural damage as the outlet nozzle is of relatively thick walled construction. Thermal loads are significant because the thick walled nozzle construction restrains the expansion of the inside nozzle surfaces under outlet sodium transients. The other prominent TLP outlet nozzle location is the nozzle to hex duct weld. However, the weld is located on the exterior surface exposed to stagnant sodium interstice temperatures and not to outlet sodium transients. As such, the structural damage caused by thermal loads in the F/A outlet hardware is worst case in the outlet nozzle, or alternately the structural damage of the hex duct to outlet nozzle weld is considered to be conservatively bounded by the structural damage of the F/A TLP outlet nozzle.

## 2.5 Attachment Assembly

The F/A attachment assembly, located adjacent to the hex duct to shield block weld, functions to support the bottom of the fuel rod assembly in both vertical and horizontal directions. The attachment assembly comprises, in combination, a pair of U-Shaped SA-316-SS support bars welded at their free ends to recesses formed in the supporting shield block, a total of 17 thin SA-316-SS attachment rails supported in lateral grooves cut in each of the support bars, and a pair of Inconel 718 locking bars which, when inserted into mating holes formed in the support bars secure the fuel rod assembly by the attachment rails to the shield block. The attachment assembly with prominent design features is identified adjacent to and including Section E-12 in the F/A design layout illustrated in Figure 2.0-1.

The attachment assembly represents the worst case F/A location for localized structural damage as the grooves machined in the support bars to accommodate the many attachment rails inherently act as stress risers. In addition, welds are provided to secure the base of the support bar legs to the top of the shield block. The latter are of interest as the welds have reduced ductility relative to the parent material. Mechanical loads acting on the support bars include deadweight and vertical OBE and SSE seismic while thermal loads comprise expansion differences caused by the response lag of the shield block relative to the support bars during inlet sodium transients.

## 2.6 Orifice Plate

The F/A orifice plate assembly, situated between the inlet nozzle and shield block, functions to passively throttle the inlet sodium flow. The orifice plate is comprised of a set of SA-316-SS perforated circular plates, nominally 1/4 in. thick, and spacers identified adjacent to and including Section F-4 in the F/A design layout illustrated in Figure 2.0-2.

The orifice assembly as comprised of thin perforated plates represents the worst case F/A location for structural damage under steady state and transient pressures induced by inlet sodium flow. In addition, thermal loads caused by the thermal lag of adjacent shield block response in relation to exhausting the diametral clearances in relation to radial constraints at the orifice plate periphery require investigation.



### 3.0 CRITERIA

In order to assure that CRBRP functional requirements are not impaired by structural damage during the first and second reactor cycles, the F/A Equipment Specification [1] includes both elastic and inelastic structural criteria from which the F/A design can be evaluated in relation to acceptability.

Fundamental in both F/A elastic and inelastic structural criteria is the use of excessive deformation as the measure of structural damage from which judgements on the impairment of F/A functional requirements and design acceptability are made. Two measures of excessive deformation are considered. The first are the peak plus accumulated deformations that occur between BOL and EOL which are related to operational F/A functional requirements. The second are the EOL residual deformations related to the dimensional tolerances specified on the design drawings which were considered necessary for BOL F/A functional requirements. For the F/A elastic criteria, limits on excessive peak plus accumulated and residual deformation which assure F/A Functional requirements are not explicitly specified. The structural criteria based on elastic analyses protect against gross deformation, tensile instability, stress rupture, excessive strain (greater than 1%) and ratchetting by limiting the values of primary and secondary stresses either to elastic domain or to a fraction of ultimate strength or rupture strength. These criteria, in general, are highly conservative and preclude the need for any strain or inelastic calculations. In the case of F/A inelastic criteria, excessive deformation limits are specified because inelastic deformations may be large in relation to operational and dimensional F/A functional requirements.

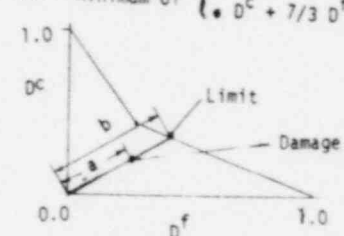
The F/A elastic and inelastic criteria also protect against crack initiation and elastic/plastic/creep instability failures that may occur before excessive deformation limits are exceeded. The modes of crack initiation failure which are protected against include both local ductile rupture and combined creep-fatigue damage. The F/A elastic criteria protect against crack initiation and elastic instability failures by imposing

limits placed on elastically calculated stresses. For the F/A inelastic criteria, strain limits protect against crack initiation failures while large deformation analysis is required to assure that elastic/plastic/creep instability failures do not occur.

The CRBRP F/A structural criteria selected for the F/A regions evaluated in this report are the inelastic structural criteria presented in the F/A Equipment Specification [1]. Accordingly, the intent of the structural evaluation of the F/A regions is to establish that crack initiation and elastic/plastic/creep instability failures do not occur before limits on excessive deformation are exceeded.

In the following subsections, the specific CRBRP F/A inelastic criteria are described in terms of background and rationale for selecting design limits, and a description of the application of the inelastic criteria for the F/A regions evaluated is presented. A summary of the CRBRP F/A inelastic criteria is given in Table 3.0-1.

TABLE 3.0-1  
CRDRP F/A INELASTIC CRITERIA AND LIMITS

Type of Failure	Mode	Criteria	Limit	F/A Region	
Crack Initiation	Local	$F_{DR} = \text{Max of } \left\{ \begin{array}{l} \bullet \frac{(e_{\text{max principal}})^{TF}}{0.3 e_f} \\ \bullet \frac{(e_{\text{max principal}})^{TF}}{e_u} \end{array} \right\}$	1	A11	
	Ductile Rupture	<p>where,</p> <p><math>e_f</math> = True Min. Fracture Strain</p> <p><math>e_u</math> = True Min. Uniform Elongation</p> <p>TF = Triaxiality Factor</p> <p><math>TF = \frac{\sqrt{2} (\sigma_1 + \sigma_2 + \sigma_3)}{\sqrt{(\sigma_1 - \sigma_2)^2 + (\sigma_2 - \sigma_3)^2 + (\sigma_3 - \sigma_1)^2}}</math></p> <p><math>\sigma_1, \sigma_2, \sigma_3</math> = Principal Stresses</p> <p><math>e_{\text{max principal}}</math> = Maximum Principal Strain (Peak + Accumulated)</p>			
Creep Fatigue		$F_{CFD} = a/b = \text{Minimum of } \left\{ \begin{array}{l} \bullet 7/3 D^c + D^f \\ \bullet D^c + 7/3 D^f \end{array} \right\}$ 	1	A11	
		<p>where,</p> <p><math>D^c</math> = Creep Damage Factor</p> <p><math>D^c = \int \frac{dt}{t_r}</math></p> <p><math>t_r</math> = Rupture Time Based on Equivalent Stress or Max. Positive Principal Stress</p> <p><math>D^f</math> = Fatigue Damage Factor</p> <p><math>D^f = \sum \frac{n}{N_f}</math></p> <p><math>n</math> = No. of Cycles</p> <p><math>N_f</math> = Allowable No. of Cycles Based on range of equivalent or Max. Principal Strain</p>			
Excessive Deformation	Peak + Accumulated	$\delta^{P+A} \leq \text{PADL}$	0.082 in.	ACLP Hex Duct	
		where,	0.020 in.	TLP Outlet Nozzle	
		-PADL = Peak + Accumulated Non-Uniform Deformation Limit, Excluding Irradiation Creep and Swelling	0.010 in.	CMP Hex Duct	
			0.005 in.	All Others	
	Residual	$\delta^R \leq \text{RDL}$	where,	0.010 in.	ACLP Hex Duct
			RDL = Residual Non-Uniform Deformation Limit, Excluding Irradiation Creep and Swelling	0.020 in.	TLP Outlet Nozzle
				0.010 in.	CMP Hex Duct
				0.005 in.	All Others

### 3.1 Background and Rationale

The structural criteria, which assure the functional requirements of the F/A in the CRBRP system over the first and second reactor cycles is not impaired, requires special considerations of nuclear fluence at elevated temperature in a liquid sodium environment. Established structural criteria for Class 1 nuclear components such as the ASME Section III Code [3] and Code Case 1592 [4] do not cover the combined effects of irradiation and elevated temperature, nor reflect the deformation limits necessary to assure the functional requirements of the F/A in the CRBR system. The proposed Structural Design Criteria for Breeder Reactor Core Components [5] provide guidelines to cover the combined effects of irradiation at elevated temperature, but recognize that specific structural criteria in terms of deformation limits which assure the functional requirements of a core component can only be specified by the Owner on a case-by-case basis.

The inelastic criteria established for the CRBRP F/A are in large part extensions of the proposed Breeder Reactor Core Components Design Criteria [5] except as modified to accommodate the specific functional requirements of the shield block, CMP and ACLP hex ducts, TLP outlet nozzle, attachment assembly, and orifice plate designs. In the following, the ASME Section III Code, Code Case 1592, and Proposed Breeder Reactor Core Components Criteria in relation to respective scope and applicability are first presented to form a background from which the rationale for the specific criteria identified in the F/A Equipment Specification [1] are identified.

#### 3.1.1 ASME Section III Code

The ASME Section III Code stress limits and design rules of Subsection NB are applicable to Class I nuclear components not exposed to nuclear fluence and operating at temperatures ( $< 800^{\circ}\text{F}$ ) where creep and relaxation effects are negligible for typical materials of construction. Accordingly, the NB rules only protect against time-independent failure modes summarized as follows:

- Crack initiation caused by ductile rupture from short term loadings,
- Crack initiation caused by fatigue under short term loading, and
- Elastic/plastic instability causing gross distortion or incremental collapse under short term loading.

The ASME Section III Code Subsection NB rules are not directly applicable to the structural evaluation of the CRBRP F/A because generally the materials are irradiated and temperatures are in excess of 800°F where time dependent creep effects may occur. In addition, the NB stress limits do not reflect the deformation limits necessary in assuring that the specific CRBR F/A functional requirements are satisfied.

### 3.1.2 Code Case 1592

The Code Case 1592 design rules are applicable to Class I nuclear components exposed to elevated temperature (> 800°F) where creep and relaxation effects are significant and irradiation effects on materials of construction are negligible. Code Case 1592 rules are formulated to include ASME Section III code stress limits and design rules to protect against time-independent failure modes with additional criteria provided to protect against time-dependent failure modes. A summary of the failure modes protected against with Code Case 1592 rules is as follows:

- Crack initiation caused by ductile rupture from combined short and long term loadings,
- Crack initiation caused by creep-fatigue interaction under combined short and long term loadings,
- Elastic/plastic/creep instability causing gross distortion or incremental collapse under short and long term loading, and

- Loss of function due to excessive deformation under short and long term loadings.

The Code Case 1592 rules are only applicable to the CRBR F/A when the effects of nuclear irradiation on the materials of construction are insignificant. For unirradiated regions of the F/A, the Code Case 1592 rules protect against time-dependent failure modes while time-independent failure modes are protected against by the NB stress limits of the ASME Section III Code. However, Code Case 1592 rules do not provide guidance in protecting against time-dependent and time-independent failure modes of F/A regions where the effects of material irradiation are significant. Further, Code Case 1592 rules only identify excessive deformation as a potential failure mode with specific limits which would assure CRBR F/A functional requirements to be specified by the Owner.

### 3.1.3 RDT Draft Criteria for Breeder Reactor Core Components [5]

The RDT Draft Criteria for Breeder Reactor Core Components are applicable to nuclear core components exposed to low (< 800°F) or elevated (> 800°F) temperatures and fluence levels where the effects of material irradiation are significant. The RDT draft rules are prescribed for Class A, B, and C Breeder Reactor core components instead of the rules for Class I nuclear components presented in the ASME Section III Code and Code Case 1592. Classification of a Breeder Reactor Core Component depends on the level of assured structural integrity required to satisfy the reliability and functional requirements of the total reactor system during specified Normal, Upset Emergency, and Faulted Events. Core components are classified as A, B, and C for decreasing levels of structural integrity designated as very high, high, and moderate respectively. The RDT draft rules protect against the same time-dependent and time-independent failure modes as Code Case 1592 and provide guidance for including the effects of irradiation on material properties. In addition, the RDT draft rules provide guidance for protecting against unstable crack propagation in materials highly embrittled by irradiation. A summary of the failure modes protected against by RDT draft rules is as follows.

- Crack initiation caused by ductile rupture from combined short and long term loading,
- Crack initiation caused by creep-fatigue interaction under combined short and long term loading,
- Elastic/plastic/creep instability causing cross distortion or incremental collapse under short and long term loading,
- Loss of reliability and function due to excessive deformation under short and long term loading, and
- Propagation of pre-existing cracks.

The RDT draft rules are generally applicable to the CRBR F/A as the effects of irradiation at elevated temperature are expected in the reactor core. The proposed RDT draft rules are mandatory in protecting against crack initiation, elastic/plastic/creep instability, and loss of function due to excessive deformation in all CRBRP components identified as Class A, B, and C. However, protection against crack propagation in RDT rules is proposed as mandatory only for CRBR core components identified as Class A by the Owner. For example, the RDT draft suggests that the CRBR C/A would be considered a Class A component because reliability and functional requirements are important during SSE while the F/A and RB/A of less importance would be Class B components and the RRS/A of even less importance classified as Class C. With regard to methods of structural evaluation, the RDT draft rules permit inelastic analysis prior to or following elastic analysis with separate limits and design margins presented for the structural evaluation method selected.

In this arrangement, the RDT Draft Criteria for Breeder Reactor Core Components provides general guidance in the classification and structural evaluation of the CRBR F/A which is not provided by ASME Section III and Code Case 1592 rules. Further, the RDT draft rules provide specific criteria which would be applicable for the CRBR F/A to protect against crack initiation,



elastic/plastic/creep instability, and crack propagation, but permit the Owner to specify alternate criteria which are rationally defensible. With regard to loss of function due to excessive deformation, the RDT rules recognize that general governing criteria can not be formulated for a core component and, for the CRBR F/A, would permit specific deformation limits relevant to its particular reliability and function to be specified by the Owner.

#### 3.1.4 CRBRP F/A Core Component

The CRBRP F/A core component criteria and limits were formulated in accordance with the general rules and guidance provided in the RDT Draft for Breeder Reactor Core Components except as modified to include additional safeguards and to more properly reflect the F/A functional requirements of the Owner as identified in the Equipment Specification [1].

In accordance with the RDT draft rules and guidelines, the CRBR F/A was considered as a Class B Breeder Reactor core component which requires a high level of assured structural integrity in protecting against crack initiation, elastic/plastic/creep instability, and excessive deformation so as to satisfy reliability and functional requirements during Normal, Upset, Emergency, and Faulted conditions specified for the reactor core. The protection against the propagation of pre-existing cracks, which is a mandatory requirement for Class A Breeder Reactor components, was not considered necessary or important for the CRBRP F/A in relation to the functional requirements of the total reactor system as a whole. A summary of the failure modes protected against by the CRBRP F/A core component criteria at the shield block, CMP and ACLP hex duct, TLP outlet nozzle, attachment assembly, and orifice plates are as follows.

- Crack initiation caused by ductile rupture from combined short and long term loading,
- Crack initiation caused by creep-fatigue interaction under combined short and long term loading,

- Elastic/plastic/creep instability causing gross distortion or incremental collapse under short and long term loading, and
- Loss of reliability and function due to excessive deformations under short and long term loading.

In the formulation of specific CRBRP F/A Structural design criteria, the fundamental difference between RDT draft rules for Breeder Reactor Core Components was that crack initiation and elastic/plastic/creep instability failure modes are only of significance if the loss of function expressed in terms of excessive deformation limits are not exceeded. Alternately, crack initiation and elastic/plastic/creep instability failure modes which occur at deformations which exceed the deformation limits necessary to assure function for the specific F/A region evaluated are not relevant. Accordingly, the CRBRP F/A inelastic structural criteria were formulated on the basis of assuring that crack initiation and elastic/plastic/creep instability failure modes would not occur before deformation associated with functional limits are exceeded. However, no explicit criteria to protect against elastic/plastic/creep instability are formulated. Instead, the protection against elastic/plastic/creep instability was to require the method of analysis that would implicitly indicate the instabilities with attendant deformations limited by the excessive deformation limits. The protection against elastic/plastic/creep instability failure modes prior to exceeding deformation limits was assured by requiring large deformation non-linear analysis for F/A regions subjected to mechanical loads which are energy unbounded and load controlled. Conversely, F/A regions with thermal loads which are energy bounded and deformation controlled, non-linear small deformation analysis is required. In this arrangement, the structural integrity of the CRBRP F/A regions reduces to assuring that crack initiation failure modes would not occur before limits on excessive deformation failure modes were exceeded.

In the following, the specific CRBRP F/A inelastic structural criteria as formulated to protect against crack initiation and excessive deformation failure modes are described and summarized.

### 3.1.4.1 Crack Initiation

The CRBRP F/A criteria to protect against crack initiation are based on the rationale developed for protecting against local ductile rupture and creep-fatigue interaction in the RDT Draft for Breeder Reactor core components [5] except as modified to provide additional safeguards. Descriptions of the local ductile rupture and creep-fatigue criteria are as follows.

#### 3.1.4.1.1 Local Ductile Rupture

In the RDT Draft for Breeder Reactor Core Components [5], the local ductile rupture criterion as a protection against crack initiation limits the local maximum peak plus accumulated principal strain ( $\epsilon_{\text{max principal}}$ ) to a safe fraction (0.3) of the true uniaxial fracture strain ( $\epsilon_f$ ) corrected for the triaxiality factor (TF) of the stress state according to the relation:

$$\epsilon_{\text{max principal}} \leq \frac{0.3}{\text{TF}} \epsilon_f$$

One difficulty in the implementation of the proposed local ductile rupture criterion is that reduction in area measurements in irradiated tensile specimens, which are related to the true strain at fracture, are difficult to obtain in practice. In addition, tensile tests of irradiated EBR-II ducts [10] indicate that true fracture strains based on initial and final reduction of area measurements significantly exceeded total elongation. Accordingly, local ductile rupture criteria based on true fracture strain may not provide adequate protection against crack initiation in irradiated materials even if reduction in area measurements could be accurately obtained.

In order to provide an additional safeguard in protecting against local ductile rupture in irradiated materials, an additional criterion based on true uniform elongation ( $\epsilon_u$ ) corrected for the triaxiality factor of the stress state was adopted for the CRBRP F/A. As the true uniform elongation ( $\epsilon_u$ ) was observed in the irradiated EBR-II tensile tests [10] to be

significantly lower than the reported fracture strains ( $\epsilon_f$ ), additional conservatism in selecting a safe fraction ( $<1$ ) was not considered necessary. The additional criterion formulated:

$$\epsilon_{\text{max principal}} \leq \frac{\epsilon_U}{TF}$$

With the understanding that the difficulty in the implementation of a local ductile rupture criterion based on true fracture strain is one of lack of data and may not be a deficiency in the criteria itself, the local ductile rupture criterion selected for the CRBRP F/A considered the minimum of true uniform elongation or fracture strain correlations in the design limit.

$$\epsilon_{\text{max principal}} \leq \text{Minimum of: } \left\{ \begin{array}{l} \bullet \frac{0.3 \epsilon_f, \text{ min}}{TF} \\ \bullet \frac{\epsilon_U, \text{ min}}{TF} \end{array} \right\}$$

In order to facilitate the CRBRP F/A structural evaluation, it was found convenient to express the local ductile rupture criterion in a dimensionless form through a ductile rupture factor ( $F_{DR}$ )

$$F_{DR} = \text{Maximum of } \left\{ \begin{array}{l} \bullet \frac{(\epsilon_{\text{max principal}}) TF}{0.3 \epsilon_f, \text{ min}} \\ \bullet \frac{(\epsilon_{\text{max principal}}) TF}{\epsilon_U, \text{ min}} \end{array} \right\}$$

Where,  $F_{DR} \leq 1$  for acceptability

$$TF = \frac{\sqrt{2} (\sigma_1 + \sigma_2 + \sigma_3)}{\sqrt{(\sigma_1 - \sigma_2)^2 + (\sigma_2 - \sigma_3)^2 + (\sigma_3 - \sigma_1)^2}}$$

$\sigma_1, \sigma_2, \sigma_3 =$  Maximum Principal Stresses

TF = 1, for TF < 1

### 3.1.4.1.2 Creep-Fatigue Damage

The RDT Draft for Breeder Reactor Core Components [5] identifies creep-fatigue damage as a means of protecting against crack initiation. The total damage (D) consists of the sum of the thermal creep ( $D^C$ ) and fatigue damage ( $D^f$ ) factors which must be less than a design margin ( $\beta$ ).

$$D = D^C + D^f < \beta$$

For Normal and Upset, and Emergency events, the RDT Draft guidelines recommend a unity design margin ( $\beta = 1$ ). On the other hand, the Code Case 1592 criterion is more conservative in protecting against creep-fatigue damage and therefore was selected for the F/A structural criteria. In order to express the calculated combined creep-fatigue damage as a fraction of the Code Case 1592 damage limit, the concept of a combined creep-fatigue damage factor ( $F_{CFD}$ ) was introduced and is illustrated in Figure 3.1-1.

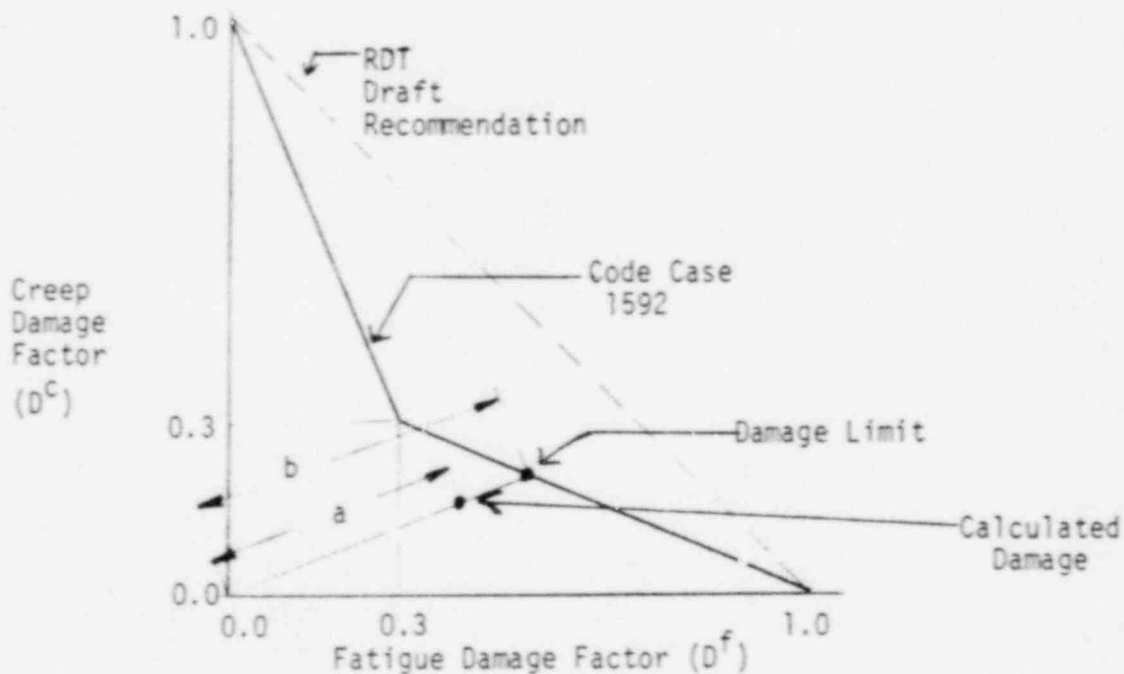


Figure 3.1-1  
Combined Creep-Damage Factor

The combined creep-fatigue damage factor ( $F_{CFD}$ ) in terms of distances a and b, which are derived from calculated creep and fatigue damage factors and the geometry of the bi-linear limits of acceptability, is given according to the relation:

$$F_{CFD} = a/b = \text{Minimum of } \left\{ \begin{array}{l} \bullet \frac{7}{3} D^C + D^f \\ \bullet D^C + \frac{1}{3} D^f \end{array} \right\}$$

In the creep damage evaluations of the  $\sigma$  regions, the creep damage factor ( $D^C$ ) was based on the stress relaxation during time-dependent loading according to the relation:

$$D_c = \int_0^{t_c} \frac{dt}{t_r}$$

where,  $t_c$  = Duration of Loading

$t_r$  = Rupture time as function of stress ( $\sigma$ ) and temperature (T)

$\sigma$  = Maximum equivalent or positive principal stress whichever provided a minimum rupture time ( $t_r$ )

In the fatigue damage evaluations of the F/A regions, the fatigue damage ( $D^f$ ) for n cycles was based on the fatigue life ( $N_f$ ) for the time-independent strain range within a single cycle according to the relation:

$$D^f = \sum_{i=1}^N \frac{n}{N_f}$$

where,

$N_f$  = Fatigue life based on maximum Von Mises Equivalent or Principal Strain Range, whichever produced a minimum number of cycles to failure.

#### 3.1.4.2 Excessive Deformations

The RDT Draft Criteria for Breeder Reactor Core Components [5] recommends that deformation limits for functional requirements be identified in the Owner Equipment Specifications and include elastic, plastic, thermal creep, and irradiation creep and swelling.

The CRBRP F/A deformation limits identified in the Equipment Specification [1] were formulated in terms of peak plus accumulated, and residual deformations which would not exceed functional requirements. The fundamental difference with those recommended by RDT draft guidelines was that the F/A functional limits formulated apply only to elastic, plastic, and thermal creep deformations during the total number of loading cycles. The F/A functional limits do not apply to irradiation creep and swelling deformations because the latter were already included in the deformation limits specified for the F/A regions on a case by case basis.

In formulating the CRBR F/A deformation limits applicable to elastic, plastic, and thermal creep deformations, a change in dimensions caused by a uniform thermal expansion were not considered to impair functional requirements. Accordingly, the dimensions and tolerances of F/A hardware as specified on the design drawings at room temperature provide a convenient reference from which to assess dimensional changes caused by loadings at elevated temperature. In this arrangement, only dimensional changes caused by non-uniform thermal expansion at elevated temperature were considered to impair F/A functional requirements.

The specification of residual deformation limits for the F/A regions on a case-by-case basis was relatively direct. Dimensional changes were not permitted to exceed the tolerances on the design drawings. For the F/A shield block, CMP and ACLP hex ducts, TLP outlet nozzle, attachment assembly, and orifice plates, the residual deformation limits (RDL) were taken from the dimensional tolerances given in the F/A Design Layout Drawing presented in Figure 2.0-2.



With regard to the peak plus accumulated deformations, the basis for specifying the limits required an assessment of whether the F/A regions were load or deformation controlled. Only the ACLP hex duct region was considered load controlled because of OBE and SSE Seismic, and Core Restraint loads. Other F/A regions including the shield block, TLP outlet nozzle, CMP hex duct, attachment assembly and orifice plate were considered primarily deformation controlled. The peak plus accumulated deformation limits (PADL) for the deformation controlled F/A regions were specified to not exceed the dimensional tolerances on the design drawing, or conservatively not exceed the respective residual deformation limit (RDL). For the ACLP hex duct region which is primarily load controlled, the PADL was determined from interaction analysis of the F/A rod bundle and hex duct under irradiation creep and swelling and directed to establishing the maximum ACLP hex duct deflection which could be accommodated without loading the fuel rods. The ACLP hex duct PADL was found to nearly approximate the clearance between the wire wrap and inside duct surface plus one wire diameter with a value of 0.082 in.

### 3.2 Application

In the application of the F/A inelastic criteria to the structural evaluation of the F/A regions, the number and characteristics of a worst case mechanical and thermal loading duty cycle was established so as to umbrella all Upset, Emergency, and Faulted Events identified in the F/A Equipment Specification [1]. The Normal events which produce little, if any, structural damage were neglected. The characteristics of the worst case duty cycle were established to include worst combinations of time independent and dependent mechanical and thermal loads, while the number of worst case duty cycles were taken as the number of worst case Upset, Emergency, and Faulted Events. The advantage of the worst case duty cycle approach in the structural evaluation of the F/A regions was that the inelastic analysis was performed on a single cycle of loading, instead of performing separate analyses for the number and characteristics of individual Upset, Emergency, and Faulted events. A description of a typical F/A region worst case duty cycle, and the number and distribution over the first and second reactor cycles is as follows.

A typical worst case duty cycle for a F/A region was assumed to be initiated by time independent short term mechanical and thermal loads followed by time dependent long term mechanical and thermal loads. The time independent loads were characterized by initial steady state temperature distributions followed by the brief thermal transient and the return to final steady state temperature distributions. Mechanical core restraint and OBE and SSE seismic loads of significance were also included as time independent loads. The time dependent loads were the steady state temperature distributions and mechanical core restraint loads which were maintained for a representative hold-time. Thereafter, the worst case duty cycle was assumed to repeat successively throughout the first and second cycles.

With regard to the number of the worst case duty cycles over the first and second reactor cycles, a total of 40 were found to typify the F/A regions evaluated. Of the total, 20 were considered to occur during the first reactor cycle of 128 FPD and 20 during second reactor cycle of 200 FPD. Accordingly, the representative hold-time in a single worst case duty cycle was conservatively based on 20 occurrences over the second reactor cycle of 200 FPD, for a 10 day hold-time. In this arrangement, a total of 40 worst case duty cycles with a 10 day hold-time per duty cycle corresponds to 400 FPD which is slightly greater and more conservative than the 328 FPD specified for the first and second reactor cycles.

### 3.2.1 Crack Initiation

#### 3.2.1.1 Local Ductile Rupture

The structural evaluations of the CRBRP F/A regions in relation to the local ductile rupture criterion were made using minimum values of true uniaxial uniform elongation ( $\epsilon_{ij, \min}$ ) and fracture strain ( $\epsilon_{f, \min}$ ) at local metal temperature and EOL fluence. The maximum principal strain ( $\epsilon_{\max \text{ principal}}$ ) was computed from EOL peak plus accumulated time-independent and dependent strain components after a total of N worst case duty cycles. The peak plus accumulated EOL strain components ( $\epsilon_{ij}^{P+A}$ ) were taken from BOL peak ( $\epsilon_{ij}^P$ ) and accumulated ( $\epsilon_{ij}^A$ ) during the first worst case duty cycle as follows.

$$\epsilon_{ij}^{P+A} = (\epsilon_{ij}^P) + \sum_{K=1}^{N-1} (\epsilon_{ij}^A)_K$$

For the first BOL duty cycle, the EOL strain components are given by the relation.

$$(\epsilon_{ij}^{P+A})_{EOL} = (\epsilon_{ij}^P)_{BOL} + (N-1) (\epsilon_{ij}^A)_{BOL}$$

As the method of computing maximum principal strains ( $\epsilon_{\max \text{ principal}}$ ) neglects shake down effects for time-independent loadings and relaxation of stresses during time-dependent loading for the (N-1) worst case loading cycles following the first cycle, the CRBRP F/A structural evaluations of local ductile rupture are conservative.

### 3.2.1.2 Creep-Fatigue Damage

In the creep damage evaluations of the F/A regions, the creep damage factor ( $D^C$ ) for a total of N worst case duty cycles was based on the relation.

$$D^C = \sum_{K=1}^N D_K^C$$

For the first BOL Duty Cycle, the EOL Creep Damage:

$$D^C = N \int_0^{t_c} \frac{dt}{t_r}$$

where,  $t_c$  = Duration of one worst case duty cycle.

$t_r$  = Rupture time

For the creep damage evaluation of a single worst case duty cycle, the minimum rupture time ( $t_r$ ) was taken from experimental data [8, 12] on pressurized tubes in a biaxial stress state ( $\sigma$ ) at temperature (T) and EOL fluence ( $\phi t$ ). Minimum rupture time ( $t_r$ ) was based on 2 standard deviations below the average experimental data. The time dependent stress ( $\sigma$ ) was taken as the maximum equivalent or positive principal stress, whichever produced the greatest creep damage in a single worst case duty cycle.

In the fatigue damage evaluations of the F/A regions, the fatigue damage ( $D^f$ ) for a total of N worst case duty cycles was based on the relation.

$$D^f = \sum_{k=1}^N D_k^f$$

For the first BOL duty cycle, the EOL fatigue damage:

$$D^f = \frac{N}{N_f}$$

Where,  $N_f$  = Fatigue Life

The fatigue life ( $N_f$ ) data for irradiated F/A materials are not currently available. The fatigue life ( $N_f$ ) for the maximum strain range ( $\Delta r$ ) within the worst case duty cycle of irradiated F/A materials was developed from the Manson Universal Slopes Method [7] commonly used for unirradiated materials. The effects of irradiation were included by applying corrections to the elastic and plastic strain ranges at EOL fluence ( $\phi t$ ) and peak metal temperature (T). For conservatism, the fatigue life ( $N_f$ ) developed for irradiated materials was reduced in accordance with the 2 on strain range and 20 on cycles (2-20 rule) recommended in the RDT Draft Core Components [5]. Simply stated, the 2-20 rule requires that the fatigue life ( $N_f$ ) relation be reduced by a factor of 2 on strain ( $\Delta \epsilon$ ) or 20 on fatigue life ( $N_f$ ), whichever provides a minimum fatigue life.

In the calculation of the maximum strain range ( $\Delta \epsilon$ ), the strain components ( $\epsilon_{ij}$ ) during the time-independent portions of the worst case duty cycle were screened to obtain extreme values ( $\epsilon'_{ij}$ ). The range between the strain components ( $\Delta \epsilon_{ij}$ ) at any point in the duty cycle and the extreme values were computed according to the relation:

$$\Delta \epsilon_{ij} = \epsilon_{ij} - \epsilon'_{ij}$$

The equivalent and maximum principal strain range were computed from the strain component ranges ( $\Delta \epsilon_{ij}$ ) at each point in the worst case duty cycle. The time-independent strain range ( $\Delta \epsilon$ ) was taken as the Von Mises equivalent or maximum principal strain range, whichever provided the smallest fatigue life ( $N_f$ ) over a single worst case duty cycle.

### 3.2.2 Excessive Deformation

The evaluation of the F/A regions for compliance with the PADL and RDL, in relation to the worst case duty cycle, was made in a manner similar to that used for the peak plus accumulated strains in the local ductile rupture evaluation. The EOL peak plus accumulated time-independent and dependent deformations ( $\delta^{P+A}$ ) after a total of N worst case duty cycles was based on the peak deformation ( $\delta^P$ ) and accumulated ( $\Delta\delta^{SS}$ ) deformation between initial and final steady state conditions at BOL.

$$\delta^{P+A} = \delta^P + \sum_{K=1}^{N-1} \delta_K^A$$

For the first BOL Duty Cycle, the EOL Peak plus accumulated deformation:

$$(\delta^{P+A})_{EOL} = (\delta^P)_{BOL} + (N-1) (\Delta\delta^{SS})_{BOL}$$

Similarly, the EOL residual deformation ( $\delta^R$ ) after N worst case duty cycles based in the difference in residual deformation ( $\delta^R$ ) between initial and final dimensions at BOL was taken as:

$$\delta^R = \sum_{K=1}^N \delta_K^R$$

For the first BOL duty cycle, the EOL regional deformation:

$$(\delta^R)_{EOL} = N(\delta^R)_{BOL}$$

For satisfactory compliance of the F/A region in relation to excessive deformation,

$$(\delta^{P+A})_{EOL} \leq \text{PADL}$$

$$(\delta^R)_{EOL} \leq \text{RDL}$$

#### 4.0 SHIELD BLOCK ANALYSIS AND EVALUATION

In the F/A shield block analysis and evaluation, a loading analysis was made that considered mechanical seismic and core restraint, and thermal steady state and transient loads in establishing the number and characteristics of a worst case duty cycle that umbrellas all expected duty cycles for the shield block region in the first and second reactor cycles. Next, an inelastic structural analysis of the shield block region was made for a single worst case BOL duty cycle to calculate the strains and dimensional changes from which EOL values were approximated. Finally, a structural evaluation of EOL strains and dimensional changes in relation to criteria which protect against crack initiation and excessive deformation was made. A summary of the loading, structural analysis and structural evaluation is presented as follows.

##### 4.1 Loading Analysis

The F/A shield block loading analysis was directed to establishing the number and characteristics of a worst case duty cycle that umbrellas both the number and characteristics of Upset, Emergency, and Faulted Events specified over the first and second reactor cycles. The number and characteristics of these events are specified in the Equipment Specification [1].

It is important to note that the worst case F/A shield block duty cycle is, in itself, hypothetical, but permits a conservative structural evaluation to be performed on a single duty cycle instead of on each of the individual events specified. In the following, the F/A shield block mechanical and thermal loads are assessed individually and in relation to each other prior to establishing the worst case duty cycle which was used in structural evaluation.

##### 4.1.1 Mechanical

The F/A shield block mechanical loads of any significance in relation to subsequent structural evaluations are deadweight and internal pressure as

OBE and SSE seismic and core restraint loads are relatively insignificant. However, in relation to thermal steady state and transient loads, even the deadweight and internal pressure loads are insignificant. Accordingly, the mechanical loads were neglected in establishing the worst case F/A shield block duty cycle for the first and second reactor cycles.

#### 4.1.2 Thermal

The F/A shield block thermal loads include the steady state and transient temperature distributions that occur during the Upset, Emergency, and Faulted Events over the first and second reactor cycles. In the definition of F/A shield block transients, the sodium temperatures at the reactor vessel inlet were conservatively assumed to be applied directly to the F/A inlets without the mitigating effects of mixing that would normally occur in the inlet plenum. As such, the transients are inherently worst case at all F/A locations in the core. Further, the description of F/A transient duty cycles was based on a worst case umbrella approach for the Upset, Emergency, and Faulted Transients. Over the first and second reactor cycles comprising 328 FPD, a total of 39 Upset transients umbrellaed by the worst of U-2b, U-11a, U-18, or U-21b were specified. Similarly, the worst of the E-4a, E-7, or E-15 was specified to umbrella the Emergency Events, while the worst F-1 or F-2 was identified to umbrella the Faulted Events.

In order to reduce the number of the specified F/A event duty cycles to a single worst case duty cycle, the Upset, Emergency, and Faulted transients were assessed by comparing the sodium temperature in terms of maximum value, rate of temperature change, and range. With regard to initial sodium temperatures, all transients were considered to be initiated at 750°F. The worst case Upset Transient was found to be the U-18 with a maximum down ramp of 2°F/second over a 420°F range. For the Emergency Transients, the E-4a was found to be the worst case with a down ramp of 2°F/second over 180°F range followed by an up ramp of 2.2°F/second over a range of 420°F. The maximum sodium temperatures reached in the U-18 and E-4a transient were 750 and 995°F respectively.



With regard to Faulted Transients, the F-1 was found to be practically indistinguishable from the Upset U-1b transient which itself was umbrellaed by the U-18. The Faulted F-2 transient was found to have a maximum sodium temperature of 1230°F which is the highest for all F/A shield block transients, but is slow acting at a maximum rate of temperature change of 0.02°F/second. As temperature differences developed in the F/A shield block would be negligible for very slow acting transients, the F-2 transient was considered less severe than the U-18 and E-4a. Further, the E-4a was considered more severe than the U-18 because the reversal in rate of temperature change through the transient would develop greater temperature differences and attendant structural damage. In this arrangement, the Emergency E-4a transient was selected as the worst case umbrella to all of the Upset, Emergency, and Faulted transients for the F/A shield block. The E-4a transient is illustrated in Figure 4.1-1.

The selection of the Emergency E-4a transient as the worst case F/A shield block transient is, in itself, not sufficient to establish the worst case F/A duty cycle. The thermal conditions following the E-4a transient and subsequent hold-times at steady state conditions are also required. The thermal conditions selected following the E-4a transient were a 2 hour soak at 600°F, a 20°F/hour heat-up rate for 2 hours, and a 5.5°F/minute heat-up rate to the steady state sodium temperature of 750°F. Thereafter, a 10 day hold-time at steady state temperatures was selected. The 10 day hold-time corresponds to 40 worst case E-4a distributed over 400 FPD which is slightly greater than the 328 FPD designated for first and second reactor cycles. The worst case F/A shield block duty cycle is illustrated in Figure 4.1-2.

The worst case F/A shield block duty cycle in terms of the E-4a transient followed by thermal conditions which return the F/A shield block region to steady state conditions followed by a 10 day hold-time prior to the initiation of the successive E-4a transient may be sufficient to establish the worst case F/A duty cycle, but is not sufficiently specific to define the corresponding temperature distributions necessary for detailed structural analysis.

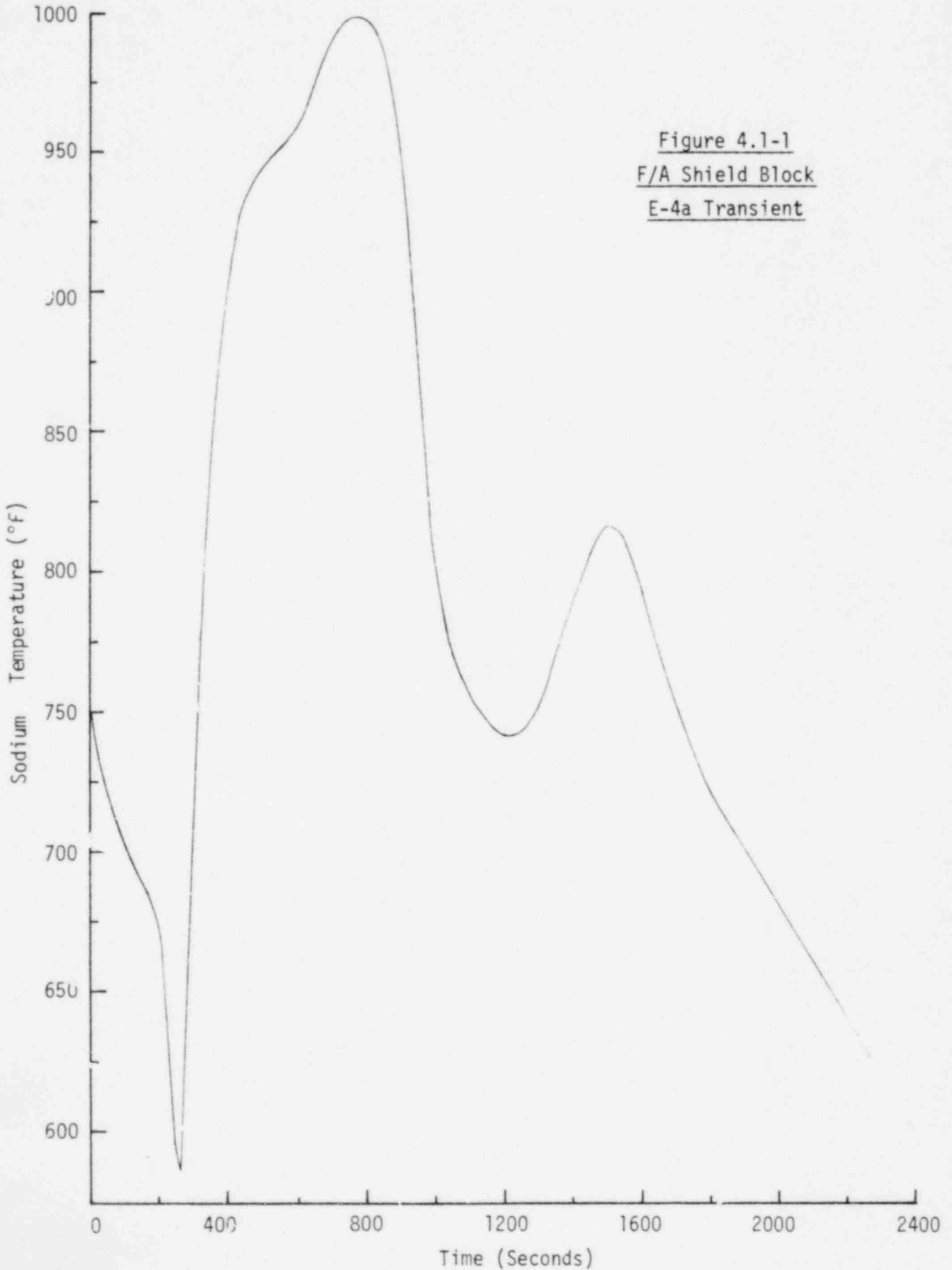
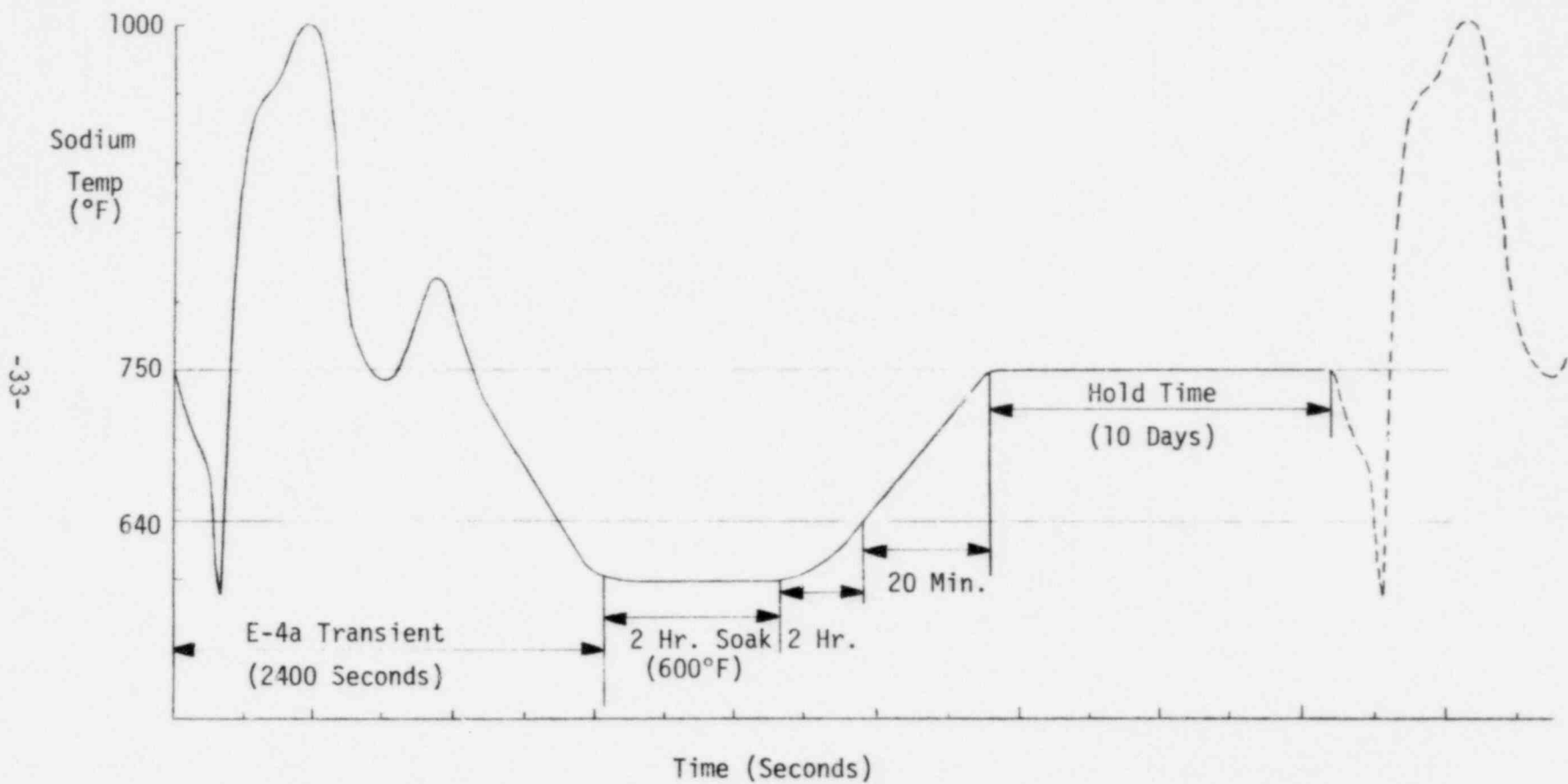


Figure 4.1-1  
F/A Shield Block  
E-4a Transient

Figure 4.1-2  
F/A Shield Block  
Worst Case Duty Cycle



In the following, the F/A shield block thermal model and geometry, boundary conditions and wetted surfaces, heat generation rates, and thermal analysis and results are described from which conclusions on the detailed temperature distributions in relation to subsequent structural analysis are presented.

#### 4.1.2.1 Model and Geometry

The F/A shield block thermal model was formulated in the ANSYS finite element program. The ANSYS program has compatibility between thermal and structural elements which permits thermal solutions of temperature distributions to be used directly in subsequent structural analysis.

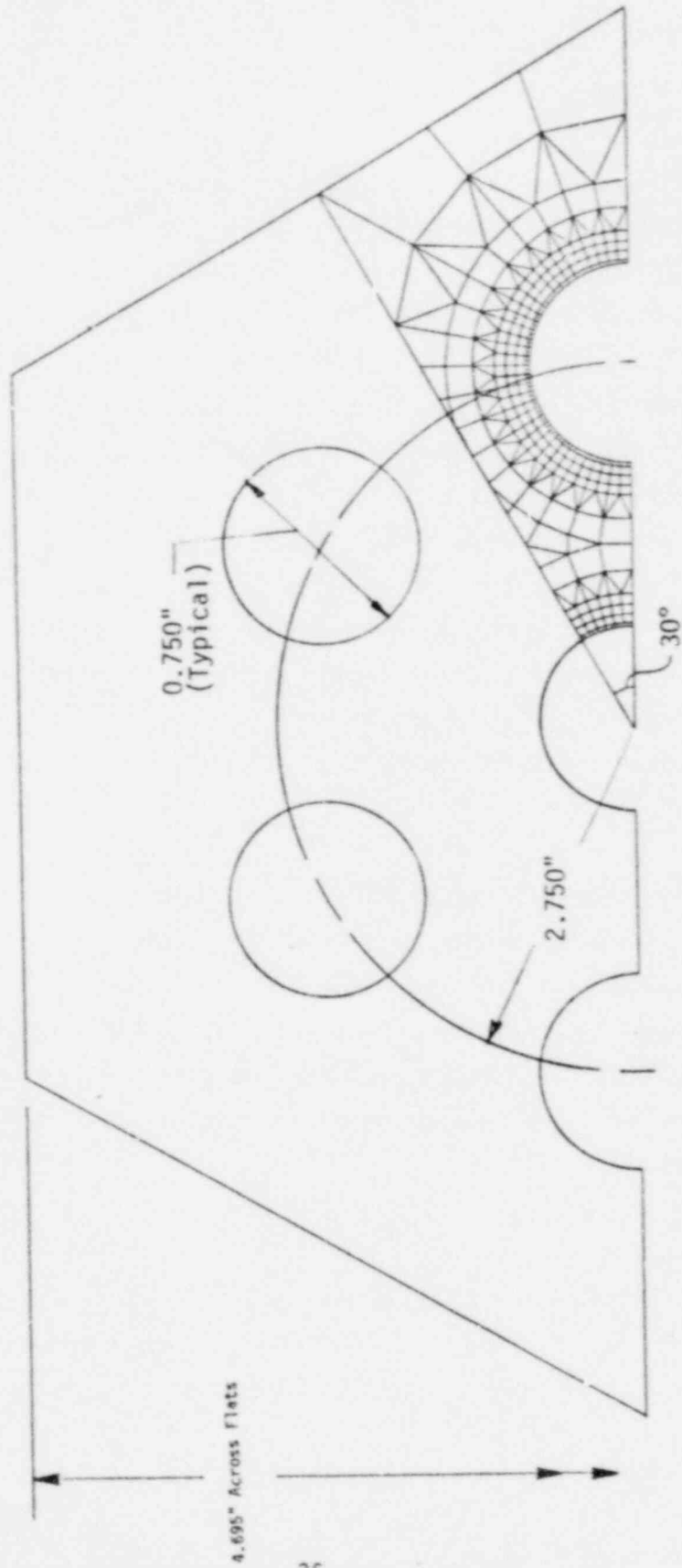
The F/A shield block region selected for analysis corresponds to a 2 dimensional slice of a symmetrical  $30^\circ$  sector taken through the 7 hole pattern provided for inlet sodium flow. The  $30^\circ$  symmetrical sector is justified as coolant flow in all 7 passages is uniform and heat generation rates are nearly uniform. The corresponding shield block geometry provides the greatest constraint for thermal expansions and represents the worst case location for structural damage for the F/A inlet hardware. The F/A shield block thermal model illustrating the dimensional extent and finite element detail of the 2 dimensional  $30^\circ$  sector geometry is presented in Figure 4.1-3.

The F/A shield block thermal model as formulated with the ANSYS program included 276 linear temperature (STIF 35) elements arranged in a mesh of 277 node points. A fine mesh was selected at the wetted surfaces directly exposed to the rapid sodium transients so the thermal skin effect would be included in subsequent structural analysis. A coarse mesh was selected at exterior surfaces exposed to stagnant sodium where skin effects are negligible.

Figure 4.1-3

F/A Shield Block Thermal Model

Dimensional Extent And Finite Element Detail



#### 4.1.2.2 Properties

The F/A shield block is constructed from SA-316-SS. The material properties necessary to derive both steady state and transient temperatures are the thermal conductivity (K), specific heat (C), and density ( $\rho$ ). The SA-316-SS properties expressed in terms of polynomials in temperature ( $T \sim ^\circ\text{F}$ ) were taken from the NSM Handbook [6] and are summarized as follows.

##### Thermal Conductivity ( $K \sim \text{BTU/in-sec-}^\circ\text{F}$ )

$$K = (0.187 \text{ E-3}) + (0.107\text{E-7}) * T$$

##### Specific Heat ( $C \sim \text{BTU/LB-}^\circ\text{F}$ )

$$C = (0.102) + (0.104 \text{ E-3}) * T - (.152\text{E-6}) * T^2 \\ + (0.1007\text{E-9}) * T^3 - (0.256\text{E-13}) * T^4$$

##### Density ( $\rho \sim \text{LB/in}^3$ )

$$\rho = 0.2885 - (0.839\text{E-5}) * T$$

#### 4.1.2.3 Boundary Conditions and Wetted Surfaces

The F/A shield block boundary conditions and wetted surfaces selected for analysis are illustrated in Figure 4.1-4.

The boundary conditions for the F/A shield block thermal analysis consisted of adiabatic conditions along the lateral surfaces of the  $30^\circ$  sector and along the exterior surface adjacent to the stagnant sodium. Along the lateral surfaces of the  $30^\circ$  sector, the boundary conditions simulate the symmetry in the uniform temperature and flow through the 7 inlet sodium passages. For the exterior surface adjacent to the stagnant sodium, an adiabatic surface simulates the symmetry of temperature between adjacent shield blocks.

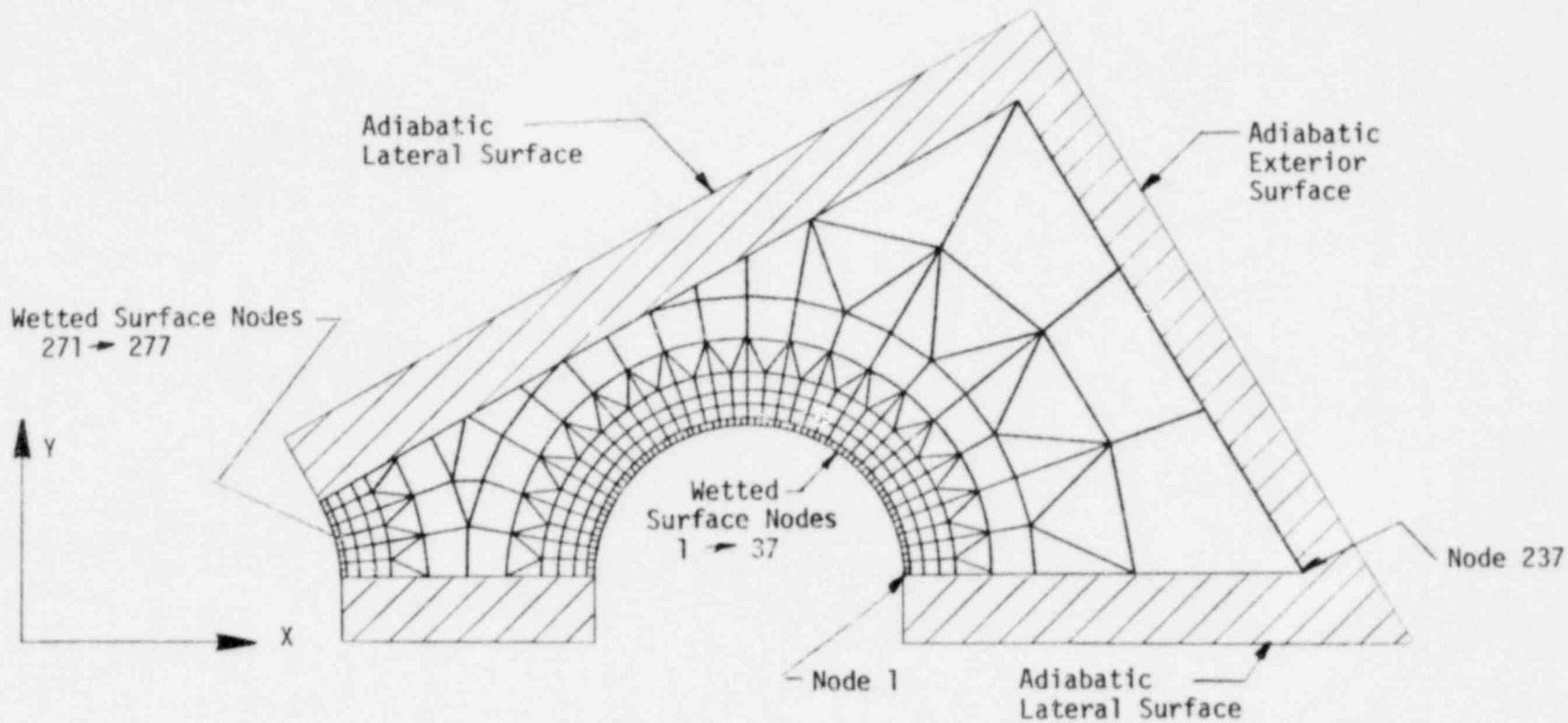


Figure 4.1-4  
F/A Shield Block  
Boundary Conditions and Wetted Surfaces



The sodium temperatures in the thermal analysis were assumed to be directly coupled to the wetted surface nodes of the portions of the flow passages included in the 30° sector of the F/A shield block. As such, thermal skin effects are conservative because the mitigating effects of a heat transfer film coefficient were neglected. The flow passage surface nodes coupled directly to the sodium temperatures were Nodes 1 through 37, increments of 1; and 271 through 277, increments of 1.

#### 4.1.2.4 Heat Generation Rates

During steady state operation, the F/A shield block is exposed to nuclear heating which was considered to collapse immediately following the initiation of the Upset, Emergency, and Faulted Transients. The nuclear heating rate per unit volume is maximum at the upper portion of the F/A shield block and decreases toward the inlet nozzle. In order to obtain a conservative estimate of temperature distributions for subsequent structural analysis, the maximum nuclear heating rate per unit volume (0.0295 BTU/in<sup>3</sup>-sec) was assumed throughout the 30° sector of the F/A shield block material. The heat generation was taken to collapse from maximum to zero in 230 milliseconds at 1.2 seconds into the E-a

#### 4.1.2.5 Analysis and Results

The ANSYS thermal analysis of the F/A shield block was arranged to provide detailed temperature distributions over the total worst case duty cycle. A total of 21 load steps were selected at prominent sodium temperature and heat generation conditions. Sodium temperatures were imposed at the wetted surface nodes and heat generation rates applied to each finite element. The first 17 load steps were taken for steady state conditions and the E-4a transient to 2400 seconds. Load Steps 1 and 2 represent steady state thermal conditions under 750°F sodium temperatures and maximum heat generation rate. Load Steps 3 and 4 provide the continuation and collapse of the heat generation rate. Load Steps 5 through 17 correspond to prominent E-4a sodium temperatures to 600°F. The 600°F soak corresponds to Load Step 18. The 20°F/hour and 5.5°F/minute heat-up rates were represented by Load Steps 19 and 20. The steady state

sodium temperatures and heat generation rate for the 10 day hold-time corresponded to Load Step 21. Prominent Load Steps in the E-4a transient are illustrated in Figure 4.1-5 and numerical values for the total worst case F/A shield block duty cycle are summarized in Table 4.1-1.

Table 4.1-1  
Worst Case F/A Shield Block Duty Cycle  
ANSYS Input Data

Load Step	Time (SEC)	Temp (°F)	Heat Gener. (BTU/SEC-IN <sup>3</sup> )
1	0.0	750	0.0295
2	0.0	750	0.0295
3	1.2	750	0.0295
4	1.43	750	0.0
5	20.	750	0.0
6	80.	710	0.0
7	200.	675	0.0
8	260.	586	0.0
9	400.	915	0.0
10	760.	1000	0.0
11	880.	975	0.0
12	1000	800	0.0
13	1140	745	0.0
14	1260	745	0.0
15	1520	820	0.0
16	1750	735	0.0
17	2400	600	0.0
18	9600	600	0.0
19	16800	640	0.00787
20	18000	750	0.00295
21	882000	750	0.00295

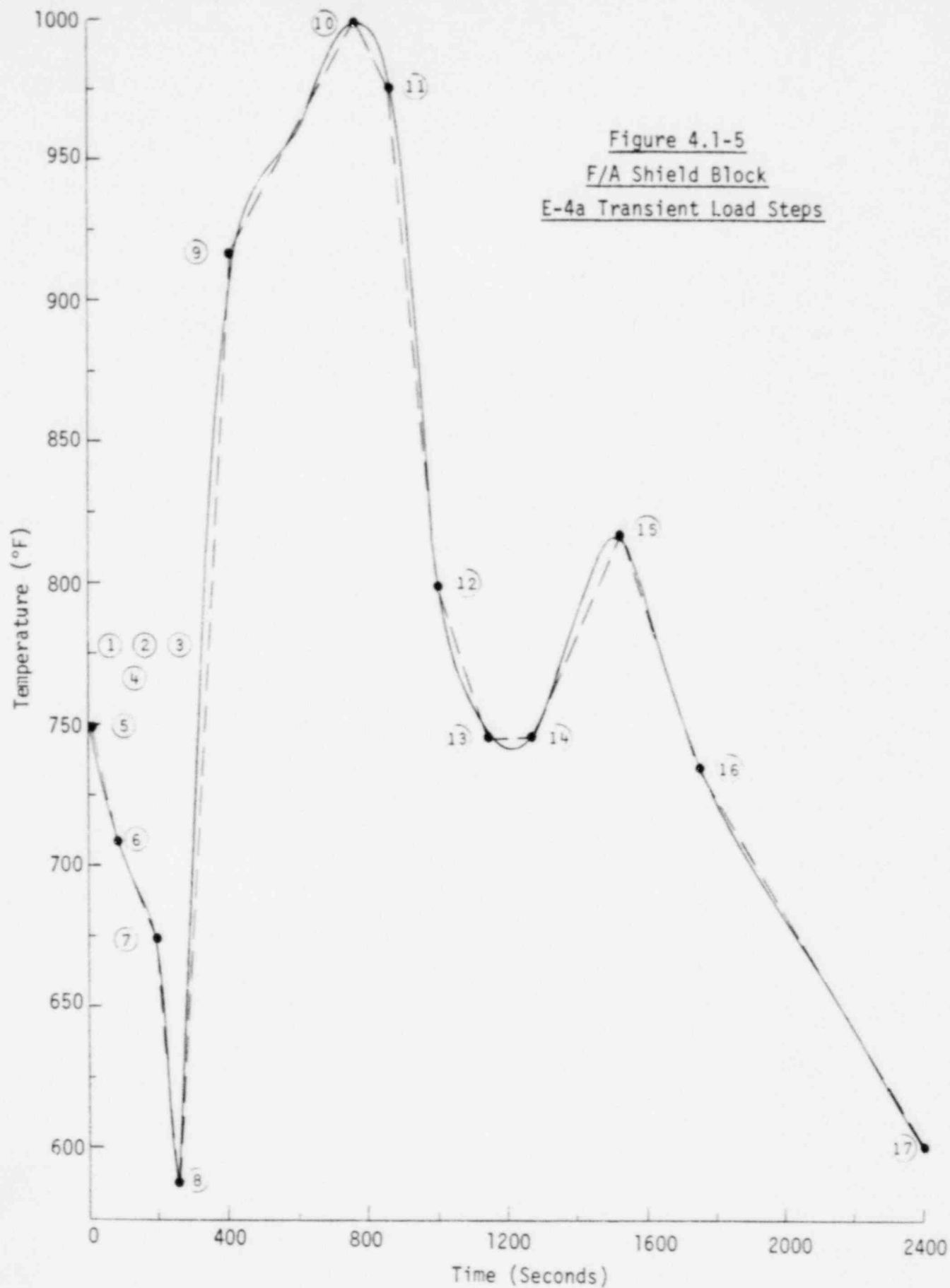


Figure 4.1-5  
 F/A Shield Block  
 E-4a Transient Load Steps

The ANSYS solution of the worst case F/A shield block duty cycle was obtained in 124 cumulative iterations using a steady state and transient convergence criteria of 1 and 5°F respectively. The temperature distributions at each cumulative iteration were saved on ANSYS Tape 4 for recall in subsequent structural analysis. In order to determine the cumulative iterations of interest in structural analysis, maximum and minimum through the wall temperature differences are most important in relation to structural damage. The F/A shield block temperature differences were based on the through-the-wall temperatures at Nodes 1 and 237 depicted in Figure 4.1-4. A plot of the temperature difference between Nodes 237 and 1, that is,  $\Delta T = T_{237} - T_1$ , in terms of cumulative iteration in the solution run is illustrated in Figure 4.1-6.

A review of the through the wall temperature difference shows that the maximum and minimum values occur at cumulative iterations 36 and 63 respectively, with a temperature difference range of 290°F. In the thermal solution run, cumulative iterations 36 and 63 correspond to the E-4a transient at 260 and 760 seconds as illustrated in Figure 4.1-1. The steady state temperature distributions at the start of the E-4a transient, and beginning and end of the 10 day hold-time correspond to cumulative iterations 4, 80, and 124. Cumulative iteration 23 represents the first positive maximum after the initial steady state conditions. Plots of the temperature distributions at cumulative iterations 2, 36, and 63 are illustrated in Figures 4.1-7 through -8 respectively.

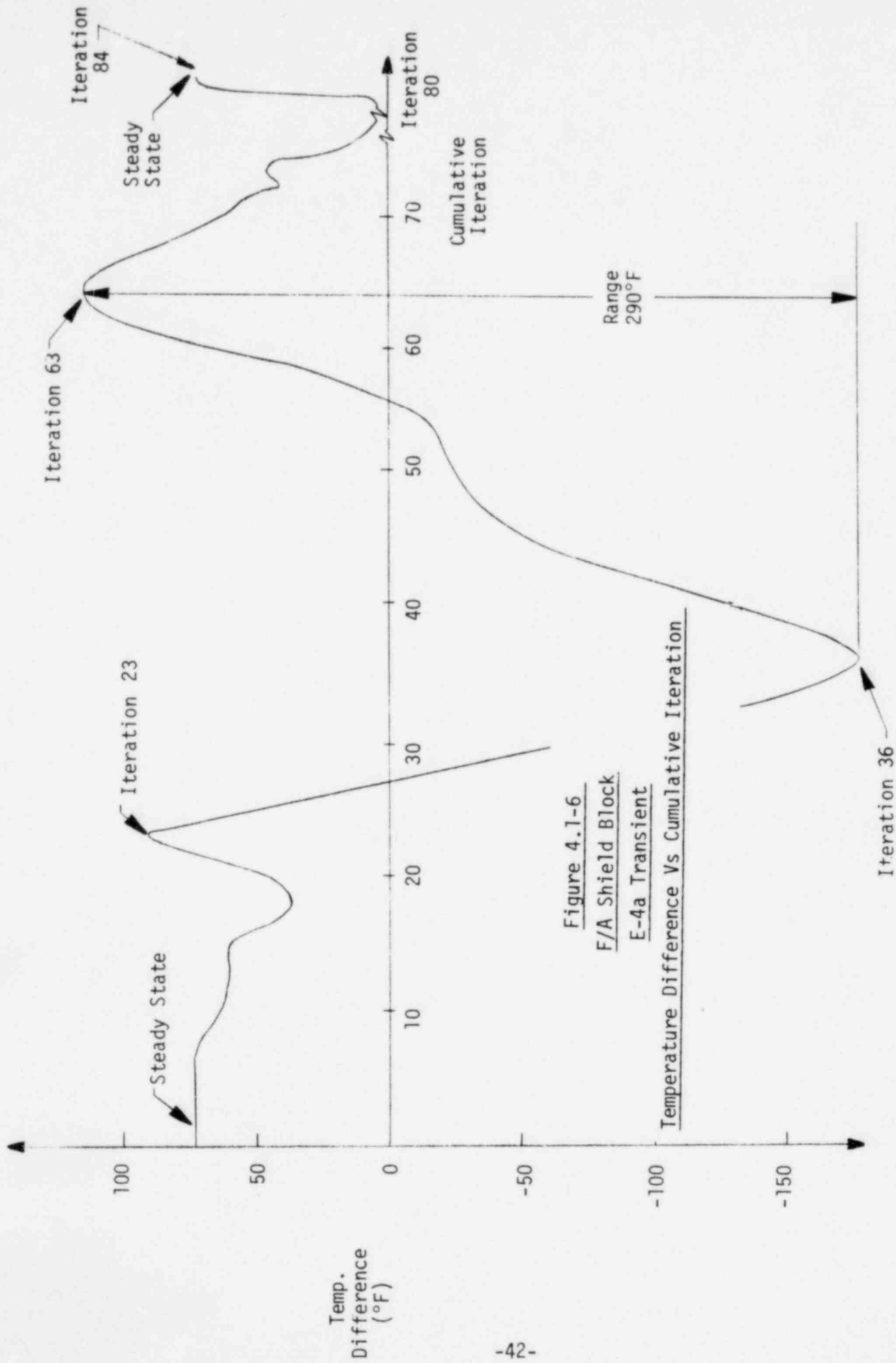


Figure 4.1-6  
 F/A Shield Block  
 E-4a Transient  
 Temperature Difference Vs Cumulative Iteration

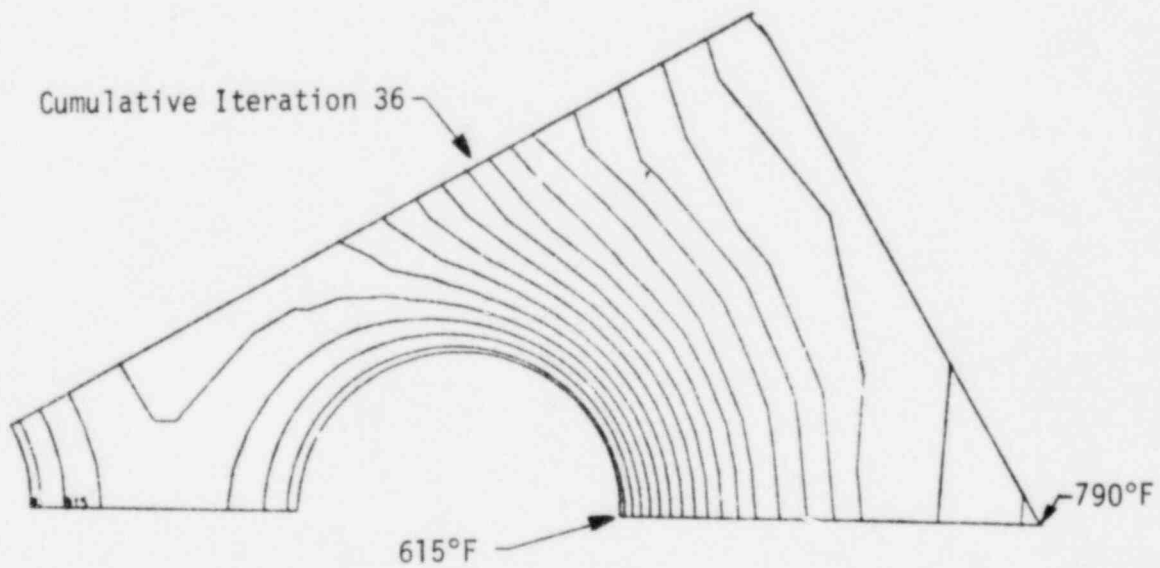
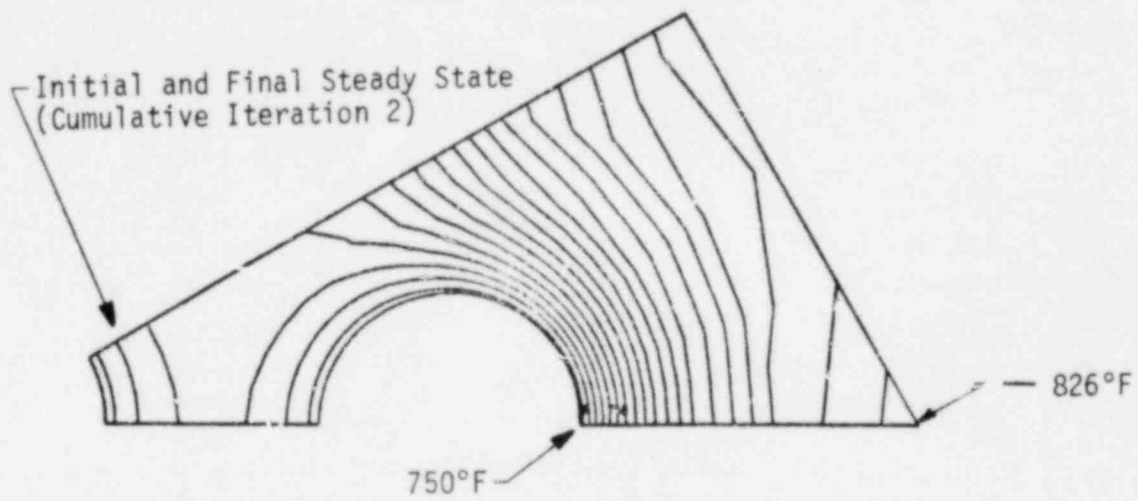


Figure 4.1-7  
F/A Shield Block  
E-4a Transient Cumulative Iterations 2 and 36  
Temperature Distributions

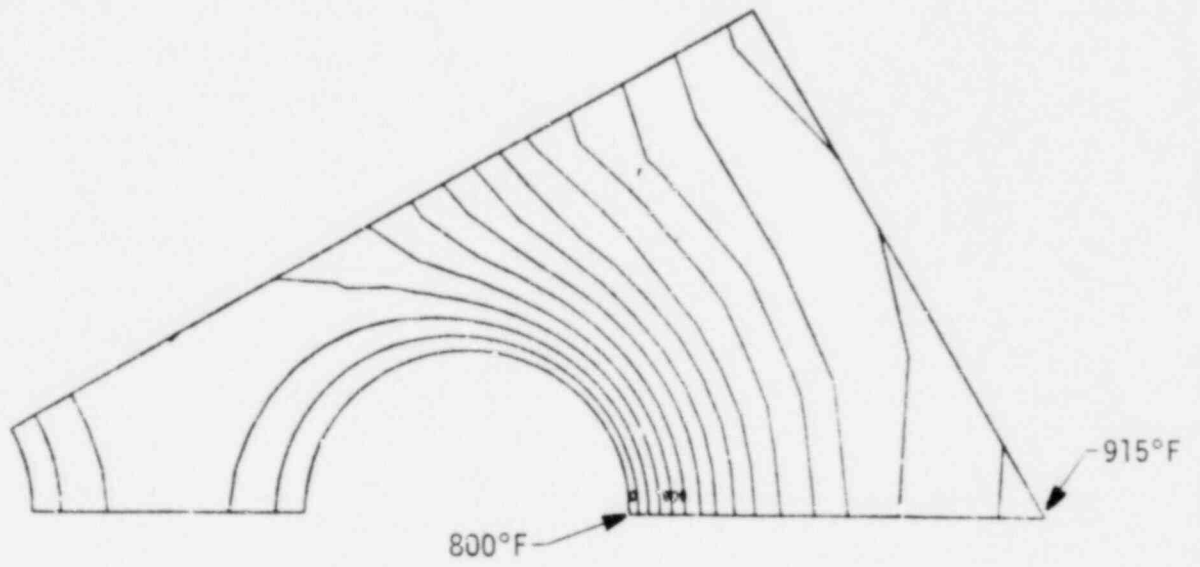


Figure 4.1-8  
F/A Shield Block  
E-4a Transient Cumulative Iteration 63  
Temperature Distribution

#### 4.1.3 Worst Case Duty Cycle

The conclusions based on the F/A shield block loading analysis in relation to establishing the worst case duty cycle with recommendations made for subsequent structural analysis were as follows.

- Mechanical loads comprising OBE and SSE seismic, core restraint, internal pressure, and dead weight were considered negligible in establishing the worst case F/A shield block duty cycle.
- Thermal loads comprising the E-4a transient in combination with thermal conditions in returning to steady state and the hold-time prior to the initiation of the next E-4a transient were considered most important in establishing the worst case F/A shield block duty cycle.

The recommendations for the specific F/A shield block loading in relation to the worst case duty cycle were based solely on time independent and dependent thermal loadings. In the specification of temperatures in the ANSYS structural analysis, the uniform temperature is a constant temperature distribution throughout while the reference temperature is the basis for deriving the thermal expansion relative to a uniform temperature or a temperature distribution corresponding to a cumulative iteration in the thermal solution run. The following worst case F/A loading cycle sequence simplified from the maximum temperature difference versus cumulative iteration plot (Figure 4.1-6) was recommended to be repeated 40 times so as to provide an upper bound to the 39 Normal and Upset Events and worst Emergency or Faulted Event.



### Time Independent

- Select a uniform temperature equal to the reference temperature at cumulative iteration 23. Load to the cumulative iteration 23 temperature distribution and unload to uniform temperature.
- Select a uniform temperature equal to the reference temperature at cumulative iteration 36. Load to the cumulative iteration 36 temperature distribution and unload to uniform temperature.
- Select a uniform temperature equal to the reference temperature at cumulative iteration 63. Load to the cumulative iteration 63 temperature distribution and unload to uniform temperature.
- Select a uniform temperature equal to the reference temperature at cumulative iteration 80. Load to the cumulative iteration 80 temperature distribution and unload to uniform temperature.

### Time Dependent

- Select a uniform temperature equal to the reference temperature at cumulative iteration 124. Load to the cumulative iteration 124 temperature distribution and hold for 10 days.

## 4.2 Structural Analysis

The F/A shield block structural Analysis was directed to deriving the stresses, strains, and dimensional changes which occur during the worst case duty cycle from which subsequent structural evaluations were made. In the following, the F/A shield block structural model, geometry, and boundary conditions are described. Next, linear and non-linear material properties including the effects of irradiation on stress-strain curves and the basis for neglecting thermal creep are presented. The selection of a reference temperature for thermal expansions in relation to the axial constraints on the region selected for analysis is described. Finally, the time independent and time dependent inelastic analysis and results for the F/A shield block are presented in preparation for subsequent structural evaluation.

### 4.2.1 Model, Geometry, and Boundary Conditions

The F/A shield block structural model was formulated in the ANSYS finite element program compatible with the prior thermal analysis. As such, the dimensional extent of the 30° sector and finite element mesh in both structural and thermal models were identical. In formulating the F/A shield block structural model, the ANSYS constant strain (STIF 2) element was used to replace the linear temperature element (STIF 35) used in the thermal model. The boundary conditions along the lateral surfaces of the 30° sector, in the manner of the conventional roller support were taken to have zero normally disposed displacement, but free to move radially. Along the surface parallel to the Global X - axis, the UY displacements were set equal to zero at Nodes 1, 37, 38, 74, 75, 111, 112, 148, 149, 185, 186, 204, 205, 223, 224, 234, 242, 249, 256, 263, 270, and 277. For the inclined surface the UY displacements, after a 30° rotation to obtain normally disposed directions, were set equal to zero at Nodes 228 through 232, 237 through 239, and 243, 250, 257, 264 and 271. The F/A shield block structural model is illustrated in Figure 4.2-1.

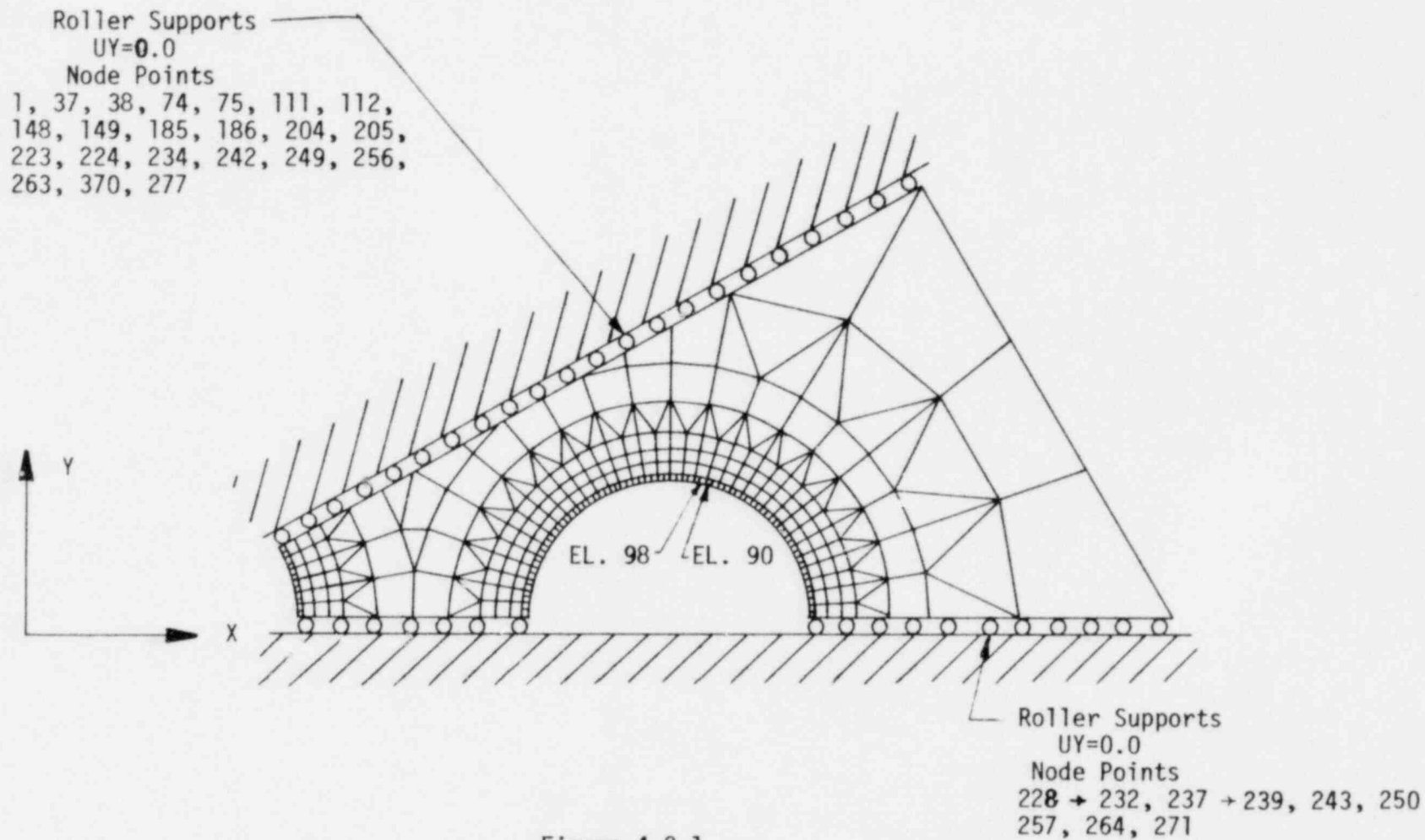


Figure 4.2-1  
F/A Shield Block  
Structural Model, Geometry, And Boundary Conditions

#### 4.2.2 Properties

The F/A shield block as constructed from SA-316-SS and initially unirradiated at BOL is irradiated to a fluence ( $E > 0.1$  Mev) of  $0.31 \times 10^{22}$  n/cm<sup>2</sup> at EOL. Operational temperatures range from 400 to 1000°F. The linear and non-linear properties of SA-316-SS under fluence and temperature selected in the F/A shield block structural analysis are described as follows.

##### 4.2.2.1 Linear

The linear SA-316-SS material properties are the Young's modulus (E), Poisson's ratio ( $\nu$ ), and the coefficient of thermal expansion ( $\alpha$ ). The linear material properties are relatively insensitive to fluence, but are functions of temperature. The corresponding linear properties as polynomial functions of temperature ( $T \sim ^\circ\text{F}$ ) were taken from the NSM Handbook [6] and are summarized as follows.

##### Young's Modulus ( $E \sim \text{PSI}$ )

$$E = (2.834E7) - (2.88E3)*T \\ - (3.69) \times T^2 + (7.71E-4)*T^3$$

##### Poisson's Ratio ( $\nu$ )

$$\nu = 0.262 + (4.26E-5)*T$$

##### Coefficient of Thermal Expansion ( $\alpha \sim 1/^\circ\text{F}$ )

$$\alpha = (10.08E-6) + (0.117E-8) *T$$

In order to reduce the non-linearity of the material properties with temperature in the ANSYS structural analysis, constant properties which provide conservative results were selected instead of the polynomial relations. The use of constant properties permits the use of the initial

stiffness matrix as computation time associated with reformulating the stiffness matrix for varying temperature distribution is eliminated.

In the F/A shield block structural analysis, the values of Young's modulus ( $24.06 \times 10^6$  psi) and Poisson's ratio (0.2966) were taken as the 800°F values for SA-316-SS. The 800°F temperature is the approximate mean of the F/A shield block during the worst case duty cycle. The value for the SA-316-SS coefficient of thermal expansion ( $11.25 \times 10^{-6}/^\circ\text{F}$ ) was taken at 1000°F. The selection of maximum coefficient of thermal expansion provides a worst case estimate of attendant damaging strains over the range of temperatures in the worst case duty cycle.

#### 4.2.2.2 Non-Linear

The non-linear SA-316-SS material property behavior required for the F/A shield block are the constitutive relations for stress and strain and thermal creep. The constitutive relations including the effects of fluence and temperature with attendant simplifications made in the F/A shield block structural analysis are described in the following.

##### 4.2.2.2.1 Stress-Strain Curves

The SA-316-SS stress-strain curves as a function of temperature and fluence are given the NSM Handbook [6] in terms of true average values. A review of the data shows that the effect of fluence is to increase the stress at a given level of strain. As such, irradiated stress-strain curves for SA-316-SS exhibit a time dependent hardening through embrittlement from BOL to EOL. For the F/A shield block, the EOL fluence ( $E > 0.1$  Mev) based on June, 1977 data is  $0.31 \times 10^{22} \text{ n/cm}^2$ . Simplifications made in the F/A structural analysis for the time dependent effects of fluence on stress-strain curves as well as the consideration of minimum instead of average properties are discussed as follows.

For the initially unirradiated F/A shield block at BOL, the SA-316-SS stress-strain curve is a minimum and increases during operational life reaching a maximum at EOL. In order to derive a representative inelastic response with the structural analysis of the F/A shield block for the worst case duty cycle, a mean stress-strain curve based the time average values of minimum BOL and maximum EOL stress-strain curves was selected for the structural analysis. The use of the time averaged mean stress - strain curves is consistent with the time averaged 40 worst case F/A duty cycles distributed uniformly over the 328 FPD between BOL and EOL. With mean stress-strain curves, the BOL fatigue damage is underestimated while the BOL creep damage is overestimated. Conversely, the mean stress-strain approach overestimates EOL fatigue damage while the EOL creep damage is underestimated. Accordingly, the F/A shield block structural analysis based on mean time averaged stress-strain curves was considered to describe the overall inelastic response to the uniform distribution of the 40 worst case duty cycles without any significant loss in accuracy.

With regard to the scatter of SA-316-SS stress-strain data at fluence and temperature, true minimum instead of true average or typical values were selected. Minimum values provide conservative inelastic response as the worst case F/A shield block duty cycle was described by the relatively slow acting thermal transients which are basically static loadings. The true minimum stress-strain curves were constructed by taking 90% of the true average stress values given the NSM Handbook [6].

In order to illustrate the F/A shield block analysis approach, the SA-316-SS stress-strain curve as the mean of true BOL and EOL stress-strain curves corrected for minimum data scatter at 800°F is presented in Figure 4.2-2. The corresponding stress-strain curve data at 800, 900, and 1000°F are presented in Table 4.2-1. The true minimum mean stress-strain curve data for SA-316-SS at 800°F was also used for F/A shield block temperatures less than 800°F. Stress-strain curve data at intermediate temperatures from those identified at 800, 900, and 1000°F were linearly interpolated.

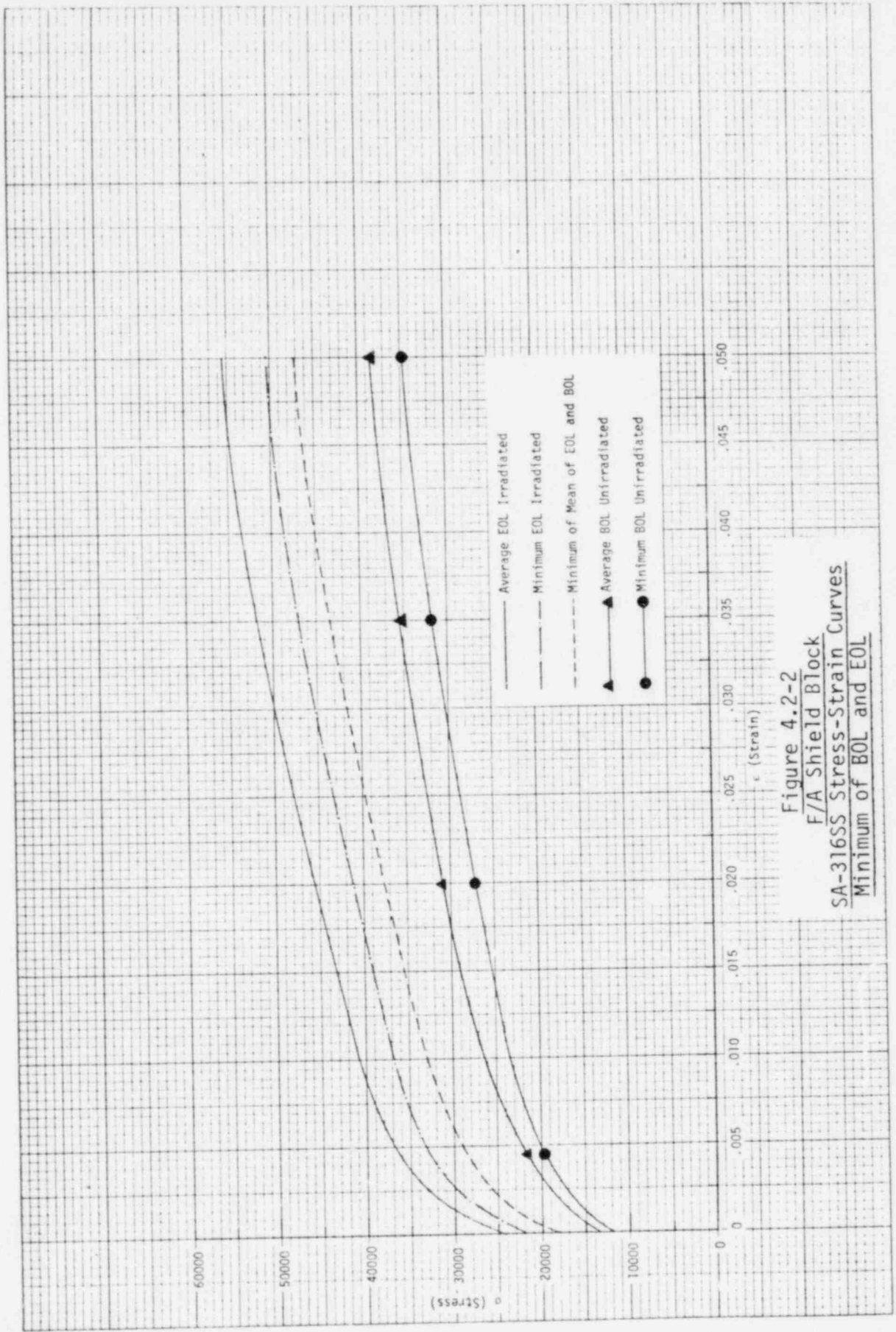


Figure 4.2-2  
 F/A Shield Block  
 SA-316SS Stress-Strain Curves  
 Minimum of BOL and EOL



Table 4.2-1  
F/A Shield Block  
True Minimum Mean of BOL and EOL Stress-Strain Data  
SA-316-SS

Temp (°F)	$10^6 E$ (psi)	Stress (PSI) at Total Strain				
		0.000748	0.003068	0.00728	0.011382	0.0518
800	24.06	17997	26600	31200	33800	47200
900	24.06	17997	25100	29400	32600	46400
1000	24.06	17997	26900	32400	34400	47000

#### 4.2.2.2.2 Thermal Creep Equations

The unirradiated SA-316-SS thermal creep-time constitutive relations as a function of stress and temperature are given in the NSM Handbook [6]. The thermal creep constitutive relations for irradiated SA-316-SS are not identified as the effects of irradiation are included in the irradiation creep equations.

For the F/A shield block, the EOL fluence is  $0.31 \times 10^{22} \text{ n/cm}^2$  with thermal creep occurring at a steady state temperature of approximately 750°F over the 10 day hold time of the worst case duty cycle. As the EOL fluence is relatively low and steady state temperatures are below 800°F, thermal creep over the worst case F/A shield block duty cycle was considered negligible. Accordingly, a study of the thermal creep constitutive relation for SA-316-SS in relation to the F/A shield block analysis with simplification similar to those made for the SA-316-SS stress-strain curves were not performed.

#### 4.2.3 Worst Case Duty Cycle Response

The structural response of the F/A shield block to the worst case duty cycle loading required the selection of reference temperatures compatible with the temperature distributions at the worst case through the wall temperature difference and axial constraints prior to deriving time



independent and dependent solutions. A description of the analysis and solutions which are required in subsequent structural evaluations is as follows.

#### 4.2.3.1 Constraints and Reference Temperature Selection

The F/A shield block structural model corresponds to a 30° sector of a lateral slice taken along the length of the shield block. Axial constraints normal to the 2 dimensional representation of the 30° sector closely simulate a plane strain condition as the length of the shield block is significantly greater than the corresponding cross-section dimensions. Accordingly, the F/A shield block was considered to be in plane strain condition for the purposes of analysis.

In a plane strain analysis under thermal loading, the ANSYS program calculates mechanical stresses induced by thermal strains ( $\epsilon_{TH}$ ) which are dependent on the coefficient of thermal expansion ( $\alpha$ ), temperature distribution ( $T$ ), and reference temperature ( $T_R$ ) according to the relation  $\epsilon_{TH} = \alpha (T - T_R)$ . As the plane strain condition requires that the total net force ( $F_n$ ) along the length vanish, the normal mechanical stresses ( $\sigma_z$ ) induced by the thermal strains ( $\epsilon_{TH}$ ) when integrated over the area ( $A$ ) must also vanish. In this arrangement, the selection of a reference temperature ( $T_R$ ) depends on the temperature distribution ( $T$ ) throughout the plane section.

The selection of a reference temperature ( $T_R$ ) that provides a net force ( $F_n$ ) across the plane section that vanishes is approximated with classical elasticity theory even though the normal ( $\sigma_z$ ) stresses may be beyond the proportional elastic limit of the material. The linear elastic approximation was considered acceptable as a first approximation to assuring a plane strain condition. For the case where the Young's modulus ( $E$ ) and coefficient of thermal expansion ( $\alpha$ ) are constant, the reference temperature ( $T_R$ ) in a plane strain finite element model is related to the normal stress distribution  $\sigma_z(x, y)$  for an arbitrarily selected reference temperature ( $T_0$ ) as follows.

$$T_R = T_0 - \frac{1}{AE\alpha} \sum_{i=1}^n \sigma_z(x, y) A_i$$

Where,

$n$  = No. of Finite Elements

$A_i$  = Area of Individual Finite Elements

$A$  = Total Plane Area

$$A = \sum_{i=1}^n A_i$$

In order to facilitate the computation of reference temperatures for the F/A shield block structural analysis, ANSYS elastic solutions for the normal stress distribution  $\sigma_z(x, y)$  at an arbitrary reference temperature ( $T_0$ ) were obtained for each of the temperature distributions corresponding to the recommended cumulative iterations in the thermal analysis solution run. ANSYS tape 12 data containing the normal stress distribution and finite element geometry were catalogued for recall by a reference temperature post processor. The F/A shield block reference temperatures ( $T_R$ ) at the recommended cumulative iterations for the worst case duty cycle are summarized in Table 4.2-2.

Table 4.2-2  
F/A Shield Block  
Reference Temperatures

Temperature Distribution (cumulative iteration)	Reference Temperature ( $T_R \sim ^\circ F$ )
4	788.8
23	635.4
36	821.4
63	860.7
80	805.3
124	788.8

#### 4.2.3.2 Analysis and Results

The ANSYS inelastic analysis of the F/A shield block structural model under the worst case duty cycle was arranged in time-independent plastic analysis associated with the short term E-4a transient followed by time-dependent creep analysis corresponding to steady state temperatures over the 10-day hold-time. The time independent and dependent analysis provide the structural response from which evaluations of crack initiation in terms of local ductile rupture and creep fatigue damage are made. With regard to dimensional changes which can exceed functional limits, the peak plus accumulated and residual deformation response during and following the worst case F/A duty cycle are required.

In order to obtain the desired results in an efficient manner, the ANSYS restart option was used to provide the loading sequence within, between and after the time independent and time dependent solutions. As elastic/plastic/creep instability would not be expected for the F/A shield block under the deformation-controlled thermal loadings, the ANSYS small strain-small deformation option was used in the inelastic analysis. A description of the time independent and dependent analysis and results is as follows.

##### 4.2.3.2.1 Time Independent

The time independent ANSYS analysis of the F/A shield block was directed to deriving the peak + accumulated strains and deformations associated with following the path dependent thermal loadings from initial steady state conditions through the E-4a transient followed by the return to final steady state conditions, but excluding the 10-day hold-time. The time independent loadings were considered as static loadings applied at zero time. A total of 3 load steps were used to determine the F/A shield block structural response to the initial steady state temperature distribution. For the E-4a transient and the return to final steady state temperature distributions, a total of 24 sequential load steps in combination with the ANSYS restart

option were used to obtain the path dependent structural response. Summaries of the F/A shield block time independent structural analysis procedures for the initial steady state conditions and E-4a transient followed by the return to final steady state conditions in terms of Load Steps, iterations, temperature distributions, reference temperatures, and descriptions are presented in Tables 4.2-3 and -4 respectively.

Table 4.2-3  
F/A Shield Block  
Time Independent Analysis Summary  
Initial Steady State Conditions

Load Steps	Iterations	Temperature Distribution (°F)	Reference Temperature (°F)	Description
1	1	788.8	788.8	Initial Steady State (Time = 0.0 sec.)
2	12	Cum. Iter. 4		
3	3	Cum. Iter. 4		

Table 4.2-4  
F/A Shield Block  
Time Independent Analysis Summary  
E-4a Transient and Return to Final Steady State Conditions

Load Step	Iterations	Temperature Distribution (°F)	Reference Temperature (°F)	Description
1	1	636.4	636.4	First E-4a Loading and Unloading (Time = 0.0)
2	14	Cum. Iter. 23		
3	5	636.4	821.4	Second E-4a Loading and Unloading (Time = 260 sec.)
4	1	821.4		
5	26	Cum. Iter. 36		
6	5	Cum. Iter. 36		
7	1	Cum. Iter. 36		
8	26	821.4		
9	5	821.4		
10	1	860.7	860.7	Third E-4a Loading and Unloading (Time = 760 sec.)
11	4	860.7		
12	18	Cum. Iter. 63		
13	8	Cum. Iter. 63		
14	1	Cum. Iter. 63		
15	19	860.7		
16	1	860.7		
17	1	805.3	805.3	Fourth E-4a Loading and Unloading (Time = 9600 sec.)
18	5	Cum. Iter. 80		
19	3	Cum. Iter. 80		
20	5	805.3		
21	1	805.3	788.8	Final Steady State (Time = 882000 sec.)
22	1	788.8		
23	10	Cum. Iter. 123		
24	1	Cum. Iter. 123		

The F/A shield block structural response to the time independent loadings was obtained with a plastic convergence ratio of 0.01. The detailed stress-strain response at each of the converged solutions were saved on ANSYS Tape 10 for subsequent recall in structural evaluations. The initial and final steady state maximum equivalent stresses were found to be 18,335 and 12,653 psi respectively. During the E-4a transient, the maximum equivalent stresses at the cumulative iterations 36 and 63 were 23,870 and 20,396 psi. The peak non-uniform deformation was found to be 0.00086 in. at cumulative iteration 36. The maximum non-uniform initial steady state deformation was 0.00035 in. Computer plots of equivalent stress and peak non-uniform deformation are presented in Figure 4.2-3 through -5.

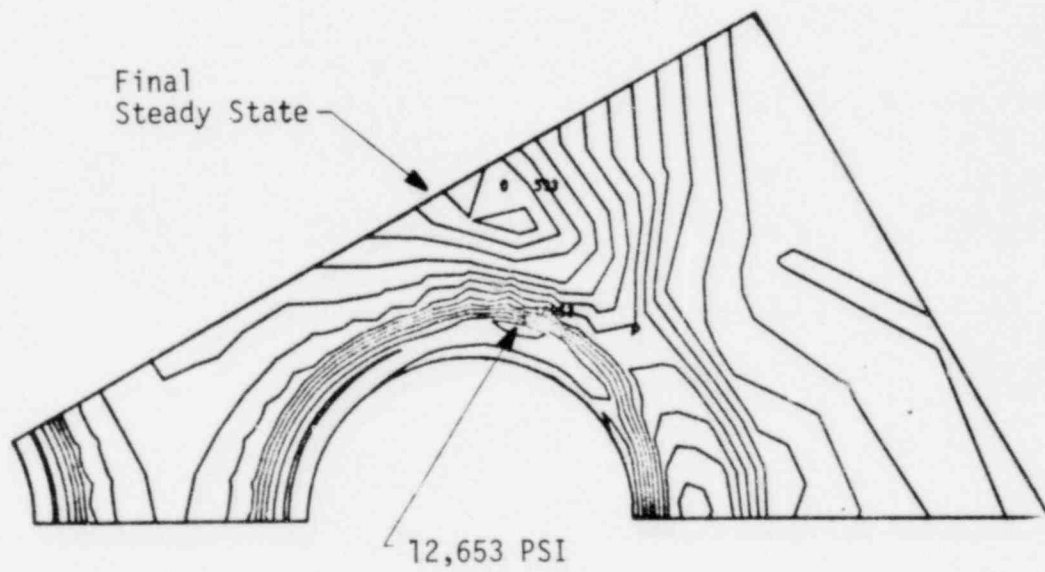
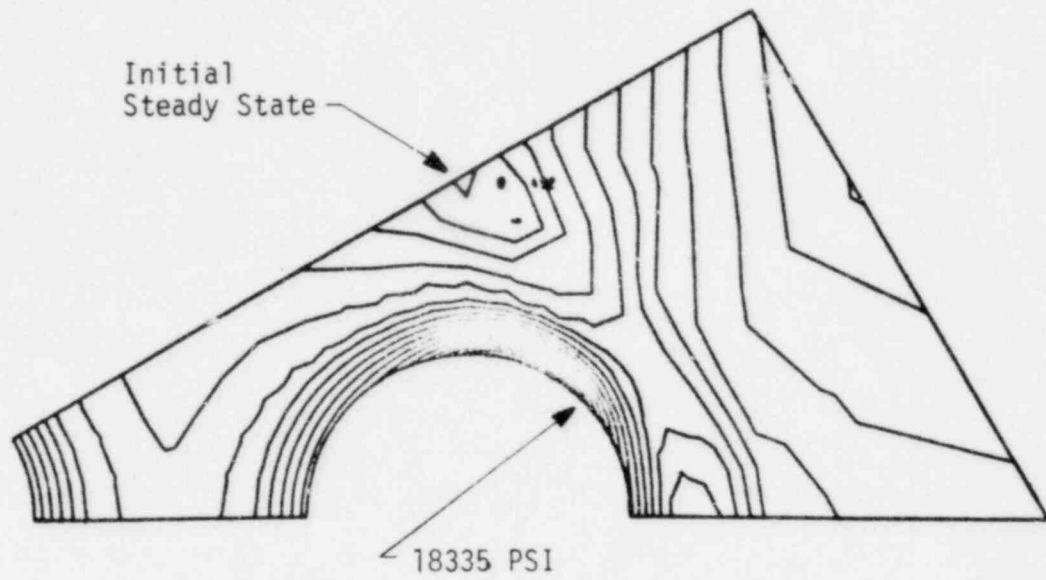


Figure 4.2-3  
F/A Shield Block  
Initial and Final Steady State Time Independent  
Equivalent Stress

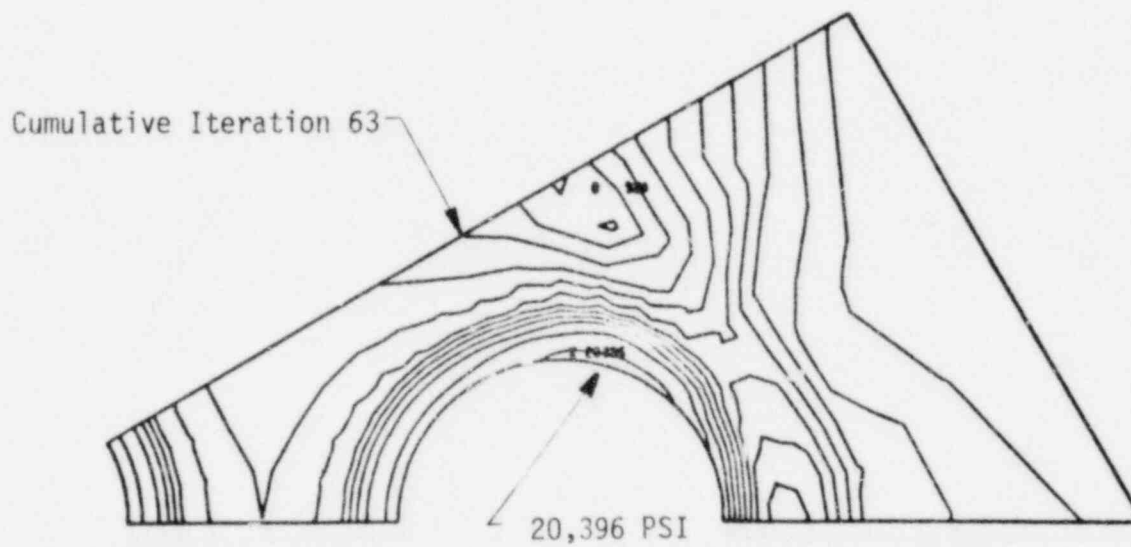
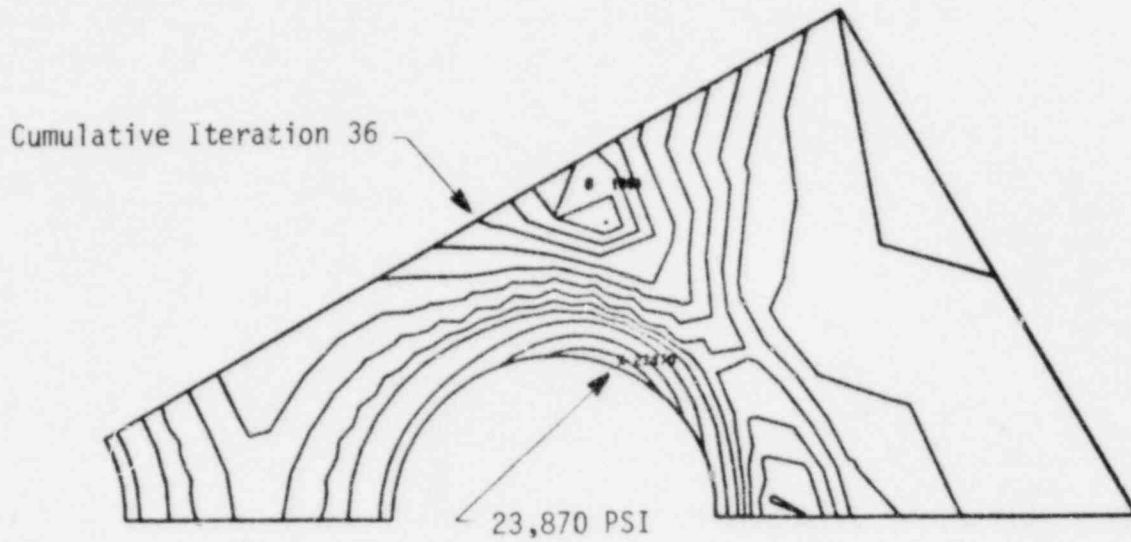


Figure 4.2-4  
F/A Shield Block  
Cumulative Iteration 36 and 63  
Time Independent Equivalent Stress



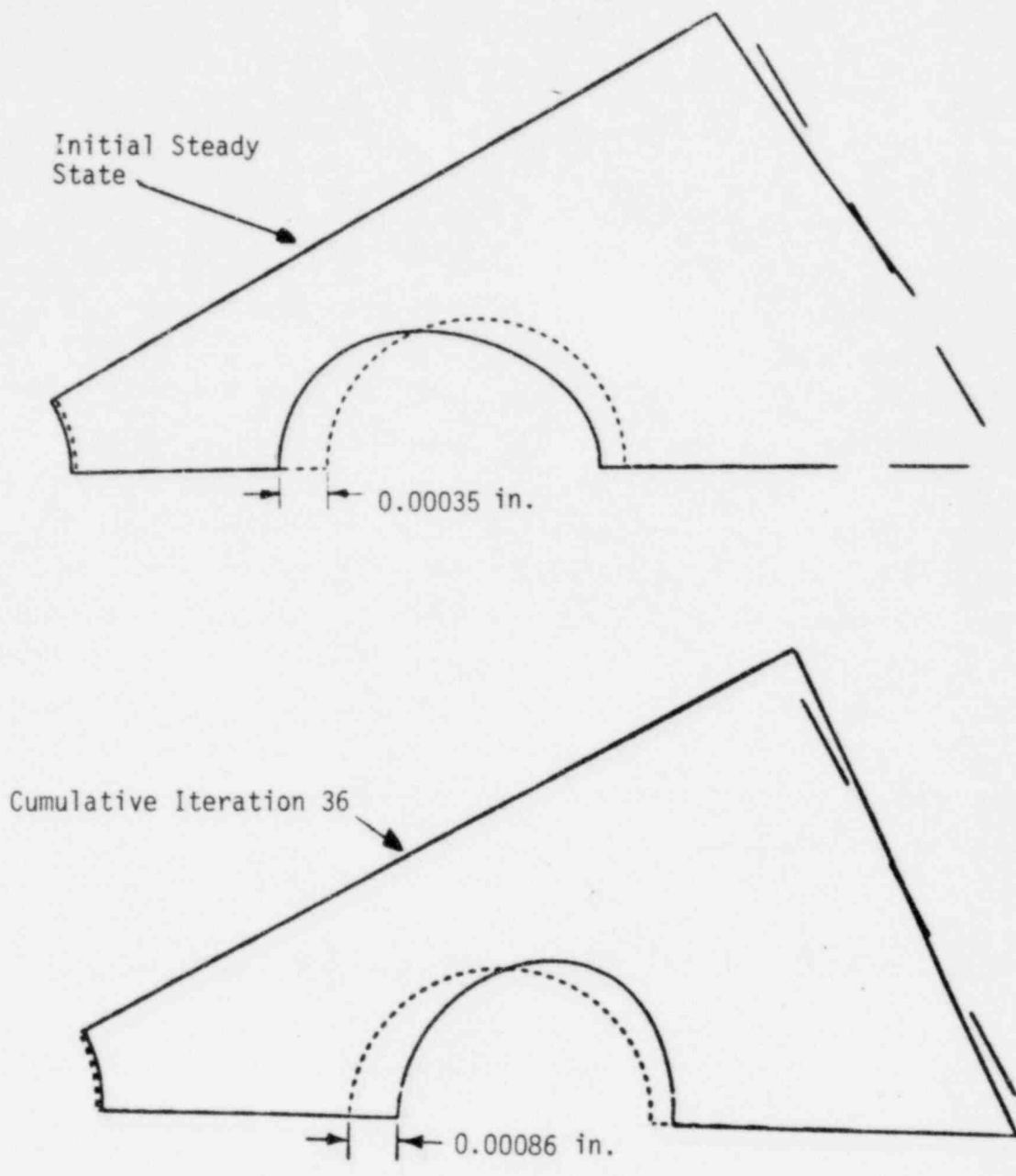


Figure 4.2-5  
F/A Shield Block  
Non-Uniform Deformations  
Time Independent

#### 4.2.3.2.2 Time Dependent

The F/A shield block time dependent ANSYS analysis was directed to deriving the residual strains and deformations associated with the 10-day hold-time following the final time independent steady state conditions. The time dependent analysis was performed in 2 Load Steps using an ANSYS restart from load step 24 of the time independent analysis for the final steady state conditions, represented by cumulative iteration 23 temperature distributions, and maintained for 10 days or 240 hours. As thermal creep was considered negligible and not included in the creep analysis, a redistribution of final steady state stresses by relaxation would not occur. Nevertheless, the final steady state structural response, although constant with time, is still required for subsequent evaluations of creep damage. An additional ANSYS restart from Load Step 26 in 2 Load Steps was performed to unload the F/A shield block to a uniform temperature so as to obtain residual deformations. A summary of the F/A shield block time dependent structural analysis procedure for the 10-day hold-time and unloading to a uniform temperature is presented in Table 4.2-5.

Table 4.2-5  
F/A Shield Block  
Time Dependent Analysis Summary  
10-Day Hold-Time and Unloading

Load Steps	Iterations	Temperature Distribution (°F)	Reference Temperature (°F)	Description
25	1	Cum. It. 23	788.8	10-Day Hold-Time
26	1	Cum. It. 23		
27	1	788.8	788.8	Unloading for Residual Deformations.
28	1	788.8		

The F/A shield block structural response to the time dependent loading was identical to the response found at the final steady state conditions of the time independent loading as thermal creep. In addition, the time dependent maximum equivalent stress and peak non-uniform deformations for the worst case duty cycle are identical to the time independent values illustrated in Figures 4.2-3 through -5.

With regard to the non-uniform deformations of the F/A shield block, the final steady state and residual values were found to be 0.00035 and 0.00004 in. respectively, and are illustrated for Figure 4.2-6.

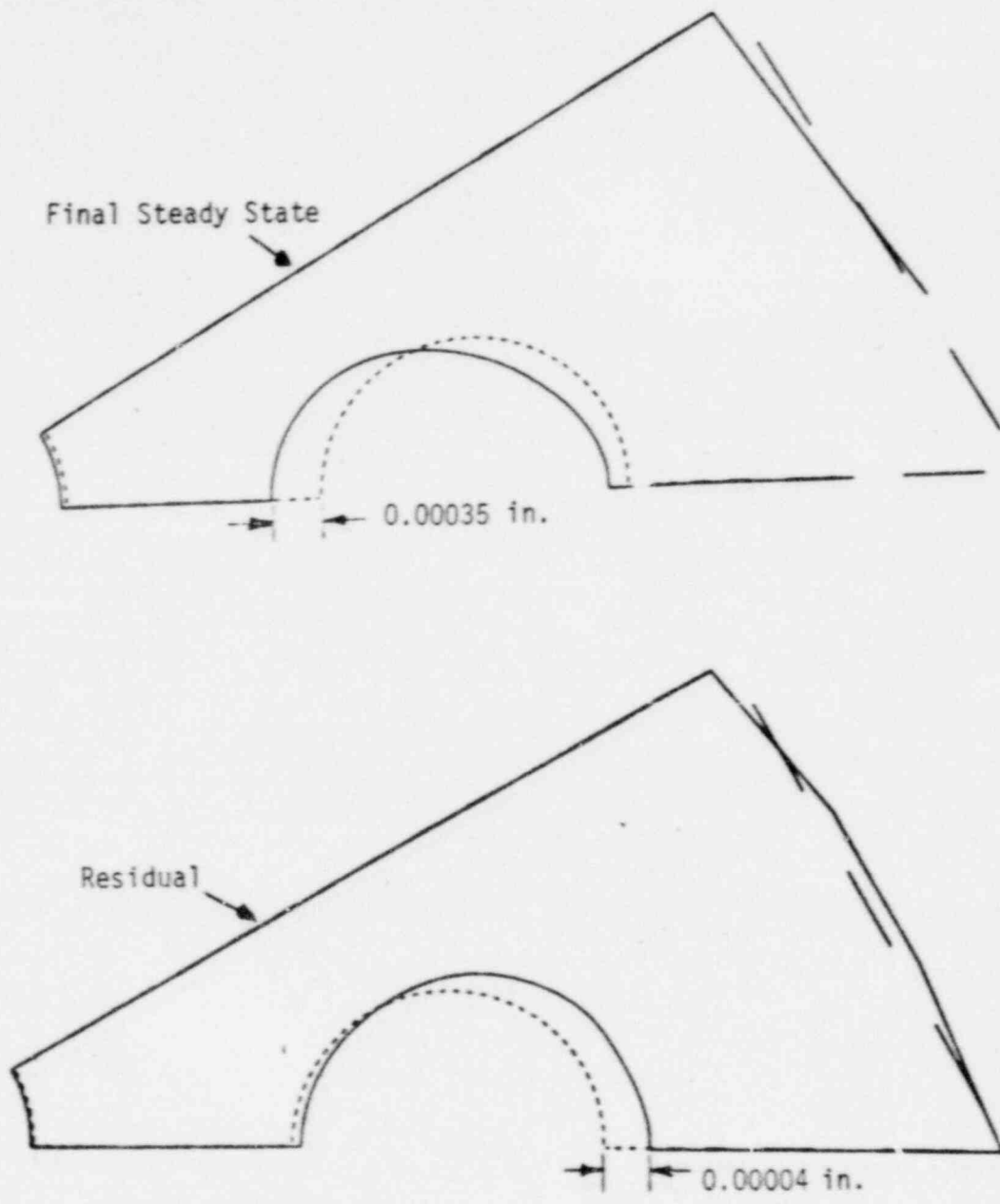


FIGURE 4.2-6  
F/A Shield Block  
Non-Uniform Deformations  
Time Dependent

### 4.3 Structural Evaluation

The F/A shield block structural evaluation was arranged to provide a comparison of the structural response for the 40 worst case duty cycles in relation to criteria which protect against crack initiation and excessive deformation failure modes and thereby assure reliability and function over the first and second reactor cycles.

The procedure for performing the F/A shield block structural evaluations of peak plus accumulated and residual deformations in relation to deformation limits was relatively direct as the inelastic deformations are known from the ANSYS displacement solutions. However, for comparisons of the stress and strain response with crack initiation failure mode criteria, the structural evaluation procedure is not direct because a detailed examination of local multiaxial stress and strain behavior in relation to uniaxial tensile and biaxial pressurized tube data is required prior to evaluating the local ductile rupture and combined creep-fatigue factors. Further, the F/A shield block model includes a large number of finite elements which must be screened to determine the worst location for crack initiation. Accordingly, an important consideration in performing a thorough structural evaluation of crack initiation is a means of processing the stress and strain response into a format that permits a ready comparison with allowable limits. In this arrangement, a special purpose damage processor was written to access the stress and strain response data written on ANSYS Tape 10 for each converged time-independent and dependent solution throughout the worst case F/A shield block duty cycle. From supplied uniaxial or biaxial materials data and crack initiation failure mode correlations, the damage processor examines the local stress and strain response of each element in the F/A shield block throughout the worst case duty cycle and identifies the element with the maximum local ductile rupture and combined creep damage factors. A description, flow chart, and listing of the damage processor is presented in Appendix A.

In the following, the F/A shield block structural evaluation of crack initiation, including allowable materials data and failure mode correlations with results for local ductile rupture and combined creep-fatigue damage, are presented. Next, the structural evaluation of F/A shield block deformations in relation to allowable limits is presented. Finally, the F/A shield block structural evaluation of crack initiation and excessive deformation failure modes is summarized.

#### 4.3.1 Crack Initiation

The F/A shield block structural evaluation of crack initiation in relation to local ductile rupture and combined creep-fatigue damage criteria over the 40 worst case duty cycles is presented in the following subsections.

##### 4.3.1.1 Local Ductile Rupture

The local ductile rupture criterion in protecting against crack initiation requires that the local ductile rupture factor ( $F_{DR}$ ) be less than unity at any point in the F/A shield block.

$$F_{DR} = \text{Maximum of } \left\{ \begin{array}{l} \bullet \frac{(\epsilon_{\max \text{ principal}})^{TF}}{0.3 \epsilon_{f, \min}} \\ \bullet \frac{(\epsilon_{\max \text{ principal}})^{TF}}{\epsilon_{u, \min}} \end{array} \right\}$$

In the following, the allowable uniaxial strains used in the F/A shield block structural evaluation and comparison of results with the local ductile rupture factor criterion are presented.

##### 4.3.1.1.1 Allowable Uniaxial Strains

The F/A shield block as constructed from SA-316-SS is unirradiated at BOL. The EOL fluence ( $E > 0.1$  Mev) is  $0.31 \times 10^{22}$  n/cm<sup>2</sup>. In addition, the F/A shield block temperatures range from 400 to 1000°F. The true minimum uniaxial uniform elongation ( $\epsilon_{u, \min}$ ) and fracture ( $\epsilon_{f, \min}$ ) strains for unirradiated and irradiated SA-316-SS as a function of temperature used

in the F/A shield block structural evaluation are described as follows.

#### 4.3.1.1.1.1 Uniform Elongation

The true irradiated uniaxial SA-316-SS uniform elongation ( $\epsilon_{u, \min}$ ) used in the F/A shield block structural evaluation were based on the minimum correlations of irradiated engineering uniform elongation ( $\bar{\epsilon}_{u, \min}$ ) recommended in the trial applications of the RDT Draft for Breeder Core Components [20-28].

The minimum engineering uniform elongation ( $\bar{\epsilon}_{u, \min}$ ) over the temperature range 700 to 1100°F as a function of fluence ( $E > 0.1$  Mev, where  $(\phi t)$  is in units of  $10^{21}$  N/cm<sup>2</sup>) is given by the relations.

$$\bar{\epsilon}_{u, \min} = 0.22, \text{ for } (\phi t) < 10^{21}$$

$$\bar{\epsilon}_{u, \min} = 0.22 \left( \frac{10^{21}}{\phi t} \right), \text{ for } (\phi t) \geq 10^{21}$$

In order to obtain true minimum irradiated uniform elongation ( $\epsilon_{u, \min}$ ) strains for the evaluation of the local ductile rupture factor ( $F_{DR}$ ) in the F/A shield block, the following relation was used.

$$\epsilon_{u, \min} = \ln (1 + \bar{\epsilon}_{u, \min})$$

#### 4.3.1.1.1.2 Fracture

The true uniaxial irradiated SA-316-SS fracture strains ( $\epsilon_{f, \min}$ ) used in the F/A shield block structural evaluation were taken directly from the minimum correlations for true fracture strain recommended in the trial applications of the RDT Draft for Breeder Reactor Core Components [5].

The true minimum irradiated fracture strain ( $\epsilon_{f, \min}$ ) over the temperature range 800 to 1400°F as a function of fluence ( $E > 0.1$  Mev, where  $(\phi t)$  is in units of  $10^{22}$  n/cm<sup>2</sup>) and temperature ( $T \sim$  °F) is given by the relations.

$$\epsilon_{f, \min} = \epsilon_f^1 \quad \text{for } (\phi t) < (\phi t)_o$$

$$\epsilon_{f, \min} = \epsilon_f^1 \left[ \frac{(\phi t)}{(\phi t)_o} \right]^n \quad \text{for } (\phi t) > (\phi t)_o$$

where,

$$\epsilon_f^1 = 0.45 \left[ \frac{T}{1000} \right]^{-3.5} \quad \text{for } 800 < T \leq 1000$$

$$\epsilon_f^1 = 0.45 \left[ \frac{T}{1000} \right]^{-5.5} \quad \text{for } 1000 < T < 1400$$

$$(\phi t)_o = 1.4 - \frac{T}{1000} \quad \text{for } 800 < T \leq 1000$$

$$(\phi t)_o = \frac{T}{1000} - 1 \quad \text{for } 1000 < T < 1400$$

$$n = -1.7 + \frac{T}{1000}$$

#### 4.3.1.1.2 Comparison with Criterion

The F/A shield block structural evaluation in relation to the worst case location for local ductile rupture was made by screening each of the finite elements over the 40 worst case duty cycles with the damage processor. The maximum local ductile rupture factor  $(F_{DR})_{\max}$  for the F/A shield block was found to occur at element 90, identified in Figure 4.2-1.

The peak BOL strain components occurred at the cumulative iteration 63 temperature distribution in the E-4a transient where the local metal temperature was 802°F. Accumulated BOL strain components were based on the difference between final and initial time independent steady state condition in the worst case duty cycle. The EOL maximum principal strain for the peak BOL and accumulated BOL strain components over 40 worst case F/A duty cycles was 0.00952 in/in. The triaxiality factor for the local stress state was 2.1 while the true minimum irradiated uniform elongation and fracture strains at EOL fluence ( $E > 0.1$  Mev,  $(\phi t) = 0.31 \times 10^{22}$  n/cm<sup>2</sup>) were 0.076 and 0.972 respectively.



In this arrangement, the maximum local ductile rupture factor  $(F_{DR})_{max}$  for the F/A shield block was found to be controlled by the uniform elongation with a value;

$$(F_{DR})_{max} = 0.263$$

As  $(F_{DR})_{max} = 0.263 < 1.0$ , the F/A shield block is not expected to experience crack initiation over the 40 worst case duty cycles based on the local ductile rupture criterion.

#### 4.3.1.2 Creep-Fatigue Damage

The creep-fatigue damage criterion in protecting against crack initiation requires that the combined creep-fatigue damage factor  $(F_{CFD})$  be less than unity at each point in the F/A shield block.

$$F_{CFD} = a/b = \text{Minimum of } \left\{ \begin{array}{l} \bullet \ 7/3 D^C + D^f \\ \bullet \ D^C + 7/3 D^f \end{array} \right\}$$

In the following, the allowable limits for fatigue life and creep rupture times used in the F/A shield block structural evaluation and a comparison of the results with the combined creep-fatigue damage criterion are presented.

#### 4.3.1.2.1 Allowable Limits

The F/A shield block as constructed from SA-316-SS is irradiated to an EOL fluence ( $E > 0.1$  Mev) of  $0.31 \times 10^{22}$  n/cm<sup>2</sup>. In addition, the F/A shield block temperatures range from 400 to 1000°F with the wetted sodium surfaces subjected to oxidation as well as interstitial transfer of carbon and oxygen. The fatigue life and time to rupture data for SA-316-SS including the effects of fluence, temperature, interstitial transfer, and surface oxidation used in the F/A shield block structural evaluation are described as follows.

#### 4.3.1.2.1.1 Fatigue Life

Currently, fatigue life correlations are not available for irradiated SA-316-SS as a function of fluence and temperature. Accordingly, the Manson Universal Slopes Method [7] was used to develop fatigue life correlations from which the fatigue damage factor ( $D^f$ ) for the F/A shield block over the 40 worst case duty cycles was derived.

In the Manson Universal Slopes Method, the slopes of elastic and plastic strain lines expressed in terms of strain range versus number of cycles on a full logarithmic plot are assumed to be the same for all materials. As applied to unirradiated SA-316-SS, the total strain range ( $\Delta\epsilon$ ) is dependent on the minimum unirradiated true fracture strain ( $\epsilon_{f,u}$ ), average unirradiated engineering ultimate strength ( $S_{u,u}$ ), Young's Modulus ( $E$ ), and cycles to failure ( $N_f$ ) by the relation:

$$\Delta\epsilon = \epsilon_{f,u}^{0.6} N_f^{-0.6} + \frac{3.5 S_{u,u} N_f^{-0.12}}{E}$$

In order to include the effects of irradiation in the fatigue life relation for SA-316-SS, reduction factors for the elastic ( $F_e$ ) and plastic ( $F_p$ ) strain ranges were used in accordance with the guidelines of the RDT Draft for Breeder Reactor Core Components [5].

$$\Delta\epsilon = F_p \epsilon_{f,u}^{0.6} N_f^{-0.6} + \frac{3.5 F_e S_{u,u} N_f^{-0.12}}{E}$$

$$\text{Where, } F_e = \left(\frac{S_{u,I}}{S_{u,u}}\right)^{k_2}$$

$$F_p = \frac{(\epsilon_{f,I})^{k_1}}{\epsilon_{f,u}}$$

$\epsilon_{f,I}$  = True Minimum Irradiated Fracture Strain

$S_{u,I}$  = Average Irradiated Engineering Ultimate Strength

$k_1, k_2$  = Experimental Constants

Without available material data, the elastic reduction factor ( $F_e$ ) and plastic reduction factor exponent ( $k_1$ ) were taken as unity. Accordingly the fatigue life relation developed for irradiated SA-316-SS was:

$$\Delta \epsilon = \epsilon_{f,I} \epsilon_{f,U}^{-0.4} N_f^{-0.6} + 3.5 \frac{S_{u,U}}{E} N_f^{-0.12}$$

The development of the irradiated SA-316-SS fatigue life relation requires the true minimum irradiated and unirradiated fracture strains ( $\epsilon_{f,I}$  and  $\epsilon_{f,U}$ ), average unirradiated engineering ultimate strength ( $S_{u,U}$ ), and Young's Modulus ( $E$ ).

- The true minimum irradiated and unirradiated fracture strains ( $\epsilon_{f,I}$  and  $\epsilon_{f,U}$ ) as a function of temperature and fluence are given in Section 4.3.1.1.2.
- The average unirradiated engineering ultimate strength ( $S_{u,U}$ ) was taken as 125% of the minimum values given in the NSM Handbook [6].  

$$S_{u,U} = 100220 - (161.42) * T + (0.368) * T^2$$

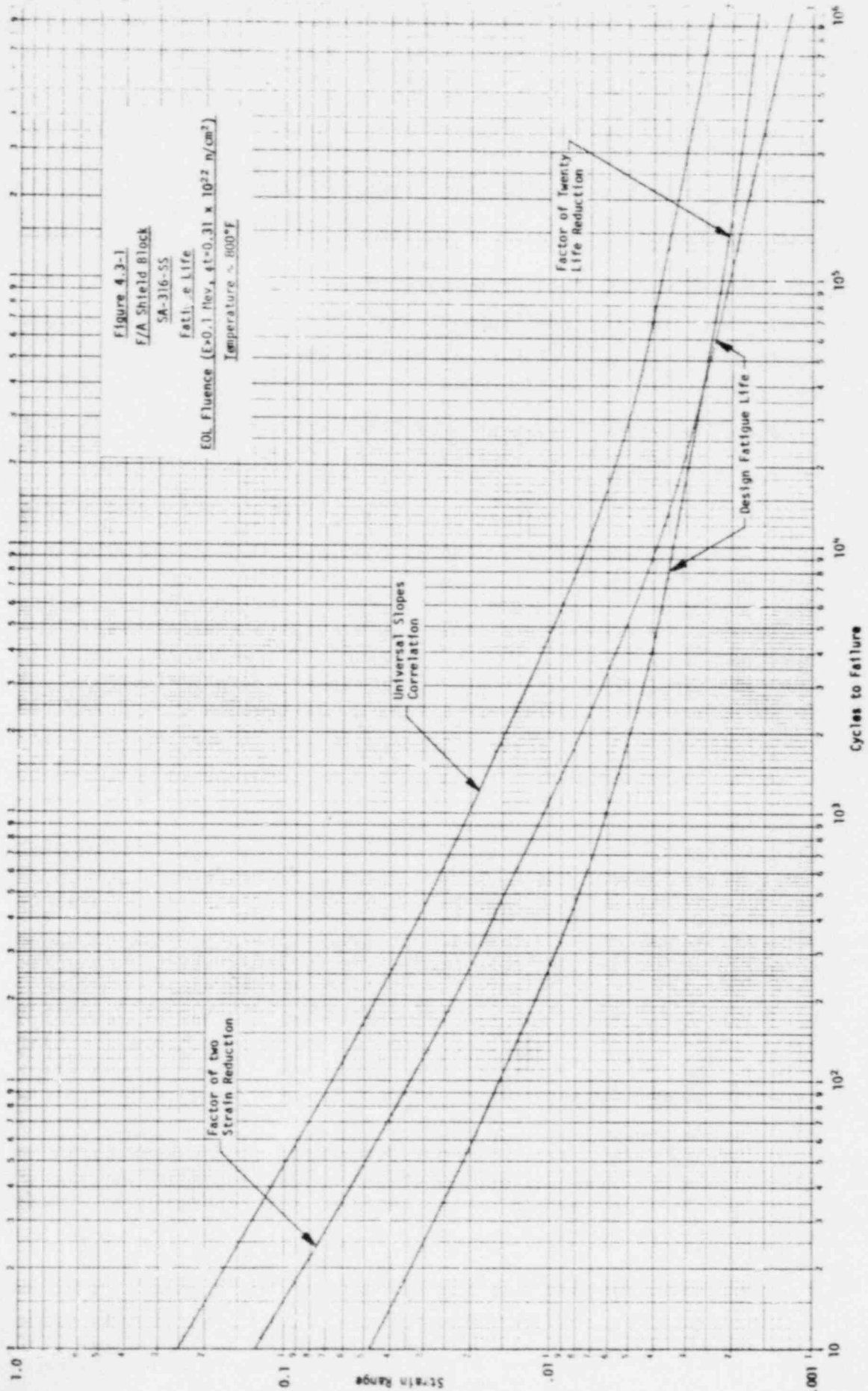
$$- (0.325E-3) * T^3 + (0.863E-7) * T^4$$

where,  $S_{u,U} \sim \text{psi}$   
 $T \sim ^\circ\text{F}$
- Young's Modulus ( $E$ ) as a function of temperature is given in Section 4.2.2.1

The irradiated SA-316-SS fatigue life relation as developed from the Manson universal slopes method and corrected for the effects of irradiation is strictly applicable only to uniaxial stress states. In order to apply the fatigue life relation to the F/A shield block, reductions in fatigue life which reflect the multiaxial stress and strain state are required. The RDT Draft Criteria for Breeder Reactor Core Components [5] recommends that equivalent strain be used for the strain range in fatigue evaluations of multiaxial stress and strain states. Another means of accounting for multiaxial effects

on fatigue life is to use the range in maximum principal strain. In the F/A shield block fatigue evaluation, the fatigue life based on equivalent or maximum principal strain, whichever produced the minimum fatigue life was adopted in order to provide an additional safeguard against fatigue failure.

An additional consideration is that the Manson Universal Slopes Method is strictly applicable only to the mean fatigue life of a material and does not account for the scatter in experimental data. The RDT Draft Criteria for Breeder Reactor Core Components [5] recommends that the 2-20 rule be used to account for the minimum fatigue life due to scatter of data about the mean. The 2-20 rule was adopted for the fatigue life correlations of irradiated SA-316-SS in the F/A shield block structural evaluation of fatigue life. Simply stated, the 2-20 rule requires that the multiaxial fatigue life be taken as the uniaxial fatigue life reduced by a factor of 2 on strain range or a factor of 20 on life, whichever is minimum. The 2-20 rule as applied to the uniaxial fatigue life relation developed for irradiated SA-316-SS using the Manson Universal Slopes Method for the F/A shield block EOL fluence ( $E > 0.1$  Mev,  $\phi t = 0.31 \times 10^{22}$  n/cm<sup>2</sup>) at 800°F is presented in Figure 4.3-1.



#### 4.3.1.2.1.2 Creep-Rupture Time

Currently, rupture time correlations are available for unirradiated and irradiated SA-316-SS based on pressurized thin walled tubes in a biaxial stress state [8]. As such, the available biaxial rupture time data with reductions for interstitial transfer and surface oxidation are sufficient for the evaluation of the creep damage factor ( $D^C$ ) for the F/A shield block over the 40 worst case duty cycle.

The creep-rupture time data [8] for unirradiated and irradiated SA-316-SS is presented in terms of the Larson-Miller Parameter (LMP). The minimum unirradiated and irradiated LMP, designated as  $(LMP)_U$  and  $(LMP)_I$ , taken as 2 standard deviations below average data, as a function of stress ( $\sigma \sim$  ksi) and fluence ( $E > 0.1$  Mev, where  $(\phi t)$  is in units of  $10^{22}$  n/cm<sup>2</sup>) are:

$$(LMP)_U = 48.91 - 5.27 \log_{10} \sigma - 2.995 (\log_{10} \sigma)^2$$

$$(LMP)_I = 52.024 - 13.353 \log_{10} \sigma - 1.311 \log_{10} (\phi t)$$

To obtain the minimum rupture time ( $t_r \sim$  HRS) at a temperature ( $T \sim$  °R  $\times 10^{-3}$ ) for either unirradiated or irradiated SA-316-SS,

$$(LMP)_U = (LMP)_I = T (20 + \log_{10} t_r)$$

Reductions in rupture time ( $t_r$ ) to account for interstitial transfer of carbon and nitrogen for SA-316-SS were found to be negligible. However, surface oxidation of SA-316-SS at wetted sodium surfaces is known to moderately affect rupture strength. The percent decrease in rupture strength for SA-316-SS from surface interaction with sodium as a function of temperature is identified in the CRBRP Core Former E-Spec [9] and summarized as a fractional reduction (FR) over a 800 to 1300°F temperature range in Table 4.3-1.

TABLE 4.3-1  
F/A SHIELD BLOCK  
FRACTIONAL REDUCTION RUPTURE STRENGTH  
SA-316-SS

Fractional Reduction (FR)	Temp. (°F)
1.0	800
1.0	900
0.97	1000
0.94	1100
0.91	1200
0.88	1300

In order to include reduction in rupture strength for both unirradiated and irradiated SA-316-SS due to sodium effects in F/A shield block evaluations of creep damage, the inelastically calculated maximum stress intensities or principal stresses ( $\sigma$ ) were increased by the reciprocal of the fractional reduction (FR) prior to evaluating the minimum rupture times ( $t_r$ ).

$$\sigma = \sigma / \text{FR}$$

In summary, the minimum rupture time ( $t_r$ ) for unirradiated SA-316-SS including reductions in rupture strength due to sodium effects used in creep damage evaluations of the F/A shield block are as follows.

$$t_r = 10 \exp \left[ \frac{((LMP)_{u,\min})^{-20}}{T} \right]$$

where,

$$(LMP)_{u,min} = 48.91 - 5.27 \log_{10} \left( \frac{\sigma}{FR} \right) - 2.995 \left( \log_{10} \frac{\sigma}{FR} \right)^2$$

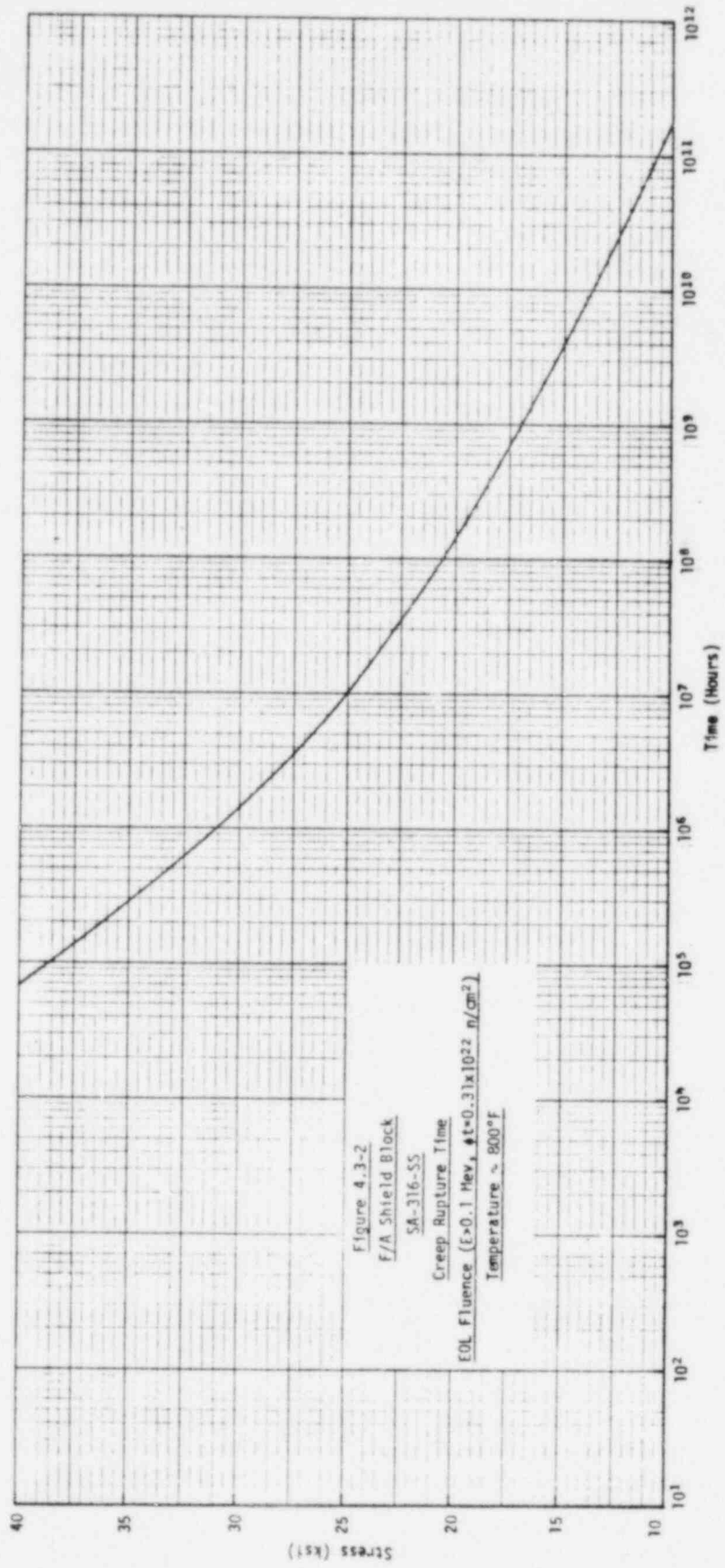
Similarly, for irradiated SA-316-SS,

where,  $t_r = 10 \exp \left[ \frac{(LMP)_{I,min}}{T} - 20 \right]$

$$(LMP)_{I,min} = 52.024 - 13.353 \log_{10} \left( \frac{\sigma}{FR} \right) - 1.3111 \log_{10} (\phi t)$$

The minimum rupture times as a function of maximum principal creep stress ( $\sigma$ ) for SA-316-SS irradiated to the EOL fluence ( $E > 0.1$  Mev,  $\phi t = C.31 \times 10^{22}$  n/cm<sup>2</sup>) at 800°F are illustrated in Figure 4.3-2.





#### 4.3.1.2.2 Comparison with Criterion

The F/A shield block structural evaluation in relation to the worst case location for combined creep-fatigue damage was made by screening each of the finite elements over the 40 worst case duty cycles with the damage processor. The maximum combined creep-fatigue damage factor  $(F_{CFD})_{max}$  for the F/A shield block was found to occur at element 98 as identified in Figure 4.2-1.

The fatigue damage factor  $(D^f)$  was found to be 0.0159 for 40 worst case duty cycles. The equivalent strain range was found to be critical and occurred between cumulative iteration 36 and 63 temperature distributions during the E-4a transient with a value of 0.0041 in/in. The peak metal temperature over the fatigue cycle was 911°F. The fatigue life for the equivalent strain range was 2505 cycles based on the EOL fluence ( $E > 0.1$  Mev,  $(\phi t) = 0.31 \times 10^{22}$  n/cm<sup>2</sup>).

The creep damage factor  $(D^c)$  was found to be  $0.668 \times 10^{-6}$  for the 40 worst case duty cycles. The principal stress was found to be critical with a value of 12,579 psi corresponding to the steady state temperature conditions at the beginning of the 10 day hold time. For the EOL fluence ( $E > 0.1$  Mev,  $(\phi t) = 0.31 \times 10^{22}$  n/cm<sup>2</sup>) at a metal temperature of 752°F, the minimum rupture time was  $1.43 \times 10^{10}$  hours.

In this arrangement, the maximum combined creep-fatigue damage factor  $(F_{CFD})_{max}$  for the F/A shield block was found to be dominated by fatigue damage while creep damage was negligible.

$$(F_{CFD})_{max} = 0.0159$$

As  $(F_{CFD})_{max} = 0.0159 < 1.0$ , the F/A shield block is not expected to experience crack initiation over the 40 worst case duty cycles based on the creep-fatigue damage criterion.

#### 4.3.2 Excessive Deformation

The F/A shield block structural evaluation of peak plus accumulated, and residual deformations in relation to functional limits over the 40 worst case duty cycles is presented in the following subsections.

##### 4.3.2.1 Peak Plus Accumulated Deformations

The peak plus accumulated deformation criterion in protecting against excessive peak deformations requires that peak plus accumulated deformations ( $\delta^{P+A}$ ) be less than the peak plus accumulated deformation limit (PADL).

$$\delta^{P+A} \leq \text{PADL}$$

The peak deformation ( $\delta^P$ ) of the F/A shield block during the worst case duty cycle at BOL was found to occur in the flow passage holes at the cumulative iteration 63 temperature distribution of the E-4a transient with a value of 0.00086 in. The initial time independent and final time dependent steady state non-uniform deformations were both found to be 0.00035 in. Accordingly, the accumulated deformation ( $\Delta\delta^{SS}$ ) between the initial and final steady state conditions for one duty cycle at BOL was 0.0 in. For 40 worst case duty cycles, the EOL peak + accumulated ( $\delta^{P+A}$ ) deformation.

$$(\delta^{P+A})_{\text{EOL}} = (\delta^P)_{\text{BOL}} + (N-1) (\Delta\delta^{SS})_{\text{BOL}}$$

$$(\delta^{P+A})_{\text{EOL}} = 0.00087 + 39 (0.0)$$

$$(\delta^{P+A})_{\text{EOL}} = 0.00087 \text{ in.}$$

For the F/A shield block, the peak plus accumulated deformation limit (PADL),

$$\text{PADL} = 0.005 \text{ in.}$$

As  $\delta^{P+A} \leq \text{PADL}$ , the F/A shield block is not expected to experience excessive peak deformation during the 40 worst case duty cycles.

#### 4.3.2.2 Residual Deformations

The residual deformation limit in protecting against excessive residual deformations requires that the residual deformation ( $\delta^R$ ) be less than the residual deformation limit (RDL).

$$\delta^R \leq \text{RDL}$$

The residual deformation ( $\delta^R$ ) between initial and final uniform conditions for one worst case duty cycle at BOL was found to be 0.00004 in. For 40 duty cycles, the residual deformation ( $\delta^R$ ) at EOL is

$$\begin{aligned}(\delta^R)_{\text{EOL}} &= N(\delta^R)_{\text{BOL}} \\ \delta^R &= 0.0016 \text{ in.}\end{aligned}$$

For the F/A shield block, the residual deformation limit (RDL) is

$$\text{RDL} = 0.005 \text{ in.}$$

As  $\delta^R \leq \text{RDL}$ , the F/A shield block is not expected to experience excessive residual deformation during the 40 worst case duty cycles.

#### 4.3.3 Summary

The F/A shield block was found to satisfy the crack initiation and excessive deformation criteria for a total of 40 worst case duty cycles. A summary of the F/A shield block structural evaluation is presented in Table 4.3-2.

TABLE 4.3-2  
F/A SHIELD BLOCK  
STRUCTURAL EVALUATION SUMMARY

Criteria		Allowable Value	Calculated Value	Margin of Safety*
Crack Initiation	Ductile Rupture Factor	1	0.263	2.80
	Combined Creep-Fatigue Damage Factor	1	0.0159	61.62
Excessive Deformation	Peak + Accumulated	0.005 in.	0.00087	4.75
	Residual	0.005 in.	0.0016 in	2.13

\* Margin of Safety =  $\frac{\text{Allowable Value}}{\text{Calculated Value}} - 1$

## 5.0 CMP HEX DUCT ANALYSIS AND EVALUATION

In the F/A CMP hex duct analysis and evaluation, a loading analysis was made that considered mechanical seismic and core restraint, and thermal steady state and transient loads in order to establish the number and characteristics of a worst case duty cycle that umbrellas all expected duty cycles for the CMP hex duct in the first and second reactor cycles. Next, an inelastic structural analysis of the CMP hex duct was made for a single worst case BOL duty cycle from which EOL values were approximated. Finally, a structural evaluation of EOL strains and dimensional changes in relation to criteria which protect against crack initiation and excessive deformation was made. A summary of the loading and structural analysis, and structural evaluation is presented as follows.

### 5.1 Loading Analysis

The F/A CMP hex duct loading analysis was directed to establishing the number and characteristics of a worst case duty cycle that umbrellas both the number and characteristics of the Upset, Emergency, and Faulted Events specified over the first and second reactor cycles. The number and characteristics of these events are specified in the Equipment Specification [1].

It is important to note that the worst case F/A CMP hex duct duty cycle is, in itself, hypothetical, but permits a conservative structural evaluation to be performed on a single duty cycle instead of on each of the individual events specified. In the following, the F/A CMP hex duct mechanical and thermal loads are assessed individually and in relation to each other prior to establishing the worst case duty cycle used in the structural evaluation.

#### 5.1.1 Mechanical

The F/A CMP hex duct mechanical loads of significance in relation to subsequent structural evaluations are the beam type bending loads induced by OBE and SSE seismic, and core restraint. Deadweight and internal pressure loadings are relatively insignificant.

Other mechanical loads postulated for the F/A CMP hex duct assume that the effects of irradiation creep and swelling are sufficient to exhaust the nominal clearances between adjacent hex ducts at the CMP so as to permit local inter-duct contact during OBE and SSE seismic events and due to core restraint under steady state operation. However, the potential for CMP inter-duct contact under seismic and core restraint loadings was assessed and found not to occur for the EOL fluence ( $E > 0.1$ ),  $(\phi t) = 9.29 \times 10^{22} \text{ N/cm}^2$ ) identified for the F/A CMP.

Accordingly, mechanical loads for the worst case F/A CMP hex duct duty cycle considered only the beam type bending loads induced by OBE and SSE seismic, and core restraint as local inter-duct contact loads do not occur and deadweight and internal pressure loads are relatively insignificant.

#### 5.1.1.1 Beam Bending

In order to perform a structural evaluation of the F/A CMP hex duct, the maximum bending stresses and strains under lateral OBE and SSE seismic, and core restraint are required. The OBE and SSE seismic bending moments ( $M$ ) were taken as the static 1-g moment ( $M_s$ ) amplified by the respective acceleration ( $a$ ) of the core barrel, while the core restraint moment ( $M_{cr}$ ) corresponding to steady state operation was taken directly.

$$M_{OBE} = [M_s] a_{OBE}$$

$$M_{SSE} = [M_s] a_{SSE}$$

$$M_{cr} = M_{cr}$$

With regard to core restraint behavior during the Upset, Emergency, and Faulted thermal transients, the temperatures of the F/A and adjacent C/A, RB/A and RRS/A hex ducts were assumed to follow the overall core temperatures, but the temperature differences across the F/A which cause

transient the core restraint bending moments were not assumed to change from steady state values. Alternately, the steady state temperature difference across the F/A hex duct cross-section at any point along its length was assumed to be the same during the thermal transients even though overall temperatures increased or decreased according to the characteristics of the transients. In this arrangement, the transient bending moments ( $M_{TR}$ ) were assumed equal to the steady state core restraint moments ( $M_{CR}$ ).

$$M_{TR} = M_{CR}$$

For the F/A CMP hex duct the cross-section modulus ( $Z$ ) and Young's Modulus ( $E$ ), the maximum bending stresses ( $\sigma$ ) and strains ( $\epsilon$ ) are given by the following relations:

$$\sigma = M/Z \text{ and } \epsilon = \sigma/E$$

Numerically, the F/A CMP hex duct section modulus ( $Z$ ) is  $2.250 \text{ in}^3$ . The Young's Modulus ( $E$ ) for the F/A CMP hex duct constructed from first core 20% CW-316-SS and operating at a steady state temperature of  $900^\circ\text{F}$  is  $23.31 \times 10^6 \text{ psi}$ . The F/A CMP hex duct maximum stresses ( $\sigma$ ) and strains ( $\epsilon$ ) under OBE and SSE seismic, core restraint and transient bending moments are summarized in Table 5.1-1.



TABLE 5.1-1  
F/A CMP HEX DUCT  
OBE AND SSE SEISMIC, AND CORE RESTRAINT  
BENDING MOMENTS, STRESSES, AND STRAINS

Loading		Core Barrel Acceleration (a)	Bending Moment (M ~ in-lb)		Max. Bending Stress ( $\sigma$ ~ PSI)	Max. Bending Strain ( $\epsilon$ ~ in/in)
			Static	Dynamic		
Seismic	OBE	1.57	1351	2121	943	4.05E-5
	SSE	2.2	1351	2972	1321	5.67E-5
Core Restraint		N/A	26213	N/A	11650	5.00E-4
Transients		N/A	26213	N/A	11650	5.00E-4

### 5.1.2 Thermal

The F/A CMP hex duct thermal loads are the steady state and transient temperature distributions that occur during the Upset, Emergency, and Faulted Events over the first and second reactor cycles. The steady state F/A CMP hex duct inside metal temperature distributions throughout Sector A of the core at BOC 1, EOC 1, BOC 2, and EOC 2 and the Upset, Emergency, and Faulted Transients defined in terms of time-dependent scale factors applied to the steady state inside metal temperatures were considered. In this arrangement, the F/A CMP hex duct thermal loads in terms of inside metal temperatures associated with BOC 1, EOC 1, BOC 2, and EOC 2 steady state as well as Upset, Emergency, and Faulted Transients were identified at any F/A location in the core.

In order to proceed with a structural evaluation of the F/A CMP hex duct, it was desirable for the sake of simplicity to consider only the worst case thermal loading. Accordingly, all F/A located in Sector A of the core were assessed in relation to the maximum inside metal wall temperature difference between a F/A and adjacent C/A or RB/A. The maximum steady inside metal wall temperature difference was found to occur at F/A A<sub>02</sub><sup>07</sup> adjacent to C/A <sub>01</sub><sup>07</sup> during BOC 1 with a value of 126°F. It is important to note that at EOC 1, BOC 2, and EOC 2, the respective inside metal temperature differences were found to decrease from BOC 1 values. As such, the BOC 1 maximum steady state inside metal temperature difference of 126°F between a F/A and adjacent C/A was clearly worst case for all F/A CMP hex ducts in the core over the first and second reactor cycles.

With regard to F/A and adjacent C/A CMP hex duct thermal transients, the Equipment Specification [1] using an umbrella approach identified the number of Upset, Emergency, and Faulted transients over the first and second reactor cycles as 1/15 of the number specified for 30 years rounded to the next whole number. Over the first and second reactor cycles comprising a total of 328 FPD, a total of 39 Upset Transients umbrellaed by the worst of U-2b or OBE were specified. Similarly, the

worst of the E-16, 60¢ Step, or U-2b during OBE were specified to umbrella the Emergency Transients while the SSE was identified to umbrella the Faulted Transients.

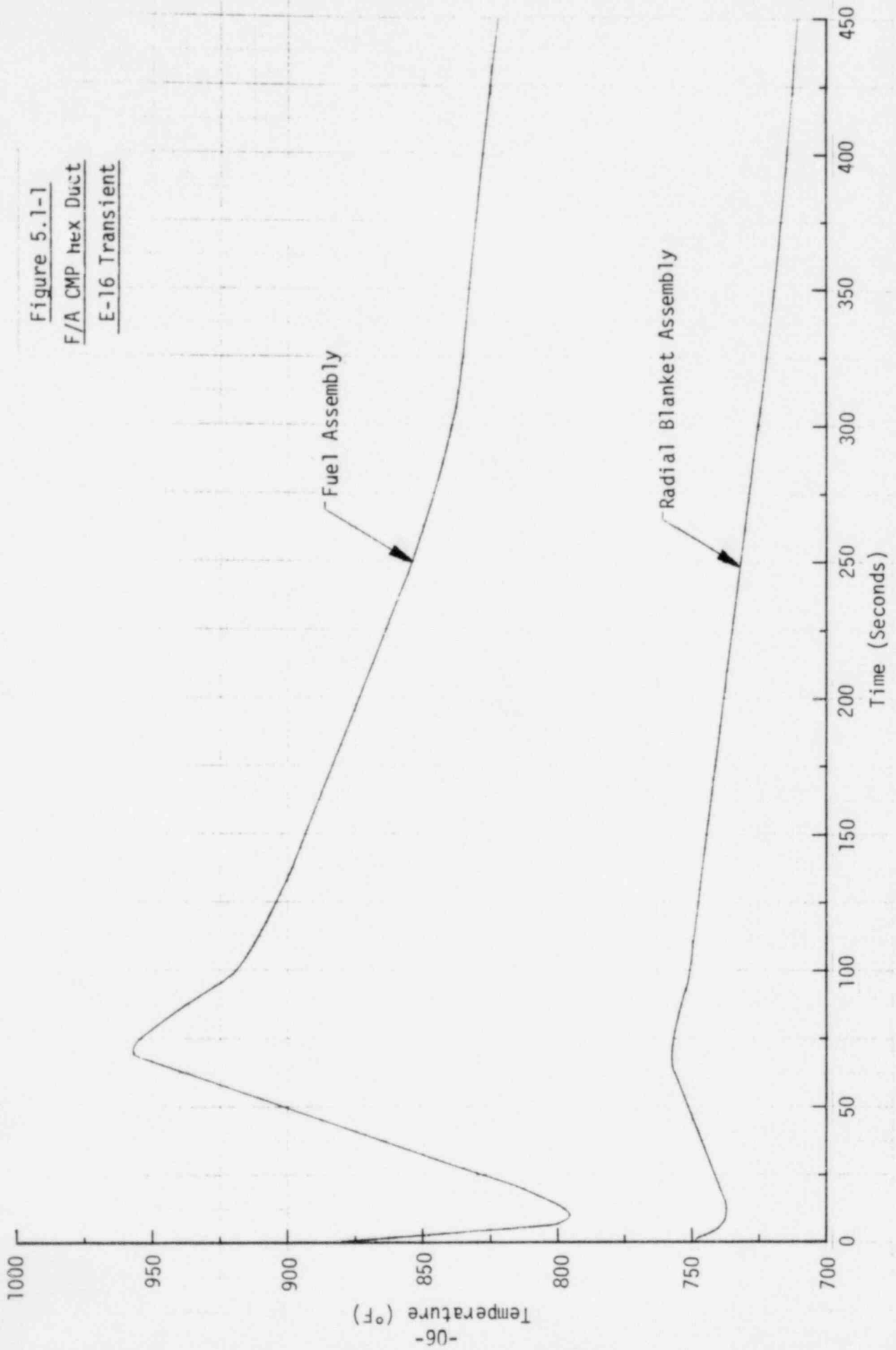
In the derivation of the F/A and adjacent C/A inside metal temperature transients for the Upset, Emergency, and Faulted transients, the upper and lower bounds for the Upset U-2b and OBE events and the Emergency 60¢ step event were considered. The upper bounds were based on quickest flow decay and maximum decay heat while the lower bounds were based on slowest flow decay and minimum decay heat. Further, the SSE Faulted Transient was found to be umbrellaed by the Emergency E-16 transient. The Upset transients comprising the upper and lower bound U-2b and OBE, and the Emergency Transients including the upper and lower bound 60¢ step, E-16, and U-2b during OBE were identified from current data.

In order to reduce the number of F/A CMP hex duct transients which umbrella the Upset and Emergency Transients to a single worst case transient, the individual transients were assessed for severity in subsequent structural evaluations by comparing the inside metal wall temperatures in terms of maximum value, rate of temperature change, and range. With regard to steady state conditions, all transients were initiated with F/A and C/A inside metal wall temperatures of 874 and 748°F which provide the worst case temperature difference of 126°F. For the Upset Transients at the F/A CMP hex duct inside metal surface, the upper and lower bound U-2b transients were assessed as slightly more severe in terms of maximum temperature with maximum rate and range of temperature indistinguishable from the upper and lower bound OBE transient. However, the adjacent C/A inside metal temperature transients for the lower bound U-2b were observed to more closely follow the F/A metal transient than in the case of the upper bound U-2b. Owing to the thermal lag in the thin walled F/A CMP hex duct, temperature differences through the wall, which are important in structural evaluations, are slightly more severe in the lower bound U-2b transient than the upper bound counterpart. With regard to the Emergency Transients, the E-16 transient in terms of

maximum value, rate of temperature change, and range was found to be clearly more severe than the upper and lower bound 60¢ step, and the U-2b during OBE transients. Further, the E-16 was also considered more severe than the lower bound U-2b transient. In this arrangement, the Emergency E-16 transient was selected as the worst case umbrella to all of the Upset, Emergency, and Faulted transients for the F/A CMP hex duct and is illustrated in Figure 5.1-1.

The selection of the Emergency E-16 transient as the worst case F/A CMP hex duct transient is, in itself, not sufficient to establish the worst case F/A CMP hex duct duty cycle. Thermal conditions following the E-16 transient and subsequent hold-times at steady state conditions are also required. The thermal conditions selected consisted of a cool-down to 600°F in 1 hour from the F/A and C/A inside metal wall temperature at 450 seconds into the E-16 transient, followed by a 1 hour heat-up to initial steady state F/A and C/A temperatures. Thereafter, a 10 day hold-time at steady state temperatures was assumed. The 10 day hold time corresponds to 40 worst case E-16 transients uniformly distributed over 400 FPD which is slightly greater than the 328 FPD specified for the first and second reactor cycles. The worst case F/A CMP hex duct duty cycle is presented in Figure 5.1-2.

The worst case F/A CMP hex duct duty cycle in terms of inside metal temperatures at initial steady state, followed by the E-16 transient, thermal conditions in returning to initial steady condition, and 10 day hold-time are not sufficiently detailed for subsequent structural evaluation. In the following, the F/A CMP hex duct thermal model and geometry, boundary conditions and wetted sodium surfaces, heat generation rates, and thermal analysis and results are described from which conclusions on detailed temperature distributions used in subsequent structural analysis are presented.



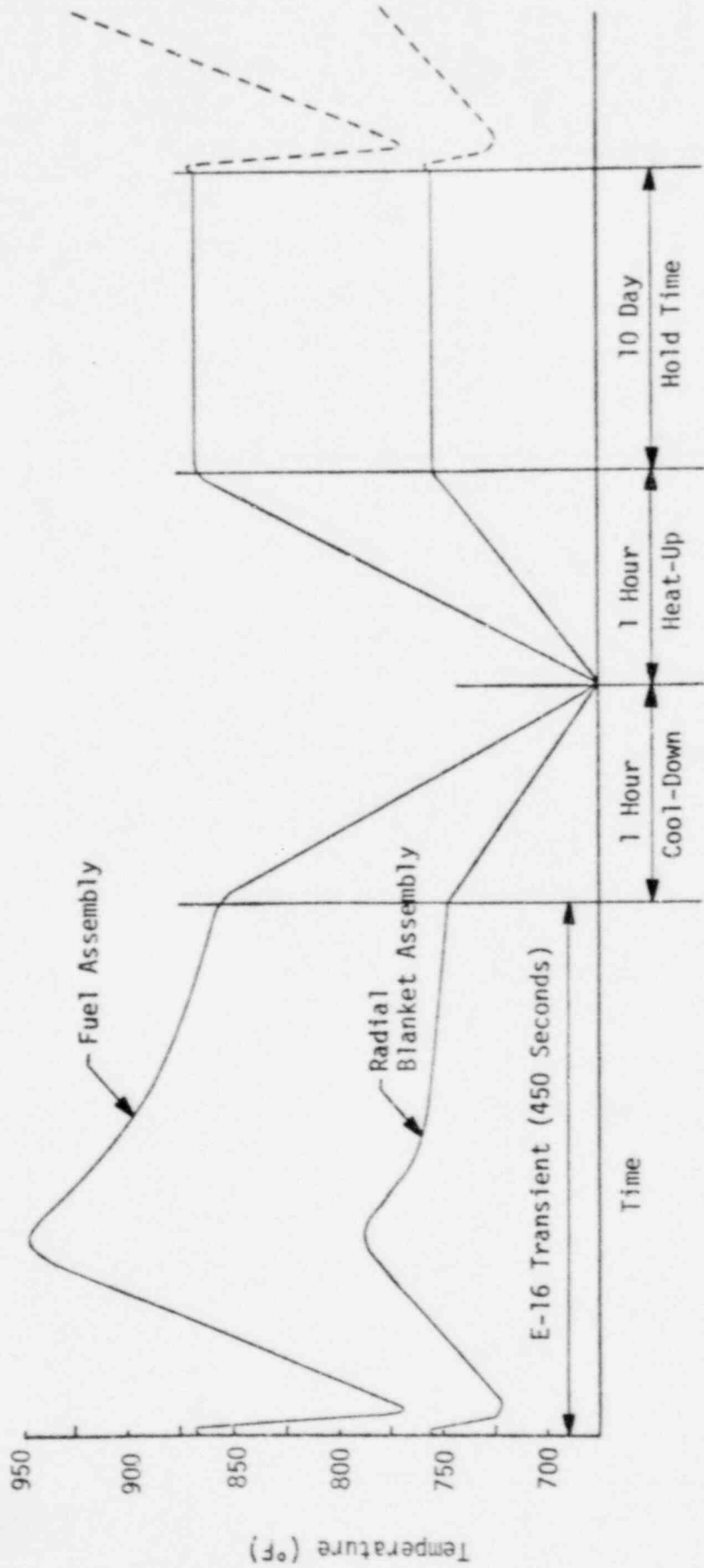


Figure 5.1-2  
 F/A CMP Hex Duct  
 Worst Case Duty Cycle

#### 5.1.2.1 Model and Geometry

The F/A CMP hex duct model was formulated in the ANSYS finite element program. The ANSYS program was selected because of the compatibility between thermal and structural elements which permits thermal solutions of temperature distributions to be used directly in subsequent structural analysis.

The F/A CMP hex duct region selected for analysis corresponds to a 2 dimensional 90° sector of the full CMP cross-section. As the worst case F/A CMP steady state and transient temperatures include adjacent C/A inside metal wall temperatures, an effective film coefficient was used to simulate the thermal resistance of the C/A wall. The effective C/A film coefficient ( $h$ ) was taken as the thermal conductivity ( $K$ ) divided by the wall thickness ( $L$ ) according to the relation,  $h = K/L$ . The effective film coefficient of the sodium in the CMP interstice gap in relation to the CMP hex duct itself was not found to be significant. The F/A CMP hex duct thermal model illustrating the dimensional extent and finite element detail is presented in Figure 5.1-3.

The F/A CMP hex duct 90° sector thermal model as formulated in the ANSYS program included a total of 354 linear temperature (STIF 35) elements in a mesh of 406 node points. A relatively fine mesh was selected in the corner adjacent to the global X-axis so as to include the thermal skin response to the thermal transients. Otherwise, a relatively coarse mesh was used throughout the 90° sector of the CMP cross-section.

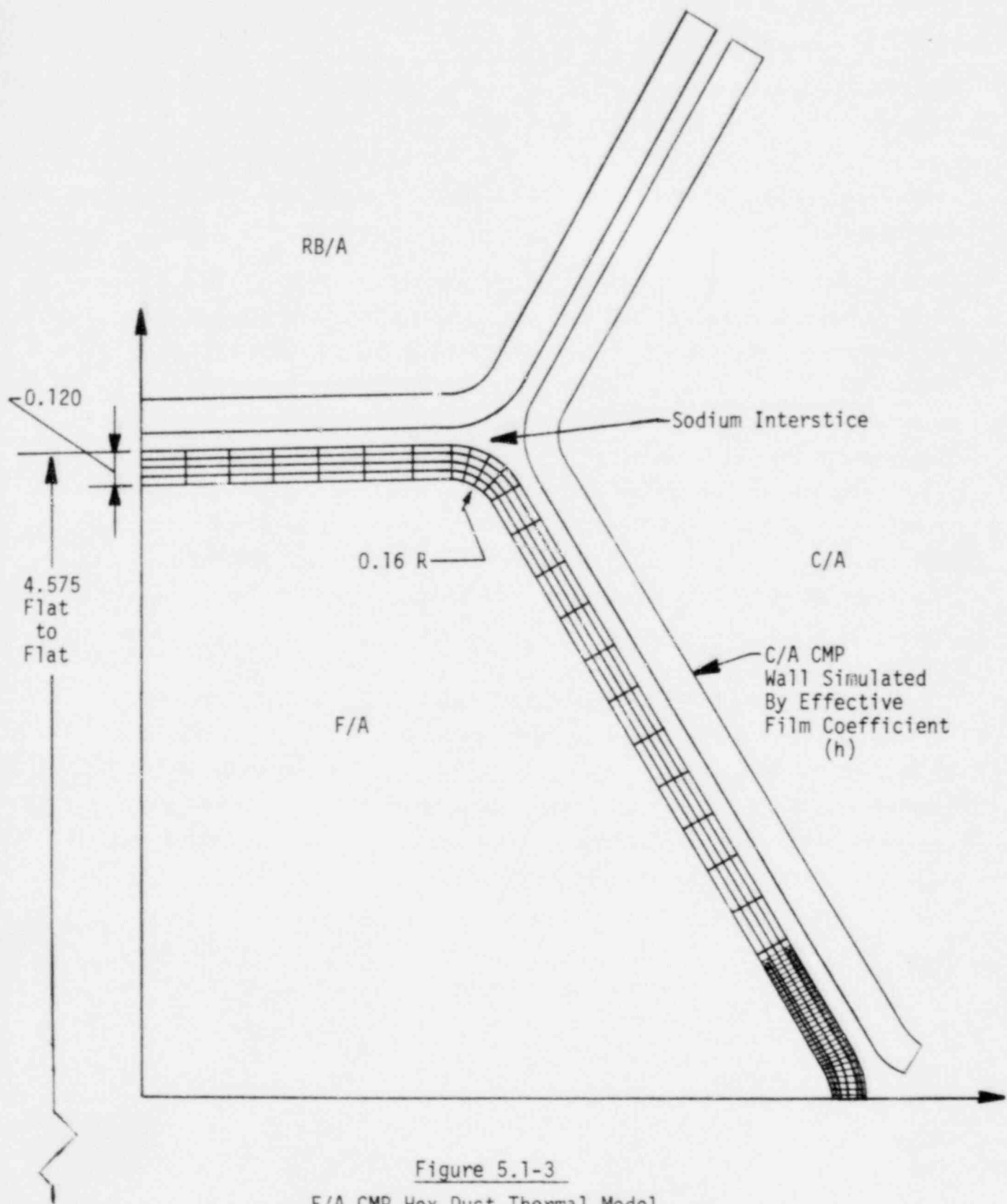


Figure 5.1-3  
 F/A CMP Hex Duct Thermal Model  
 Dimensional Extent and Finite Element Detail



#### 5.1.2.2 Properties

The F/A CMP hex duct is constructed from first core 20% CW-316-SS. The thermal conductivity (K), specific heat (C), and density ( $\rho$ ) of 20% CW-316-SS are known to not significantly differ from SA-316-SS values. Accordingly, the first core 20% 316-SS properties used in the F/A CMP hex duct thermal analysis were identical to the SA-316-SS properties identified for the F/A shield block described in Section 4.1.2.2.

#### 5.1.2.3 Boundary Conditions and Wetted Surfaces

The F/A CMP hex duct boundary conditions and wetted surfaces selected in the thermal analysis are illustrated in Figure 5.1-4.

Boundary conditions for the thermal analysis consisted of adiabatic conditions along the lateral surfaces coincident with the Global X and Y axes of the 90° sector model. In simulating the thermal resistance of the C/A CMP hex duct wall, the effective film coefficient ( $h=0.00164$  BTU/in<sup>2</sup>-sec-°F) was based on a thermal conductivity ( $K=0.000197$  BTU/in-sec-°F) and wall thickness ( $L=0.12$  in). The effective film coefficient ( $h$ ) was specified at the free surfaces of all elements forming the exterior of the F/A CMP hex duct which included elements 10 through 58, increments of 12; 254 through 262, increments of 8; and 266 through 354, increments of 4.

The wetted interior F/A CMP surfaces were assumed to respond immediately to the inside metal wall temperatures of the worst case F/A CMP duty cycle. Local variations in wetted interior surface temperatures were neglected. Instead, all F/A CMP hex duct interior surface node temperatures were globally coupled to each other and included Nodes 1 through 61, increments of 12; 73 through 280, increments of 9; and 287 through 402, increments of 5.

With regard to the wetted interior C/A CMP surfaces which are exposed to inside metal wall temperatures, local temperature variations were also neglected and a global variation assumed in the form of a Bulk Temperature. The bulk temperatures were specified in accordance with C/A inside metal

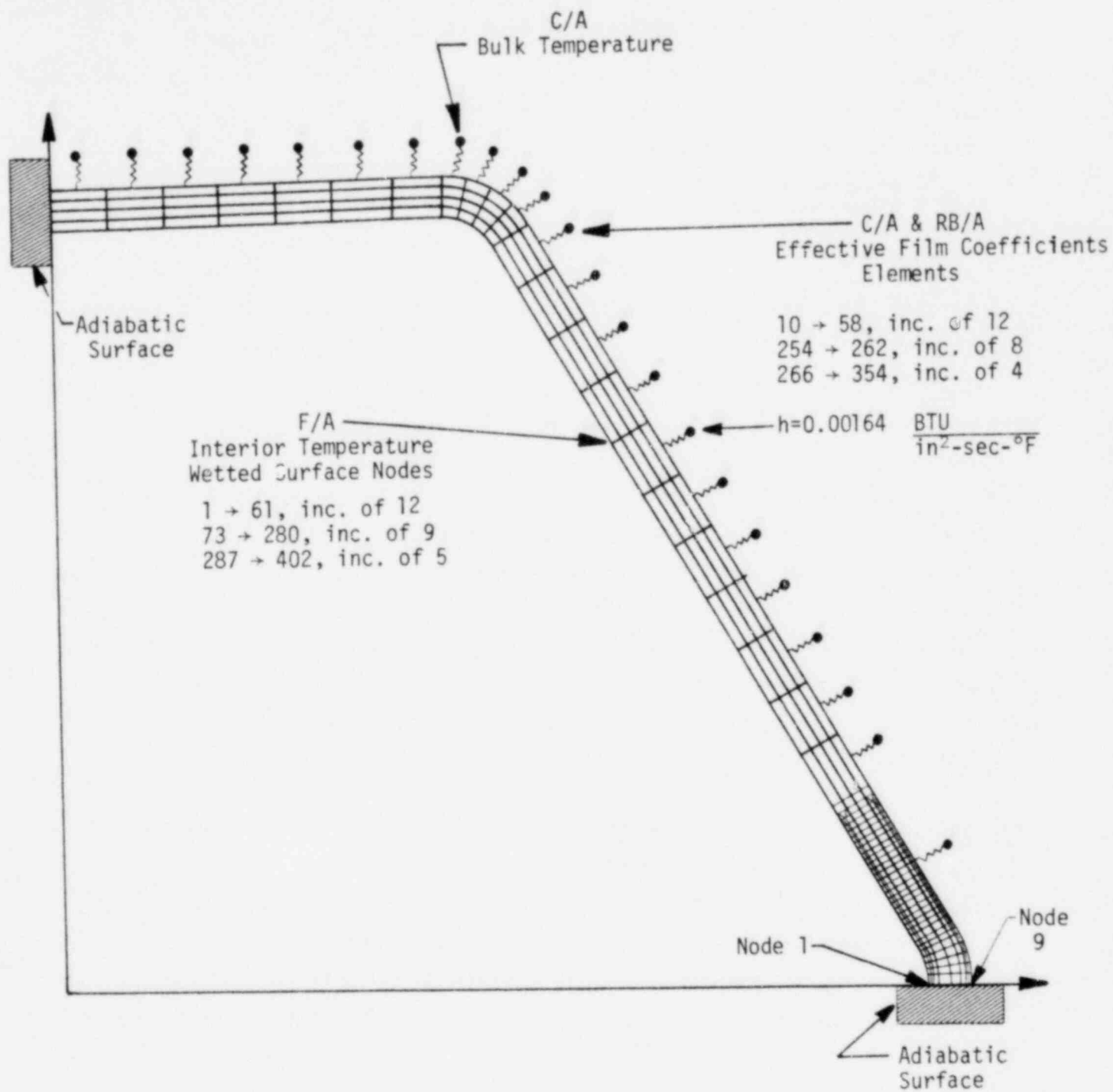


Figure 5.1-4  
F/A CMP Hex Duct  
Boundary Conditions and Wetted Surfaces

Surface temperature variations of the worst case F/A CMP hex duty cycle and applied to the F/A through the effective C/A wall film coefficients.

#### 5.1.2.4 Heat Generation Rates

During steady state operation, the F/A CMP hex duct is exposed to nuclear heating. The expected maximum and average CMP heating rates were 58 and 45 watts/cc respectively. The steady state F/A CMP metal temperatures include the average heating rate over the core region. Accordingly, only the difference between the maximum and average heating rates of 13 watts/cc or 0.20 BTU/in<sup>3</sup>-sec should be considered in the derivation of detailed CMP hex duct temperatures.

For the F/A CMP hex duct exposed to a heat generation rate (Q) with thermal conductivity (K) and wall dimension (L), the temperature difference ( $\Delta T$ ) is given by:

$$\Delta T = QL^2/2K$$

$$\Delta T = \frac{0.20 \text{ BTU/in}^3\text{-sec} (0.12 \text{ in})^2}{2(2.87 \times 10^{-4} \text{ BTU/in-sec-}^\circ\text{F})}$$

$$\Delta T = 5.01^\circ\text{F}$$

For the F/A CMP hex duct, the steady state temperature difference ( $\Delta T_{SS}$ ) caused by sodium flow was 126°F. As  $\Delta T \ll \Delta T_{SS}$ , the steady state temperature is insignificant, and heat generation rates were neglected in the thermal analysis

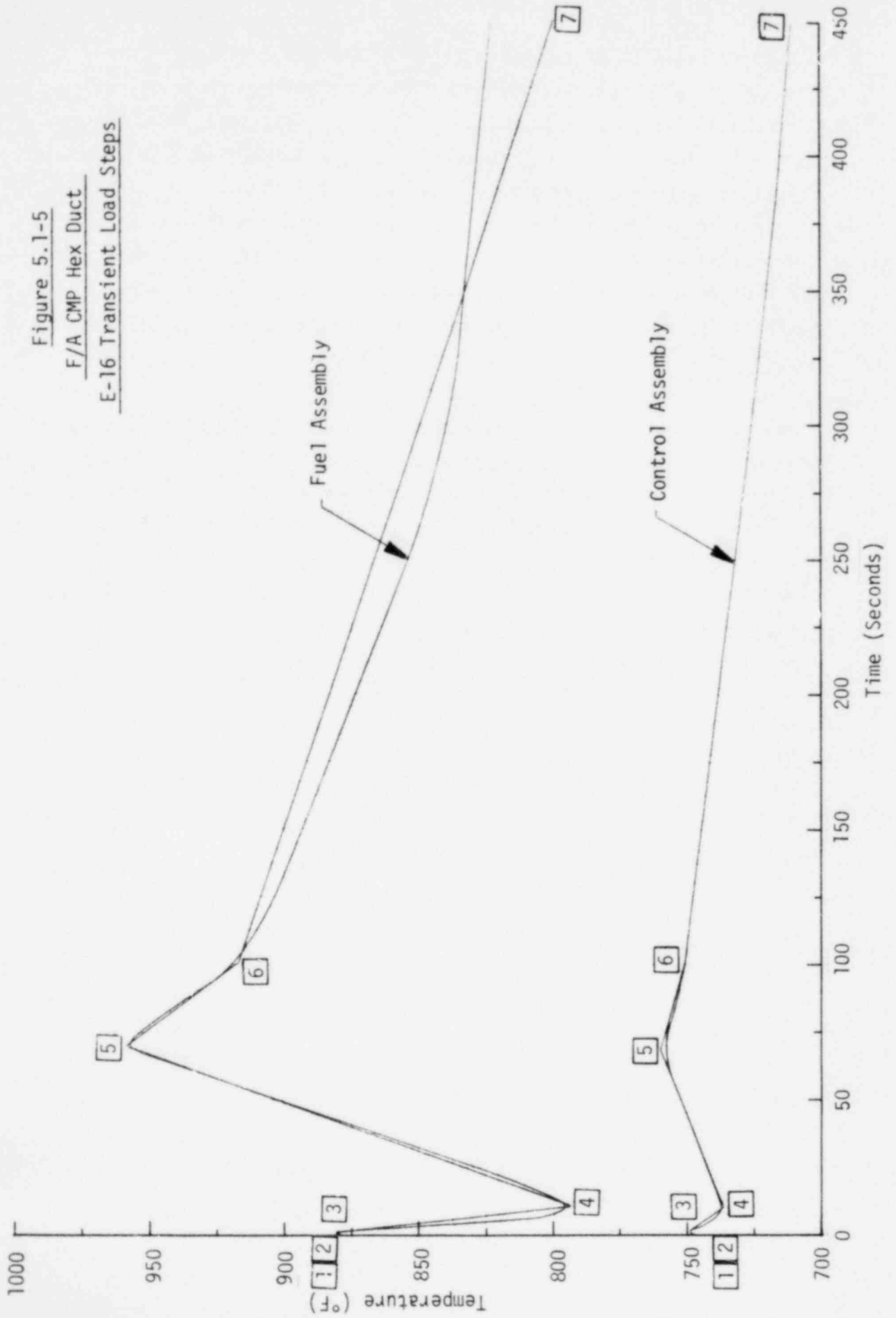
### 5.1.2.5 Analysis and Results

The ANSYS thermal analysis of the F/A CMP hex duct was arranged to provide detailed temperature distributions over the total worst case duty cycle. A total of 10 load steps were selected at prominent F/A and C/A inside metal surface temperatures. The first 7 Load Steps characterized the initial steady state conditions and the E-16 transient to 450 seconds. Load Steps 1 and 2 represent initial steady state conditions while Load Steps 3 through 7 correspond to the E-16 transient. Load Step 8 corresponds to the 1 hour cool-down to 600°F. The return to final steady state temperatures with the 1 hour heat-up was accomplished in Load Step 9. The final steady state temperatures held for 10 days were obtained in Load Step 10. Prominent Load Steps in the E-16 transient are illustrated in Figure 5.1-5 and numerical values for the full worst case F/A CMP hex duct duty cycle are presented in Table 5.1-2.

TABLE 5.1-2  
WORST CASE F/A CMP HEX DUCT DUTY CYCLE  
ANSYS INPUT DATA

Load Step	Time (Sec)	Temp (°F)	
		F/A	C/A
1	0.0	874	748
2	0.0	874	748
3	1.0	880	752
4	7.5	788	738
5	63	910	758
6	100	920	750
7	450	800	710
8	4050	600	600
9	7650	874	748
10	900000	874	748

Figure 5.1-5  
 F/A CMP Hex Duct  
 E-16 Transient Load Steps



The ANSYS solution of the worst case F/A CMP hex duct duty cycle was obtained in 47 cumulative iterations using a static and transient convergence criteria of 1 and 5°F, respectively. The temperature distributions at each cumulative iteration were saved on ANSYS Tape 4 for recall in subsequent structural analysis. In order to determine the cumulative iterations of interest in structural analysis, maximum and minimum through the wall temperature differences are most important in relation to structural damage. The F/A CMP hex duct temperature differences based on the through-the-wall temperatures at nodes 1 and 9 depicted in Figure 5.1-4 are illustrated in Figure 5.1-6.

A review of the through-the-wall temperature differences shows that the maximum and minimum values occur at cumulative iterations 27 and 37 respectively, with a range of 95°F. In the thermal solution run, cumulative iteration corresponds to the E-16 transient Figure 5.1-1. The initial steady state condition corresponds to cumulative iteration 2 with a temperature difference of 80°F. Plots of the temperature distributions throughout the F/A CMP hex duct thermal model at cumulative iterations 2 and 27 are presented in Figure 5.1-7.

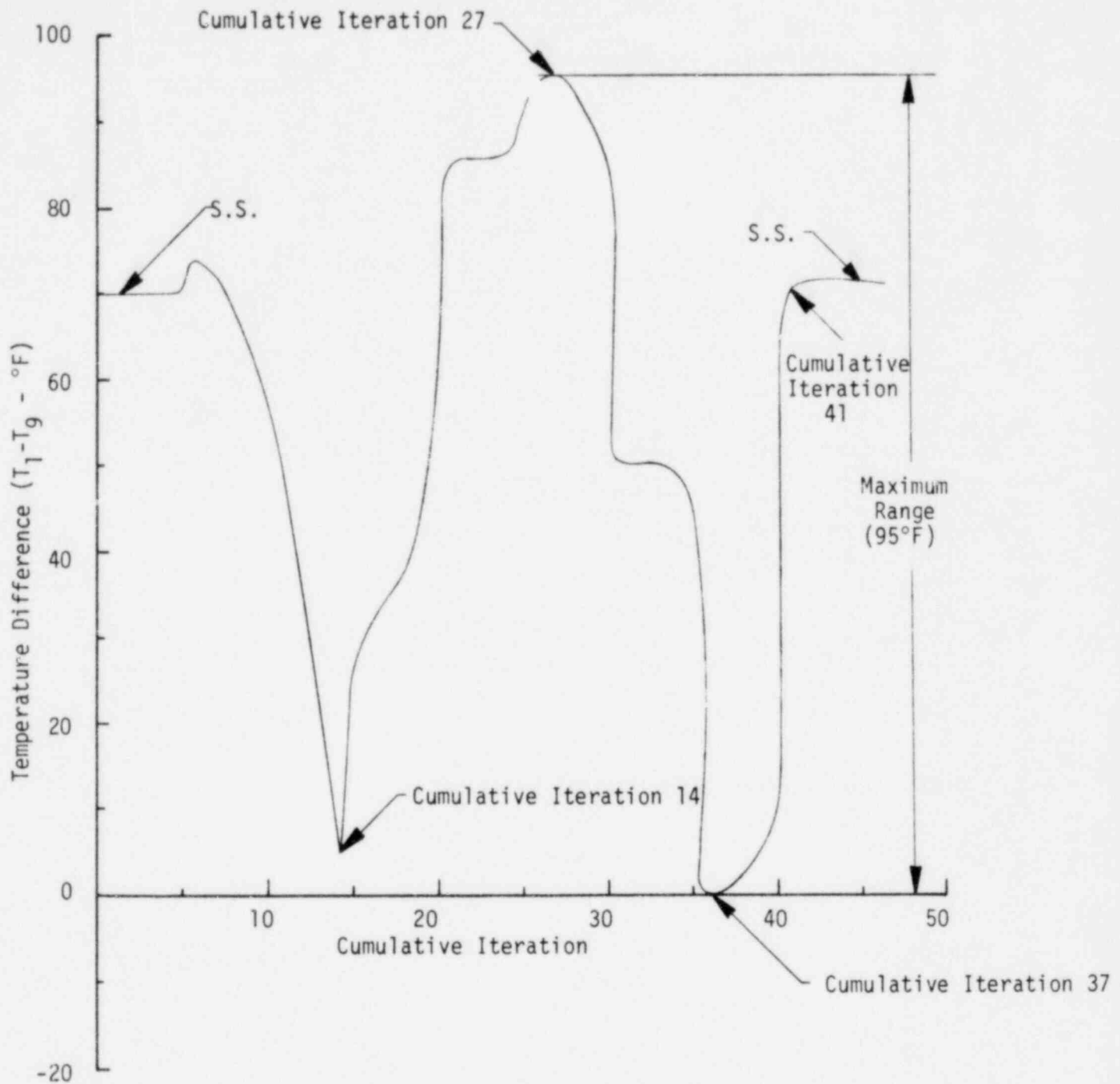


Figure 5.1-6  
 F/A CMP Hex Duct  
 E-16 Transient  
 Temperature Difference vs. Cumulative Iteration

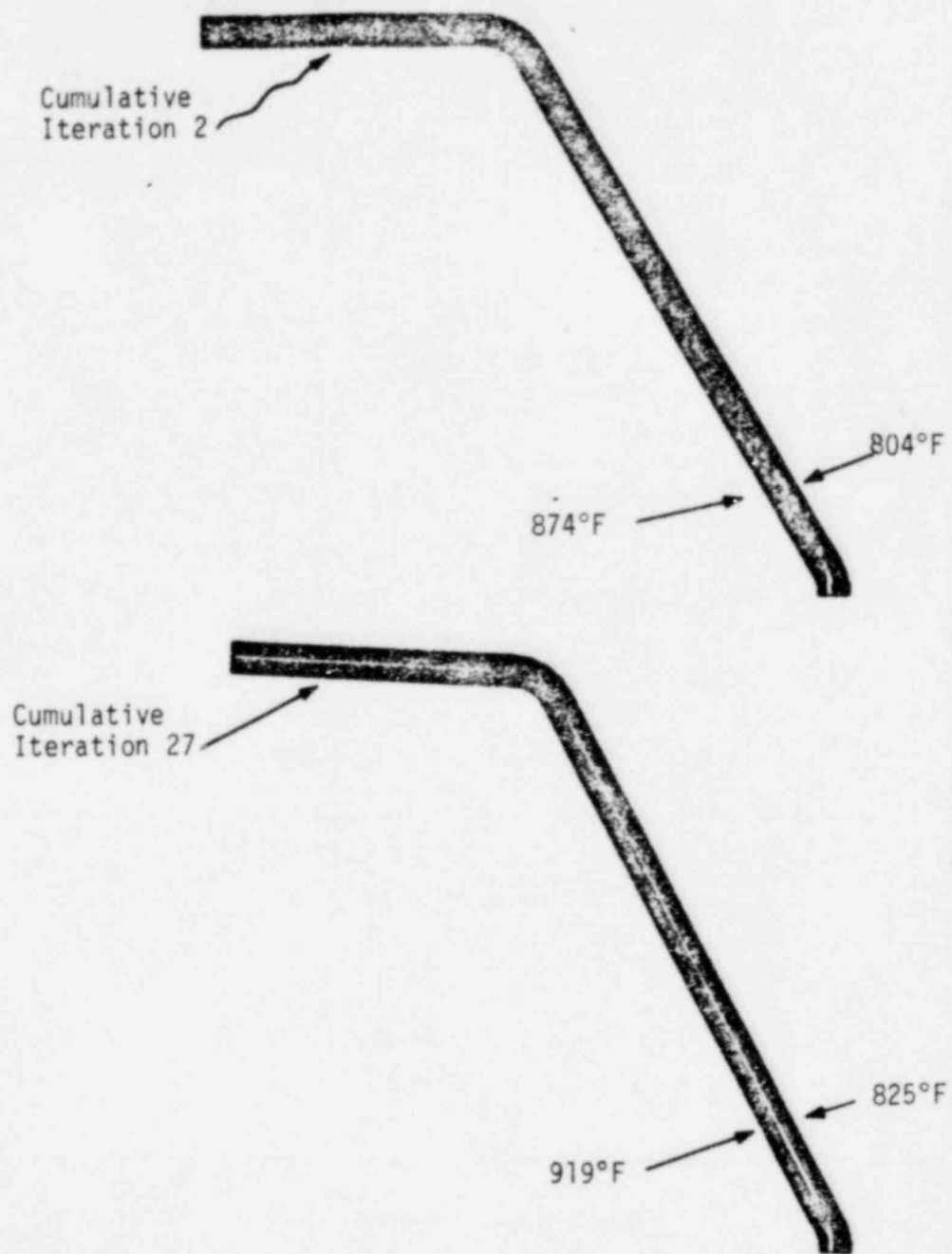


Figure 5.1-7  
F/A CMP Hex Duct  
E-16 Transient Cumulative Iterations 2 and 27  
Temperature Distributions



### 5.1.3 Worst Case Duty Cycle

The conclusions based on the F/A CMP hex duct loading analysis in relation to establishing the worst case duty cycle with recommendations for subsequent structural analysis were as follows.

- Mechanical loads comprising OBE and SSE beam bending, internal pressure, and deadweight were considered insignificant. Local inter-duct contact loads are non-existent. Only beam bending loads caused by core restraint under steady state operation were considered to be of significance in establishing the worst case F/A CMP hex duct duty cycle.
- Thermal loads associated with the E-16 transient in combination with the thermal conditions in returning to steady state and the hold-time prior to the initiation of the next E-16 transient were considered most important in establishing the worst case F/A CMP hex duct duty cycle.

The recommendations for the specific F/A CMP hex duct loading in relation to the worst case duty cycle were arranged into combined mechanical and thermal time independent and dependent loadings. The following sequence for the worst case F/A CMP hex duct cycle was recommended to be repeated 39 times so as provide an upper bound to the 39 specified Upset events, and the worst Emergency or Faulted event.

#### Time Independent

- Select a uniform temperature equal to the reference temperature at cumulative iteration 2. Load to the cumulative iteration 2 temperature distribution and apply the steady state core restraint bending moment. Unload to uniform temperature.
- Select a uniform temperature equal to the reference temperature at cumulative iteration 27. Load to the cumulative iteration 27 temperature distribution and apply the transient bending moment. Unload to uniform temperature.

- Select a uniform temperature equal to the reference temperature at cumulative iteration 2. Load to the cumulative iteration 2 temperature distribution and apply the steady state core restraint bending moment.

#### Time Dependent

- Hold the cumulative iteration 2 temperature distribution in combination with the steady state core restraint bending moment for 10 days.

## 5.2 Structural Analysis

The F/A CMP hex duct structural analysis was directed to deriving the stresses, strains and dimensional changes which occur during the worst case duty cycle from which structural evaluations were made. In the following, the F/A CMP hex duct structural model, geometry, and boundary conditions are described. Next, linear and non-linear material properties including the effects of irradiation on stress-strain curves and simplifications made in the thermal creep equations are presented. Further, reference temperature selection for thermal expansions in relation to axial constraints is described. Finally, the time independent and dependent inelastic analysis and results for the F/A CMP hex duct are presented in preparation for subsequent structural evaluation.

### 5.2.1 Model, Geometry and Boundary Conditions

The F/A CMP hex duct model was formulated in the ANSYS finite element program so as to be compatible with the temperature distributions of the thermal model. The F/A CMP geometry was taken to be identical to that used for the thermal analysis, except that the film coefficients simulating the C/A CMP wall thermal resistance were deleted.

In formulating the F/A CMP hex duct structural model, the ANSYS constant strain (STIF 2) structural element was used to replace the linear temperature (STIF 35) thermal element. The boundary conditions along the lateral surfaces of the 90° sector coincident with the global X and Y axes, in the manner of the conventional roller support, were taken to have zero normally disposed displacements, but free to move laterally. Along the surface coincident with the global X axis, the UY displacements at nodes 1 through 9 were set equal to zero. For the surface coincident with the global Y axis, the UX displacements at nodes 402 through 406 were set equal to zero. The F/A CMP hex duct structural model is illustrated in Figure 5.2-1.

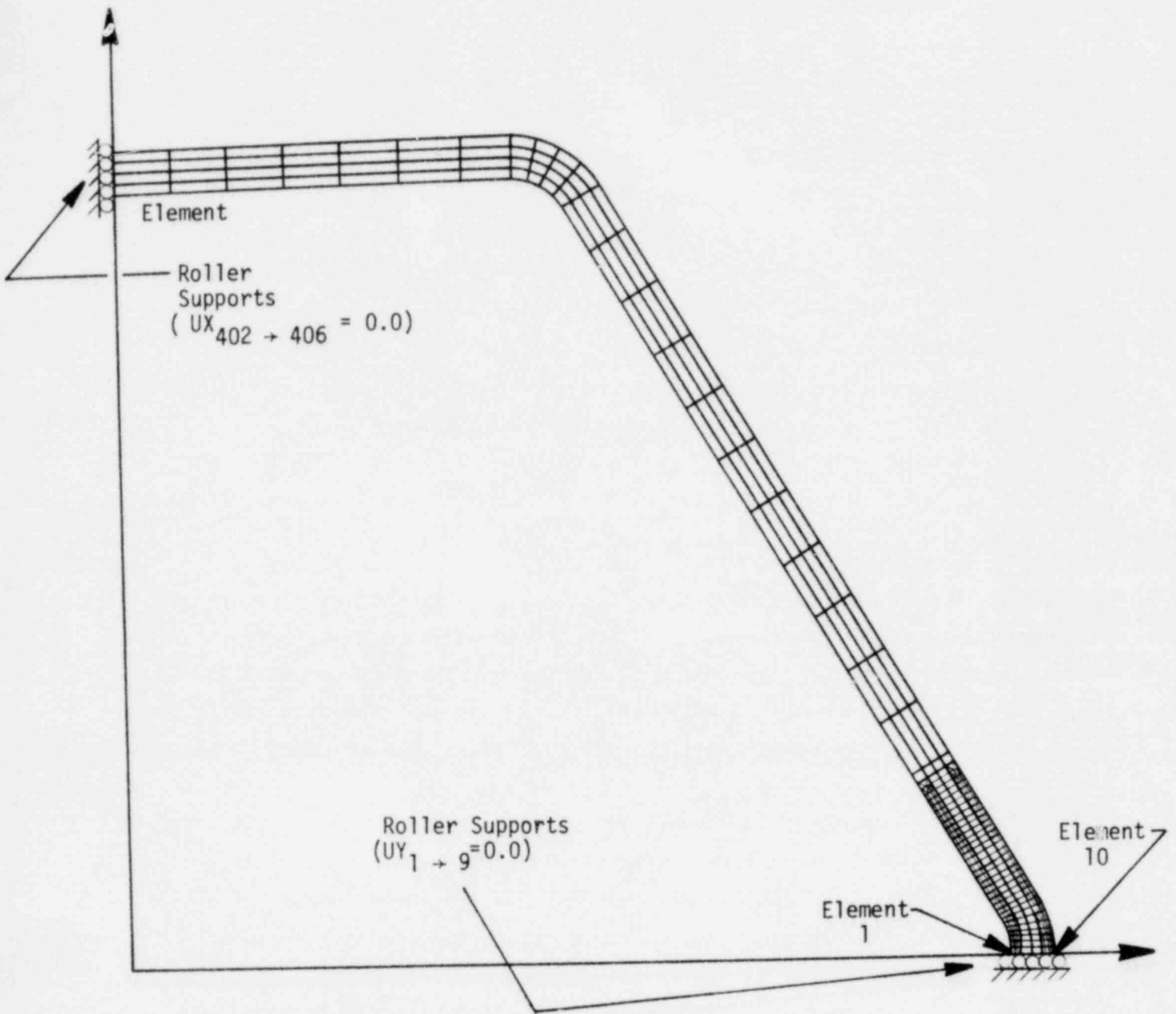


Figure 5.2-1  
 F/A CMP Hex Duct  
 Structural Model, Geometry, and Boundary Conditions

## 5.2.2 Properties

The F/A CMP hex duct as constructed from first core 20% CW-316-SS and initially unirradiated at BOL is irradiated to a fluence ( $E > 0.1$  Mev,  $(\phi t) = 9.29 \times 10^{22}$  N/CM<sup>2</sup>) at EOL. The linear and non-linear properties of first core 20% CW-316-SS under fluence and temperature with simplifications used in the F/A CMP hex duct analysis are described as follows.

### 5.2.2.1 Linear

The linear 20% CW-316-SS properties including the Young's Modulus (E), Poisson's ratio ( $\nu$ ), and coefficient of thermal expansion ( $\alpha$ ) are known to not significantly differ from SA-316-SS values. Accordingly, the first core 20% CW-316-SS properties used in the F/A CMP hex structural analysis were identical to the SA-316-SS properties identified for the F/A shield block described in Section 4.2.2.1.

### 5.2.2.2 Non-Linear

The non-linear first core 20% CW-316-SS material property behavior required in the F/A CMP hex duct structural analysis are the time independent stress-strain curves and the time dependent thermal creep equations.

#### 5.2.2.2.1 Stress-Strain Curves

Currently, stress-strain properties of first core 20 percent CW-316-SS are not extensively known as prior experimental effort has been primarily directed to N-Lot steel. The available stress-strain properties of first core steel [11] are limited to fluence ( $E > 0.1$  Mev) to  $3 \times 10^{22}$  N/CM<sup>2</sup> over a temperature range from 1000 to 1200°F. As the CMP hex duct EOL fluence ( $E > 0.1$  Mev) is  $9.29 \times 10^{22}$  N/CM<sup>2</sup>, the available data requires extrapolation in order to obtain first core 20% CW-316-SS stress-strain data for use in the F/A CMP hex duct analysis.

In the F/A CMP hex duct analysis, the first core 20% CW-316-SS stress-strain data of importance are the proportional elastic limit stresses as time independent mechanical and thermal loadings are relatively low and elastic analysis was justified.

The available first core 20% CW-316-SS true minimum proportional elastic limit stress ( $\sigma_{PEL}$ ) was taken as 86 percent of the minimum engineering yield stress ( $\sigma_{Y, MIN}$ ).

$$\sigma_{PEL} = 0.86 \sigma_{Y, MIN}$$

The minimum engineering yield stress ( $\sigma_Y \sim$  KSI) data identified in Reference [11] was fit to a polynomial in temperature ( $T \sim$  °F  $\times 10^{-2}$ ) according to the relation:

$$\sigma_{Y, MIN} = 60.596 - 0.817 * T - 0.0601 * T^2$$

Numerical values of the true minimum proportional elastic limit stress ( $\sigma_{PEL}$ ) as a function of temperature are summarized in Table 5.2-1.

Table 5.2-1  
F/A CMP Hex Duct  
Minimum Yield and Proportional Elastic Limit Stress  
First Core 20% CW-316-SS

Temp (°F)	$\sigma_{Y, MIN}$ (KSI)	$\sigma_{PEL}$ (KSI)
800	50.21	43.18
850	49.31	42.41
900	48.37	41.60
950	47.41	40.77
1000	45.42	39.06

#### 5.2.2.2.2 Thermal Creep Equations

The steady state F/A CMP hex duct temperatures cover the temperature range of 800 to 875°F. Calculations for these conditions with the unirradiated 20% CW-316-SS thermal creep equations for thermal creep of N-lot (interim NSMH equations [12]) and first core [24] lots indicate that thermal creep was negligible. Accordingly, thermal creep during time dependent mechanical and thermal loadings was neglected for the F/A CMP hex duct.

### 5.2.3 Worst Case Duty Cycle Response

The structural response of the F/A CMP hex duct to the worst case duty cycle loading comprised of combined mechanical and thermal loadings required an analytical approach different from that used for the F/A shield block and outlet nozzle where thermal loadings alone formed the basis for the respective duty cycles. The structural response associated with the time independent and time dependent thermal loadings were derived independently of the mechanical loading response and combined by superposition. Superposition of thermal and mechanical structural response, in terms of stresses and strains, was justified because the F/A CMP hex duct remained linear elastic throughout the worst case duty cycles. The superposition of mechanical stresses and strains is described in the F/A CMP hex duct structural evaluation. In the following, the analysis and thermal structural response solutions for the F/A CMP hex duct are presented.

#### 5.2.3.1 Constraints and Reference Temperature Selection

The F/A CMP hex duct corresponds to a 90° sector of a lateral slice taken through the length of the hex duct at CMP. For through the wall thermal loadings, axial constraints normal to the 2 dimensional 90° sector closely simulate a plane strain condition as the length of the hex duct is significantly greater than corresponding cross-sectional dimensions. Accordingly, the F/A CMP hex duct was considered to be in a plane strain condition for the purposes of deriving the structural response to thermal loadings.

The method of selecting a reference temperature in relation to an arbitrary temperature distribution imposed on an ANSYS plane strain model was described for the F/A shield block in Section 4.2.3.1. Using the same method for the F/A CMP hex duct, the reference temperatures for the recommended cumulative iterations in the worst case duty cycle are summarized in Table 5.2-2.



TABLE 5.2-2  
F/A CMP Hex Duct  
REFERENCE TEMPERATURES

Temperature Distribution (Cum. Iter.)	Reference Temperature (°F)
2	836.6
27	872.5

5.2.3.2 Analysis and Results

The ANSYS elastic analysis of the F/A CMP hex duct structural model under the worst case thermal duty cycle was arranged into a time independent analysis of the short term E-16 transient followed by a time dependent analysis at steady state temperatures over the 10 day hold-time. In order to obtain the thermal structural response in an efficient manner, the ANSYS restart option was used to follow the loading sequence within, between, and after the time independent and dependent loadings. As elastic or creep instability would not be expected for the F/A CMP hex duct under the deformation controlled thermal loadings, the ANSYS small-strain small deformation option was used in the elastic analysis. Descriptions of the time independent and dependent analysis and results are as follows.

5.2.3.2.1 Time Independent

The time independent ANSYS analysis of the F/A CMP hex duct was directed to deriving the peak elastic strains and deformations associated with the thermal loadings from initial steady state through the E-16 transient followed by a return to final steady state, but excluding the 10 day hold-time. The time independent loadings were considered as static loads applied at zero time. A total of 8 sequential ANSYS Load Steps in combination with the restart option were used to obtain the time independent structural response of the F/A CMP hex duct, a summary of which is presented in Table 5.2-3.

TABLE 5.2-3  
F/A CMP HEX DUCT  
TIME INDEPENDENT ANALYSIS SUMMARY  
INITIAL STEADY STATE, E-16 TRANSIENT, AND FINAL STEADY STATE

Load Step	Iterations	Temperature Distribution (°F)	Reference Temperature (°F)	Description
1	1	836.6	836.6	Initial Steady State (0.0 SEC.)
2	1	Cum. Iter. 2	836.6	
3	1	836.6	836.6	
4	1	872.5	872.5	E-16 Transient (100 SEC.)
5	1	Cum. Iter. 27	872.5	
6	1	872.5	872.5	
7	1	836.6	836.6	Final Steady State (7650 SEC.)
8	1	Cum. Iter. 2	836.6	

The F/A CMP hex duct structural response to the time independent loadings in terms of elastic stresses and strains were saved on ANSYS Tape 10 for subsequent recall in structural evaluations. The initial and final time independent steady state maximum equivalent stress was found to be 13,128 psi. During the E-16 transient, the maximum equivalent stress at cumulative iteration 27 was 17,179 psi. The peak non-uniform deformation was found to occur at cumulative iteration 27 with a value of 0.00026 in., while the maximum initial and final steady state non-uniform deformations were 0.00017 in. Computer plots of time independent equivalent stress and deformations are presented in Figures 5.2-2 and -3.

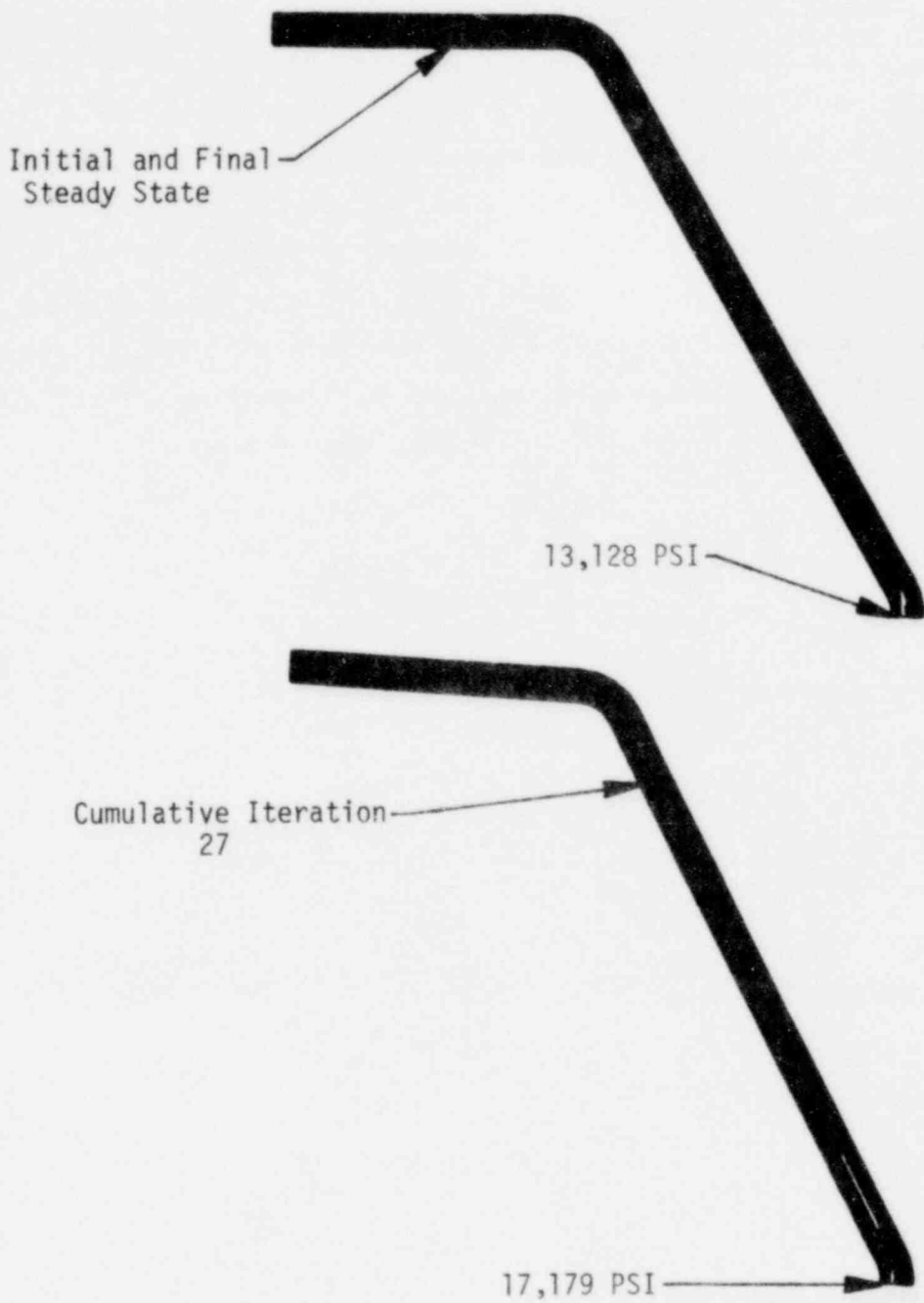


Figure 5.2-2  
F/A CMP Hex Duct  
Steady State and Cumulative Iteration 27  
Equivalent Stress  
Time Independent

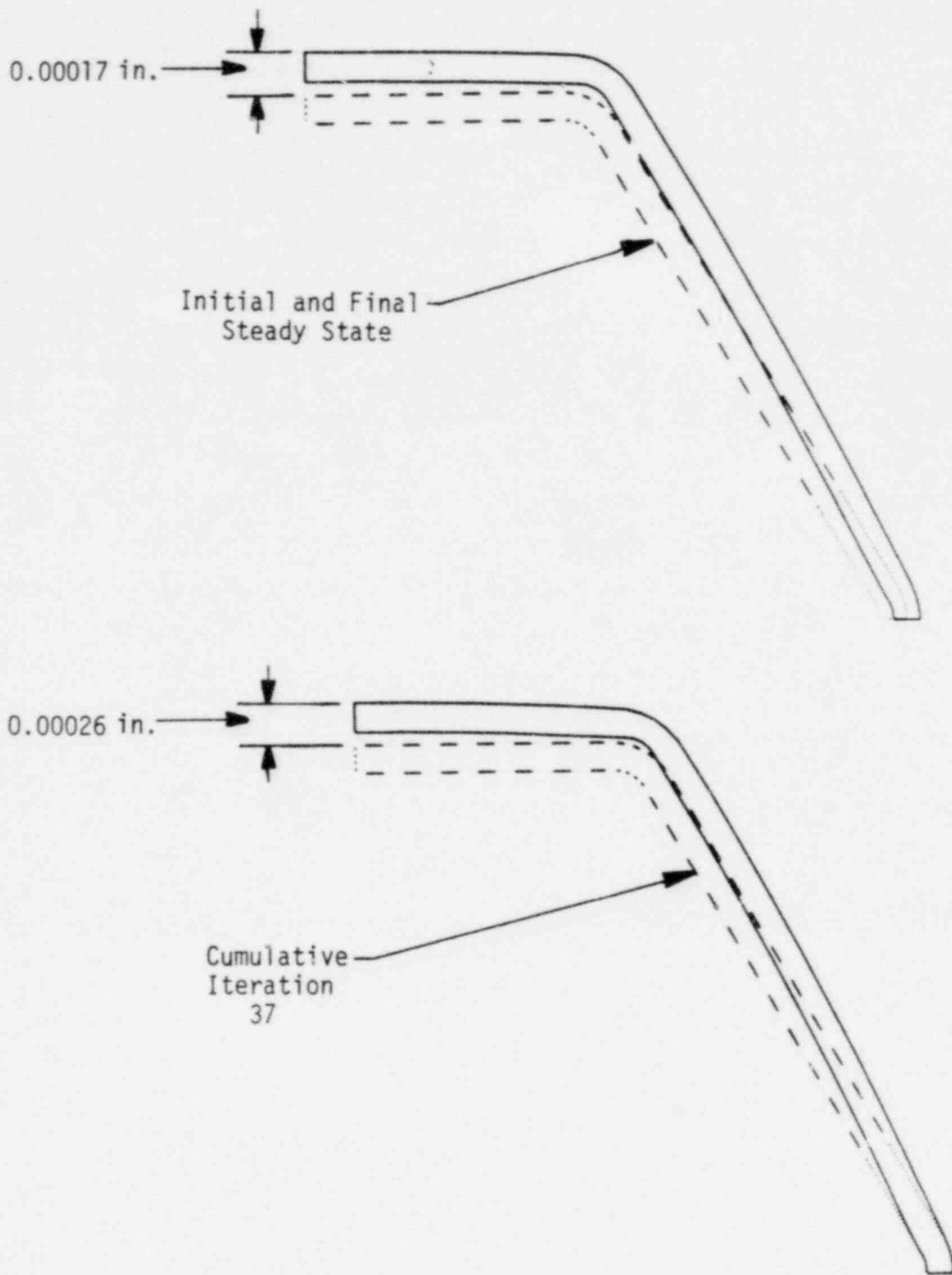


Figure 5.2-3  
 F/A CMP Hex Duct  
 Steady State and Cumulative Iteration 27  
 Non-Uniform Deformations  
 Time Independent

#### 5.2.3.2.2 Time Dependent

The time dependent ANSYS analysis of the F/A CMP hex duct was directed to deriving the final time dependent steady state structural response associated with the 10 day hold-time at final time independent steady state conditions. The time dependent analysis was performed with Load Step 9 using an ANSYS restart from Load Step 8 of the time independent analysis at the cumulative iteration 2 temperature distribution and maintained for 10 days or 240 hours. As thermal creep was neglected in the time dependent analysis, a redistribution of the time independent stresses would not occur. Accordingly, only one iteration at a creep time step of 240 hours was used in Load Step 9.

The F/A CMP hex duct structural response for the time dependent loading was identical to the time independent final steady state response as thermal creep was neglected. Accordingly, the final time dependent steady state maximum equivalent stress and non-uniform deformations are identical to the final time dependent values illustrated in Figures 5.2-2 and -3.

With regard to the residual non-uniform deformations of the F/A CMP hex duct, none would occur because the F/A CMP hex duct remains linear elastic over the worst case duty cycle.

### 5.3 Structural Evaluations

The F/A CMP hex duct structural evaluation was arranged to provide a comparison of the structural response for the 39 worst case duty cycles in relation to criteria which protect against crack initiation and excessive deformation failure modes and thereby assure F/A CMP hex duct function over the first and second reactor cycles.

The procedure for performing the F/A CMP hex duct structural evaluations in relation to crack initiation and excessive deformation criteria was identical to that used for the F/A shield block thermal stresses and strains presented in Section 4.3, except as modified to superpose the time independent transient and time dependent core restraint mechanical bending stresses and strains. A linear superposition of the thermal and mechanical bending stresses and strains is justified, as combined stresses are less than the proportional elastic limit stresses identified for first core 20% CW-316-SS in Table 5.2-1.

In order to perform a true superposition of mechanical bending stresses and strains with the thermal stresses and strains in the 90° sector of the F/A CMP hex duct, a linear variation of mechanical bending stress and strain about the neutral axis of the CMP hex duct would be summed algebraically with the local thermal stresses and strains. However, a true superposition was not made. Instead, a simpler, yet conservative, approach was adopted which consisted of superposing the peak outer fiber mechanical bending stresses and strains uniformly over the full cross-section of the F/A CMP hex duct 90° sector. In essence, the full F/A CMP hex duct cross-section was placed in a uniaxial stress and strain state equal to the peak outer fiber bending values. By using both positive and negative peak outer fiber bending values, the true superposition of mechanical and thermal stresses and strains was conservatively bracketed between tensile and compressive values. The peak bending stresses and strains for the mechanical transient and core restraint bending moments used in the superposition were 11,650 psi and  $5 \times 10^{-4}$  in/in as identified in Table 5.1-1.

The superposition of peak outer fiber mechanical and thermal stresses and strains was made in conjunction the structural evaluation of crack initiation failure modes using the damage processor. Local ductile rupture and combined creep-fatigue damage factors were computed for each element in the F/A CMP hex duct model for 3 sets of mechanical bending stress-strain values, that is, (+ 11,650 PSI, + 5 x 10<sup>-4</sup> in/in), (- 11,650 PSI, - 5 x 10<sup>-4</sup> in/in), and (0 PSI, 0 in/in). Of these sets of mechanical bending stresses and strains, the worst combination with the local thermal stress and strain state in terms of maximum local ductile rupture and combined creep-fatigue damage factors were used in comparison with allowable limits.

A summary of the F/A CMP hex duct structural evaluation and summary of results is presented as follows.

### 5.3.1 Crack Initiation

The F/A CMP hex duct structural evaluation of crack initiation in relation to local ductile rupture and combined creep-fatigue damage criteria over the 39 worst case duty cycles is presented in the following subsections.

#### 5.3.1.1 Local Ductile Rupture

The local ductile rupture criterion in protecting against crack initiation requires that the ductile rupture factor ( $F_{DR}$ ) be less than unity at each point in the F/A CMP hex duct.

$$F_{DR} = \text{Maximum of} \left( \begin{array}{l} \bullet \frac{(\epsilon_{\max \text{ principal}})_{TF}}{0.3 \epsilon_{f, \min.}} \\ \bullet \frac{(\epsilon_{\max \text{ principal}})_{TF}}{\epsilon_{u, \min.}} \end{array} \right)$$



In the following, the allowable uniaxial strains used in the F/A CMP hex duct structural evaluation and comparison of results with the local ductile rupture factor criterion are presented.

#### 5.3.1.1.1 Allowable Uniaxial Strains

The F/A CMP hex duct as constructed from first core 20% CW-316-SS is unirradiated at BOL. The EOL fluence ( $E > 0.1$  Mev) is  $9.29 \times 10^{22}$  N/cm<sup>2</sup>. In addition, the F/A CMP hex duct temperatures range from 600 to 1000°F. The true minimum uniaxial uniform elongation ( $\epsilon_{u, \min}$ ) and fracture ( $\epsilon_{f, \min}$ ) strains for unirradiated and irradiated first core 20% CW-316-SS as a function of fluence and temperature used in the F/A CMP hex duct structural evaluation are described as follows.

##### 5.3.1.1.1.1 Uniform Elongation

Currently, uniform elongation data [11] for first core 20% CW-316-SS is limited to a fluence ( $E > 0.1$  Mev,  $(\phi t) = 3 \times 10^{22}$  N/cm<sup>2</sup>) and a temperature range of 1000 to 1200°F. In order to apply the available first core 20% CW-316-SS data to the F/A CMP fluence and temperatures, extrapolations were made. Specifically, the minimum engineering uniform elongation ( $\bar{\epsilon}_{u, \min} \sim$  in/in) data was fit to a polynomial in temperature ( $T \sim 10^{-2}$  °F) according to the relation:

$$\bar{\epsilon}_{u, \min} = 0.128 + 0.0108 * T + 0.000938 * T^2 - 0.00018 * T^3$$

The true minimum uniform elongation ( $\epsilon_{u, \min}$ ) used in the F/A CMP hex duct structural evaluation in terms of the minimum engineering uniform elongation ( $\bar{\epsilon}_{u, \min}$ ) were taken as:

$$\epsilon_{u, \min} = \ln (1 + \bar{\epsilon}_{u, \min})$$

#### 5.3.1.1.1.2 Fracture

Uniaxial fracture strain data for first core 20% CW-316-SS is currently not available for use in the F/A CMP hex duct structural evaluation. Accordingly, the true uniaxial fracture strain based on unirradiated and irradiated SA-304-SS and SA-316-SS recommended by General Electric for 20% CW-316-SS in the trial applications of the RDT Draft for Breeder Reactor Core Components [15-23] identified for the F/A shield block in Section 4.3.1.1.1 were also used in the structural evaluation of F/A CMP hex duct.

#### 5.3.1.1.2 Comparison with Criterion

The F/A CMP hex duct structural evaluation in relation to the worst case location for local ductile rupture was made by screening each of the finite elements over the 39 worst case duty cycles with the damage processor. Individual structural evaluations were made for the 3 sets of bending stresses and strains in order to obtain the worst case superposition. The maximum F/A CMP hex duct local ductile rupture factor ( $F_{DR}$ )<sub>max</sub> was found to occur for the case of tensile superposition at element 10 as identified in Figure 5.2-1.

The peak BOL strain components occurred at the cumulative iteration 27 temperature distribution in the E-16 transient where the local metal temperature was 827°F. Accumulated BOL strain components were based on the difference between final time dependent and initial time independent steady state conditions. The EOL maximum principal strain for the peak BOL and accumulated BOL strain components over the 39 worst case F/A CMP hex duct duty cycles was 0.00099 in/in. The triaxiality factor for the local stress state was 1.692. The true minimum irradiated uniform elongation and fracture strains at EOL fluence ( $E > 0.1$  Mev,  $(\phi t) = 9.29 \times 10^{22}$  N/cm<sup>2</sup>) were 0.166 and 0.0768 in/in respectively.

In this arrangement, the maximum local ductile rupture factor  $(F_{DR})_{max}$  for the F/A CMP hex duct was found to be controlled by the fracture strain with a value,

$$(F_{DR})_{max} = 0.0727$$

As  $(F_{DR})_{max} < 1.0$ , the F/A CMP hex duct is not expected to experience crack initiation over the 39 worst case duty cycles based on the local ductile rupture criterion.

#### 5.3.1.2 Creep-Fatigue Damage

The creep-fatigue damage criterion in protecting against crack initiation requires that the combined creep fatigue damage factor  $(F_{CFD})$  be less than unity at each point in the F/A CMP hex duct.

$$F_{CFD} = a/b = \text{Minimum of } \left\{ \begin{array}{l} \bullet 7/3 D^C + D^f \\ \bullet D^C + 7/3 D^f \end{array} \right\}$$

In the following, the allowable limits for fatigue life and creep-rupture times used in the F/A CMP hex duct structural evaluation and a comparison of results with the combined creep-fatigue damage factor criterion are presented.

##### 5.3.1.2.1 Allowable Limits

The F/A CMP hex duct as constructed from first core 20% CW-316-SS is irradiated to an EOL fluence ( $E > 0.1$  Mev) of  $9.29 \times 10^{22}$  n/cm<sup>2</sup>. In addition, the F/A CMP hex duct temperatures range from 600 to 1000°F with the wetted sodium surfaces subjected to oxidation as well as interstitial transfer of carbon and oxygen. The fatigue life and time to rupture data for first core 20% CW-316-SS including the effects of fluence, temperature, interstitial transfer, and surface oxidation used in the F/A CMP hex duct structural evaluation are described as follows.

### 5.3.1.2.1.1 Fatigue Life

Currently, fatigue life correlations are not available for irradiated first core 20% CW-316-SS as a function of fluence and temperature. Accordingly, the Manson Universal Slopes Method [7] was used to develop fatigue life correlations from which the fatigue damage factor ( $D^f$ ) for the F/A CMP hex duct over the 39 worst case duty cycles was derived.

In the Manson Universal Slopes Method, the slopes of elastic and plastic strain lines expressed in terms of strain range versus number of cycles on a full logarithmic plot are assumed to be the same for all materials. As applied to unirradiated 20% CW-316-SS, the total strain range ( $\Delta\epsilon$ ) is dependent on the minimum unirradiated true fracture strain ( $\epsilon_{f,u}$ ), average unirradiated engineering ultimate strength ( $S_{u,u}$ ), Young's Modulus ( $E$ ), and cycles to failure ( $N_f$ ) by the relation:

$$\Delta\epsilon = \epsilon_{f,u}^{0.6} N_f^{-0.6} + \frac{3.5 S_{u,u}}{E} N_f^{-0.12}$$

In order to include the effects of irradiation in the fatigue life relation for SA-316-SS, reduction factors for the elastic ( $F_e$ ) and plastic ( $F_p$ ) strain ranges were used in accordance with the guidelines of the RDT Draft for Breeder Reactor Core Components [5].

$$\Delta\epsilon = F_p \epsilon_{f,u}^{0.6} N_f^{-0.6} + \frac{3.5 F_e S_{u,u}}{E} N_f^{-0.12}$$

$$\text{Where, } F_e = \left(\frac{S_{u,I}}{S_{u,u}}\right)^{k_2}$$

$$F_p = \left(\frac{\epsilon_{f,I}}{\epsilon_{f,u}}\right)^{k_1}$$

$\epsilon_{f,I}$  = True Minimum Irradiated Fracture Strain

$S_{u,I}$  = Average Irradiated Engineering Ultimate Strength

$k_1, k_2$  = Experimental Constants

Without available material data, the elastic and plastic exponents ( $k_1$ ,  $k_2$ ) were taken as unity. Accordingly the fatigue life relaxation developed for irradiated SA-316-SS was:

$$\Delta \epsilon = \epsilon_{f,I} \epsilon_{f,u}^{-0.4} N_f^{-0.6} + 3.5 \frac{S_{u,I}}{E} N_f^{-0.12}$$

The development of the irradiated first core 20% CW-316-SS fatigue life relation required the true minimum irradiated and unirradiated fracture strains ( $\epsilon_{f,I}$  and  $\epsilon_{f,u}$ ), average irradiated engineering ultimate strength ( $S_{u,I}$ ), and Young's Modulus ( $E$ )

- The true minimum irradiated and unirradiated fracture strains ( $\epsilon_{f,I}$  and  $\epsilon_{f,u}$ ) as a function of temperature and fluence are given in Section 4.3.1.1.2.
- The average irradiated engineering ultimate strength ( $S_{u,I}$ ) was based on the available first core 20% CW-316-SS data [11]. A polynomial fit to the available data was made for the average engineering ultimate ( $S_{u,I} \sim \text{KSI}$ ) as a function of temperature ( $T \sim ^\circ\text{F} \times 10^{-2}$ ).

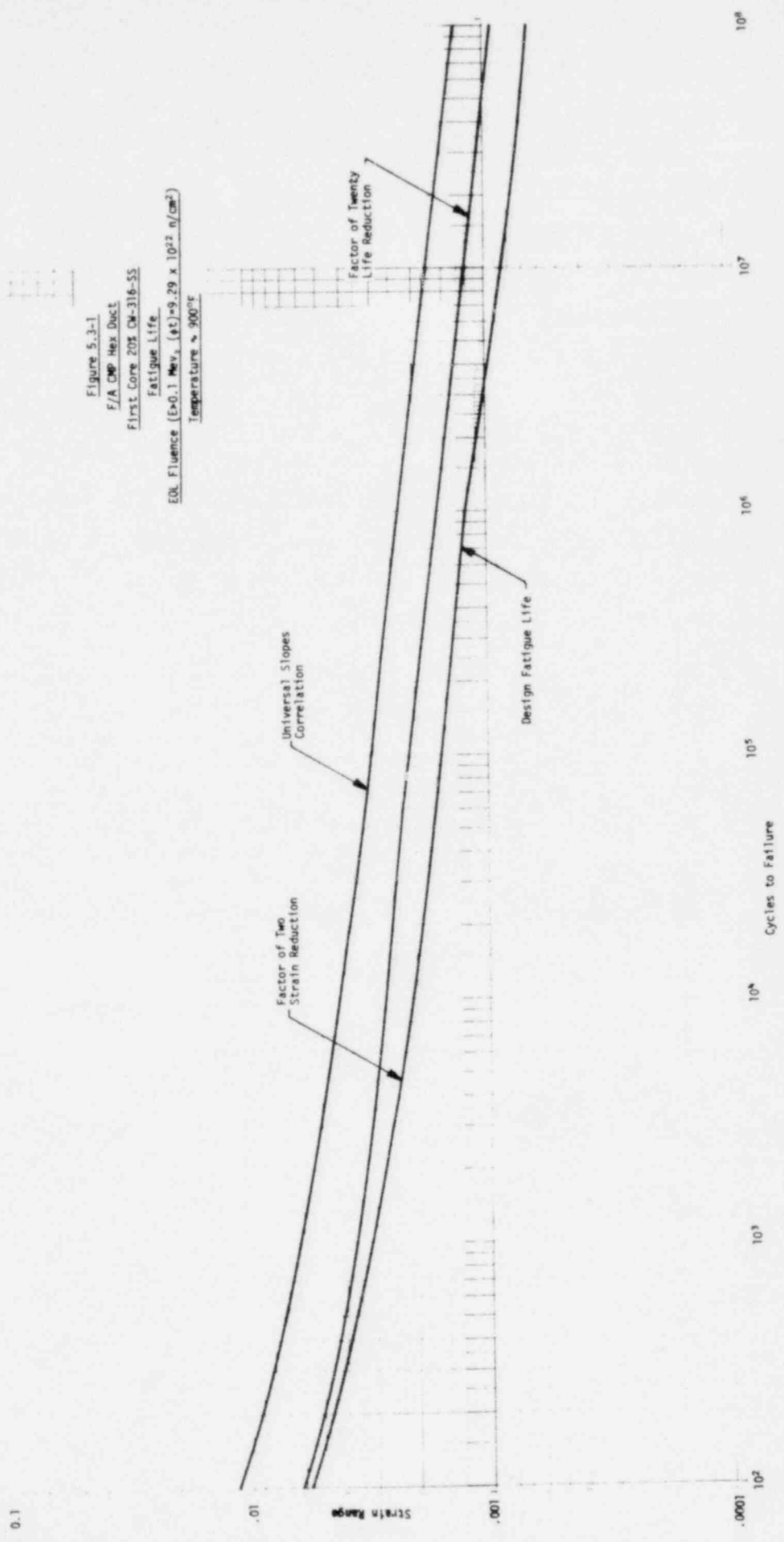
$$S_{u,I} = 78.92 + 3.68 * T - 0.47 * T^2$$

- Young's Modulus ( $E$ ) as a function of temperature is given in Section 4.2.2.1

The irradiated first core 20% CW-316-SS fatigue life relation as developed from the Manson universal slopes method and corrected for the effects of irradiation is strictly applicable only to uniaxial stress states. In order to apply the fatigue life relation to the F/A CMP hex duct, reductions in fatigue life which reflect the multiaxial stress and strain state are required. The RDT Draft for Breeder Reactor Core Components [5] recommends that equivalent strain be used for the strain range in fatigue evaluations of multiaxial stress and strain states. Another means of accounting for

multiaxial effects on fatigue life is to use the range on maximum principal strain. In the F/A CMP hex duct fatigue evaluation, the fatigue life based on equivalent or maximum principal strain, whichever produced the minimum fatigue life was adopted in order to provide an additional safeguard against fatigue failure.

An additional consideration is that the Manson Universal Slopes Method is strictly applicable only to the mean fatigue life of a material and does not account for the scatter in experimental data. The RDT Draft for Breeder Reactor Core Components [5] recommends that the 2-20 rule be used to account for the minimum fatigue life due to scatter of data about the mean. The 2-20 rule was adopted for the fatigue life correlations of irradiated first core 20% CW-316-SS in the F/A CMP hex duct structural evaluation of fatigue life. Simply stated, the 2-20 rule requires that the multiaxial fatigue life be taken as the uniaxial fatigue life reduced by a factor of 2 on strain range or a factor of 20 on life, whichever is minimum. The 2-20 rule as applied to the uniaxial fatigue life relation developed for irradiated first core 20% CW-316-SS using the Manson Universal Slopes Method for the F/A CMP hex duct EOL fluence ( $E > 0.1$  Mev,  $\phi t = 9.29 \times 10^{22}$  n/cm<sup>2</sup>) at 900°F is presented in Figure 5.3-1.



### 5.3.1.2.1.2 Creep Rupture Time

Currently, creep-rupture time correlations are not available for irradiated first core 20% CW-316-SS. However, creep rupture time correlations have been developed [12] for irradiated N-lot 20% CW-316-SS based on thin walled pressurized tubes irradiated to fluences ( $E > 0.1$  Mev), from  $0.21$  to  $0.90 \times 10^{22}$  n/cm<sup>2</sup> over a temperature range of 1000 to 1400°F. Owing to the lack of irradiated first core steel creep rupture data and correlations, the N-lot 20% CW-316-SS creep rupture correlations were used in the evaluation of creep damage factor ( $D^C$ ) for the F/A CMP hex duct over the 39 worst case duty cycles.

The creep rupture time correlations for irradiated N-lot 20% CW-316-SS given in [12] are presented in terms of the mean Larson-Miller Parameter (LMP). A logarithmic bilinear correlation between LMP and maximum principal stress ( $\sigma$  ksi) was developed in terms of temperature ( $T$  °R) and time ( $t_r$  Hrs). The transition stress ( $\sigma_x$  ksi) is given by:

$$\sigma_x = 69.405e^{[-4.85 \times 10^{-4}T]}$$

The  $\sigma$ -LMP correlations are given by:

$$\text{LMP} = 64292 - 7762 \ln(\sigma), \sigma \geq \sigma_x$$

$$\text{LMP} = 44270 + 2.295T - 3040 \ln(\sigma), \sigma < \sigma_x$$

No specific fluence term appears in the correlation. It was found that a difference existed between irradiated and unirradiated data, but that a change in fluence had no detectable effect on the correlation.

The mean rupture time ( $t_r$ ) is given by the relation:

$$t_r = 10 \exp \left[ \frac{\text{LMP}}{T} - 20 \right]$$



In order to correct for the spread in the experimental creep rupture-time data for N-lot 20% CW-316-SS, the minimum irradiated creep rupture times, based on 1.926 standard deviations below the mean on the LMP, were used in the F/A CMP hex duct structural evaluations of creep damage. The mean and minimum rupture times at the F/A CMP hex duct fluence [ $E > 0.1 \text{ Mew}$ ,  $(\phi t) = 9.29 \times 10^{22} \text{ n/cm}^2$ ] and 900°F as a function of maximum principal stress ( $\sigma$ ) are illustrated in Figure 5.3-2.

FIGURE 5.3-2

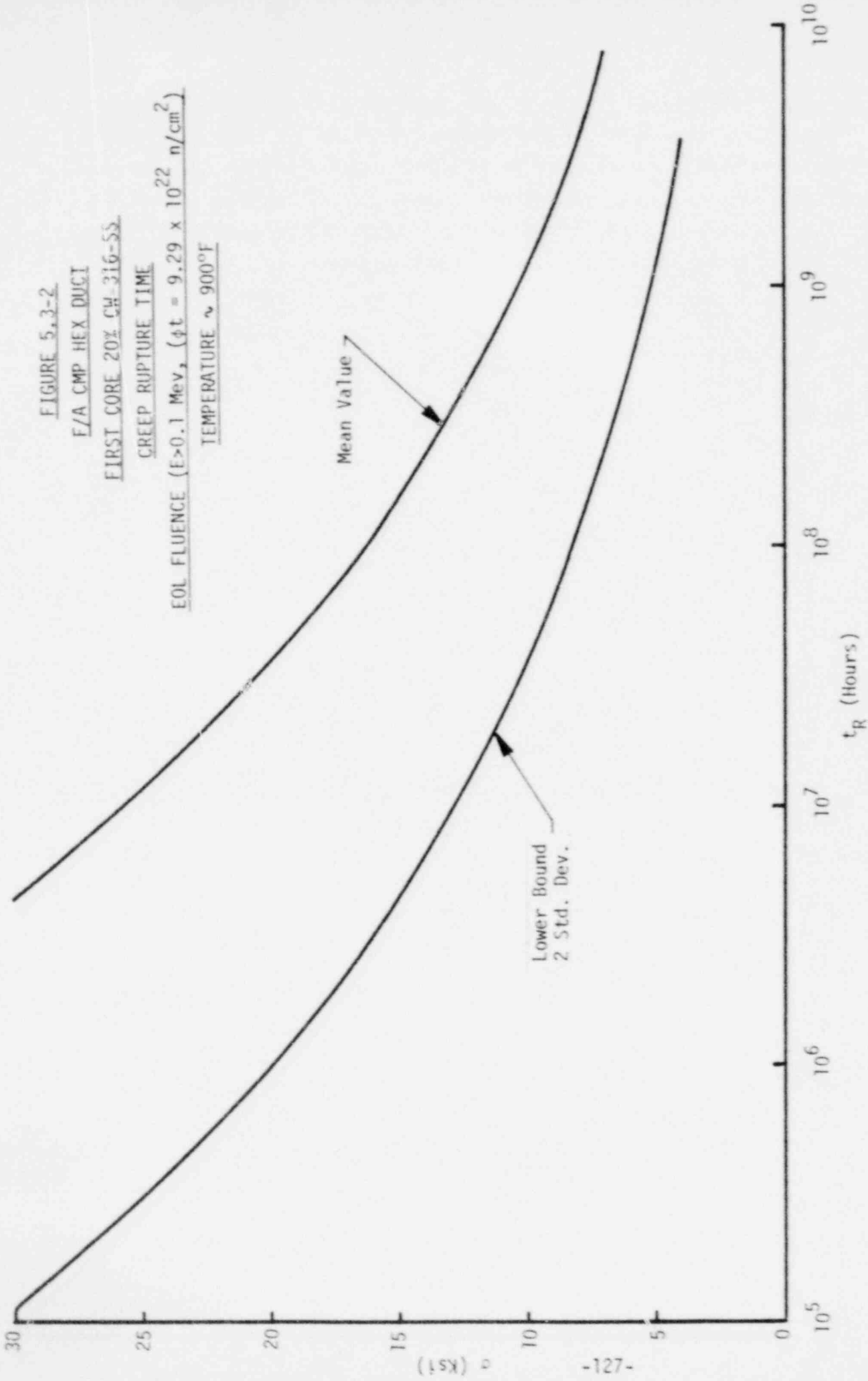
F/A CMP HEX DUCT

FIRST CORE 20% CW-316-SS

CREEP RUPTURE TIME

EOL FLUENCE ( $E > 0.1$  Mev,  $\phi t = 9.29 \times 10^{22}$  n/cm<sup>2</sup>)

TEMPERATURE  $\sim 900^\circ\text{F}$



### 5.3.1.2.2 Comparison and Criterion

The F/A CMP hex duct structural evaluation in relation to the worst case location for combined creep-fatigue damage was made by screening each of the finite elements over the 39 worst case duty cycles with the damage processor. Individual structural evaluations were made for the 3 sets of bending stresses and strains in order to obtain the worst case superposition. The maximum F/A CMP hex duct combined creep-fatigue damage factor  $(F_{CFD})_{max}$  was found to occur for the case of compressive superposition at Element 1 as identified in Figure 5.2-1.

The fatigue damage factor ( $D^f$ ) was found to be  $0.657 \times 10^{-6}$  for the 39 worst case duty cycles. The equivalent strain range was found to be critical and occurred between cumulative iteration 27 and a uniform temperature distribution during the E-16 transient with a value of 0.00065 in/in. The peak local metal temperature during the E-16 transient was 918°F. The fatigue life for the equivalent strain range was  $59.3 \times 10^6$  cycles based on the EOL fluence ( $E > 0.1$  Mev,  $(\phi t) = 9.29 \times 10^{22}$  n/cm<sup>2</sup>).

The creep damage factor ( $D^c$ ) was found to be 0.00515 for the 39 worst case duty cycles. The equivalent stress was found to be critical with a value of 21,387 psi corresponding to the steady state operation at the beginning of the 10 day hold-time. For the EOL fluence ( $E > 0.1$  Mev,  $(\phi t) = 9.29 \times 10^{22}$  n/cm<sup>2</sup>) at a metal temperature of 872°F, the minimum rupture time was  $1.82 \times 10^6$  hours.

In this arrangement, the maximum combined creep-fatigue damage factor  $(F_{CFD})_{max}$  for the F/A CMP hex duct was found to be dominated by creep damage while fatigue damage was negligible.

$$(F_{CFD})_{max} = 0.0052$$

As  $(F_{CFD})_{max} < 1.0$ , the F/A CMP hex duct is not expected to experience crack initiation over the 39 worst case duty cycles based on the creep-fatigue damage criterion.

### 5.3.2 Excessive Deformation

The F/A CMP hex duct structural evaluation of peak + accumulated, and residual deformations in relation to functional limits is presented in the following subsections.

#### 5.3.2.1 Peak Plus Accumulated Deformations

The peak plus accumulated deformation criterion in protecting against excessive deformation requires that peak plus accumulated deformations ( $\delta^{P+A}$ ) be less than the peak plus accumulated deformation limit (PADL).

$$\delta^{P+A} \leq \text{PADL}$$

The peak deformation ( $\delta^P$ ) of the F/A CMP hex duct during the worst case duty cycle at BOL was found to occur at the cumulative iteration 27 temperature distribution with a value of 0.00026 in. As the F/A CMP hex duct remained linear elastic, the initial time independent and final time dependent steady state deformation were identical with a value of 0.00017 in. Accordingly, the accumulated deformation ( $\Delta\delta^{SS}$ ) between initial and final steady state conditions over one duty cycle at BOL was 0.0 in. For 39 worst case duty cycles, the EOL peak plus accumulated deformation,

$$(\delta^{P+A})_{\text{EOL}} = (\delta^P)_{\text{BOL}} + (N-1) (\Delta\delta^{SS})$$

$$(\delta^{P+A})_{\text{EOL}} = 0.00026 + 38 (0.0)$$

$$(\delta^{P+A})_{\text{EOL}} = 0.00026 \text{ in.}$$

For the F/A CMP hex duct, the peak plus accumulated deformation limit (PADL)

$$\text{PADL} = 0.010 \text{ in.}$$

As  $\delta^{P+A} < \text{PADL}$ , the F/A CMP hex duct is not expected to experience excessive peak deformation over the 39 worst case duty cycles.

### 5.3.2.2 Residual Deformations

The residual deformation limit in protecting against excessive residual deformation requires that the residual deformation ( $\delta^R$ ) be less than the residual deformation limit (RDL).

$$\delta^R \leq \text{RDL}$$

The residual deformation ( $\delta^R$ ) between initial and final uniform conditions for the F/A CMP hex duct are identically zero because the deformations are linear elastic. Accordingly,  $\delta^R \leq \text{RDL}$  and the F/A CMP hex duct inherently satisfies excessive residual deformation limits.

### 5.3.3 Summary

The F/A CMP hex duct was found to satisfy the crack initiation and excessive deformation criteria for a total of 39 worst case duty cycles. A summary of the F/A CMP hex duct structural evaluation is presented in Table 5.3-1.

TABLE 5.3-1  
F/A CMP HEX DUCT  
STRUCTURAL EVALUATION SUMMARY

Criteria		Allowable Value	Calculated Value	Margin* of Safety
Crack Initiation	Ductile Rupture Factor	1	0.0727	12.76
	Combined Creep-Fatigue Damage Factor	1	0.0052	191.3
Excessive Deformation	Peak Plus Accumulated	0.010 in.	0.00026 in	37.4
	Residual	0.010 in.	0 in.	$\infty$

\* Margin of Safety =  $\frac{\text{Allowable Value}}{\text{Calculated Value}} - 1$

## 6.0 ACLP HEX DUCT ANALYSIS AND EVALUATION

In the F/A ACLP hex duct analysis and evaluation, a loading analysis was made that considered mechanical seismic and core restraint, and thermal steady state and transient loads in order to establish the number and characteristics of a worst case duty cycle that umbrellas all expected duty cycles for the ACLP hex duct in the first and second reactor cycles. Next, an inelastic structural analysis of the ACLP hex duct was made for a single worst case BOL duty cycle from which EOL values were approximated. Finally, a structural evaluation of EOL strains and dimensional changes in relation to criteria which protect against crack initiation and excessive deformation was made. A summary of the loading and structural analysis, and structural evaluation is presented as follows.

### 6.1 Loading Analysis

The F/A ACLP hex duct loading analysis was directed to establishing the number and characteristics of a worst case duty cycle that umbrellas both the number and characteristics of the Upset, Emergency, and Faulted Events specified over the first and second reactor cycles. The number and characteristics of these events are specified in the Equipment Specification [1].

It is important to note that the worst case F/A ACLP hex duct duty cycle is, in itself, hypothetical, but permits a conservative structural evaluation to be performed on a single duty cycle instead on each of the individual events specified. In the following, the F/A ACLP hex duct mechanical and thermal loads are assessed individually and in relation to each other prior to establishing the worst case duty cycle used in the structural evaluation.

#### 6.1.1 Mechanical

The F/A ACLP hex duct mechanical loads of significance in relation to subsequent structural evaluations are the beam type bending and local contact loads induced by OBE and SSE seismic, and core restraint. Deadweight and internal pressure loadings are relatively insignificant.

#### 6.1.1.1 Beam Bending

In order to perform a structural evaluation of the F/A ACLP hex duct, the maximum bending stresses and strains under lateral OBE and SSE seismic, and core restraint are required. The OBE and SSE seismic bending moments (M) are given in terms of the static 1-g moment ( $M_s$ ) amplified by the respective acceleration (a) of the core barrel, and the core restraint moments ( $M_{CR}$ ) corresponding to steady state operation are given directly.

$$M_{OBE} = [M_s] a_{OBE}$$

$$M_{SSE} = [M_s] a_{SSE}$$

$$M_{CR} = M_{CR}$$

With regard to core restraint behavior during the Upset, Emergency, and Faulted thermal transients, the temperatures of the F/A and adjacent C/A, RB/A and RRS/A hex ducts were assumed to follow the overall core temperatures, but the temperature differences across the F/A which cause the beam bending moments are not expected to change significantly from steady state values. Accordingly, the core restraint bending moments during the transients were not assumed to change from steady state values. Alternately, the steady state temperature differences across the F/A hex duct cross-section at any point along its length was assumed to be the same during the thermal transients even though overall temperatures increased or decreased according to the characteristics of the transients. In this arrangement, the transient bending moments ( $M_{TR}$ ) were assumed equal to the steady state core restraint moments ( $M_{CR}$ )

$$M_{TR} = M_{CR}$$

In order to determine the maximum ACLP bending stresses and strains, the ACLP bending moments were screened for each F/A. The maximum ACLP core restraint ( $M_{CR}$ ) and transient ( $M_{TR}$ ) moments were found to occur at F/A A<sup>09</sup><sub>01</sub> with a value of 48,860 in-lb. The maximum 1-g static bending moment ( $M_s$ ), applicable to all F/A, was found to be 2600 in-lb.

For the F/A ACLP hex duct the cross-section modulus ( $Z$ ) and Young's modulus ( $E$ ), the maximum bending stresses ( $\sigma$ ) and strains ( $\epsilon$ ) are given by the following relations:

$$\sigma = M/Z \text{ and } \epsilon = \sigma/E$$

Numerically, the F/A ACLP hex duct section modulus ( $Z$ ) is 3.929 in<sup>3</sup>. The Young's Modulus ( $E$ ) for the ACLP hex duct as constructed from 20% CW-316-SS and operating at a steady temperature of 1000°F is  $22.54 \times 10^6$  psi. The F/A ACLP hex duct maximum stresses ( $\sigma$ ) and strains ( $\epsilon$ ) under OBE and SSE seismic, core restraint and transient bending moments are summarized in Table 6.1-1.



TABLE 6.1-1  
F/A ACLP HEX DUCT  
OBE AND SSE SEISMIC, AND CORE RESTRAINT  
BENDING MOMENTS, STRESSES, AND STRAINS

Loading		Core Barrel Acceleration (a)	Bending Moment (M ~ in-lb)		Max. Bending Stress ( $\sigma$ ~ PSI)	Max. Bending Strain ( $\epsilon$ ~ in/in)
			Static	Dynamic		
Seismic	OBE	1.57	2600	4082	1039	4.61E-5
	SSE	2.2	2600	5720	1456	6.46E-5
Core Restraint		N/A	48860	N/A	12436	5.52E-4
Transients		N/A	48860	N/A	12436	5.52E-4

#### 6.1.1.2 Local Contact

The F/A ACLP local contact loads are the inter-duct loads that occur at the corners and faces of a F/A ACLP load pad under lateral OBE and SSE seismic excitation, or are induced by the core restraint system during steady state and transient thermal operation.

An important consideration in the structural evaluation of the F/A ACLP is whether the local inter-duct loads are load or deformation controlled, or some combination thereof. However, the local inter-duct behavior of the F/A ACLP hex ducts in relation to whether the structural response due to lateral seismic and core restraint is load or deformation controlled is not fully understood at this time. Currently, the local ACLP inter-duct loads are thought to be load controlled only when the attendant deformations are less than the gaps that exist between adjacent assemblies.

The most common example of a load controlled condition occurs when a F/A ACLP hex duct experiences compressive 2 face loading from adjacent ducts across 2 opposing flats, but the outwardly disposed deformations at the unloaded corners are not sufficient to exhaust the gaps and initiate contact with the adjacent ACLP hex ducts. Once the unloaded corners contact the respective adjacent ACLP hex ducts, the 2 face loading of the duct under consideration becomes deformation controlled. By the same argument, the ACLP hex ducts which were applying the 2 face loads to the duct under consideration are also undergoing deformation and load redistribution. Alternately, the 2 face loads applied to the ACLP hex duct are themselves deformation controlled and in a strict sense are not load controlled.

In a pure deformation controlled CRBR core with a rigid core former ring and core barrel, the local inter-duct ACLP hex duct loads approach a pure hydrostatic loading with a uniform deformation pattern throughout the ACLP cross-section. In actuality, a small amount of load controlled behavior characterized by 2 face loading and non-uniform cross-section deformations would occur because of nominal gap variations, temperature differences,

core former ring and core barrel flexibilities and exterior ACLP hex duct dimensional tolerances. However, system analysis of actual CRBR core behavior under lateral seismic and steady state or transient thermal operation with the detail necessary to assure displacement compatibility at the contact surfaces of each ACLP hex duct within the flexibility of the core formers and barrel is beyond current state-of-the-art analytical procedures. Current analytical procedures only approximate true displacement compatibility between CRBR core assemblies in order to obtain practical solutions. As such, systems analysis of CRBRP seismic and core restraint response provide conservative loads for ACLP duct structural evaluations which, neglect the mitigating effects of actual deformation controlled core behavior.

In the following, the F/A local contact ACLP hex duct seismic loads during OBE and SSE, and induced by core restraint during steady state and transient thermal conditions are described. Also, conservatisms in the local contact F/A ACLP hex duct loads to be used in the structural evaluation are cited.

#### 6.1.1.2.1 OBE and SSE Seismic

The F/A local contact ACLP hex duct loads are based on the Planar Core Model (PCM) presented in the Core Inter-Duct Analysis Document [13].

The PCM used to derive the F/A ACLP hex duct local contact loads under lateral OBE and SSE seismic excitation was based on a 2 dimensional 180° sector of the CRBR core at the ACLP. A lateral 1g acceleration was imposed on the 2 dimensional 180° sector of the CRBR core at the ACLP with a portion of the full weight of each F/A, RB/A, C/A, and RRS/A lumped at the corners of the respective ACLP cross-sections. Owing to the detail of the PCM, a true simulation of inter-duct contact using non-linear gap elements at each of the 12 possible contact points for each core assembly was not practical. Instead, a semi-linear analytical approach consisting of interposing linear springs between each pair of contact points was adopted. As the linear springs permit tensile loads to be developed, a manual iterative procedure was used to obtain a compression only solution. In

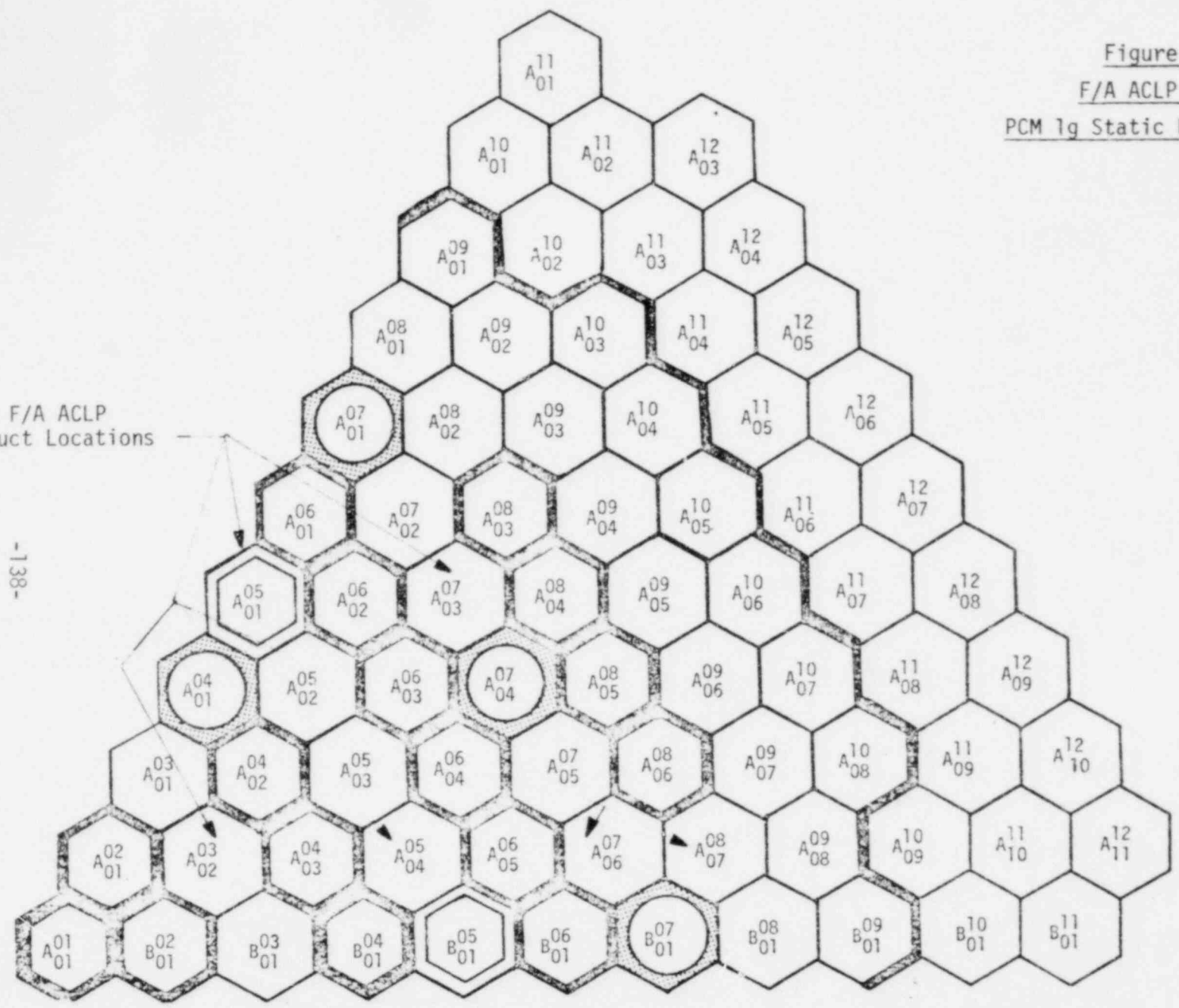
essence, the inter-duct loads were inspected after each linear solution and, if found to be tensile, the spring stiffness was reduced until the majority of inter-duct loads were compressive. In this arrangement, the local F/A ACLP loads derived by the PCM are considered conservative for the following reasons.

- The PCM considered full load transfer of the ACLP region to the ACLP core former. However, the bending action of individual or groups of core assemblies would actually transfer a portion of the ACLP load to the TLF outlet nozzle and core support plate. Accordingly, PCM local contact loads for the F/A ACLP hex ducts under lateral 1-g static acceleration are larger in magnitude from what would be expected in the CRBR core.
- The PCM simulated compression only local contact through linear springs which were reduced in stiffness to provide minimal tensile loads. However, the duct corners were permitted to overlap each other in the process. Accordingly, true displacement compatibility consistent with the deformation controlled loading of the F/A ACLP hex ducts and adjacent ACLP hex ducts which would tend to produce hydrostatic loading was not obtained. As such, the PCM local contact loads for the F/A ACLP hex duct under lateral 1-g static acceleration include 2 face loads larger in magnitude from what would be expected in the CRBR core.

In order to establish the worst case F/A ACLP hex duct local contact OBE and SSE seismic loads, F/A locations in a 60° sector of the core were identified for structural evaluation as illustrated in Figure 6.1-1.

Figure 6.1-1  
 F/A ACLP Hex Duct  
 PCM 1g Static Load Locations

Worse F/A ACLP  
 Hex Duct Locations



1g Acceleration  
 →

The method of selecting the worst case F/A ACLP hex duct local contact seismic loads for structural evaluation was directed to establishing a set of static 1 g loads for a 90° sector of the ACLP hex duct cross-section which are representative of the 12 loads on each of the 6 F/A locations. In essence, a set of 3 loads ( $F_1$ ,  $F_2$ , and  $F_3$ ) in a 90° sector of the ACLP hex duct cross-section were selected to represent the 12 loads ( $W_{11}$ ,  $W_{12}$ ,  $W_{21}$ ,  $W_{22}$ ,  $W_{31}$ ,  $W_{32}$ ,  $W_{41}$ ,  $W_{42}$ ,  $W_{51}$ ,  $W_{52}$ ,  $W_{61}$ ,  $W_{62}$ ) on each of the F/A ACLP hex ducts. The load designation scheme is illustrated in Figure 6.1-2.

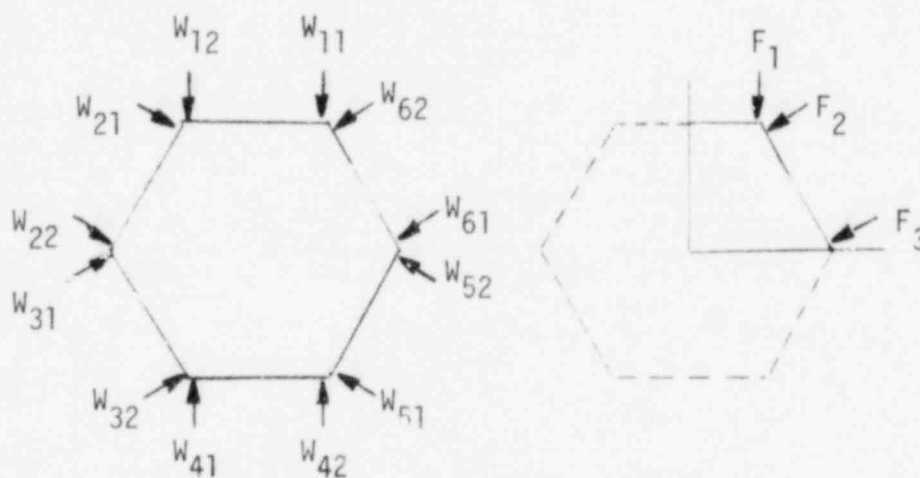


Figure 6.1-2  
F/A ACLP Hex Duct  
Method of Selecting Static 1g Loads

The values of the representative static 1g loads on the 90° sector ACLP hex sector of each F/A were derived from the following method of averaging.

$$F_1 = \frac{W_{11} + W_{12} + W_{41} + W_{42}}{4}$$

$$F_2 = \frac{W_{21} + W_{32} + W_{51} + W_{62}}{4}$$

$$F_3 = \frac{W_{22} + W_{31} + W_{52} + W_{61}}{4}$$

A summary of the static 1g loads ( $F_1$ ,  $F_2$ ,  $F_3$ ) for each of the 6 F/A locations is given in Table 6.1-2.

TABLE 6.1-2  
F/A ACLP HEX DUCT  
AVERAGE 1g 90° SECTOR LOADS

F/A Location	Average 90° Sector Loads (LBS)		
	F <sub>1</sub>	F <sub>2</sub>	F <sub>3</sub>
A <sub>03</sub> A <sub>02</sub>	2278	1313	2080
A <sub>05</sub> A <sub>01</sub>	2670	238	1643
A <sub>05</sub> A <sub>04</sub>	2658	345	1930
A <sub>07</sub> A <sub>03</sub>	2515	835	2150
A <sub>07</sub> A <sub>06</sub>	2993	1223	2155
A <sub>08</sub> A <sub>07</sub>	2768	568	2105

The average static 1g loads in the 90° sector of a F/A ACLP hex duct cross-section represent a symmetrical set of loads with attendant structural damage which is an approximation to the damage that would occur for the actual non-symmetrical set of loads over the 360° sector of the F/A ACLP hex duct cross-section. However, the disadvantage with the average 1g 90° sector load is that individual structural evaluations would be required for each of the 6 F/A ACLP hex duct locations because a simple assessment of the worst case loading is not possible. Consequently, the individual F/A loads (F<sub>1</sub>, F<sub>2</sub>, F<sub>3</sub>) were, in turn, averaged for the 6 F/A locations so as to simplify structural evaluations, and yet also provide a reasonable set of 90° sector F/A ACLP hex duct loads. The average 1g F/A loads (F<sub>1</sub>)<sub>av</sub>, (F<sub>2</sub>)<sub>av</sub>, and (F<sub>3</sub>)<sub>av</sub> used in the F/A ACLP hex duct structural evaluation were obtained by averaging the F/A loads (F<sub>1</sub>, F<sub>2</sub>, F<sub>3</sub>) in Table 6.1-2.

$$(F_1)_{av} = 2647 \text{ LBS}$$

$$(F_2)_{av} = 754 \text{ LBS}$$

$$(F_3)_{av} = 2010 \text{ LBS}$$

In order to determine the dynamic OBE and SSE seismic F/A ACLP hex duct loads ( $F_{DYN}$ ), the static 1g loads ( $F_s$ ) were increased by the dynamic accelerations ( $a$ ) of the core barrel.

$$F_{DYN, OBE} = [F_s] a_{OBE}$$

$$F_{DYN, SSE} = [F_s] a_{SSE}$$

For the OBE seismic acceleration ( $a_{OBE} = 1.57$  g), the worst case F/A ACLP hex duct loads are:

$$(F_1)_{av, OBE} = 4156 \text{ LBS.}$$

$$(F_2)_{av, OBE} = 1184 \text{ LBS.}$$

$$(F_3)_{av, OBE} = 3156 \text{ LBS.}$$

Similarly, for the SSE seismic acceleration ( $a_{SSE} = 2.2$  g).

$$(F_1)_{av, SSE} = 5823 \text{ LBS.}$$

$$(F_2)_{av, SSE} = 1658 \text{ LBS.}$$

$$(F_3)_{av, SSE} = 4422 \text{ LBS.}$$

#### 6.1.1.2.2 Steady State and Transient Core Restraint

The F/A local contact ACLP hex duct loads are based on the 2 dimensional Core Restraint Model (CRM).

The F/A ACLP hex duct local contact core restraint loads under steady state reactor operation were derived using a 2 dimensional CRM which incorporates simplified 3 dimensional assembly interaction effects. The CRM is based on a string of F/A, C/A, RB/A, and RRS/A assemblies extending from the center of the core to the ACLP and TLP core former rings. Assemblies were simulated using 2 dimensional beams with gap elements at the inlet nozzle, ACLP, and TLP to represent contact with the inlet module and adjacent assemblies. Each assembly in the model is assigned the stiffness and interaction characteristics of a hexagonal ring of assemblies.

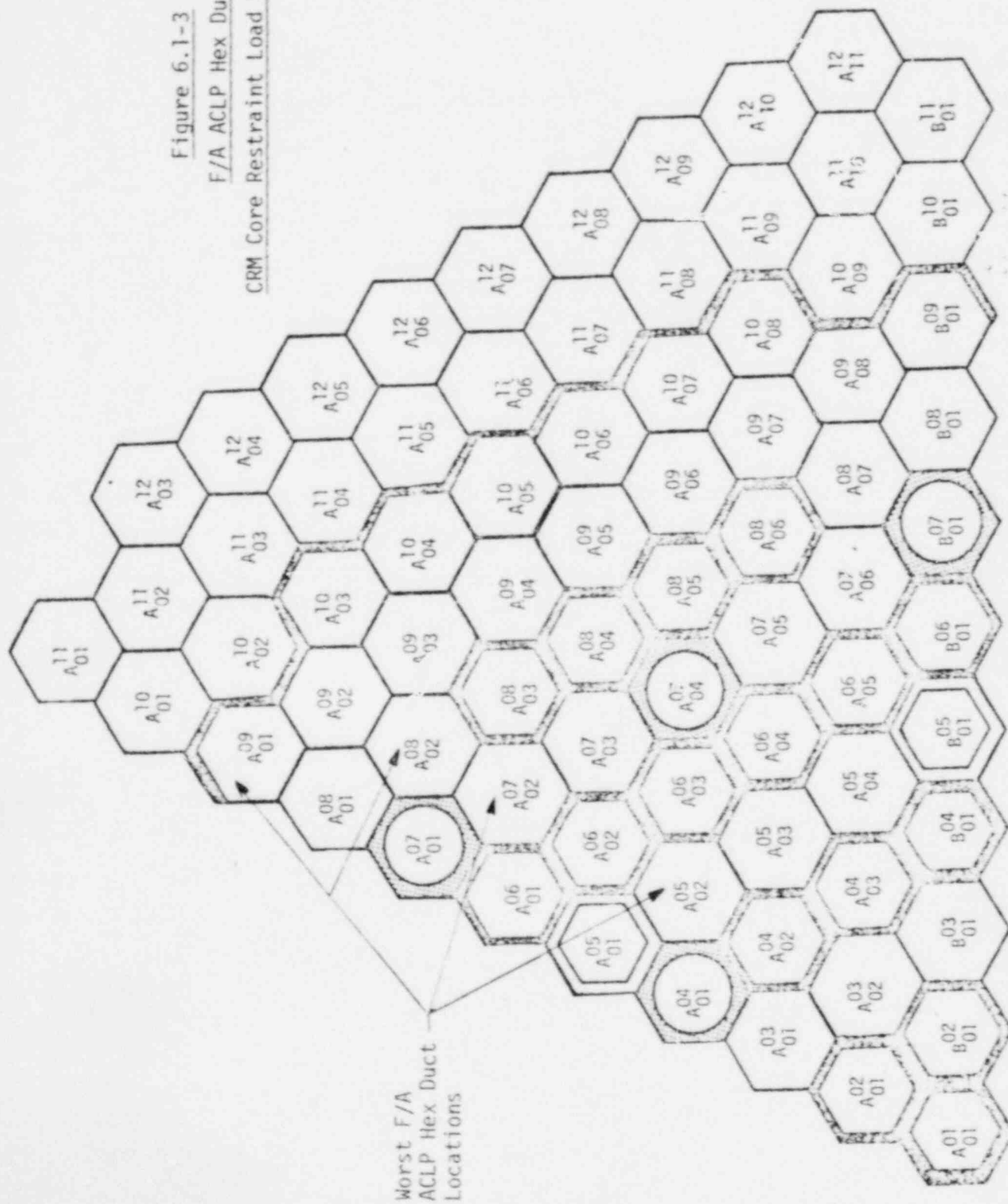


Owing to the simplicity of the CRM, a true simulation of non-linear inter-duct contact consisting of gap and stiffness simulation at each of the 12 possible contact points on each core assembly ACLP and TLP location was not obtained. Nevertheless, a reasonable approximation of F/A ACLP hex duct load to be used for structural evaluation were obtained for the following reasons.

- The CRM local contact F/A ACLP hex duct loads were based a 1.4 uncertainty on the steady state temperatures. Accordingly, the 40% increase in temperature difference across the cross-sections of the core assemblies in the string of core assemblies produces larger F/A ACLP hex duct loads than would be expected in the CRBR core, even if true displacement compatibility were obtained.
- The CRM local contact F/A ACLP hex duct loads were based on a uniform gap distribution of 0.010 in. where as the nominal CRBR gap at operating conditions is 0.015 in. Accordingly, the F/A ACLP hex duct local contact loads during steady state CRBR thermal operation as constrained by the ACLP and TLP core formers and derived by the CRM are higher than would be expected in the actual CRBR core.

In order to establish the worst case F/A ACLP hex duct local contact core restraint loads, 4 F/A locations in a 30° sector of the core were identified for structural evaluation as illustrated in Figure 6.1-3.

Figure 6.1-3  
 F/A ACLP Hex Duct  
 CRM Core Restraint Load Locations



The method of selecting the F/A with the worst case ACLP hex duct local contact steady state core restraint loads for structural evaluation was directed to establishing a set of loads for a 90° sector of the ACLP hex duct cross-section which are representative of the 2 face loads at each of the 6 faces in each of the 4 F/A locations. Alternately, a set of 3 loads ( $F_1$ ,  $F_2$ , and  $F_3$ ) in a 90° sector of the ACLP cross-section were selected to represent the 6 sets of 2 face loads ( $W_1, \dots, W_6$ ) on each of the F/A ACLP hex ducts. The load designation scheme is illustrated in Figure 6.1-4.

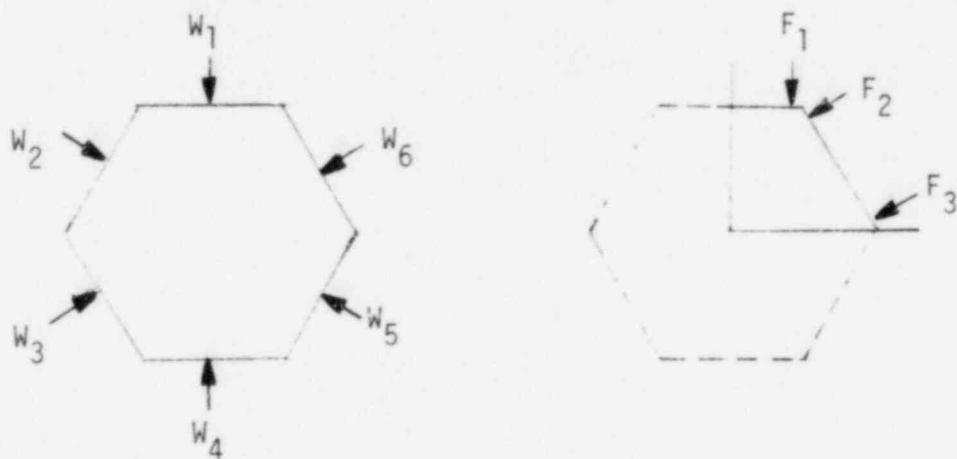


Figure 6.1-4  
F/A ACLP Hex Duct  
Method of Selecting Core Restraint Loads

The values of the core restraint loads on the 90° sector of each F/A were derived by the following method of averaging.

$$F_1 = \frac{W_1 + W_4}{4}$$

$$F_2 = \frac{W_2 + W_3 + W_5 + W_6}{8}$$

$$F_3 = \frac{W_2 + W_3 + W_5 + W_6}{8}$$

A summary of the steady state core restraint loads ( $F_1$ ,  $F_2$ ,  $F_3$ ) for each of the 4 F/A locations is given in Table 6.1-3.

TABLE 6.1-3  
F/A ACLP HEX DUCT  
AVERAGE STEADY STATE CORE RESTRAINT 90° SECTOR LOADS

F/A Location	Average 90° Sector Loads (LBS)		
	$F_1$	$F_2$	$F_3$
A <sub>02</sub> <sup>08</sup>	432	298	298
A <sub>02</sub> <sup>07</sup>	210	230	230
A <sub>02</sub> <sup>05</sup>	0	122	122
A <sub>01</sub> <sup>09</sup>	0	42	42

The average steady state core restraint loads in the 90° sector of a F/A ACLP hex duct cross-section represent a symmetrical set of loads with attendant structural damage is an approximation to the damage that would occur over the 360° sector of the F/A ACLP hex duct cross-section. Unlike the local contact seismic loads, the worst case core restraint loads were selected by simple inspection of the individual loads at the 4 F/A locations given in Table 6.1-3. The F/A location A<sub>02</sub><sup>08</sup> steady state core restraint loads were selected as worst case in F/A ACLP hex duct structural evaluations.

$$F_1 = 432 \text{ LBS}$$

$$F_2 = 298 \text{ LBS}$$

$$F_3 = 298 \text{ LBS}$$

The worst case F/A ACLP hex duct local contact core restraint loads apply only to steady state thermal performance of the CRBR core. With regard to transient CRBR core restraint behavior during Upset, Emergency, and Faulted thermal transients, the temperatures of the core assemblies change locally over the brief duration of the transients. In relation to the global temperature change of the full CRBRP core as constrained by the ACLP and TLP core formers, significant difference in local contact ACLP hex duct contact loads from that would occur during steady state behavior is not expected. Accordingly, the ACLP hex duct local contact loads ( $F_{TR}$ ) during the transient behavior of the CRBR core were assumed to be identical to the steady state loads ( $F_{SS}$ ) for the purposes of structural evaluation.

$$F_{TR} = F_{SS}$$

### 6.1.2 Thermal

The F/A ACLP hex duct thermal loads are the steady state and transient temperature distributions that occur during the Upset, Emergency, and Faulted Events over the first and second reactor cycles. The steady state F/A ACLP hex duct inside metal temperature distributions throughout Sector A of the core at BOC 1, EOC 1, BOC 2, and EOC 2 and the Upset, Emergency, and Faulted Transients defined in terms of time-dependent scale factors applied to the steady state inside metal temperatures were considered. In this arrangement, the F/A ACLP hex duct thermal loads in terms of inside metal temperatures associated with BOC 1, EOC 1, BOC 2, and EOC 2 steady state as well as Upset, Emergency, and Faulted Transients were identified at any F/A location in the core.

In order to proceed with a structural evaluation of the F/A ACLP hex duct, it was desirable for the sake of simplicity to consider only the worst case thermal loading. Accordingly, all F/A located in Sector A of the core were assessed in relation to the maximum inside metal wall temperature difference between a F/A and adjacent C/A or RB/A. The maximum steady state inside metal wall temperature difference was found to occur at F/A A<sub>05</sub><sup>09</sup> adjacent to RB/A A<sub>04</sub><sup>08</sup> during BOC 1 with a value of 219°F. It is important to note that at EOC 1, BOC 2, and EOC 2, the respective inside metal temperature differences were found to decrease from BOC 1 values with an average temperature difference over the first and second reactor cycles of 152°F. A greater maintained steady state inside metal wall temperature difference over the first and second reactor cycles is observed for F/A A<sub>02</sub><sup>07</sup> adjacent to C/A A<sub>01</sub><sup>07</sup>. For the latter, a maximum temperature difference of 217°F is seen to occur at EOC 1 while the average temperature over the first and second reactor cycles is 200°F. Accordingly, the F/A A<sub>02</sub><sup>07</sup> adjacent to C/A A<sub>01</sub><sup>07</sup> with a respective average inside metal surface temperature difference of 200°F was considered as worst case for steady state temperature distributions in subsequently F/A ACLP hex duct structural evaluations.

With regard to F/A and adjacent C/A ACLP hex duct thermal transients, the Equipment Specification [1] using an umbrella approach identified the number of Upset, Emergency, and Faulted transients over the first and second reactor cycles as 1/15 of the number specified for 30 years rounded to the next whole number. Over the first and second reactor cycles comprising a total of 328 FPD, a total of 39 Upset Transients umbrellaed by the worst of U-2b or OBE were specified. Similarly, the worst of the E-16, 60c Step, or U-2b during OBE were specified to umbrella the Emergency Transients while the SSE was identified to umbrella the Faulted Transients.

In the derivation of the F/A and adjacent C/A inside metal temperature transients for the Upset, Emergency, and Faulted transients, the upper and lower bounds for the Upset U-2b and OBE events and the Emergency 60c step event were identified from June, 1977 data. The upper bounds were based on quickest flow decay and maximum decay heat while the lower bounds were based on slowest flow decay and minimum decay heat. Further, the SSE Faulted Transient was found to be umbrellaed by the Emergency E-16 transient. The Upset transients comprising the upper and lower bound U-2b and OBE, and the Emergency Transients including the upper and lower bound 60c step, E-16, and U-2b during OBE are identified.

In order to reduce the number of F/A ACLP hex duct transients which umbrella the Upset, and Emergency Transients to a single worst case transient, the individual transients were assessed for severity in subsequent structural evaluations by comparing the inside metal wall temperatures in terms of maximum value, rate of temperature change, and range. In the assessment, the F/A  $A_{04}^{09}$  adjacent to RB/A  $A_{04}^{08}$  steady state temperature difference of 219°F with F/A and RB/A inside metal surface temperatures of 1056 and 837°F were used. For the Upset Transients at the F/A ACLP hex duct inside metal surface, the upper and lower bound U-2b transients with maximum rate and range of temperature indistinguishable from the upper and lower bound OBE transient. However, the adjacent RB/A inside metal temperature transients for the lower bound U-2b were observed to more closely follow the F/A metal transient than in the case of the upper bound U-2b. Owing to the thermal lag in the thin walled F/A ACLP hex duct, temperature differences through the wall, which are important in structural evaluations, are slightly more severe in the lower bound U-2b transient than the upper bound counterpart. With regard to the Emergency Transients, the E-16 transient in terms of maximum value, rate of temperature change, and range was found to be clearly more severe than the upper and lower bound 60¢ step, and the U-2b during OBE transients. Further, the E-16 was also considered more severe than the lower bound U-2b transient. In this arrangement, the Emergency E-16 transient was considered to umbrella all Upset, Emergency, and Faulted transients for the F/A ACLP hex duct and is illustrated in Figure 6.1-5.



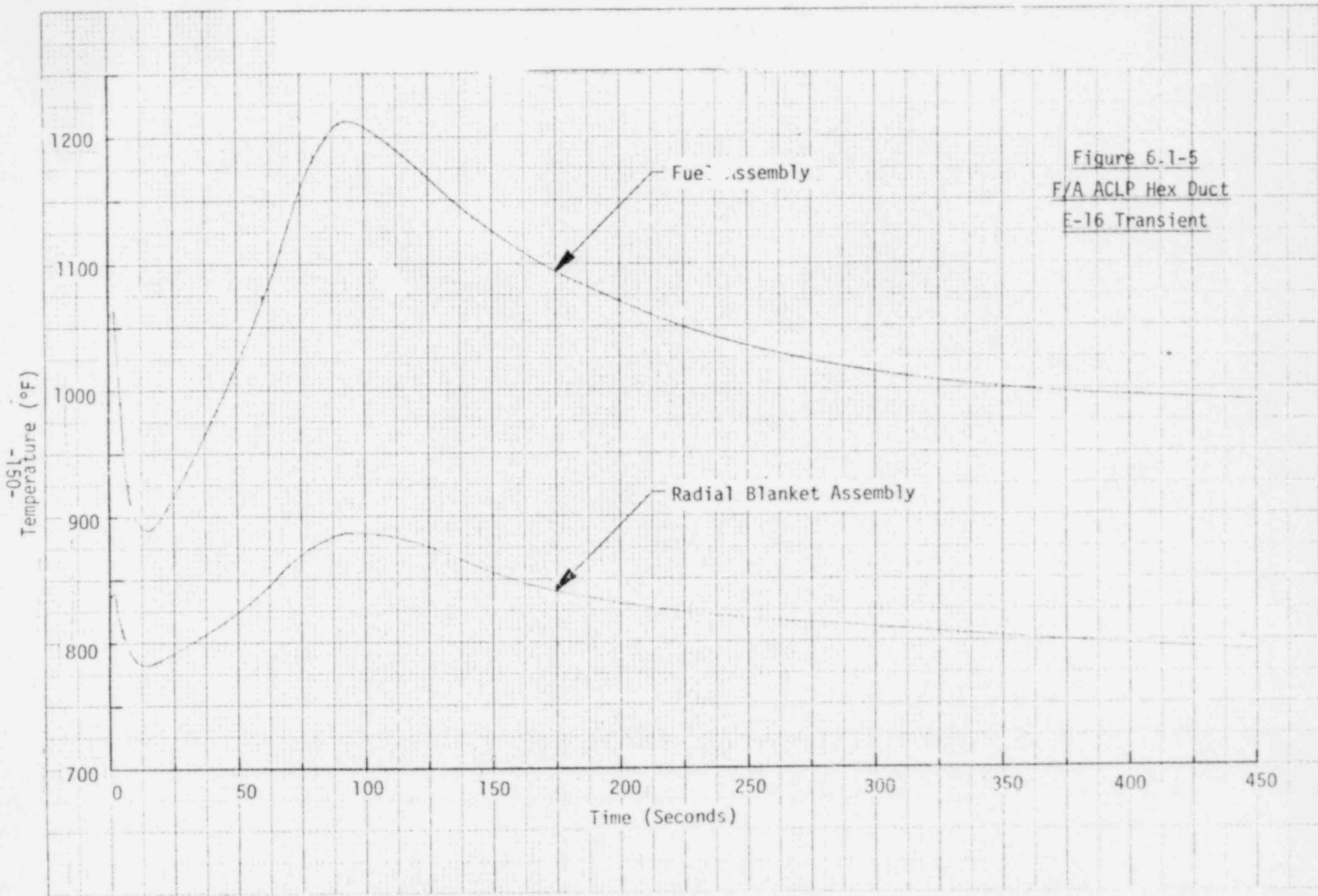
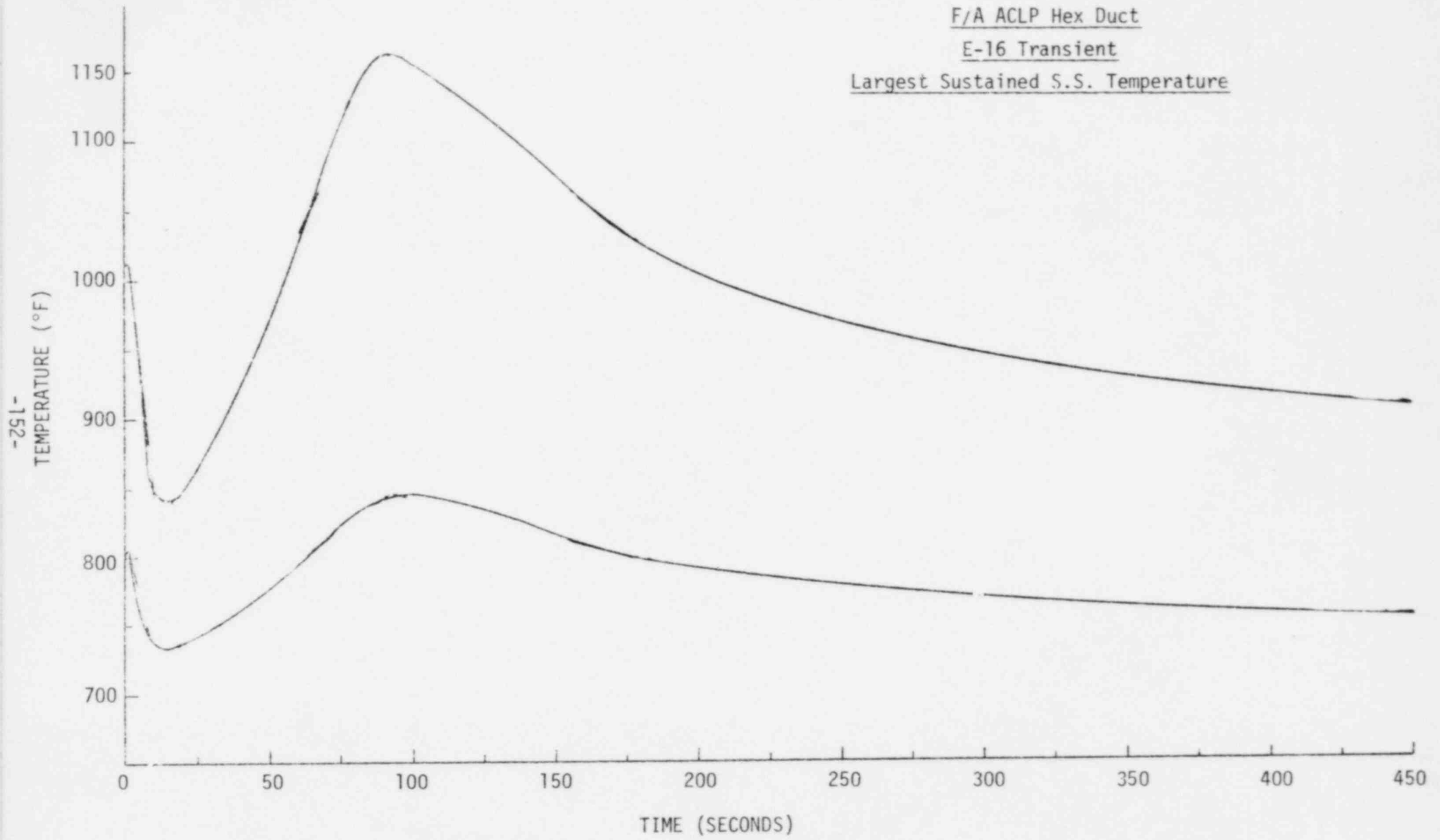


Figure 6.1-5  
F/A ACLP Hex Duct  
E-16 Transient

In the F/A ACLP hex duct structural evaluation, the E-16 transient based on the response of F/A  $A_{02}^{07}$  adjacent to C/A  $A_{01}^{07}$  with the larger sustained steady state inside metal surface temperature was used instead of E-16 transient based on F/A and RB/A used in the transient assessment. In addition, the F/A  $A_{02}^{07}$  metal temperatures at each of the six inside surface were averaged at BOC 1, EOC 1, BOC 2, and EOC 2 were averaged to minimize conservatism in steady state temperature variations. The corresponding average inside surface temperatures were found to reasonably approximate sustained F/A and C/A temperatures of 1000 and 800°F with a temperature difference of 200°F over the first and second reactor cycles. In this arrangement, the Emergency E-16 transient with the largest sustained steady state temperature difference was selected as the worst case umbrella to all Upset, Emergency, and Faulted transients for the F/A ACLP hex duct structural evaluation and is illustrated in Figure 6.1-6.

The selection of the Emergency E-16 transient with the largest sustained steady state temperature difference as the worst case F/A ACLP hex duct transient is, in itself, not sufficient to establish the worst case F/A ACLP hex duct duty cycle. Thermal conditions following the E-16 transient and subsequent hold-times at steady state conditions are also required. The thermal conditions selected consisted of a cool-down to 699°F in 1 hour from the F/A and C/A inside metal wall temperature at 450 seconds into the E-16 transient, followed by a 1 hour heat-up to initial steady state F/A and C/A temperatures. Thereafter, a 10 day hold-time at steady state temperature was assumed. The 10 day hold time corresponds to 40 worst case E-16 transients uniformly distributed over 400 FPD which is slightly greater than the 328 FPD specified for the first and second reactor cycles. The worst case F/A ACLP hex duct duty cycle is presented in Figure 6.1-7.

Figure 6.1-6  
F/A ACLP Hex Duct  
E-16 Transient  
Largest Sustained S.S. Temperature



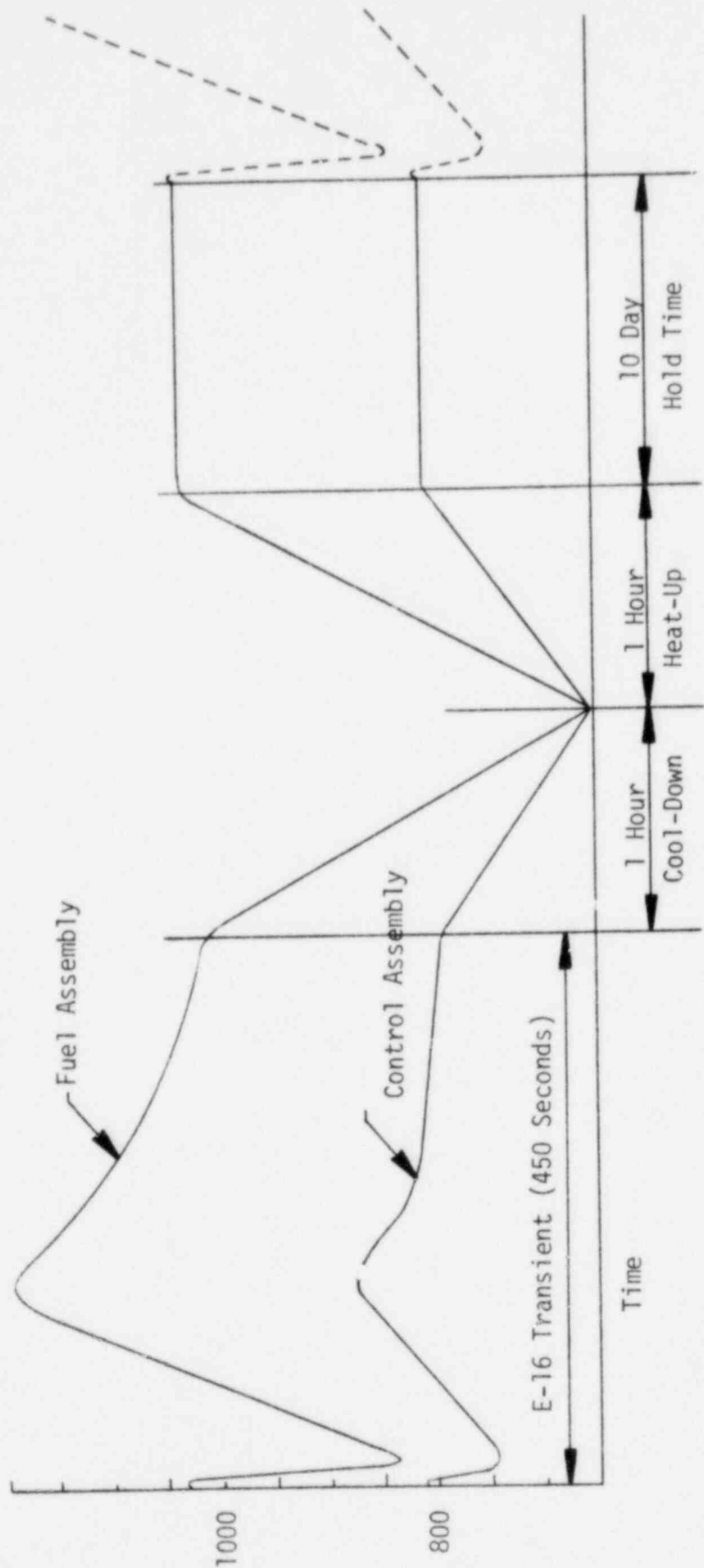


Figure 6.1-7  
 F/A ACLP Hex Duct  
 Worst Case Duty Cycle

The worst case F/A ACLP hex duct duty cycle in terms of inside metal temperatures at initial steady state, followed by the E-16 transient, thermal conditions in returning to initial steady condition, and 10 day hold-time are not sufficiently detailed for subsequent structural evaluation. In the following, the F/A ACLP hex duct thermal model and geometry, boundary conditions and wetted sodium surfaces, heat generation rates, and thermal analysis and results are described from which conclusions on detailed temperature distributions used in subsequent structural analysis are presented.

#### 6.1.2.1 Model and Geometry

The F/A ACLP hex duct model was formulated in the ANSYS finite element program. The ANSYS program was selected because of the compatibility between thermal and structural elements which permits thermal solutions of temperature distributions to be used directly in subsequent structural analysis.

The F/A ACLP hex duct region selected for analysis corresponds to a 2 dimensional 90° sector of the full ACLP cross-section. As the worst case F/A ACLP steady state and transient temperatures include adjacent C/A inside metal wall temperatures, an effective film coefficient was used to simulate the thermal resistance of the C/A wall. The effective C/A film coefficient ( $h$ ) was taken as the thermal conductivity ( $K$ ) divided by the wall thickness ( $L$ ) according to the relation,  $h = K/L$ . The effective film coefficient of the sodium in the ACLP interstice gap in relation to the ACLP hex duct itself was not found to be significant. The F/A ACLP hex duct thermal model illustrating the dimensional extent and finite element detail is presented in Figure 6.1-8.

The F/A ACLP hex duct 90° sector thermal model as formulated in the ANSYS program included a total of 294 linear temperature (STIF 35) elements in a mesh of 341 node points. A relatively fine mesh was selected in the corner adjacent to the global X-axis so as to include the thermal skin response to the thermal transients. Otherwise, a relatively coarse mesh was used throughout the 90° sector of the ACLP cross-section.

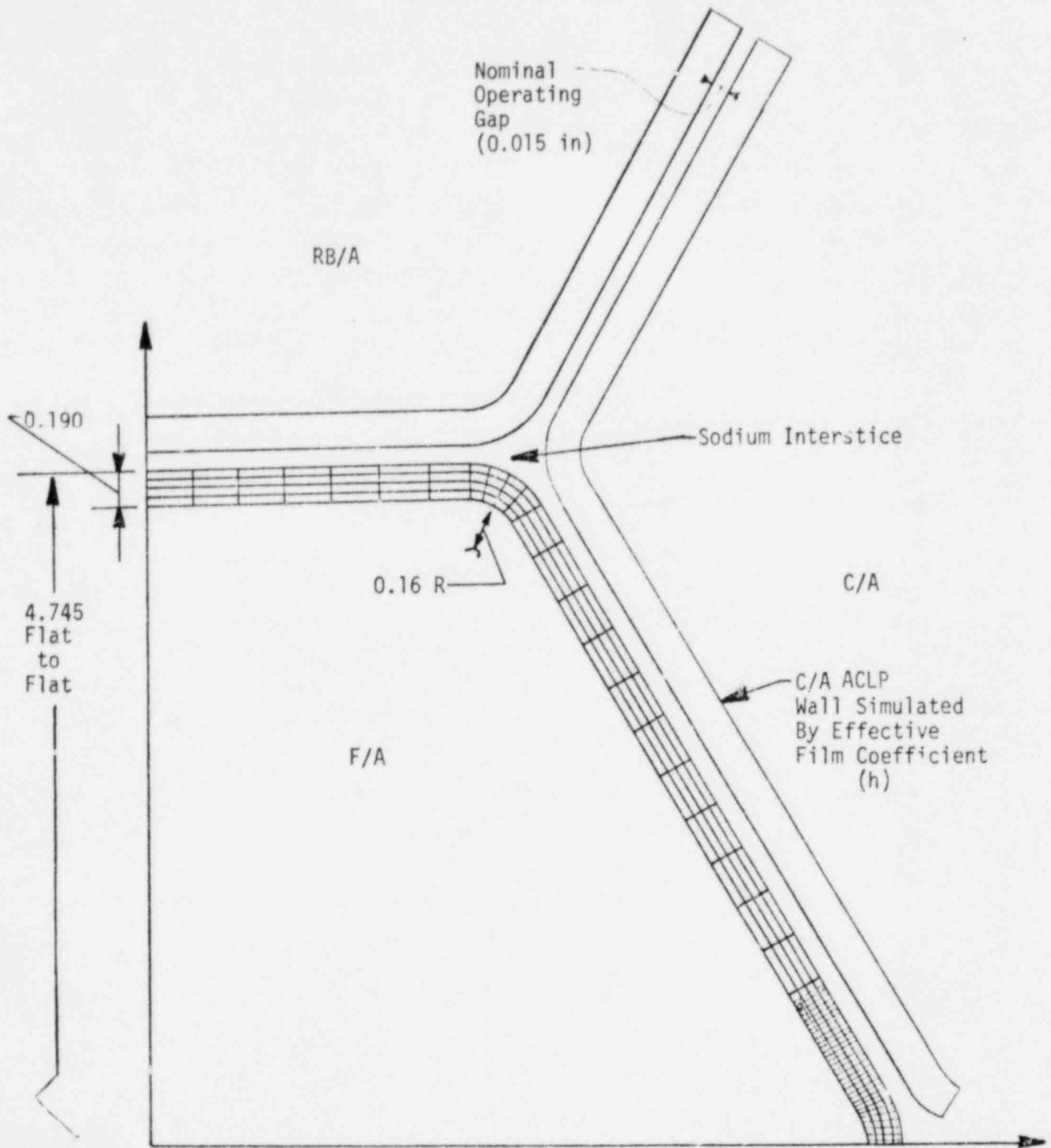


Figure 6.1-8  
 F/A ACLP Hex Duct  
 Dimensional Extent and Finite Element Detail

### 6.1.2.2 Properties

The F/A ACLP hex duct is constructed from first core 20% CW-316-SS. The thermal conductivity (K), specific heat (C), and density ( $\rho$ ) of 20% CW-316-SS are known to not significantly differ from SA-316-SS values. Accordingly, the first core 20% 316-SS properties used in the F/A ACLP hex duct thermal analysis were identical to the SA-316-SS properties identified for the F/A shield block described in Section 4.1.2.2.

### 6.1.2.3 Boundary Conditions and Wetted Surfaces

The F/A ACLP hex duct boundary conditions and wetted surfaces selected in the thermal analysis are illustrated in Figure 6.1-9.

Boundary conditions for the thermal analysis consisted of adiabatic conditions along the lateral surfaces coincident with the Global X and Y axes of the 90° sector model. In simulating the thermal resistance of the C/A ACLP hex duct wall, the effective film coefficient ( $h=0.00104$  BTU/in<sup>2</sup>-sec-°F) was based on a thermal conductivity ( $K=0.000197$  BTU/in-sec-°F) and wall thickness ( $L=0.190$  in). The effective film coefficient ( $h$ ) was specified at the free surfaces of all elements forming the exterior of the F/A ACLP hex duct which included elements 8 through 40, increments of 8; 49 through 153, increments of 8; element 163; elements 169 through 223, increments of 6, and 230 through 296, increments of 6.

The wetted interior F/A ACLP surfaces were assumed to response immediately to the inside metal wall temperatures of the worst case F/A ACLP duty cycle. Local variations in wetted interior surface temperatures were neglected. Instead, all F/A ACLP hex duct interior surface node temperatures were globally coupled to each other and included Nodes 1 through 172, increments of 9; and 181 through 315, increments of 7.

With regard to the wetted interior C/A ACLP surfaces which are exposed to inside metal wall temperatures, local temperature variations were also neglected and a global variation assumed in the form of a bulk temperature. The bulk temperatures were specified in accordance with C/A inside metal

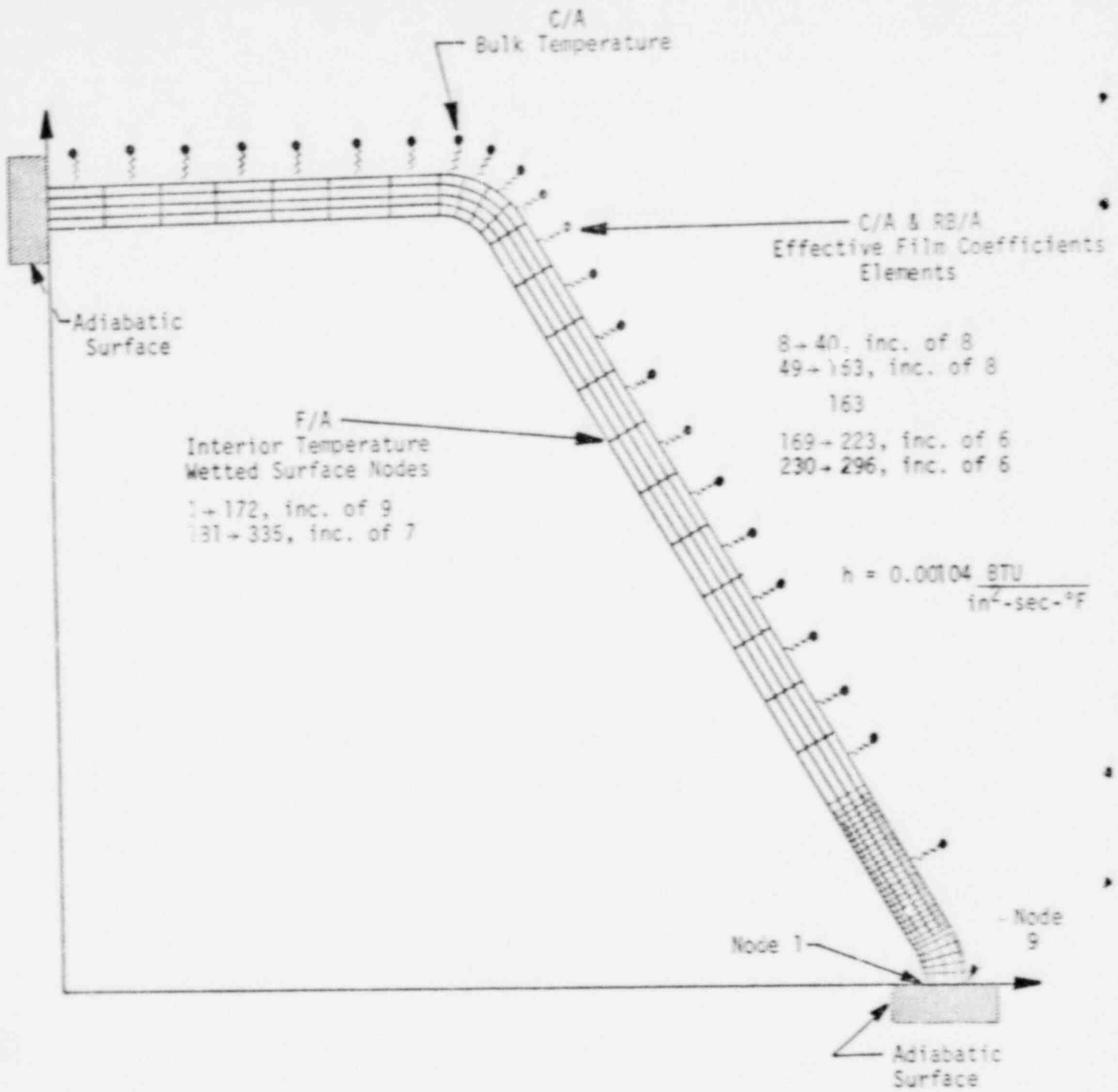


Figure 6.1-9  
F/A ACLP Hex Duct  
Boundary Conditions and Wetted Surface.



surface temperature variations of the worst case F/A ACLP hex duct cycle and applied to the F/A through the effective C/A wall film coefficients.

#### 6.1.2.4 Heat Generation Rates

During steady state operation, the F/A ACLP hex duct is exposed to nuclear heating. The maximum heating rate per unit volume was relatively uniform with a value of 1.919 watts/cc or 0.0295 BTU/in<sup>3</sup>-sec. For the F/A ACLP hex duct exposed to a heat generation rate (Q) with thermal conductivity (K) and wall dimension (L), the temperature difference ( $\Delta T$ ) is given by:

$$\Delta T = QL^2/2K$$

$$\Delta T = \frac{(0.0295 \text{ BTU/in}^3\text{-sec}) (0.205 \text{ in})^2}{2(2.87 \times 10^{-4} \text{ BTU/in-sec}^\circ\text{F})}$$

$$\Delta T = 2.16 \text{ }^\circ\text{F}$$

For the F/A ACLP hex duct, the steady state temperature difference ( $\Delta T_{ss}$ ) caused by sodium flow was 200°F. As  $\Delta T \ll \Delta T_{ss}$ , the steady state temperature is insignificant, and heat generation rates were neglected in the thermal analysis.

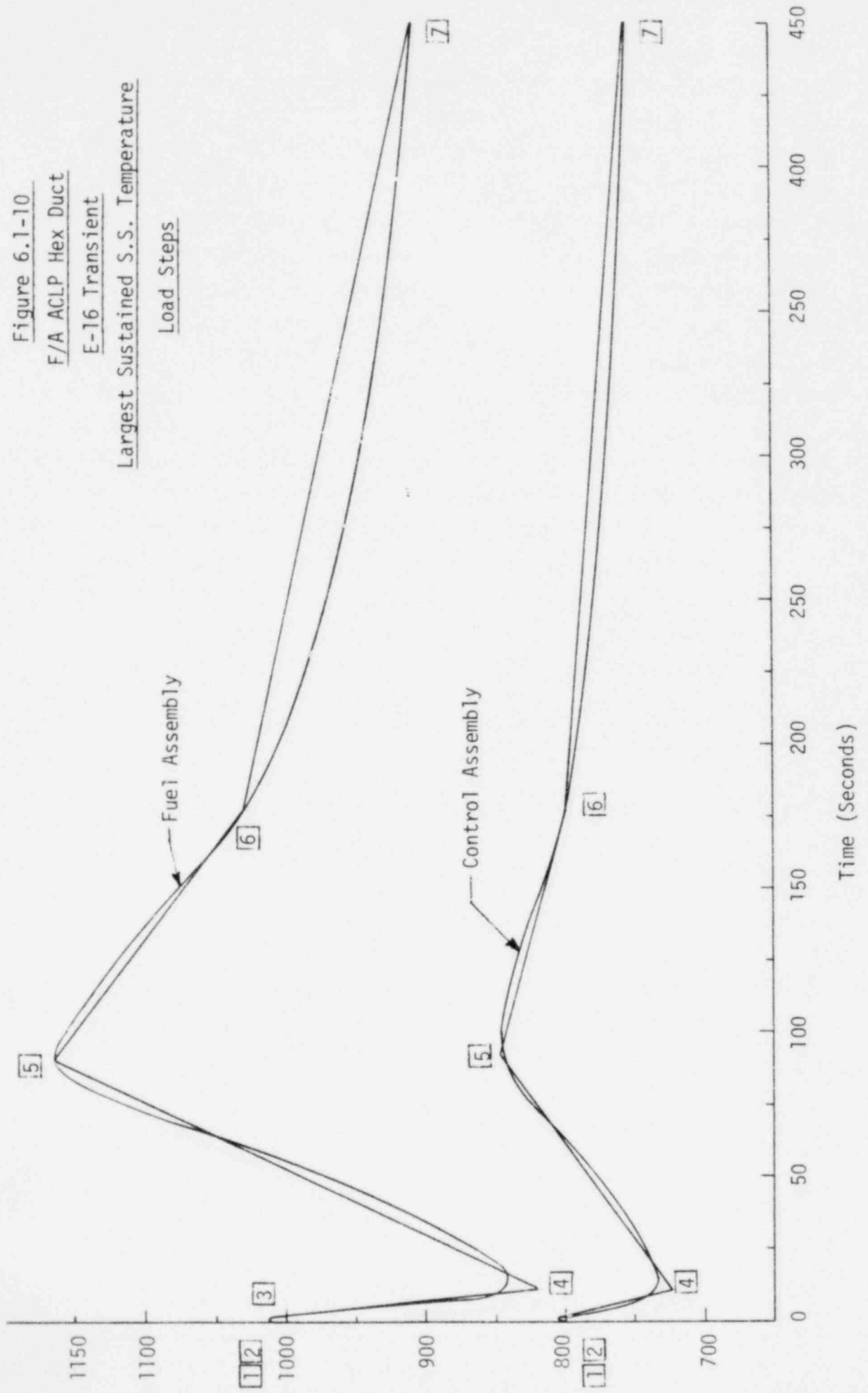
### 6.1.2.5 Analysis and Results

The ANSYS thermal analysis of the F/A ACLP hex duct was arranged to provide detailed temperature distributions over the total worst case duty cycle. A total of 10 load steps were selected at prominent F/A and C/A inside metal surface temperatures. The first 7 Load Steps characterized the initial steady state conditions and the E-16 transient to 450 seconds. Load Steps 1 and 2 represent initial steady state conditions while Load Steps 3 through 7 correspond to the E-16 transient. Load Step 8 corresponds to the 1 hour cool-down to 600°F. The return to final steady state temperatures with the 1 hour heat-up was accomplished in Load Step 9. The final steady state temperatures held for 10 days were obtained in Load Step 10. Prominent Load Steps in the E-16 transient are illustrated in Figure 6.1-10 and numerical values for the full worst case F/A ACLP hex duct duty cycle are presented in Table 6.1-4.

TABLE 6.1-4  
WORST CASE F/A ACLP HEX DUCT DUTY CYCLE  
ANSYS INPUT DATA

Load Step	Time (Sec)	Temp (°F)	
		F/A	C/A
1	0.0	1000	800
2	0.0	1000	800
3	2.0	1010	805
4	12.5	820	735
5	90	1155	845
6	175	1030	800
7	450	1010	755
8	4050	600	600
9	7650	1000	800
10	900000	1000	800

Figure 6.1-10  
 F/A ACLP Hex Duct  
 E-16 Transient  
 Largest Sustained S.S. Temperature  
 Load Steps



The ANSYS solution of the worst case F/A ACLP hex duct duty cycle was obtained in 74 cumulative iterations using a static and transient convergence criteria of 1 and 5°F respectively. The temperature distributions at each cumulative iteration were saved on ANSYS Tape 4 for recall in subsequent structural analysis. In order to determine the cumulative iterations of interest in structural analysis, maximum and minimum through the wall temperature differences are most important in relation to structural damage. The F/A ACLP hex duct temperature differences were based on the through-the-wall temperatures at nodes 1 and 9 depicted in Figure 6.1-9. A plot of the F/A ACLP hex duct temperature differences is presented in Figure 6.1-11.

A review of the through-the-wall temperature differences shows that the maximum and minimum values occur at cumulative iterations 32 and 61 respectively, with a range of 174°F. In the thermal solution run, cumulative iteration 32 corresponds to the E-16 transient at 90 seconds as illustrated in Figure 6.1-6. The initial steady state condition corresponds to cumulative iteration 2 with a temperature difference of 110°F. Plots of the temperature distributions throughout the F/A ACLP hex duct thermal model at cumulative iterations 2 and 32 are presented in Figure 6.1-12.

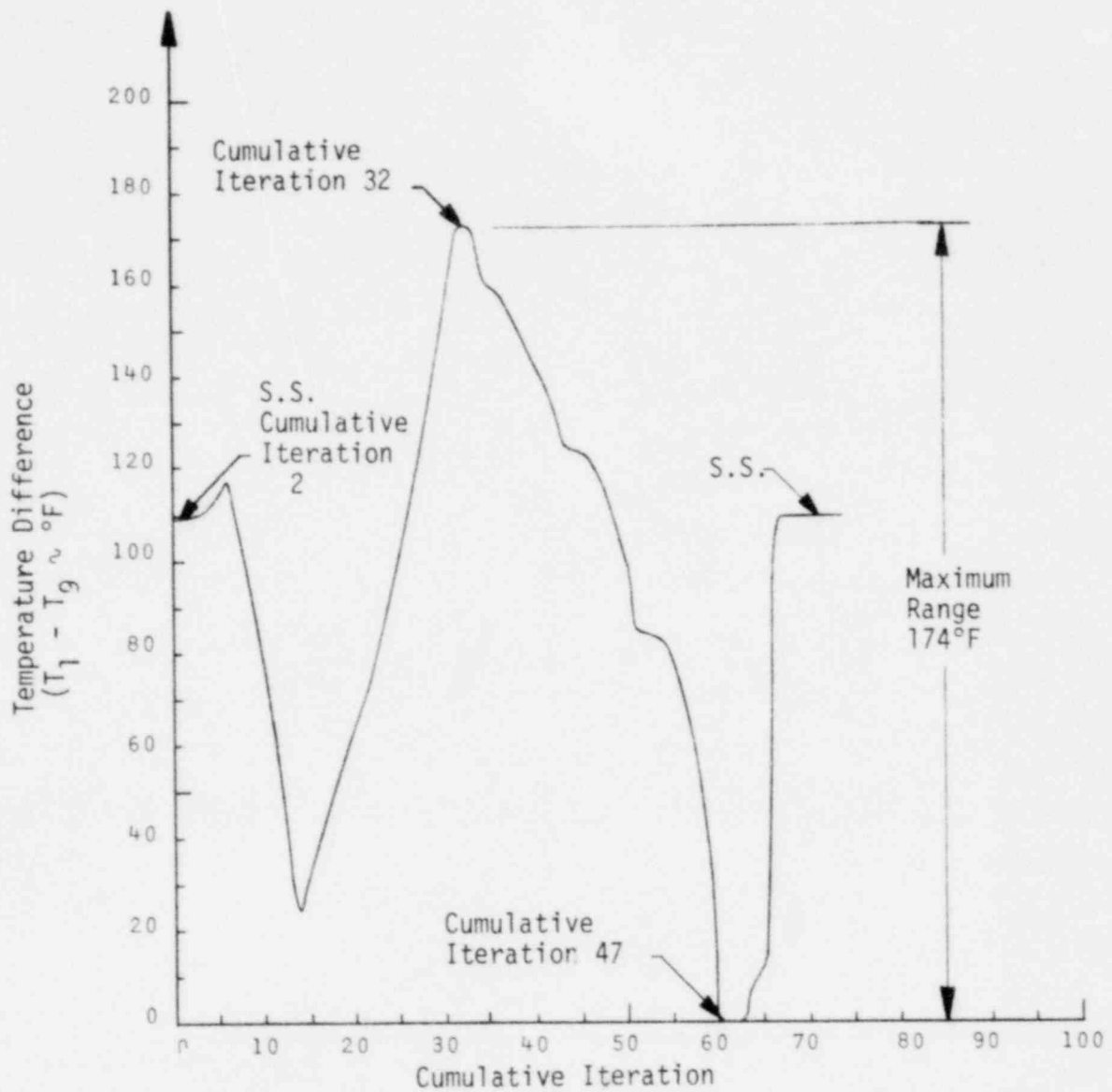


Figure 6.1-11  
 F/A ACLP Hex Duct  
 E-16 Transient  
 Temperature Difference vs. Cumulative Iteration

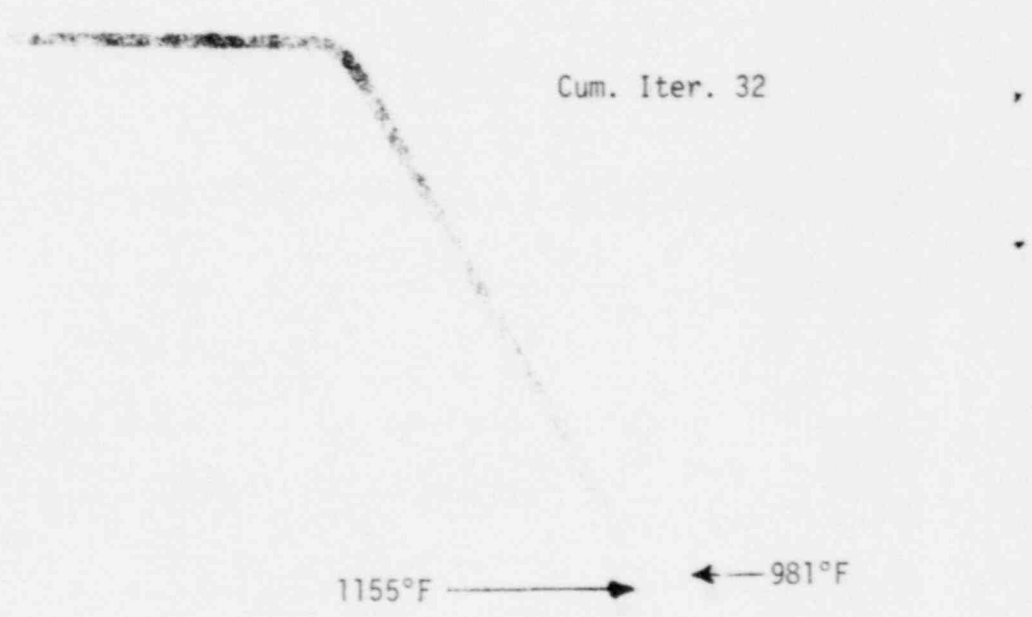
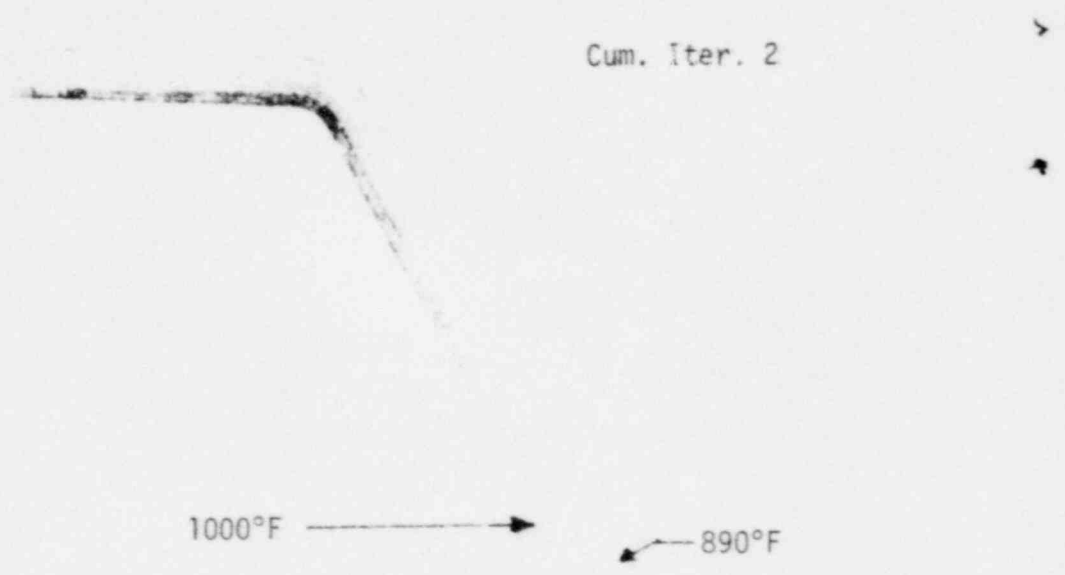


Figure 6.1-12  
 F/A ACLP Hex Duct  
 E-16 Transient  
 Cumulative Iteration 2 and 32 Temperature Distributions

### 6.1.3 Worst Case Duty Cycle

The conclusions based on the F/A ACLP hex duct loading analysis in relation to establishing the worst case duty cycle with recommendations for subsequent structural analysis were as follows.

- Mechanical loads comprising OBE and SSE beam bending, internal pressure, and deadweight were considered insignificant. Steady state and transient beam bending moments were considered negligible relative to local contact loads and SSE loads are more severe than OBE local contact loads. Only local contact loads caused by core restraint under steady state and transient operation, and during SSE seismic events were considered to be of significance in establishing the worst case F/A ACLP hex duct duty cycle.
- Thermal and mechanical core restraint loads associated with the E-16 transient in combination with the thermal conditions in returning to steady state and the hold-time prior to the initiation of the next E-16 transient were considered most important in establishing the worst case F/A ACLP hex duct duty cycle.

In order to provide a consistent basis for combining the local contact steady state and transient core restraint and SSE seismic loads with the E-16 steady state and transient thermal loads, a 90° sector of the ACLP cross -section was selected. The local ACLP hex duct contact loads were conservatively assumed to be load controlled even though attendant deformations may mitigate actual structural response due the restraint of adjacent ACLP hex ducts.

The recommendations for the specific F/A ACLP hex duct loading were to apply a first and second worst case duty cycle of time independent and dependent loading. The first worst case duty cycle comprising successive SSE seismic loads applied at peak E-16 transient temperatures and core restraint loads was to be applied only once. The second worst case duty cycle comprising the E-16 transient temperatures and core restraint loads,

but excluding additional SSE loads, was considered to be repeated 38 times. In this arrangement, the recommended number and characteristics of the first and second worst case F/A ACLP hex duct duty cycles provide an upper bound to the 39 specified 'Upset events and the worst Emergency or Faulted event.

#### First Cycle - Time Independent (One Application)

- Select a uniform temperature equal to the reference temperature at cumulative iteration 2. Load to the cumulative iteration 2 temperature distribution and apply the steady state core restraint local contact loads. Unload to uniform temperature.
- Select a uniform temperature equal to the reference temperature at cumulative iteration 32. Load to the cumulative iteration 32 temperature distribution and apply the transient core restraint local contact loads. Apply successive SSE seismic local contact loads until shakedown is observed. Unload to uniform temperature.
- Select a uniform temperature equal to the reference temperature at cumulative iteration 2. Load to the cumulative iteration 2 temperature distribution and apply the steady state core restraint local contact loads.

#### First Cycle - Time Dependent (One Application)

- Hold the cumulative iteration 2 temperature distribution in combination with the 2 face steady state core restraint local contact loads for 10 days.

#### Second Cycle - Time Independent (Repeat 38 times)

- Select a uniform temperature equal to the reference temperature at cumulative iteration 2. Load to the cumulative iteration 2 temperature distribution and apply the steady state core restraint local contact loads. Unload to uniform temperature.



- Select a uniform temperature equal to the reference temperature at cumulative iteration 32. Load to the cumulative iteration 32 temperature distribution and apply the transient core restraint local contact loads. Unload to uniform temperature.
- Select a uniform temperature equal to the reference temperature at cumulative iteration 2. Load to the cumulative iteration 2 temperature distribution and apply the steady state core restraint local contact loads

Second Cycle - Time Dependent (Repeat 38 times)

- Hold the cumulative iteration 2 temperature distribution in combination with the 2 face steady state core restraint local contact loads for 10 days.

## 6.2 Structural Analysis

The F/A ACLP hex duct structural analysis was directed to deriving the stresses and strains, and dimensional changes which occur during the first and second worst case duty cycles from which structural evaluations were made. In the following, the F/A ACLP hex duct structural model, geometry, and boundary conditions are described. Next, linear and non-linear material properties including the effects of irradiation on stress-strain curves and simplification made in the thermal creep equations are presented. Further, reference temperature selection for thermal expansions in relation to axial constraints is described. Finally, the first and second worst case duty cycle time independent and dependent inelastic analysis and results for the F/A ACLP hex duct are presented in preparation for subsequent structural evaluation.

### 6.2.1 Model, Geometry and Boundary Conditions

The F/A ACLP hex duct model was formulated in the ANSYS finite element program so as to be compatible with the temperature distributions of the thermal model. The F/A ACLP geometry was taken to be identical to that used for the thermal analysis, except that the film coefficients simulating the C/A ACLP wall thermal resistance were deleted.

In formulating the F/A ACLP hex duct structural model, the ANSYS constant strain (STIF 2) structural element was used to replace the linear temperature (STIF 35) thermal element. The boundary conditions along the lateral surfaces of the 90° sector coincident with the global X and Y axes, in the manner of the conventional roller support, were taken to have zero normally disposed displacements. Coincident with the global X axis, the UY displacements at nodes 1 through 9 were set equal to zero. For the surface coincident with the global Y axis, the UX displacements at nodes 335 through 341 were set corners of the ACLP hex duct cross-section. With the 90° sector of the ACLP formulated in a plane strain condition, the local contact loads ( $F_1$ ,  $F_2$ ,  $F_3$ ) were expressed in terms of a load/length basis by dividing each load by the 4 in. ACLP pad length. The F/A ACLP hex duct structural model is illustrated in Figure 6.2-1.

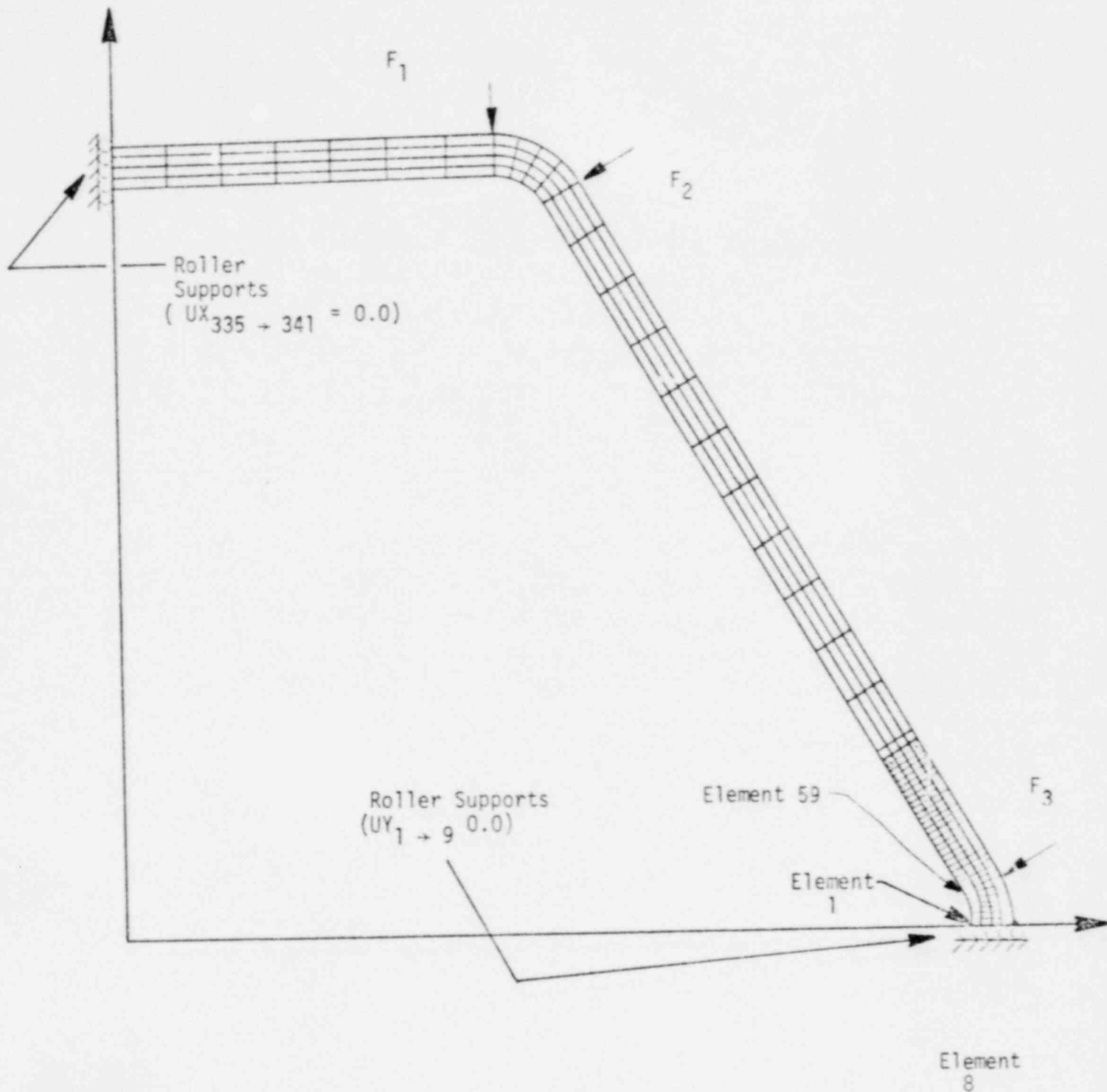


FIGURE 6.2-1  
 F/A ACLP Hex Duct  
 Structural Model, Geometry, and Boundary Conditions

## 6.2.2 Properties

The F/A ACLP hex duct as constructed from first core 20 percent CW-316-SS is initially unirradiated to a fluence ( $E > 0.1$  Mev,  $(\phi t) = 0.59 \times N/CM^2$ ) at EOL. The linear and non-linear properties of first core 20% CW-316-SS under fluence and temperature with simplifications used in the F/A ACLP hex duct analysis are described as follows.

### 6.2.2.1 Linear

The linear 20% CW-316-SS properties including the Young's Modulus (E), Poisson's ratio ( $\nu$ ), and coefficient of thermal expansion ( $\alpha$ ) are known to not significantly differ from SA-316-SS values. Accordingly, the first core 20% CW-316-SS properties used in the F/A ACLP hex structural analysis were identical to the SA-316-SS properties identified for the F/A shield block described in Section 4.2.2.1.

### 6.2.2.2 Non-Linear

The non-linear first core 20% CW-316-SS material property behavior required in the F/A ACLP hex duct structural analysis are the time independent stress-strain curves and the time dependent thermal creep equations, and irradiation creep and swelling equations.

#### 6.2.2.2.1 Stress Strain Curves

Currently, stress-strain properties of irradiated first core 20% CW-316-SS are not extensively known as prior experimental effort has been primarily directed to N-Lot steel. The available stress-strain properties of first core steel [11] are limited to fluence ( $E > 0.1$  Mev) of  $3 \times 10^{22}$  N/CM<sup>2</sup> over a temperature range from 1000 to 1200°F. As the ACLP hex duct EOL fluence ( $E > 0.1$  Mev) is  $0.59 \times 10^{22}$  N/CM<sup>2</sup>, the available data requires extrapolation in order to obtain irradiated first core 20% CW-316-SS stress-strain data for use in the F/A ACLP hex duct analysis. With regard to unirradiated first core 20% CW-316-SS stress-strain data, unirradiated N-Lot data is representative and was taken for the F/A ACLP hex duct analysis.

In constructing the F/A ACLP hex duct stress-strain which are compatible with the worst case duty cycles uniformly distributed over the first and second reactor cycles, a mean of true minimum BOL and the minimum EOL stress-strain values was taken. Minimum properties were selected to provide conservative inelastic stress and strain response because mechanical and thermal ACLP hex duct loads were assumed to be applied slowly in an essentially static manner. For elastic BOL and EOL response of the F/A ACLP hex duct, the Young's Modulus for unirradiated and irradiated first core 20% CW-316-SS was taken to be identical to the Young's Modulus for unirradiated SA-316-SS as described for the F/A shield block in Section 4.2.2.1. In the following, the unirradiated and irradiated stress-strain data used in the F/A ACLP hex duct analysis are identified.

The average unirradiated engineering stress-strain data for N-lot 20% CW-316-SS used to represent unirradiated first core steel in the inelastic response of the F/A ACLP hex duct is given in the NSM Handbook [6]. Minimum unirradiated engineering N-Lot stress strain data was taken as 80% of average values. The minimum engineering unirradiated proportional elastic limit stress ( $\bar{\sigma}_{PEL,u}$ ), yield stress ( $\bar{\sigma}_{Y,u}$ ), ultimate stress ( $\bar{\sigma}_{u,u}$ ), and uniform elongation strain ( $\bar{\epsilon}_{u,u}$ ), where stress and strain is in units of KSI and in/in respectively, in terms of temperature ( $T \sim ^\circ F$ ) is given according to the relations.

$$\bar{\sigma}_{PEL,u} = 0.80 \bar{\sigma}_{Y,u}$$

$$\begin{aligned} \bar{\sigma}_{Y,u} = & 76.89 - 0.10*T + (1.208E-3)*T^2 - (0.817E-5)*T^3 + (3.04E-8)*T^4 \\ & - (6.75E-11)*T^5 + (0.931E-13)*T^6 - (7.99E-17)*T^7 + (4.14E-20)*T^8 \\ & - (1.18E-23)*T^9 + (1.42E-27)*T^{10} \end{aligned}$$

$$\begin{aligned} \bar{\sigma}_{u,u} = & 97.62 - (0.812E-1)*T + (6.67E-4)*T^2 - (2.69E-6)*T^3 + (4.98E-9)*T^4 \\ & - (4.58E-12)*T^5 + (2.04E-15)*T^6 - (3.46E-19)*T^7 \end{aligned}$$

$$\begin{aligned} \bar{\epsilon}_{u,u} = & 0.104 + (4.81E-4)*T - (7.0E-6)*T^2 + (4.33E-8)*T^3 - (1.49E-10)*T^4 \\ & + (3.0E-13)*T^5 - (3.64E-16)*T^6 + (2.70E-19)*T^7 - (1.19E-22)*T^8 + (2.89E-26)*T^9 \\ & + (2.95E-30)*T^{10} \end{aligned}$$

The minimum irradiated engineering stress-strain data for first core 20% CW-316-SS used for the F/A ACLP hex duct at EOL fluence ( $E > 0.1$  Mev,  $(\phi t) = 0.59 \times 10^{22}$  n/cm<sup>2</sup>) were taken from the available first core data [11]. The minimum irradiated engineering proportional elastic limit stress ( $\bar{\sigma}_{PEL,I}$ ), yield stress ( $\bar{\sigma}_{Y,I}$ ), ultimate stress ( $\bar{\sigma}_{u,I}$ ), and uniform elongation ( $\bar{\epsilon}_{u,I}$ ) in terms of temperature ( $T \sim ^\circ F \times 10^{-2}$ ) are as follows.

$$\bar{\sigma}_{PEL,I} = 0.86 \bar{\sigma}_{Y,I}$$

$$\bar{\sigma}_{Y,I} = 60.596 - 0.817*T - 0.0601*T^2$$

$$\bar{\sigma}_{u,I} = 78.92 + 3.68*T - 0.47*T^2$$

$$\bar{\epsilon}_{u,I} = 0.128 + 0.0108*T + 0.000938*T^2 - 0.00018*T^3$$

In order to obtain true minimum stress-strain data from minimum engineering data for unirradiated BOL and irradiated EOL conditions of the F/A ACLP hex duct, the following relations between true stress and strain ( $\sigma, \epsilon$ ) and engineering stress and strain ( $\bar{\sigma}, \bar{\epsilon}$ ) were used.

$$\sigma_{PEL,u} = \bar{\sigma}_{PEL,u}$$

$$\sigma_{PEL,I} = \bar{\sigma}_{PEL,I}$$

$$\sigma_{Y,u} = \bar{\sigma}_{Y,u}$$

$$\sigma_{Y,I} = \bar{\sigma}_{Y,I}$$

$$\sigma_{u,u} = (1 + \bar{\epsilon}_{u,u}) \bar{\sigma}_{u,u}$$

$$\sigma_{u,I} = (1 + \bar{\epsilon}_{u,I}) \bar{\sigma}_{u,I}$$

$$\epsilon_{u,u} = \ln(1 + \bar{\epsilon}_{u,u})$$

$$\epsilon_{u,I} = \ln(1 + \bar{\epsilon}_{u,I})$$

The mean of true minimum unirradiated BOL and true minimum irradiated EOL stress-strain for the F/A ACLP hex duct over a temperature range of 800 to 1200°F are summarized in Table 6.2-1.

TABLE 6.2-1  
F/A ACLP HEX DUCT  
TRUE MINIMUM MEAN OF BOL AND EOL  
STRESS-STRAIN DATA

Temp. (°F)	Young's Modulus (PSI X 10 <sup>6</sup> )	Stress (PSI) at Total Strain (in/in)				
		0.00178	0.00378	0.01	0.04	0.08
800	24.06	42830	55390	56900	62700	68500
900	23.31	41490	53940	55360	60790	66220
1000	22.53	40100	51920	53290	58500	63800
1100	21.72	38660	48470	49810	54960	60100
1200	20.89	37180	43300	44650	49830	55000

In order to illustrate the approach adopted to represent the mean of true minimum unirradiated BOL and irradiated EOL stress-strain data for the F/A ACLP hex duct during the worst case duty cycles, the respective average, minimum, and mean stress-strain curves for first core 20% CW-316-SS at 1000°F are presented in Figure 6.2-2.

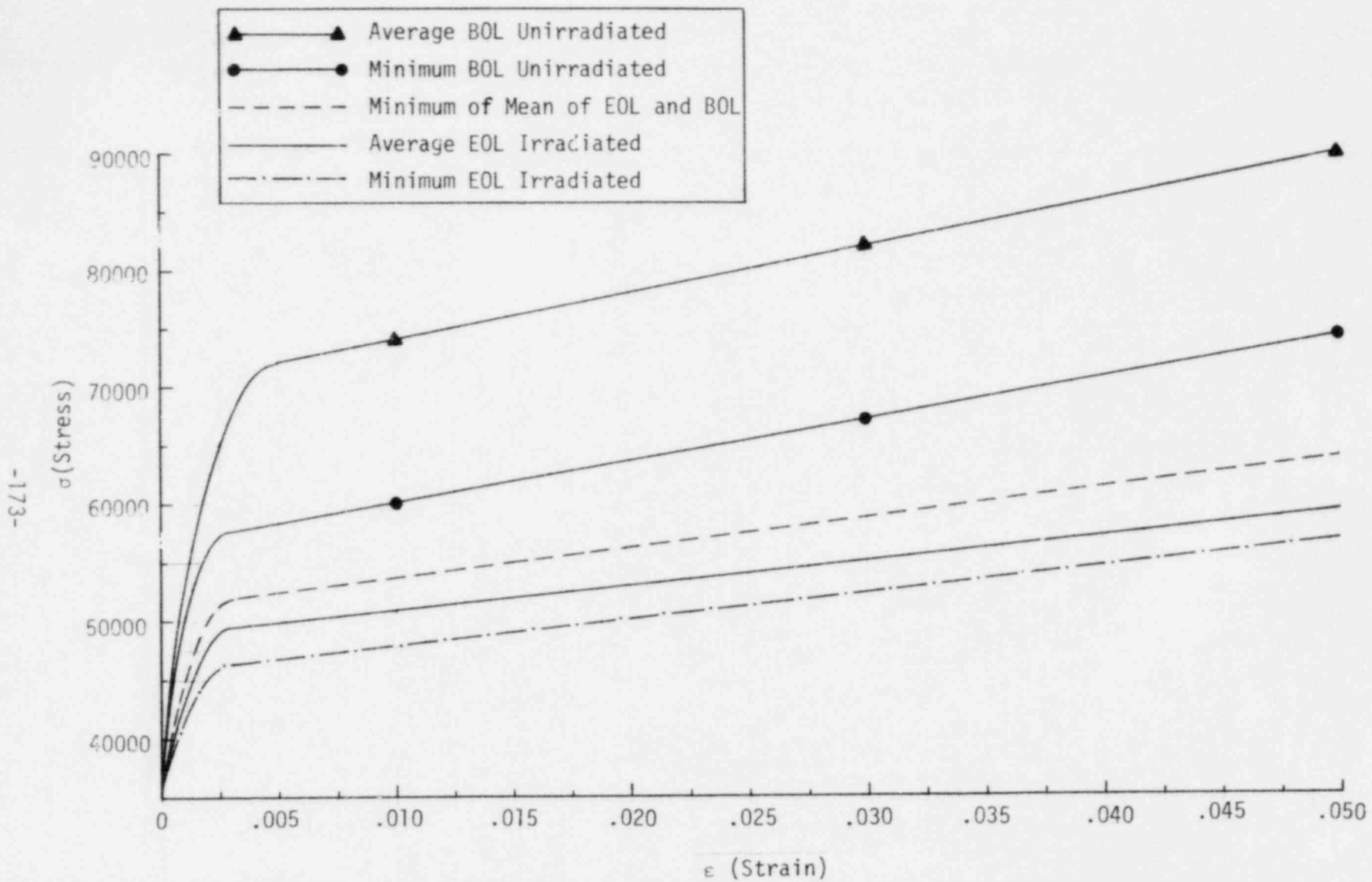


FIGURE 6.2-2  
 F/A ACLP HEX DUCT  
 FIRST CORE 20% CW-316-SS STRESS-STRAIN CURVES  
 MINIMUM MEAN OF BOL AND EOL AT 1000°F



#### 6.2.2.2.2 Thermal Creep Equations

The thermal creep equations for irradiated and unirradiated first core 20% CW-316-SS are currently being developed and have not been placed into an approved form for use in the F/A ACLP hex duct analysis. However, thermal creep equations for unirradiated N-Lot 20% CW-316-SS are identified as the interim NSM Handbook relations [12] are available which tends to approximate first core steel thermal creep. Accordingly, the N-Lot 20% CW-316-SS thermal creep equations were used in the F/A ACLP hex duct analysis.

The thermal creep equations for N-Lot 20% CW-316-SS are expressed in terms of a hoop strain ( $\epsilon_c$ ) and stress ( $\sigma$ ) as the experimental data was based on pressurized thin walled tubes. In applying the pressurized thin walled tube data to multiaxial stress states in the F/A ACLP hex duct, equivalent stress ( $\sigma_e$ ) and strain ( $\epsilon_e$ ) were used according to the relations:

$$\sigma_e = \frac{\sqrt{3}}{2} \sigma \text{ and } \epsilon_e = \frac{2}{\sqrt{3}} \epsilon_c$$

The thermal creep equations for hoop strain ( $\epsilon_c$ ) and strain rate ( $\dot{\epsilon}_c$ ) from the pressurized thin walled tube data is presented in both integrated and rate form.

$$\epsilon_c = A\sigma \cosh^{-1} (1 + rt) + P\sigma^n t^m + Q\sigma^n t^{2.5}$$

$$\frac{d\epsilon_c}{dt} = \frac{A\sigma r}{\sqrt{2rt + r^2 t^2}} + m P\sigma^n t^{m-1} + 2.5 Q\sigma^n t^{1.5}$$

In applying the thermal creep equations to the worst case F/A ACLP hex duct duty cycle, the relaxation of thermal stresses occurs during the 10 day hold time. As the duty cycles are assumed to be successively repeated, it was desirable for the sake of conservatism to neglect the primary creep and only consider secondary creep. However, the form of the thermal creep equations used to represent the pressurized thin walled

tube data does not permit a separation of primary and secondary creep. Accordingly, both primary and secondary thermal creep were considered to occur simultaneously in successive duty cycles. The approach is considered only slightly non-conservative as thermal creep was not expected to be significant at the steady state operational temperature of 1000°F. A summary of the N-Lot thermal creep equation for hoop strain ( $\epsilon_c \sim \%$ ) and stress ( $\sigma \sim \text{PSI}$ ), time ( $t \sim \text{HRS}$ ), and temperature ( $T \sim ^\circ\text{K}$ ) are presented as follows.

$$\ln A = \left\{ \begin{array}{l} -8.94451 - \frac{4.3314 \times 10^3}{T} \\ \text{or} \\ -1.3748 - \frac{1.07471 \times 10^4}{T} \end{array} \right.$$

whichever yields the smaller value of  $\ln A$

$$\ln r = \left\{ \begin{array}{l} -2.99573 \\ \text{or} \\ 291.069 - \frac{926\,425.0}{T} + \frac{1.0114 \times 10^9}{T^2} - \frac{3.70757 \times 10^{11}}{T^3} \end{array} \right.$$

whichever yields the larger value of  $\ln r$

$$n = \left\{ \begin{array}{l} 6.3 \quad \text{for } T \leq 922.039^\circ\text{K} (1200^\circ\text{F}) \\ \text{or} \\ -124.593 + 0.283804T - 1.539 \times 10^{-4} T^2 \\ \quad \text{for } T > 922.039^\circ\text{K} (1200^\circ\text{F}) \end{array} \right.$$

$$m = \left\{ \begin{array}{l} 0.533 \quad \text{for } T \leq 922.039 \\ \text{or} \\ 44.5365 - 0.0954482 T + 5.17593 \times 10^{-5} T^2 \\ \quad \text{for } T > 922.039^\circ\text{K} (1200^\circ\text{F}) \end{array} \right.$$

$$\ln P = \begin{cases} 35.3606 - \frac{8.96596 \times 10^4}{T} & \text{for } T < 810.928^\circ\text{F} (1000^\circ\text{F}) \\ \text{or} \\ 5131.26 - \frac{1.35198 \times 10^7}{T} + \frac{1.17285 \times 10^{10}}{T^2} - \frac{3.39674 \times 10^{12}}{T^3} & \end{cases}$$

$$\text{for } 1033.15^\circ\text{K} (1400^\circ\text{F}) \geq T \geq 810.928^\circ\text{K} (1000^\circ\text{F})$$

$$\ln Q = \begin{cases} -453.917 + \frac{5.91409 \times 10^5}{T} - \frac{2.39794 \times 10^8}{T^2} & \text{for } T < 810.928^\circ\text{K} (1000^\circ\text{F}) \\ \text{or} \\ -89.2335 & \text{for } 866.483^\circ\text{K} (1100^\circ\text{F}) \geq T \geq 810.928^\circ\text{K} (1000^\circ\text{F}) \\ \text{or} \\ 1179.06 - \frac{2.19791 \times 10^6}{T} + \frac{9.52226 \times 10^8}{T^2} & \end{cases}$$

$$\text{for } 1033.15^\circ\text{K} (1400^\circ\text{F}) \geq T \geq 866.483^\circ\text{K} (1100^\circ\text{F})$$

### 6.2.2.2.3 Irradiation Creep and Swelling Equations

The irradiation creep and swelling equations for first core 20% CW-316-SS are currently being developed and have not been placed into an approved form for use in the F/A ACLP hex duct analysis. However, irradiation creep and swelling equations for N-Lot 20% CW-316-SS are available which tend to approximate first core steel irradiation creep and swelling behavior and were used in the F/A ACLP hex duct analysis.

The irradiation creep equations for N-Lot 20% CW-316-SS include both deviatoric and dilational effects. The equivalent deviatoric creep strain ( $\bar{\epsilon} \sim \text{in/in}$ ) is related to the equivalent stress ( $\bar{\sigma} \sim \text{psi}$ ) according to the relation:

$$\bar{\epsilon}/\bar{\sigma} = A [1 - e^{-f/b}] + cf + D S_0$$

where;

$$A[1 - e^{-f/b}] = \text{Primary creep term}$$

$$cf = \text{Secondary creep term}$$

$$DS_0 = \text{Swelling Term}$$

In the worst case F/A ACLP hex duct duty cycle, the relaxation of thermal stresses by irradiation creep occurs during the 10 day hold-time. However, the ACLP hex duct region is exposed to an insignificant EOL fluence ( $E > 0.1 \text{ Mev}$ ,  $(\phi t) = 0.59 \times 10^{22} \text{ n/cm}^2$ ) and little, if any, stress relaxation due to irradiation creep and swelling would be expected. In order to simplify the time dependent analysis as well as providing slightly conservative creep damage results, irradiation creep and swelling were neglected. The effects on time dependent elastic/plastic/creep instability and functional limits which would be enhanced by including irradiation creep and swelling were not considered significant.

### 6.2.3 Worst Case Duty Cycle Response

The structural response of the F/A ACLP hex duct to the first and second worst case duty cycles required the selection of reference temperatures compatible with the temperature distributions at the worst case through the wall temperature differences and axial constraints prior to deriving the time independent and dependent solutions. A description of the analysis and solutions which are required in subsequent structural evaluation is as follows.

#### 6.2.3.1 Constraints and Reference Temperature Selection

The F/A ACLP hex duct structural model corresponds to a 90° sector of a lateral slice taken through the length of the ACLP cross-section. Axial constraints normal to the 2 dimensional 90° sector reasonably simulate a plane strain condition as the length of the ACLP is comparable to the corresponding cross-sectional dimensions. Accordingly, the F/A ACLP hex duct was considered to be in a plane strain condition for the purposes of analysis.

The method of selecting a reference temperature in relation to an arbitrary temperature distribution imposed in an ANSYS plane strain model was described for the F/A shield block in Section 4.2.3.1. Using the same method for the F/A ACLP hex duct, the reference temperatures for the recommended cumulative iterations in the worst case duty cycle are summarized in Table 6.2-2.

TABLE 6.2-2  
F/A ACLP Hex Duct  
Reference Temperatures

Temperature Distribution (Cum. Iter.)	Reference Temperature ( $T_R \sim ^\circ\text{F}$ )
2	948.4
32	1072.7

### 6.2.3.2 Analysis and Results

The ANSYS inelastic analysis of the first and second worst case duty cycles was arranged in time independent and dependent loadings. The first worst case duty cycle time independent loads included the initial steady state thermal and steady state core restraint loads, the E-16 transient thermal and transient core restraint load, 2 successive peak SSE loads at maximum E-16 transient thermal and transient core restraint loads, and a return to final steady state thermal and core restraint loads. A 10 day hold-time under steady state thermal and core restraint loads comprised the time dependent loads of the first worst case duty cycle. The second worst case duty cycle time independent loads were identical to those of the first duty cycle except that the SSE loads were not repeated. The time dependent loads for the second worst case duty cycle were identical to those of the first duty cycle.

In order to follow the path dependent ACLP hex duct structural response to the first and second worst case duty cycles, the ANSYS restart option was used. In addition, the ANSYS small strain-large deformation option was used in the event that the deformations associated with the mechanical core restraint and SSE seismic loads were sufficient to initiate the collapse of the F/A ACLP hex duct due to elastic/plastic/creep instability.

#### 6.2.3.2.1 First Cycle - Time Independent

The F/A ACLP hex duct structural response to the time independent loadings of the first worst case duty cycle was obtained in 20 sequential ANSYS load steps in combination with the restart option. The first cycle time independent loadings were considered as static loadings applied at zero time. A summary of the time independent thermal and mechanical loadings for the first cycle time independent analysis is presented in Table 6.2-3.

TABLE 6.2-3

## F/A ACLP HEX DUCT

## FIRST CYCLE TIME INDEPENDENT ANALYSIS SUMMARY

## INITIAL STEADY STATE, E-16 TRANSIENT/MECHANICAL LOADS, AND FINAL STEADY STATE

Load Step	Iterations	Temperature Distribution (°F)	Reference Temperature (°F)	Mechanical Loads ( $F_1, F_2, F_3$ )	Description
1	1	948.4	948.4	None	Initial Steady State (0.0 sec)
2	1	Cum.Iter. 2	948.4	None	
3	1	Cum.Iter. 2	948.4	CR	
4	1	948.4	948.4	CR	
5	1	1072.7	1072.7	CR	E-16 Transient (90 sec)
6	1	Cum.Iter. 32	1072.7	CR	
7	1	Cum.Iter. 32	1072.7	CR	E-16 Transient (90 sec) First Cycle of SSE Loads
8	5	Cum.Iter. 32	1072.7	CR + 0.5 SSE	
9	9	Cum.Iter. 32	1072.7	CR + 1.0 SSE	
10	1	Cum.Iter. 32	1072.7	CR + 0.5 SSE	
11	1	Cum.Iter. 32	1072.7	CR	
12	1	Cum.Iter. 32	1072.7	CR	E-16 Transient (90 sec)
13	1	Cum.Iter. 32	1072.7	CR + 0.5 SSE	
14	2	Cum.Iter. 32	1072.7	CR + 1.0 SSE	Second Cycle of SSE Loads
15	1	Cum.Iter. 32	1072.7	CR + 0.5 SSE	
16	1	Cum.Iter. 32	1072.7	CR	
17	1	Cum.Iter. 32	1072.7	CR	
18	1	1072.7	1072.7	CR	E-16 Transient (4050 sec)
19	1	948.4	948.4	CR	Final Steady State (7650 sec)
20	1	Cum.Iter. 2	948.4	CR	

The F/A ACLP hex duct structural response to the first cycle time independent loadings was obtained with a plastic convergence ratio of 0.01. The detailed stress-strain response at each of the converged solutions was saved on ANSYS Tape 10 for subsequent recall in structural evaluations. The initial and final first cycle time independent steady state maximum equivalent stresses were found to be 24,038 and 20,082 psi respectively. During the E-16 transient, the maximum equivalent stresses at the cumulative iteration 32 temperature distribution with the first peak SSE loads was 46,168 psi. The peak non-uniform deformation was found to be 0.01256 in. at cumulative iteration 32. The initial and final steady state non-uniform deformations were 0.00187 and 0.00245 in. respectively. Computer plots of equivalent stress and peak non-uniform deformation are presented in Figures 6.2-3 through -5.



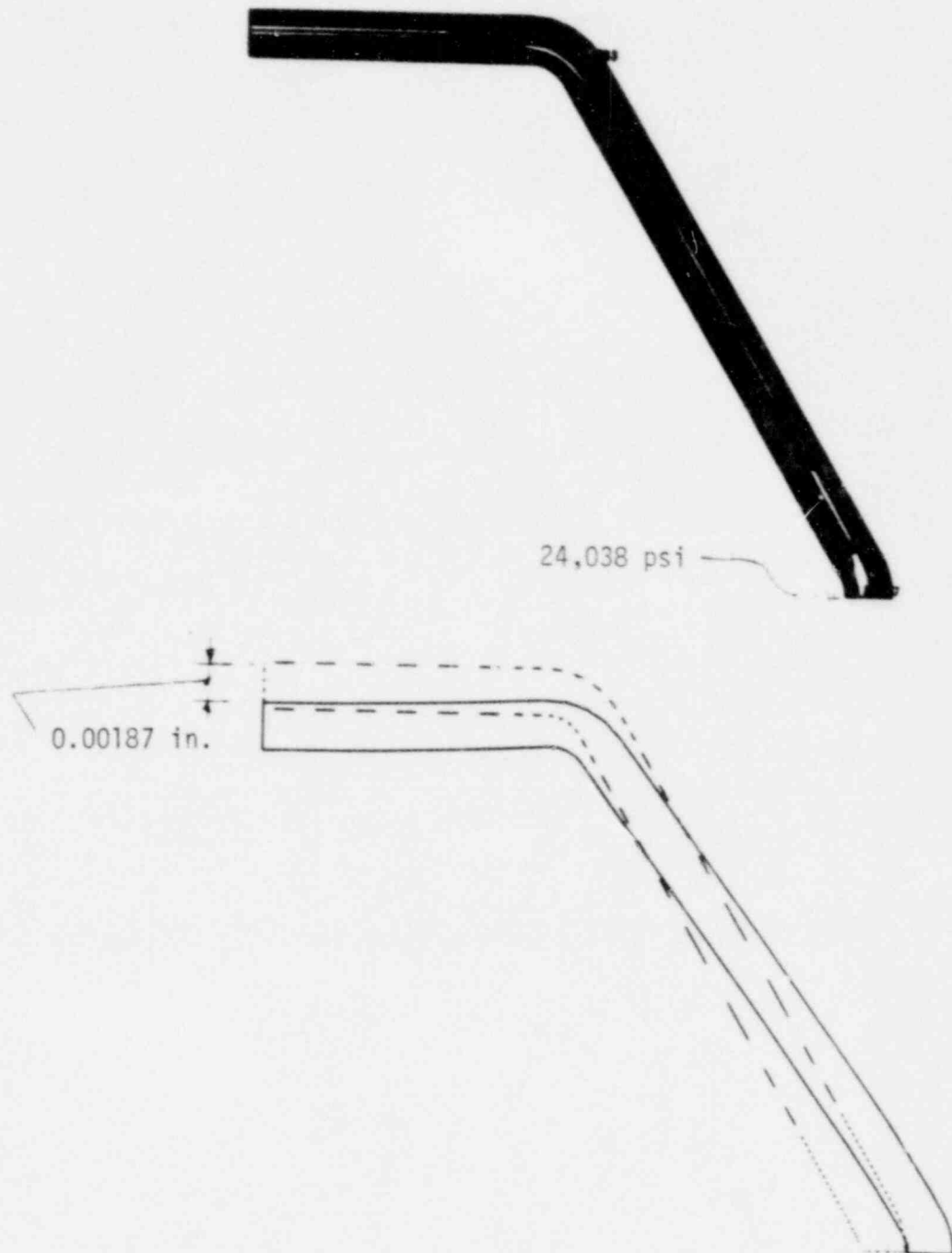


FIGURE 6.2-3  
F/A ACLP HEX DUCT  
FIRST CYCLE - TIME INDEPENDENT  
INITIAL STEADY STATE  
EQUIVALENT STRESS AND PEAK NON-UNIFORM DEFORMATION

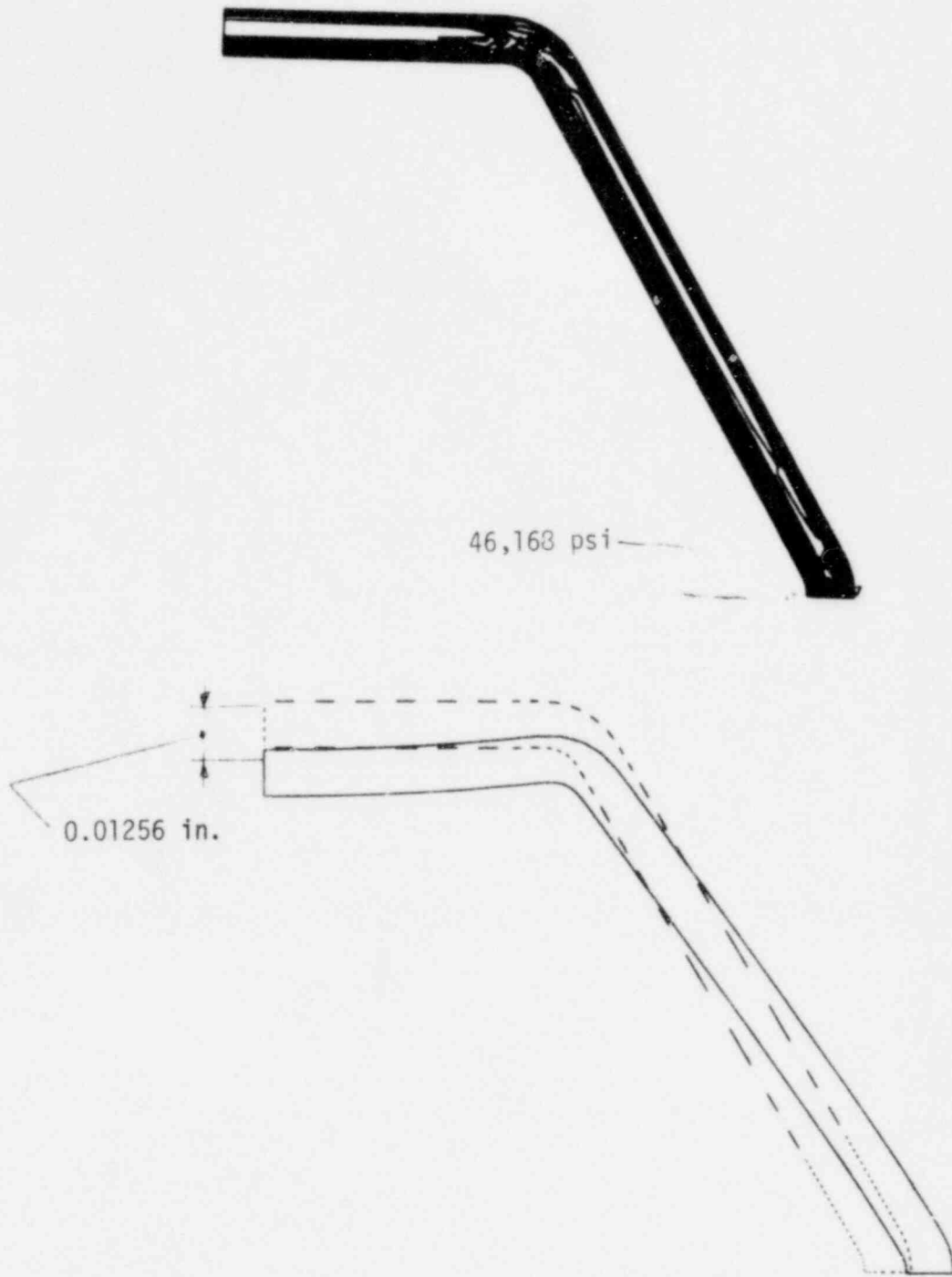


FIGURE 6.2-4  
 F/A ACLP HEX DUCT  
 FIRST CYCLE - TIME INDEPENDENT  
 CORE RESTRAINT AND SSE LOADS WITH CUMULATIVE ITERATION 32 TEMPERATURE DISTRIBUTION  
 EQUIVALENT STRESS AND PEAK NON-UNIFORM DEFORMATION

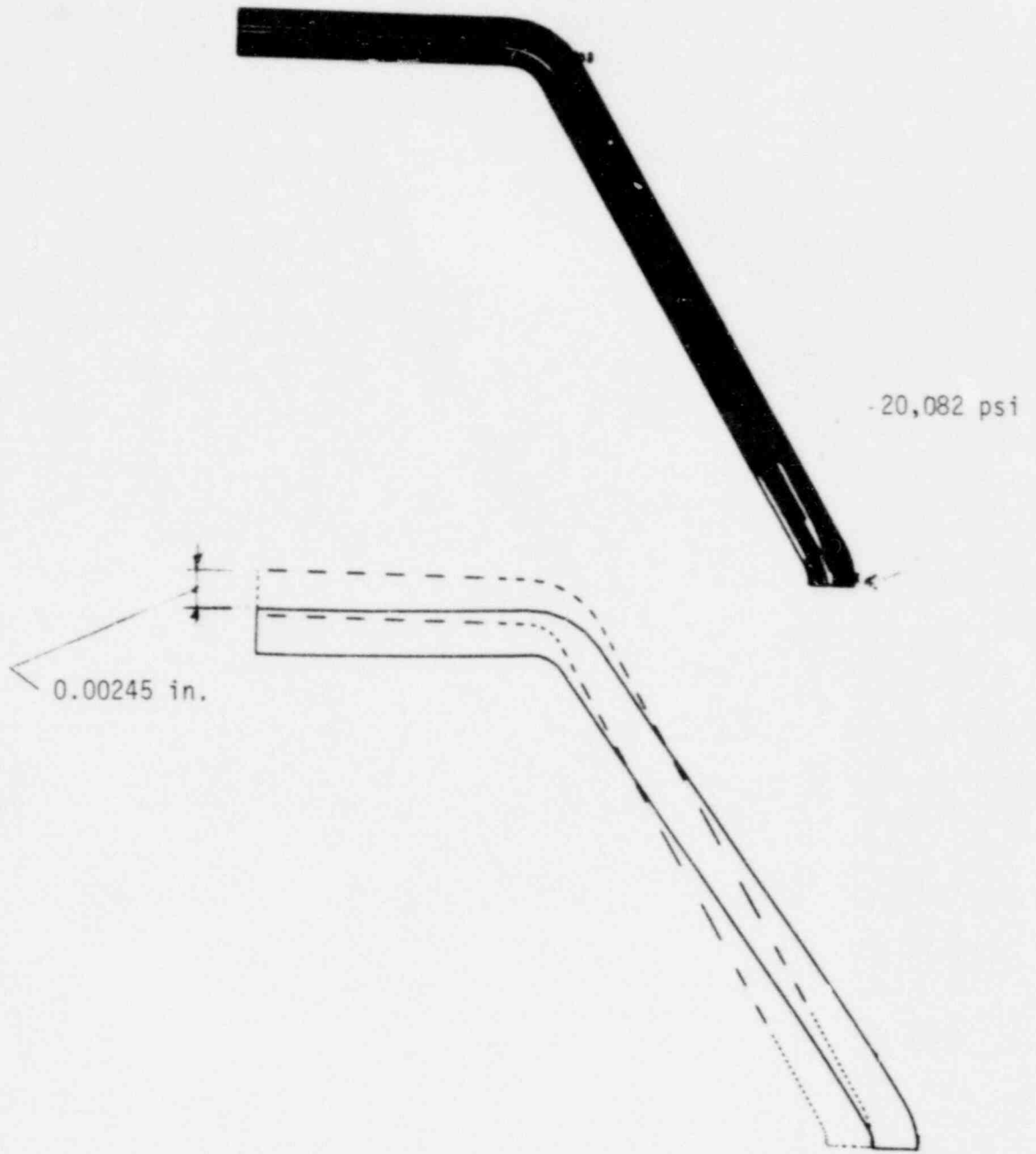


FIGURE 6.2-5  
F/A ACLP HEX DUCT  
FIRST CYCLE - TIME INDEPENDENT  
FINAL STEADY STATE  
EQUIVALENT STRESS AND PEAK NON-UNIFORM DEFORMATION

### 6.2.3.2.2 First Cycle - Time Dependent

The F/A ACLP hex duct structural response to the time dependent loadings of the first worst case duty cycle was obtained in load steps 21 through 23 with an ANSYS restart from load step 20 of the first cycle time independent analysis. A creep time step of 5 hours was used initially to follow the primary creep and increased to a 10 hour time step for the remainder of the 10 day hold time. Subsequent ANSYS restarts were made for load steps 24 through 26 to obtain the residual deformations after the first worst case duty cycle. A summary of the first cycle time dependent mechanical and thermal loadings is presented in Table 6.2-4.

TABLE 6.2-4  
F/A ACLP HEX DUCT  
FIRST CYCLE TIME DEPENDENT ANALYSIS SUMMARY  
10 DAY HOLD-TIME AND UNLOADING

Load Step	Iter.	Time (Hrs.)	Temperature Distribution (°F)	Reference Temperature (°F)	Mechanical Loads (F <sub>1</sub> , F <sub>2</sub> , F <sub>3</sub> )	Description
21	1	0.0	Cum.Iter. 2	948.4	CR	10 Day Hold-Time
22	6	30	Cum.Iter. 2	948.4	CR	
23	21	240	Cum.Iter. 2	948.4	CR	
24	1	240	Cum.Iter. 2	948.4	CR	Unloading For Residual Deformations
25	1	240	948.4	948.4	None	
26	3	240	948.4	948.4	None	

The F/A ACLP hex duct structural response to the first cycle time dependent loading was obtained with a creep convergence ratio of 0.25. The detailed stress-strain response was saved on ANSYS Tape 10 for subsequent recall in structural evaluations. The F/A ACLP hex duct structural response at the end of the 10 day hold-time, designated as the time dependent final steady state condition, was not found to significantly differ from the time independent final steady state response because of negligible relaxation

of stresses and deformations under primary and secondary thermal creep. The maximum equivalent stress and peak non-uniform deformation in the F/A ACLP hex duct at the first cycle time dependent final steady state condition were found to be 17,915 psi and 0.00267 in. as illustrated in Figure 6.2-6.

With regard to the residual stresses and deformations of the F/A ACLP hex duct, maximum values of 18,605 psi and 0.00055 in. were found for the first worst case duty cycle as illustrated in Figure 6.2-7.

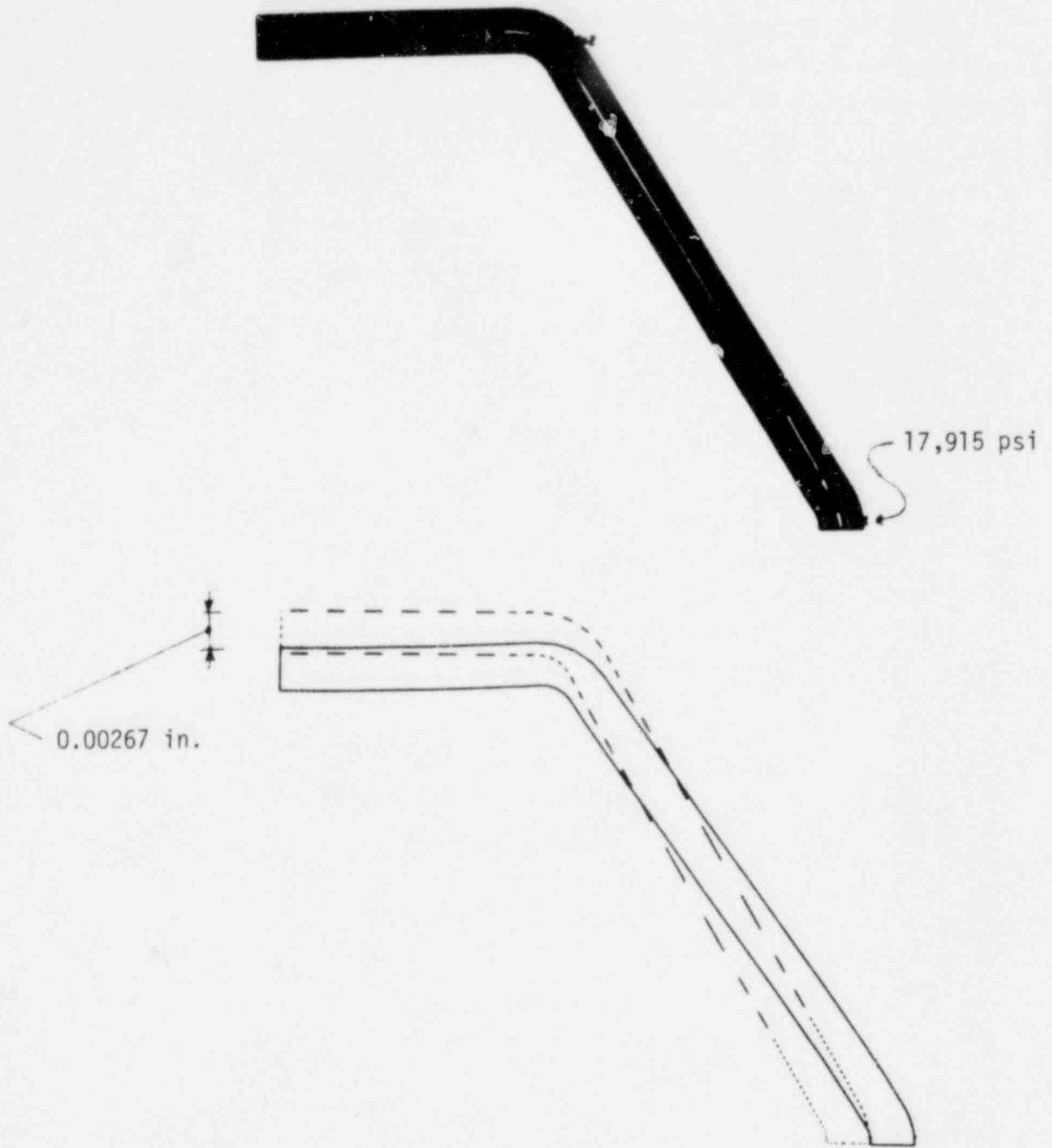


FIGURE 6.2-6  
F/A ACLP HEX DUCT  
FIRST CYCLE - TIME DEPENDENT  
FINAL STEADY STATE  
EQUIVALENT STRESS AND NON-UNIFORM DEFORMATION

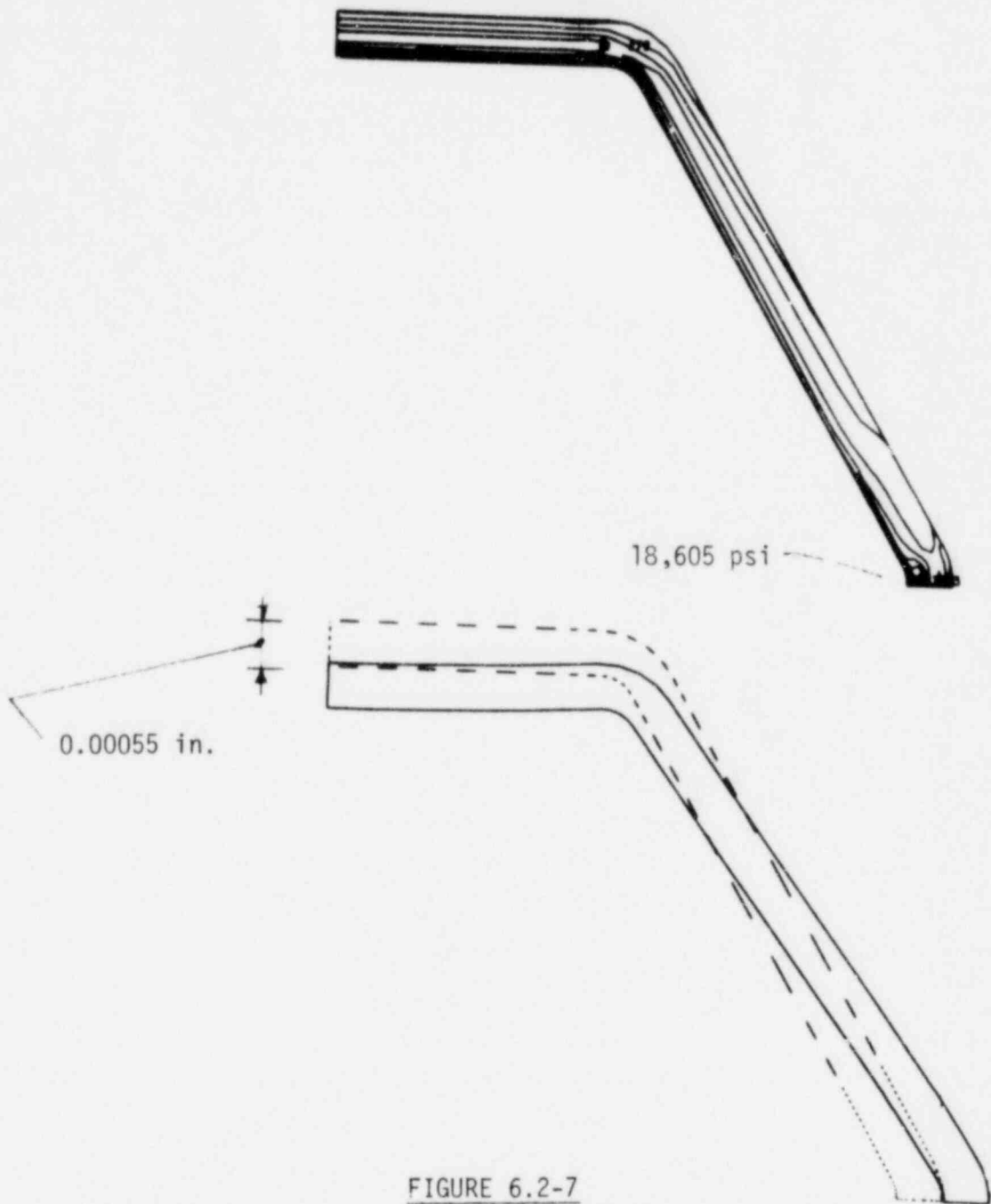


FIGURE 6.2-7  
F/A ACLP HEX DUCT  
FIRST CYCLE - TIME DEPENDENT  
UNLOADING FOR RESIDUALS  
EQUIVALENT STRESS AND NON-UNIFORM DEFORMATION

### 6.2.3.2.3 Second Cycle - Time Independent

The F/A ACLP hex duct structural response to the time independent loadings of the second worst case duty cycle was obtained in load steps 27 through 30 with an ANSYS restart from load step 26 of the first cycle time dependent analysis. The second cycle time independent loadings were considered as static loadings applied at 240 hours. A summary of the time independent thermal and mechanical loadings for the second cycle time independent analysis is presented in Table 6.2-5.

TABLE 6.2-5  
F/A ACLP HEX DUCT  
SECOND CYCLE TIME INDEPENDENT ANALYSIS SUMMARY  
INITIAL STEADY STATE, E-16 TRANSIENT, AND FINAL STEADY STATE

Load Step	Iter.	Temperature Distribution (°F)	Reference Temperature (°F)	Mechanical Loads (F <sub>1</sub> , F <sub>2</sub> , F <sub>3</sub> )	Description
27	1	1072.4	1072.4	CR	
28	3	1072.4	1072.4	CR	E-16 Transient (90 sec)
29	1	Cum.Iter. 32	1072.4	CR	Loading and Unloading
30	1	1072.4	1072.4	CR	

The F/A ACLP hex duct structural response to the second cycle time independent loadings was obtained with a plastic convergence ratio of 0.01 and saved on ANSYS Tape 10 for subsequent recall in structural evaluations. During the E-16 transient, the maximum equivalent stress was found to occur at the cumulative iteration 32 temperature distribution with a value of 27,063 psi. The maximum equivalent stress at the final steady state condition was found to be 17,908 psi. The peak non-uniform deformations at the cumulative iteration 32 temperature distribution and final steady state condition were found to be 0.00273 and 0.00267 in. respectively. Computer plots of equivalent stress and peak non-uniform deformation are presented in Figures 6.2-8 and -9.



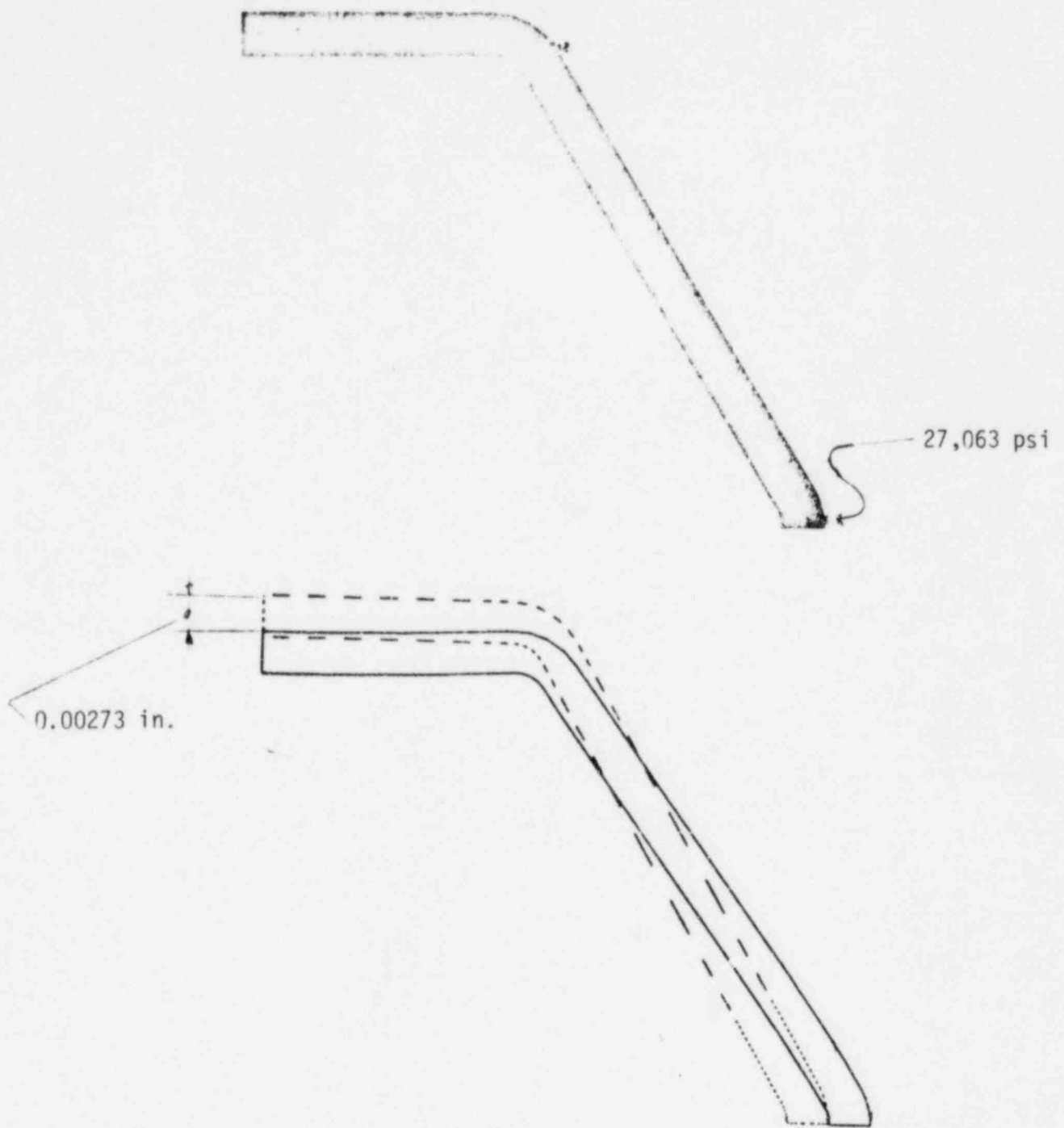


FIGURE 6.2-8  
 F/A ACLP HEX DUCT  
 SECOND CYCLE-TIME INDEPENDENT  
 CUMULATIVE ITERATION 32 TEMPERATURE DISTRIBUTION  
 EQUIVALENT STRESS AND PEAK NON-UNIFORM DEFORMATION

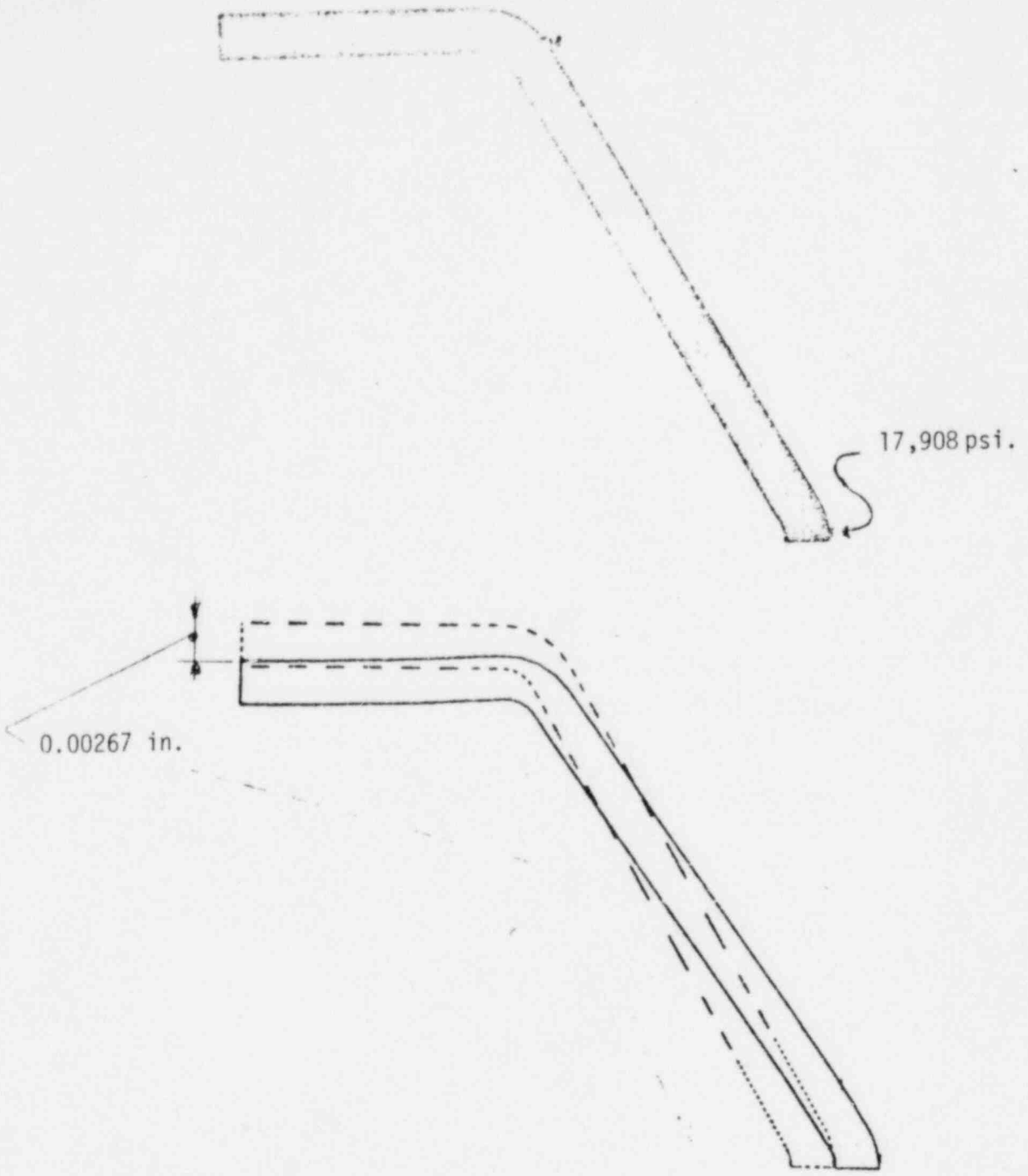


FIGURE 6.2-9  
F/A ACLP HEX DUCT  
SECOND CYCLE-TIME INDEPENDENT  
FINAL STEADY STATE  
EQUIVALENT STRESS AND NON-UNIFORM DEFORMATION

#### 6.2.3.2.4 Second Cycle - Time Dependent

The F/A ACLP hex duct structural response to the time dependent loadings of the second worst case duty cycle was obtained in load steps 31 through 34 with an ANSYS restart from load step 30 the second cycle time independent analysis. A creep time step of 10 hours was maintained throughout the 10 day hold-time. A subsequent ANSYS restart was made from load step 34 to obtain the residual deformations after the second worst case duty cycle. A summary of the second cycle time dependent mechanical and thermal loadings is presented in Table 6.2-6.

TABLE 6.2-6  
F/A ACLP HEX DUCT  
SECOND CYCLE TIME DEPENDENT ANALYSIS SUMMARY  
10 DAY HOLD TIME AND UNLOADING

Load Step	Iter.	Time (Hrs.)	Temperature Distribution (°F)	Reference Temperature (°F)	Mechanical Loads (F <sub>1</sub> , F <sub>2</sub> , F <sub>3</sub> )	Description
31	1	240	948.4	948.4	CR	Initiate and hold for ten days
32	3	240	948.4	948.4	CR	
33	1	240	Cum.Iter. 2	948.4	CR	
34	24	480	Cum.Iter. 2	948.4	CR	
35	1	480	948.4	948.4	None	Unloading for Residual Deformations

The F/A ACLP hex duct structural response to the second cycle time dependent loading was obtained with a creep convergence ratio of 0.25 with the stress-strain response saved on ANSYS Tape 10 for subsequent recall in structural evaluations. The maximum equivalent stress and peak non-uniform deformation in the F/A ACLP hex duct at the second cycle time dependent final steady state condition were found to be 17,498 psi and 0.00272 in. as illustrated in Figure 6.2-10.

With regard to the residual stresses and deformations of the F/A ACLP hex duct, maximum values of 18,786 psi and 0.00083 in. were found for the second duty cycle as illustrated in Figure 6.2-11.

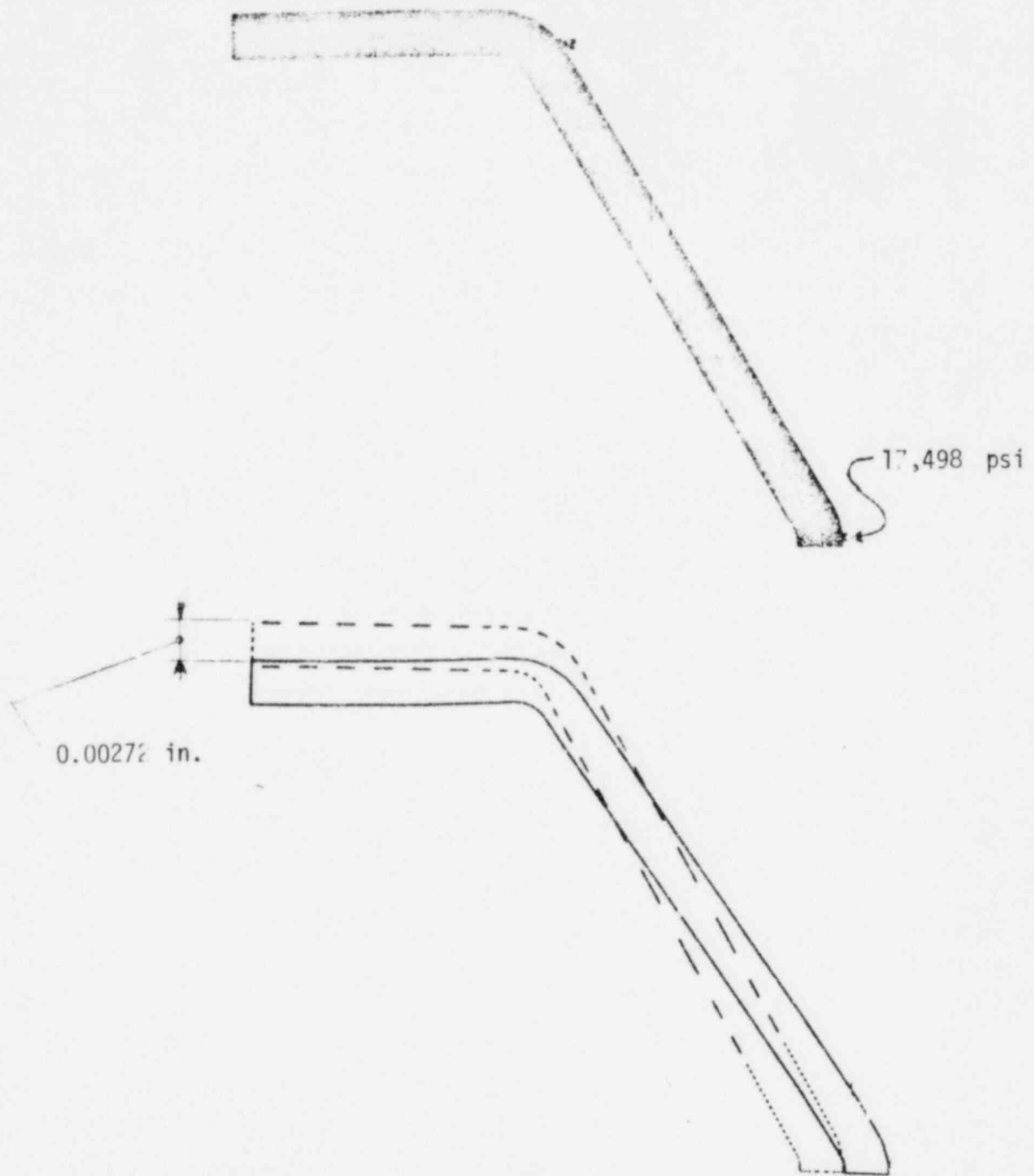


FIGURE 6.2-10  
F/A ACLP HEX DUCT  
SECOND CYCLE-TIME DEPENDENT  
FINAL STEADY STATE  
EQUIVALENT STRESS AND NON-UNIFORM DEFORMATION

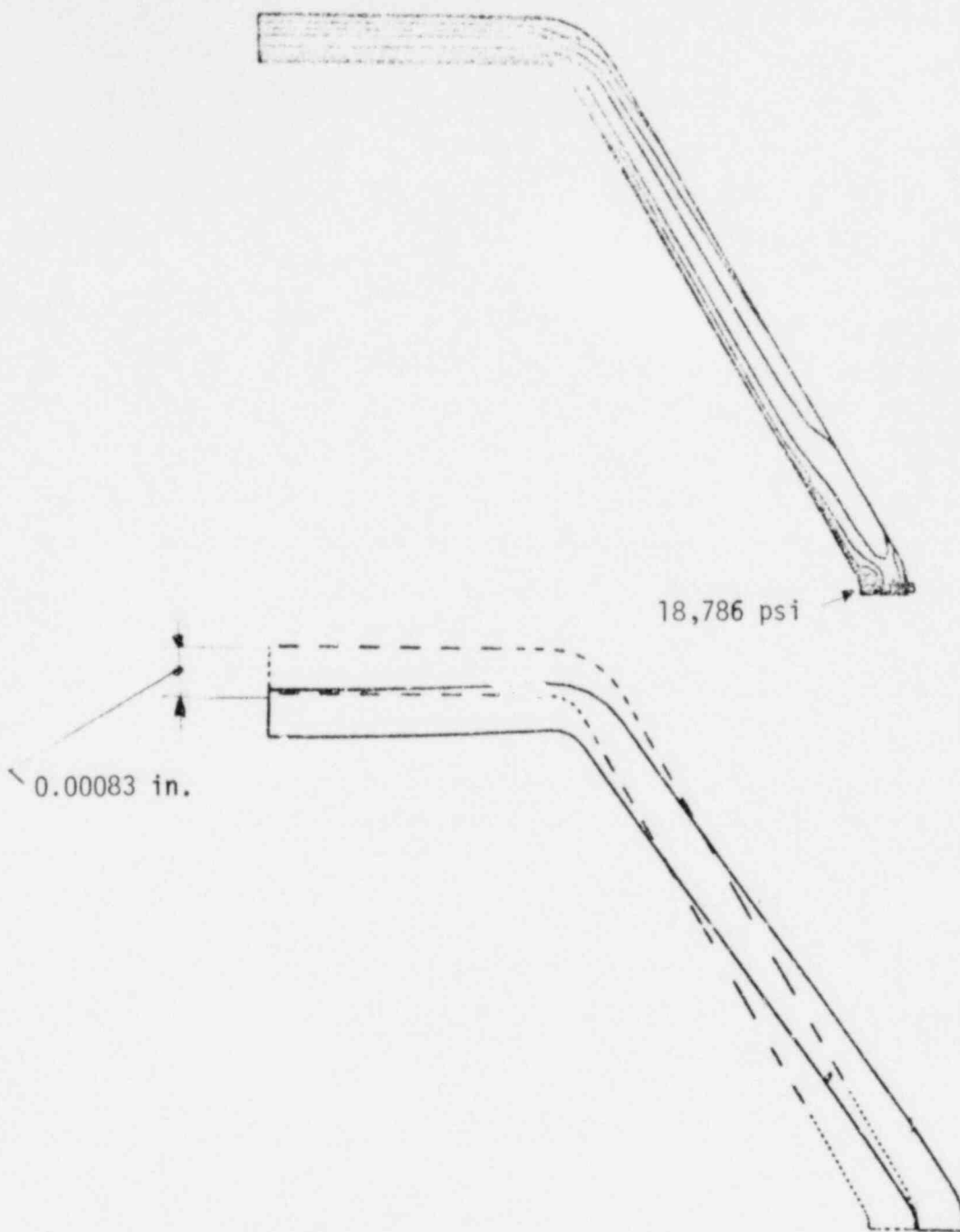


FIGURE 6.2-11  
F/A ACLP HEX DUCT  
SECOND CYCLE-TIME DEPENDENT  
UNLOADING FOR RESIDUALS  
EQUIVALENT STRESS AND NON-UNIFORM DEFORMATION

### 6.3 Structural Evaluation

The F/A ACLP hex duct structural evaluation was arranged to provide a comparison of the structural response for the 39 worst case duty cycles in relation to criteria which protect against crack initiation and excessive deformation failure modes and thereby assure F/A ACLP hex duct over the first and second reactor cycles.

The procedure for performing the F/A ACLP hex duct structural evaluation differed from that used for the F/A shield block and TLP outlet nozzle in that the structural response for the first and second worst case duty cycles had to be combined. The combination was made by considering one of the first duty cycles and 38 of the second duty cycles so as to obtain the required total of 39 worst case duty cycles. A description of F/A ACLP structural evaluation is presented as follows.

#### 6.3.1 Crack Initiation

The F/A ACLP hex duct structural evaluation of crack initiation in relation to local ductile rupture and combined creep-fatigue damage criteria over the 39 worst case duty cycles is presented in the following subsections.

##### 6.3.1.1 Local Ductile Rupture

The local ductile rupture criterion for protecting against crack initiation requires that the ductile rupture factor ( $F_{DR}$ ) be less than unity at each point in the F/A ACLP hex duct.

$$F_{DR} = \text{Maximum of } \left\{ \begin{array}{l} \bullet \frac{(\epsilon_{\max \text{ principal}})^{TF}}{0.3 \epsilon_{f, \min}} \\ \bullet \frac{(\epsilon_{\max \text{ principal}})^{TF}}{\epsilon_{u, \min}} \end{array} \right\}$$

In the following, the allowable uniaxial strains used in the F/A ACLP hex duct structural evaluation and comparison of results with the local ductile rupture factor criterion are presented.

#### 6.3.1.1.1 Allowable Uniaxial Strains

The F/A ACLP hex duct as constructed from first core 20% CW-316-SS is unirradiated at BOL. The EOL fluence ( $E > 0.1$  Mev) based on June 1977 data is  $0.59 \times 10^{22}$  n/cm<sup>2</sup>. In addition, the F/A ACLP hex duct temperatures range from 700 to 1150°F. The true uniaxial uniform elongation ( $\epsilon_{u, \min}$ ) for irradiated first core 20% CW-316-SS used for the F/A ACLP hex duct was identical to that used for the CMP hex duct presented in Section 5.3.1.1.1.1. The fracture strain ( $\epsilon_{f, \min}$ ) for unirradiated and irradiated first core 20% CW-316-SS used in the F/A ACLP hex duct structural evaluation was taken from recommendations in the trial applications of the RDT Draft Criteria for Breeder Reactor Core Components [15-23] and is identical to that taken for the F/A shield block structural evaluation presented in Section 4.3.1.1.1.

#### 6.3.1.1.2 Comparison with Criterion

The F/A ACLP hex duct structural evaluation in relation to local ductile rupture considered the first duty cycle to occur only once while the second duty cycle was repeated 38 times. In determining the maximum principal strain for comparison with the local ductile rupture criterion, the peak strain components were taken from the combined mechanical and thermal loads in the first duty cycle while accumulated strain components were taken from the 38 repeated second duty cycles. The peak and accumulated strain components were computed separately for the first and second duty cycles using the damage processor and combined by hand to determine the ductile rupture factor ( $F_{DR}$ ) for the 39 worst case duty cycles.

In the F/A ACLP hex duct, the maximum local ductile rupture factor ( $F_{DR}$ )<sub>max</sub> during the 39 worst case duty cycles was found to occur at element 1, as identified in Figure 6.2-1.

For the first duty cycle at BOL, the peak strain components occurred under the combined core restraint and SSE seismic mechanical loads, and the thermal loads corresponding to the cumulative iteration 32 temperature distribution of the E-16 transient. The local stress state was found to have a triaxiality factor of -2.075 but was taken as unity for conservatism in the structural evaluation. For the local metal temperature of 1146°F, the true minimum irradiated uniform elongation and fracture strains at EOL fluence ( $E > 0.1$  Mev,  $(\phi t) = 0.59 \times 10^{22}$  n/cm<sup>2</sup>) were 0.100 and 0.134 in/in respectively. The peak BOL strain components  $(\epsilon_{ij}^P)_{BOL}$  were:

$$(\epsilon_{ij}^P)_{BOL} = \left\{ \begin{array}{l} \epsilon_{xx}^P = 0.002757 \\ \epsilon_{yy}^P = -0.003618 \\ \gamma_{xy}^P = 0.000612 \\ \epsilon_{zz}^P = -0.000832 \end{array} \right\}$$

In the second duty cycle at BOL, the accumulated strain components occur between initial time independent and final time dependent steady state conditions. The local stress states were found to have negative triaxiality factors, but were both taken as unity in combining the strain components. The difference between final and initial steady state, strain components  $(\Delta \epsilon_{ij}^A)$  at BOL were:

$$(\Delta \epsilon_{ij}^A)_{BOL} = \left\{ \begin{array}{l} \Delta \epsilon_{xx}^A = 0.0000190 \\ \Delta \epsilon_{yy}^A = -0.0000100 \\ \Delta \gamma_{xy}^A = 0.0000020 \\ \Delta \epsilon_{zz}^A = 0.0 \end{array} \right\}$$

After a total of  $N = 39$  worst case duty cycles, the peak plus accumulated strain components  $(\epsilon_{ij}^{P+A})$  at EOL were:

$$(\epsilon_{ij}^{P+A})_{EOL} = (\epsilon_{ij}^P)_{BOL} + (N-1)(\Delta \epsilon_{ij}^A)_{BOL}$$



$$(\epsilon_{ij}^{P+A})_{EOL} = \left\{ \begin{array}{l} \epsilon_{xx}^{P+A} = 0.003479 \\ \epsilon_{yy}^{P+A} = -0.003998 \\ \gamma_{xy}^{P+A} = 0.000688 \\ \epsilon_{zz}^{P+A} = -0.000832 \end{array} \right\}$$

The EOL maximum principal strain ( $\epsilon_{\text{max principal}}$ ) based on the EOL peak plus accumulated strain components was:

$$\epsilon_{\text{max principal}} = 0.00349 \text{ in/in}$$

Accordingly, the maximum local ductile rupture factor  $(F_{DR})_{\text{max}}$  was found to be controlled by the fracture strain with a value;

$$(F_{DR})_{\text{max}} = 0.087$$

As  $(F_{DR})_{\text{max}} < 1.0$ , the F/A ACLP hex duct is not expected to experience crack initiation over the 39 worst case duty cycles based on the local ductile rupture criterion.

### 6.3.1.2 Creep-Fatigue Damage

The creep-fatigue damage criterion in protecting against crack initiation requires that the combined creep-fatigue damage factor ( $F_{CFD}$ ) be less than unity at each point in the F/A ACLP hex duct.

$$F_{CFD} = a/b = \text{Minimum of } \left\{ \begin{array}{l} \bullet 7/3 D^C + D^f \\ \bullet D^C + 7/3 D^f \end{array} \right\}$$

In the following, the allowable limits for fatigue life and creep-rupture times used in the F/A ACLP hex duct structural evaluation and a comparison of the results with the combined creep-fatigue damage factor criterion are presented.

#### 6.3.1.2.1 Allowable Limits

The F/A ACLP hex duct as constructed from first core 20% CW-316-SS is unirradiated at BOL. The EOL fluence ( $E > 0.1$  Mev) based on June 1977 data is  $0.59 \times 10^{22}$  n/cm<sup>2</sup>. In addition, the F/A ACLP hex duct temperatures range from 700 to 1150°F. The fatigue life and creep rupture time relations used in the F/A ACLP hex duct structural evaluation were identical to those used in the F/A CMP hex duct structural evaluation presented in Section 5.3.1.1.1. The fatigue life and creep rupture time relations representative of F/A ACLP hex duct peak and steady state metal temperature at EOL fluence are illustrated in Figures 6.3-1 and -2 respectively.

FIGURE 6.3-1  
 F/A ACLP HEX DUCT  
 FIRST CORE 20% CW-316-SS  
 FATIGUE LIFE  
 $EOL \text{ FLUENCE } (E \times 0.1 \text{ Mev, } t = .59 \times 10^{22} \text{ n/cm}^2)$   
 TEMPERATURE  $\sim 1150^\circ\text{F}$

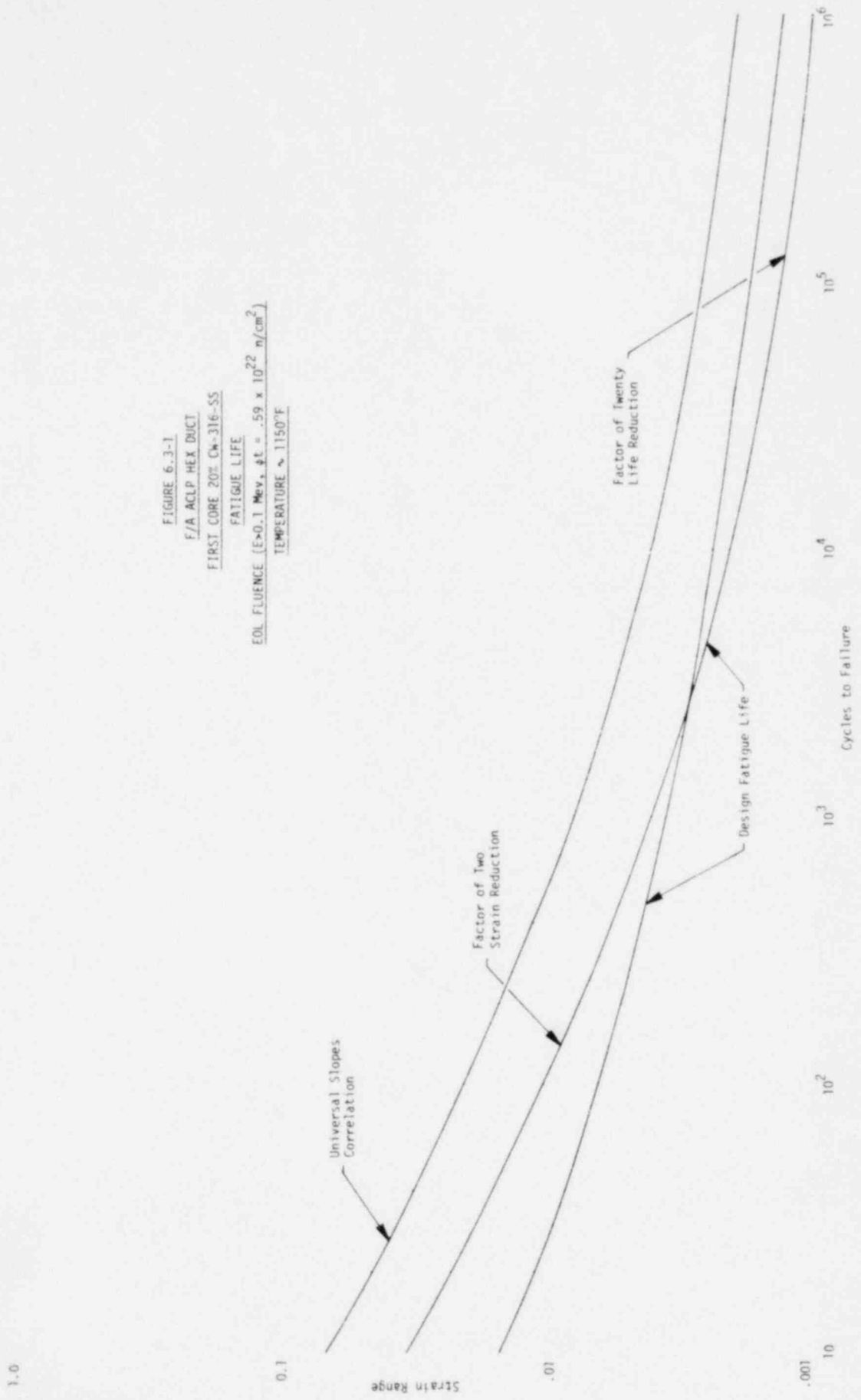


FIGURE 6.3-2

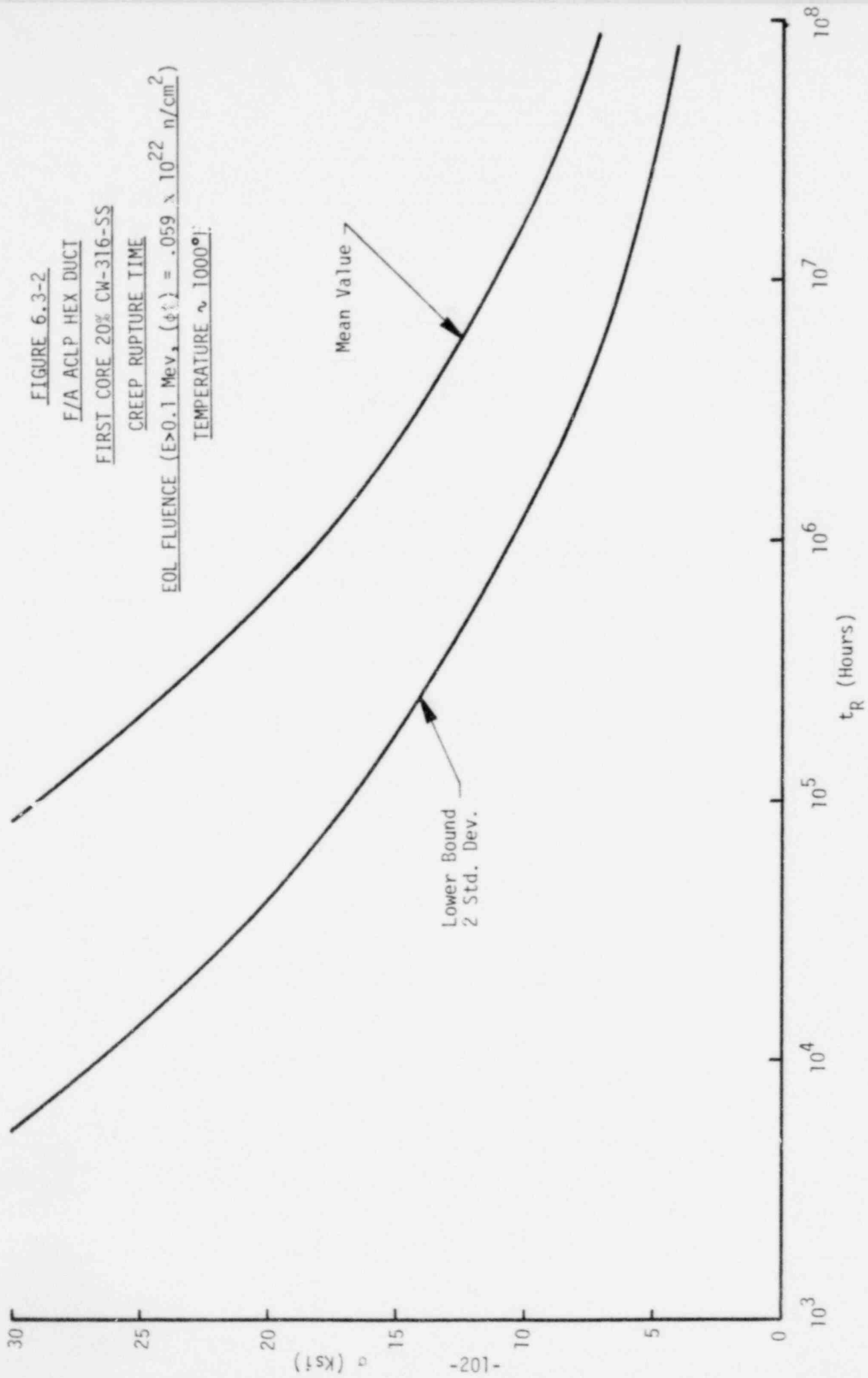
F/A ACLP HEX DUCT

FIRST CORE 20% CW-316-SS

CREEP RUPTURE TIME

EOL FLUENCE ( $E > 0.1$  Mev,  $\phi$ ) =  $0.059 \times 10^{22}$  n/cm<sup>2</sup>

TEMPERATURE  $\sim 1000^\circ$



### 6.3.1.2.2 Comparison with Criterion

The F/A ACLP hex duct structural evaluation in relation to the combined creep-fatigue damage was based on the first duty cycle applied only once while 38 of the second duty cycles were considered. The creep and fatigue damage factors ( $D^C$ ,  $D^f$ ) were computed separately for the first and second duty cycles with the damage processor and combined by hand to obtain the total combined creep-fatigue damage factor ( $F_{CFD}$ ) for the 39 worst case duty cycles.

In the F/A ACLP hex duct, the maximum combined creep-fatigue damage factor ( $F_{CFD})_{max}$  during the 39 worst case duty cycles was found to occur at element 59, as identified in Figure 6.2-1.

The fatigue damage factor ( $D_1^f$ ) for the first duty cycle was found to be 0.0000154 while the fatigue damage factor ( $D_2^f$ ) for 38 of the second duty cycles was 0.0000186. The peak metal temperature in both the first and second duty cycles was 1134°F corresponding to the E-16 transient cumulative iteration 32 temperature distribution. The maximum principal and equivalent strain ranges were found to be critical in the first and second duty cycles respectively. For the first duty cycle, the maximum principal strain range was found to occur between the first peak SSE load application and a uniform temperature distribution with a value of 0.00147 in/in. In the second duty cycle, the maximum equivalent strain range occurred between a uniform temperature and the E-16 transient cumulative iteration 32 temperature distribution with a value of 0.000882 in/in. Based on the F/A ACLP hex duct EOL fluence ( $E > 0.1$  Mev,  $(\phi t) = 0.59 \times 10^{22}$  n/cm<sup>2</sup>), the fatigue cycles to failure for the maximum strain ranges of the first and second duty cycles were  $0.65 \times 10^6$  and  $2.04 \times 10^6$ . Accordingly, the total fatigue damage factor ( $D^f$ ) in terms of the first cycle fatigue damage factor ( $D_1^f$ ) combined with the fatigue damage factor ( $D_2^f$ ) for the 38 second duty cycles.

$$\begin{aligned}D^f &= D_1^f + D_2^f \\D^f &= 0.0000154 + 0.0000186 \\D^f &= 0.0000340\end{aligned}$$

The creep damage factor ( $D_1^C$ ) for the first duty cycle was found to be 0.000946 while the creep damage factor ( $D_2^C$ ) for 38 of the second duty cycles was 0.0242. The steady state local metal temperature in both first and second duty cycles was 938°F. The maximum equivalent stress was found to be critical in both first and second duty cycles. In the first duty cycle with a duration of 240 hours, the initial and final time dependent maximum equivalent stresses were 17,059 and 14,177 psi. For the 38 second duty cycles with a duration of 9120 hours, the initial and final time dependent maximum principal stresses were 14,148 and 13,618 psi. Based on the F/A ACLP hex duct EOL fluence ( $E > 0.1$  Mev,  $(\phi t) = 0.59 \times 10^{22}$  n/cm<sup>2</sup>), the mean minimum rupture times for the maximum equivalent stresses during the first and second duty cycles were  $0.254 \times 10^6$  and  $0.377 \times 10^6$  hours. Accordingly, the total creep damage factor ( $D^C$ ) in terms of the first cycle creep damage factor ( $D_1^C$ ) combined with the creep damage factor ( $D_2^C$ ) for the 38 second duty cycles was

$$D^C = D_1^C + D_2^C$$

$$D^C = 0.000946 + 0.0242$$

$$D^C = 0.0251$$

In this arrangement, the maximum combined creep-fatigue damage factor  $(F_{CFD})_{max}$  for the F/A ACLP hex duct is given by the relation:

$$(F_{CFD})_{max} = \frac{a}{b} = \text{Minimum of } \left\{ \begin{array}{l} \bullet \frac{7}{3} D^C + D^f \\ \bullet D^C + \frac{7}{3} D^f \end{array} \right\}$$

$$(F_{CFD})_{max} = 0.0108$$

As  $(F_{CFD})_{max} < 1.0$ , the F/A ACLP hex duct is not expected to experience crack initiation over the 39 worst case duty cycles based on the creep-fatigue damage criterion.

### 6.3.2 Excessive Deformation

The F/A ACLP hex duct structural evaluation of peak plus accumulated, and residual deformations in relation to functional limits over the 39 worst case duty cycles is presented in the following subsections.

#### 6.3.2.1 Peak Plus Accumulated Deformations

The peak plus accumulated deformation criterion in protecting against excessive deformations requires that peak plus accumulated deformations ( $\delta^{P+A}$ ) be less than the peak plus accumulated deformation limit (PADL).

$$\delta^{P+A} \leq \text{PADL}$$

The F/A ACLP hex duct peak BOL deformation ( $\delta^P$ ) was 0.01256 in. and occurred during the combined core restraint and SSE seismic mechanical loads and the thermal loads associated with the cumulative iteration 32 temperature distribution of the E-16 transient of the first duty cycle. The accumulated BOL deformation ( $\delta^A$ ) was based on the initial time independent and final time dependent steady state conditions of the second duty cycle. For the initial and final deformation values of 0.00267 and 0.00272 in., the accumulated steady state deformation ( $\Delta\delta^{SS}$ ) in the second duty cycle at BOL was 0.00005 in. For the 39 worst case F/A ACLP hex duct duty cycles, the EOL peak plus accumulated deformation ( $\delta^{P+A}$ ) is given by the relation

$$(\delta^{P+A})_{\text{EOL}} = (\delta^P)_{\text{BOL}} + (N-1) (\Delta\delta^{SS})_{\text{BOL}}$$

$$(\delta^{P+A})_{\text{EOL}} = 0.0126 + (38) (0.00005)$$

$$(\delta^{P+A})_{\text{EOL}} = 0.0145$$

For the F/A ACLP hex duct, the peak plus accumulated deformation limit (PADL) is

$$\text{PADL} = 0.082 \text{ in.}$$

As  $\delta^{P+A} < \text{PADL}$ , the F/A ACLP hex duct is not expected to experience excessive peak deformation over the 39 worst case duty cycles.

#### 6.3.2.2 Residual Deformations

The residual deformation limit in protecting against excessive deformation requires that the residual deformation ( $\delta^R$ ) be less than the residual deformation limit (RDL).

$$\delta^R \leq \text{RDL}$$

The F/A ACLP hex duct residual BOL deformations ( $\delta^R$ ) after the first and second duty cycles were found to be 0.00055 and 0.00083 in. respectively. Accordingly, the change in residual deformations ( $\Delta\delta^R$ ) in successive second duty cycles would be 0.00028 in. For the 39 worst case F/A ACLP hex duct duty cycles, the EOL residual deformation is given by the relation.

$$(\delta^R)_{\text{EOL}} = (\delta^R) + (N-1)(\Delta\delta^R)$$

$$(\delta^R)_{\text{EOL}} = 0.00055 + 38 (0.00028)$$

$$(\delta^R)_{\text{EOL}} = 0.011 \text{ in.}$$

For the F/A ACLP hex duct, the residual deformation limit (RDL) across the flats is 0.010 in. However, the RDL for a single hex duct flat is 0.005 in. As  $(\delta^R)_{\text{EOL}} > 0.005$  in., the F/A ACLP hex duct residual deformation at EOL approximated from the response of the first and second duty cycles at BOL is not acceptable.

Accordingly, the response to a third duty cycle was derived using the same procedure identified for the second duty cycle. The F/A ACLP hex duct residual BOL deformation after the third duty cycle was 0.00086 in. For the 39 worst case F/A ACLP hex duct duty cycles, the EOL residual deformation estimated from the second and third duty cycles at BOL is given by the relation.



$$(\delta^R)_{EOL} = 0.00083 + 37 (0.00086 - 0.00083)$$

$$(\delta^R)_{EOL} = 0.00194 \text{ in.}$$

As  $\delta^R < RDL$ , the F/A ACLP hex duct is not expected to experience excessive residual deformation over the 39 worst case duty cycles.

### 6.3.3 Summary

The F/A ACLP hex duct was found to satisfy the crack initiation and excessive deformation criteria. A summary of the F/A ACLP hex duct structural evaluation is presented in Table 6.3-1.

TABLE 6.3-1  
F/A ACLP HEX DUCT  
STRUCTURAL EVALUATION SUMMARY

Criteria		Allowable Value	Calculated Value	Margin of Safety*
Crack Initiation	Ductile Rupture Factor	1	0.087	10.49
	Combined Creep-Fatigue Damage Factor	1	0.0108	91.59
Excessive Deformation	Peak + Accumulated	0.082 in	0.0145	4.65
	Residual	0.005 in	0.00194	1.58

$$* \text{ Margin of Safety} = \frac{\text{Allowable Value}}{\text{Calculated Value}} - 1$$

## 7.0 TLP OUTLET NOZZLE ANALYSIS AND EVALUATION

In the F/A TLP outlet nozzle analysis and evaluation, a loading analysis was made that considered mechanical seismic and core restraint, and thermal steady state and transient loads in order to establish the number and characteristics of a worst case duty cycle that umbrellas all expected duty cycles for the outlet nozzle in the first and second reactor cycles. Next, an inelastic structural analysis of the outlet nozzle was made for a single worst case BOL duty cycle to calculate the strains and dimensional changes from which EOL values were approximated. Finally, a structural evaluation of EOL strains and dimensional changes in relation to criteria which protect against crack initiation and excessive deformation was made. A summary of the loading and structural analysis, and structural evaluation is presented as follows.

### 7.1 Loading Analysis

The F/A outlet nozzle loading analysis was directed to establishing the number and characteristics of a worst case duty cycle that umbrellas both the number and characteristics of Upset, Emergency and Faulted Events specified over the first and second reactor cycles. The number and characteristics of these events are specified in the Equipment Specification [1].

It is important to note that the worst case F/A outlet nozzle duty cycle is, in itself, hypothetical, but permits a conservative structural evaluation to be performed on a single duty cycle instead on each of the individual events specified. In the following, the F/A outlet nozzle mechanical and thermal loads are assessed individually and in relation to each other prior to establishing the worst case duty cycle used in the structural evaluation.

#### 7.1.1 Mechanical

The F/A outlet nozzle mechanical load of significance in relation to subsequent structural evaluations is internal pressure, as dead weight, OBE and

SSE seismic, and core restraint are relatively insignificant. However, in relation to thermal steady state and transient loads, even internal pressure loads are insignificant. Accordingly, mechanical loads were neglected in establishing the worst case F/A outlet nozzle duty cycle for the first and second reactor cycles.

#### 7.1.2 Thermal

The F/A outlet nozzle thermal loads are the steady state and transient temperature distributions that occur during the Upset, Emergency, and Faulted events over the first and second reactor cycles. The steady state F/A outlet nozzle inside metal temperature distributions throughout Sector A of the core at BOC 1, EOC 1, BOC 2, and EOC 2 and the Upset, Emergency, and Faulted transients defined in terms of time-dependent scale factors applied to the steady state inside metal temperatures were considered. In this arrangement, the F/A outlet nozzle thermal loads in terms of inside metal temperatures associated with BOC 1, EOC 1, BOC 2, and EOC 2 steady state conditions as well as during Upset, Emergency and Faulted transients were identified at any F/A location in the core.

In order to proceed with a structural evaluation of the F/A outlet nozzle, it was desirable for the sake of simplicity to consider only the worst case thermal loading. Accordingly, all F/A located in Sector A of the core were assessed in relation to the maximum inside metal wall temperature difference between a F/A and adjacent C/A or RB/A. The maximum steady state inside metal wall temperature difference was found to occur at F/A A<sub>04</sub><sup>09</sup> adjacent to RB/A A<sub>04</sub><sup>08</sup> during BOC 1 with a value of 214°F. It is important to note that at EOC 1, BOC 2 and EOC 2, the respective inside metal temperature differences were found to decrease from BOC 1 values. As such, the BOC 1 maximum steady state inside metal temperature difference of 214°F between a F/A and adjacent RB/A was clearly worst case for all F/A outlet nozzles in the core over the first and second reactor cycles.

With regard to F/A and adjacent RB/A outlet nozzle thermal transients, the Equipment Specification [1] using an umbrella approach identified the number of Normal, Upset, Emergency, and Faulted transients over the first and second reactor cycles as 1/15 of the number specified for 30 years rounded to the next whole number. Over the first and second reactor cycles comprising a total of 328 FPD, a total of 39 Upset transient events umbrellaed by the worst of U-2b or OBE were specified. Similarly, the worst of the E-16, 60¢ Step, or U-2b during OBE were specified to umbrella the Emergency Transients while the SSE was identified to umbrella the Faulted Transients.

In the derivation of the F/A and adjacent RB/A inside metal temperature transients for the Upset, Emergency, and Faulted events, the identified upper and lower bounds for the Upset U-2b and OBE events and the Emergency 60¢ step event. The upper bounds were based on quickest flow decay and maximum decay heat while the lower bounds were based on slowest flow decay and minimum decay heat. Further, the SSE Faulted Transient was found to be umbrellaed by the Emergency E-16 transient. The Upset transients comprising the upper and lower bound U-2b and OBE, and the Emergency Transients including the upper and lower bound 60¢ step, E-16, and U-2b during OBE are based on June 1977 loads.

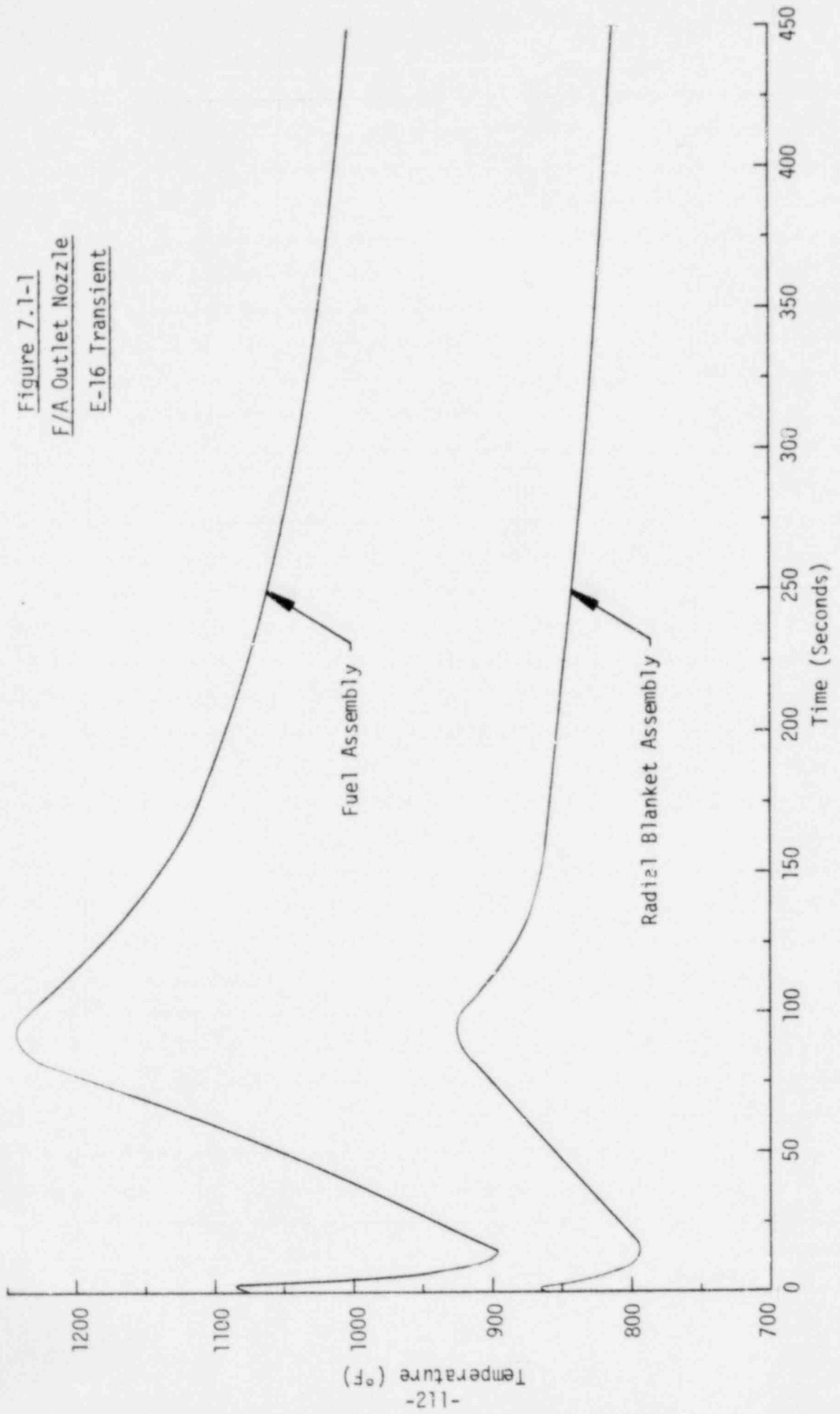
In order to reduce the number of F/A outlet nozzle transients which umbrella the Upset and Emergency Transients to a single worst case transient, the individual transients were assessed for severity in subsequent structural evaluations by comparing the inside metal wall temperatures in terms of maximum value, rate of temperature change, and range. With regard to steady state conditions, all transients were initiated with F/A and RB/A inside metal wall temperatures of 1076 and 862°F which provide the worst case temperature difference of 214°F. For the Upset transients at the F/A outlet nozzle inside metal surface, the upper and lower bound U-2b transients were assessed as slightly more severe in terms of maximum temperature with maximum rate and range of temperature indistinguishable from the upper and lower bound

OBE transient. However, the adjacent RB/A inside metal temperature transients for the lower bound U-2b were observed to more closely follow the F/A metal transient than in the case of the upper bound U-2b. Owing to the thermal lag in the thick walled F/A outlet nozzle, temperature differences through the wall, which are important in structural evaluations, are more severe in the lower bound U-2b transient than the upper bound counterpart. With regard to the Emergency transients, the E-16 transient in terms of maximum value, rate of temperature change, and range was found to be clearly more severe than the upper and lower bound 60¢ step, and the U-2b during OBE transients. Further, the E-16 was also considered more severe than the lower bound U-2b transient. In this arrangement, the Emergency E-16 transient was selected as the worst case umbrella to all the Upset, Emergency, and Faulted transients for the F/A outlet nozzle and is illustrated in Figure 7.1-1.

The selection of the Emergency E-16 transient as the worst case F/A outlet nozzle transient is, in itself, not sufficient to establish the worst case F/A outlet nozzle duty cycle. Thermal conditions following the E-16 transient and subsequent hold-times at steady state conditions are also required. The thermal conditions selected consisted of a cool-down to 600°F in 1 hour from the F/A and RB/A inside metal wall temperature at 450 seconds into the E-16 transient, followed by a 1 hour heat-up to initial steady state F/A and RB/A temperatures. Thereafter, a 10 day hold-time at steady state temperatures was assumed. The 10 day hold time corresponds to 40 worst case E-16 transients uniformly distributed over 400 FPD which is slightly greater than the 328 FPD specified for the first and second reactor cycles. The worst case F/A outlet nozzle duty cycle is presented in Figure 7.1-2.

The worst case F/A outlet nozzle duty cycle in terms of inside metal temperatures at initial steady state, followed by the E-16 transient, thermal conditions in returning to initial steady condition, and 10 day hold-time are not sufficiently detailed for subsequent structural evaluation. In the following, the F/A outlet nozzle thermal model and geometry,

Figure 7.1-1  
F/A Outlet Nozzle  
E-16 Transient



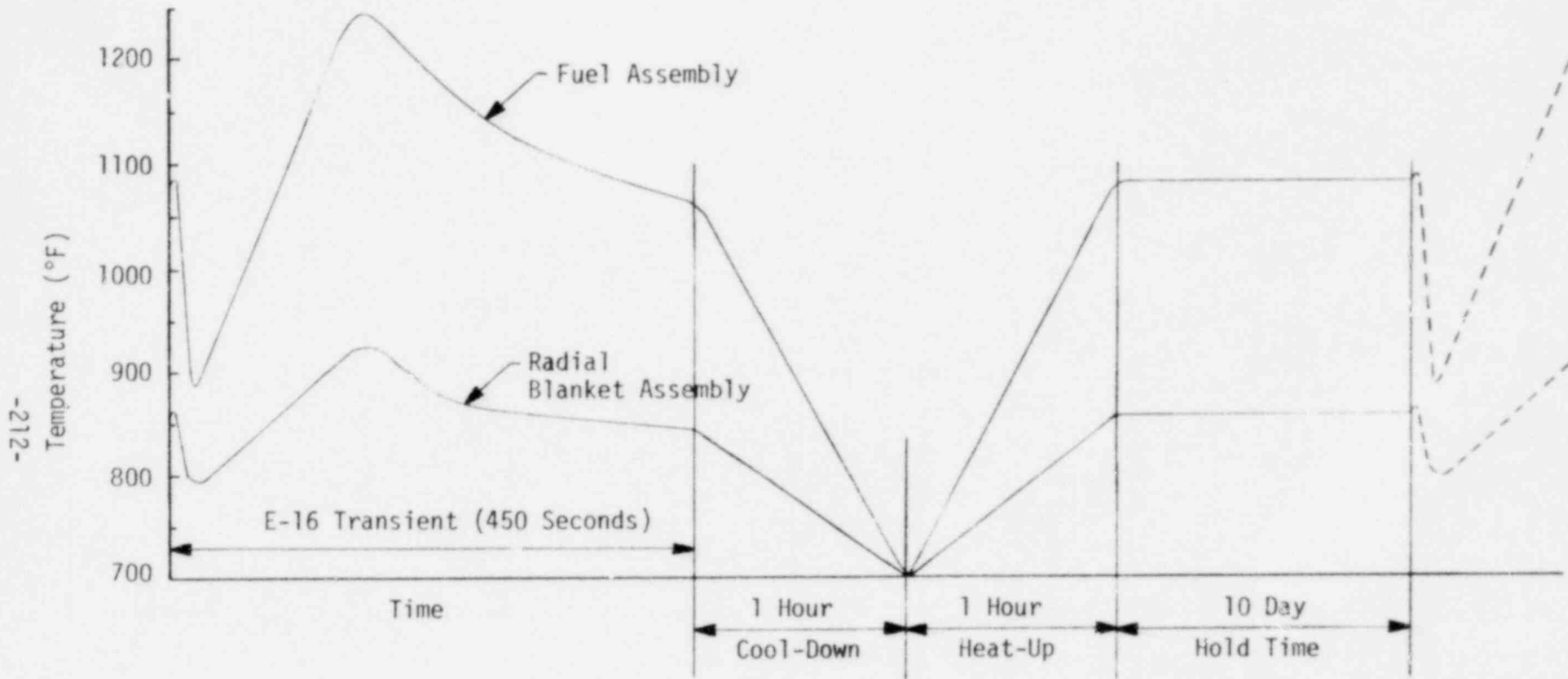


Figure 7.1-2  
 F/A Outlet Nozzle  
 Worst Case Duty Cycle

boundary conditions and wetted sodium surfaces, heat generation rates, and thermal analysis and results are described from which conclusions on detailed temperature distributions used in subsequent structural analysis are presented.

#### 7.1.2.1 Model and Geometry

The F/A outlet nozzle model was formulated in the ANSYS finite element program. The ANSYS program has compatibility between thermal and structural elements which permits thermal solutions of temperature distributions to be used directly in subsequent structural analysis.

The F/A outlet nozzle region selected for analysis corresponds to a 2 dimensional slice of a symmetrical 30° sector taken through the fluted pattern provided to protect the fuel rods from inadvertant placement of RB/A. As the worst case F/A outlet nozzle duty cycle includes adjacent RB/A inside metal wall temperatures, a flat slab simulation of the RB/A was also included in the thermal model. The 30° symmetrical sector is justified as outlet sodium flow and heat generation rates are uniform. The F/A outlet nozzle thermal model illustrating the dimensional extent and finite element detail is presented in Figure 7.1-3.



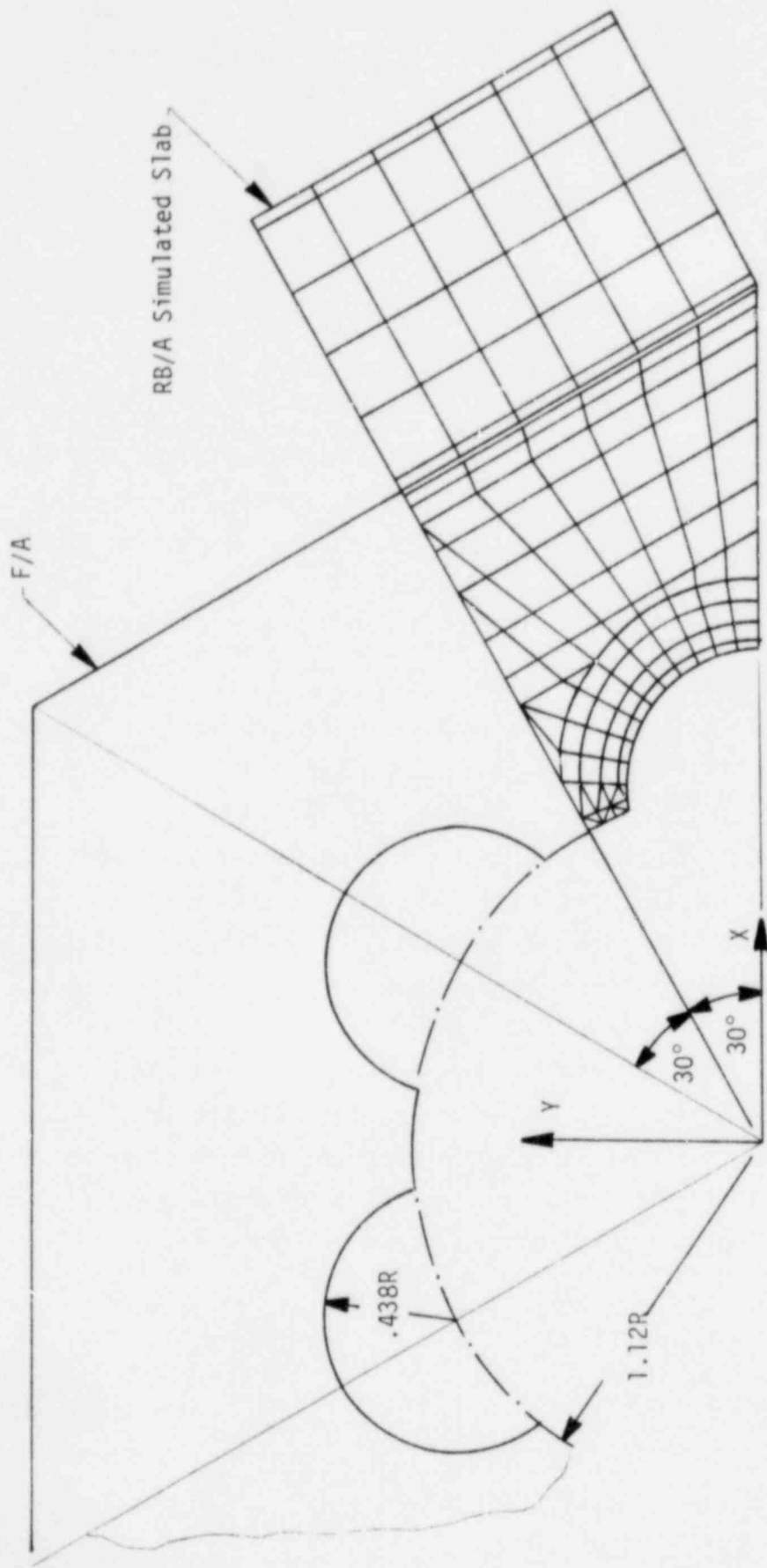


Figure 7.1-3  
F/A Outlet Nozzle Thermal Model  
Dimensional Extent and Finite Element Detail

The F/A outlet nozzle thermal model as formulated in the ANSYS program included a total of 149 linear temperature (STIF 35) elements in a mesh of 366 node points. The F/A outlet nozzle was modeled with 113 elements while the simulation of the adjacent RB/A as a flat slab was modeled with 36 elements. The F/A and RB/A elements were assigned different element types in the thermal model so that the RB/A elements could be deleted in the structural analysis solutions. A relatively fine mesh was selected at the wetted sodium surfaces of the F/A outlet nozzle so as to include the thermal skin response to the thermal transients.

#### 7.1.2.2 Properties

The F/A and adjacent RB/A outlet nozzles are both constructed from SA-316-SS. The thermal conductivity (K), specific heat (c), and density ( $\rho$ ) properties used in the thermal analysis were identical to those used for the F/A shield block as presented in Section 4.1.2.2.

#### 7.1.2.3 Boundary Conditions and Wetted Surfaces

The F/A and adjacent RB/A boundary conditions and wetted surfaces selected in the thermal analysis are illustrated in Figure 7.1-4.

Boundary conditions for the thermal analysis consisted of adiabatic conditions along the lateral surfaces of the 30° F/A outlet nozzle and the flat slab simulation of the RB/A outlet nozzle. Conductive conditions were assumed at the sodium interstice between the exterior surfaces of the F/A and RB/A. Owing to the relatively high thermal conductivity ( $K_s$ ) of sodium in combination with the small interstice gap (G), the effective film coefficient ( $h = K_s/G$ ) is high. Accordingly, the node points along the F/A and RB/A exterior surfaces were locally coupled to each other in the thermal analysis. The F/A node 13 was coupled to the RB/A node 300, and so forth along the sodium interstice as follows.

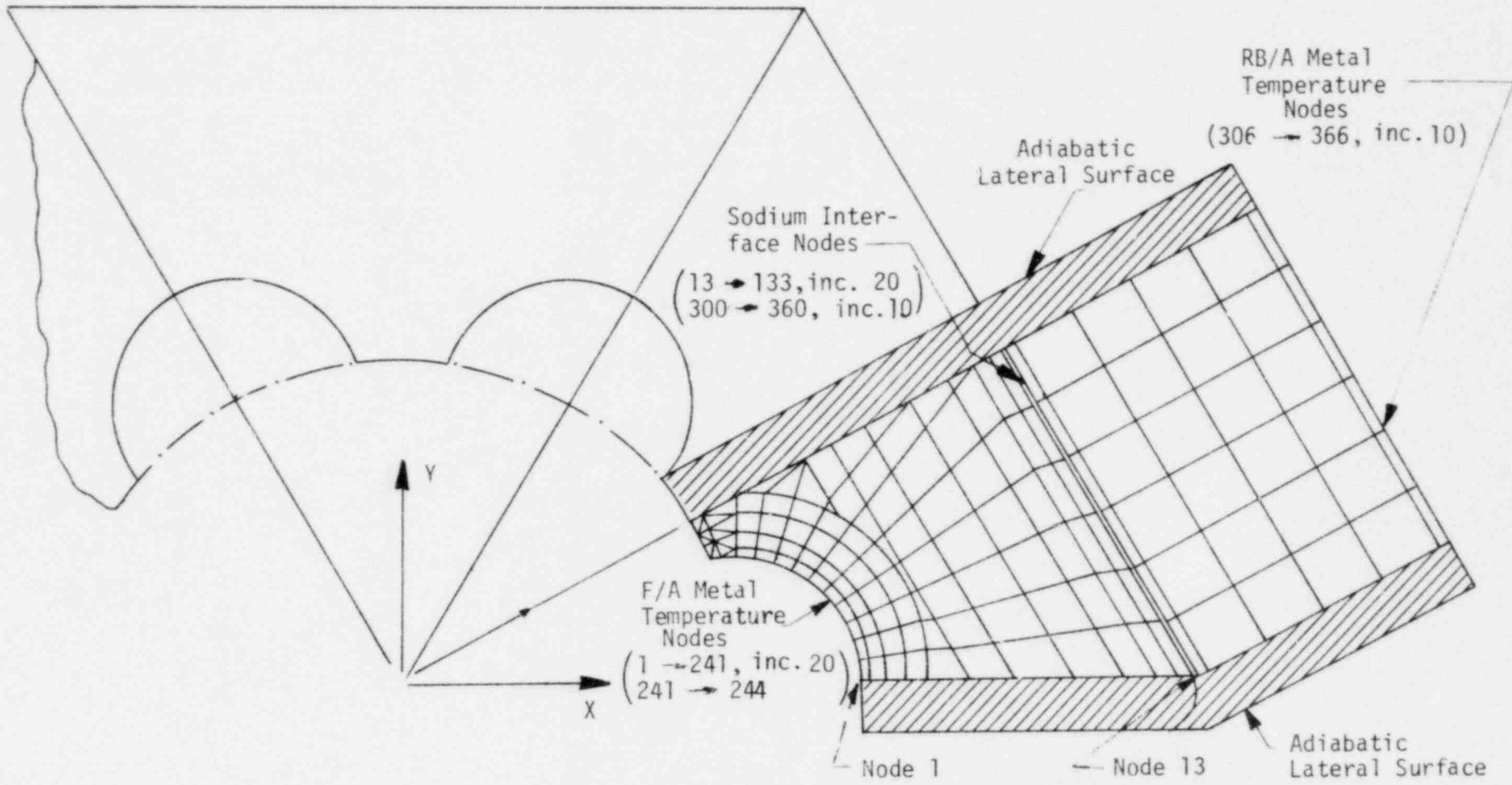


Figure 7.1-4  
F/A Outlet Nozzle  
Boundary Conditions and Wetted Surfaces

$$F/A \left\{ \begin{array}{l} 13 = 300 \\ 33 = 310 \\ 53 = 320 \\ 73 = 330 \\ 93 = 340 \\ 113 = 350 \\ 133 = 360 \end{array} \right\} RB/A$$

The wetted interior surfaces of the F/A and RB/A were assumed to respond immediately to the respective inside metal wall temperatures of the worst case F/A outlet nozzle duty cycle. Local variations in wetted interior surface temperatures were neglected. Instead, all F/A outlet nozzle interior surface node point temperatures were globally coupled to each other and included nodes 1 through 241, in increments of 20; and 241 through 244. Similarly, the interior surface node point temperatures for the flat slab simulation of the RB/A were globally coupled to each other at node points 306 through 366 in increments of 10.

#### 7.1.2.4 Heat Generation Rates

During steady state operation the F/A outlet nozzle is exposed to nuclear heating. Based on June 1977 Data, the maximum heating rate/per unit volume is relatively uniform with a value of 0.038 watts/cc or 0.00059 BTU/in<sup>3</sup>-sec. For the F/A outlet nozzle exposed to a heat generation rate (Q) with thermal conductivity (K) and wall dimension (L), the temperature difference ( $\Delta T$ ) is given by:

$$\begin{aligned} \Delta T &= QL^2/2K \\ \Delta T &= \frac{(0.00059 \text{ BTU/in}^3 \text{ -sec}) (2.33 \text{ in})^2}{2(2.87 \times 10^{-4} \text{ BTU/in-sec-}^\circ\text{F})} \\ \Delta T &= 5.88^\circ\text{F} \end{aligned}$$

For the F/A outlet nozzle, the steady state temperature difference ( $\Delta T_{ss}$ ) caused by sodium flow was 214°F. As  $\Delta T \ll \Delta T_{ss}$ , the effect of heat generation rate on the steady state temperature distribution is small and heat generation rates were neglected in the thermal analysis.

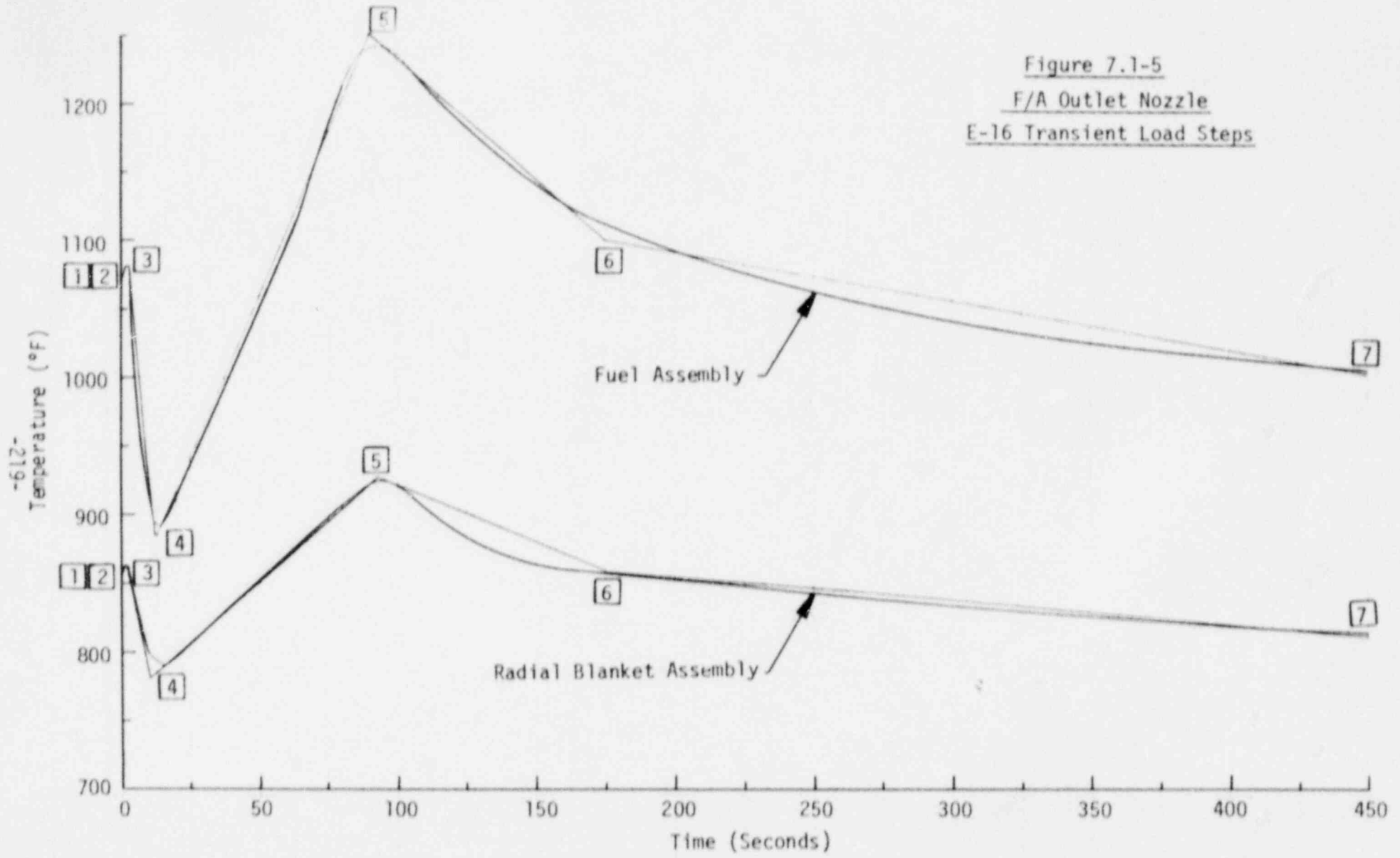
### 7.1.2.5 Analysis and Results

The ANSYS thermal analysis of the F/A outlet nozzle was arranged to provide detailed temperature distributions over the total worst case duty cycle. A total of 10 load steps were selected at prominent F/A and RB/A inside metal surface temperatures. The first 7 load steps characterized the initial steady state conditions and the E-16 transient to 450 seconds. Load Steps 1 and 2 represent initial steady state conditions while Loads Steps 3 through 7 correspond to the E-16 transient. Load Step 8 corresponds to the 1 hour cool-down to 600°F. The return to final steady state temperatures with the 1 hour heat-up was accomplished in Load Step 9. The final steady state temperatures held for 10 days were obtained in Load Step 10. Prominent load steps in the E-16 transient are illustrated in Figure 7.1-5 and numerical values for the full worst case F/A outlet nozzle duty cycle are presented in Table 7.1-1.

TABLE 7.1-1  
WORST CASE F/A OUTLET NOZZLE DUTY CYCLE  
ANSYS INPUT DATA

Load Step	Time (Sec.)	Temp. (°F)	
		F/A	RB/A
1	0.0	1076	862
2	0.0	1076	862
3	2	1085	865
4	12.5	885	780
5	90	1250	925
6	175	1100	860
7	450	1000	810
8	4050	600	600
9	7650	1076	862
10	900000	1076	862

Figure 7.1-5  
F/A Outlet Nozzle  
E-16 Transient Load Steps



The ANSYS solution of the worst case F/A outlet nozzle duty cycle was obtained in 79 cumulative iterations using a static and transient convergence criteria of 1 and 5°F respectively. The temperature distributions at each cumulative iteration were saved on ANSYS Tape 4 for recall in subsequent structural analysis. In order to determine the cumulative iterations of interest in structural analysis, maximum and minimum through the wall temperature differences are most important in relation to structural damage. The F/A outlet nozzle temperature differences were based on the through-the-wall temperatures at nodes 1 and 13 depicted in Figure 7.1-4. A plot of the temperature difference between nodes 13 and 1, that is,  $\Delta T = T_{13} - T_1$ , in terms of cumulative iterations is presented in Figure 7.1-6.

A review of the through-the-wall temperature differences shows that the maximum and minimum values occur at cumulative iterations 16 and 31 respectively, with a range of 383°F. In the thermal solution run, cumulative iterations 16 and 31 correspond to the E-16 transient at 12.5 and 90 seconds as illustrated in Figure 7.1-1. The initial steady state condition corresponds to cumulative iteration 3 with a temperature difference of 135°F. Plots of the temperature distribution throughout the F/A outlet nozzle thermal model at cumulative iterations 3, 16, and 31 are presented in Figure 7.1-7.

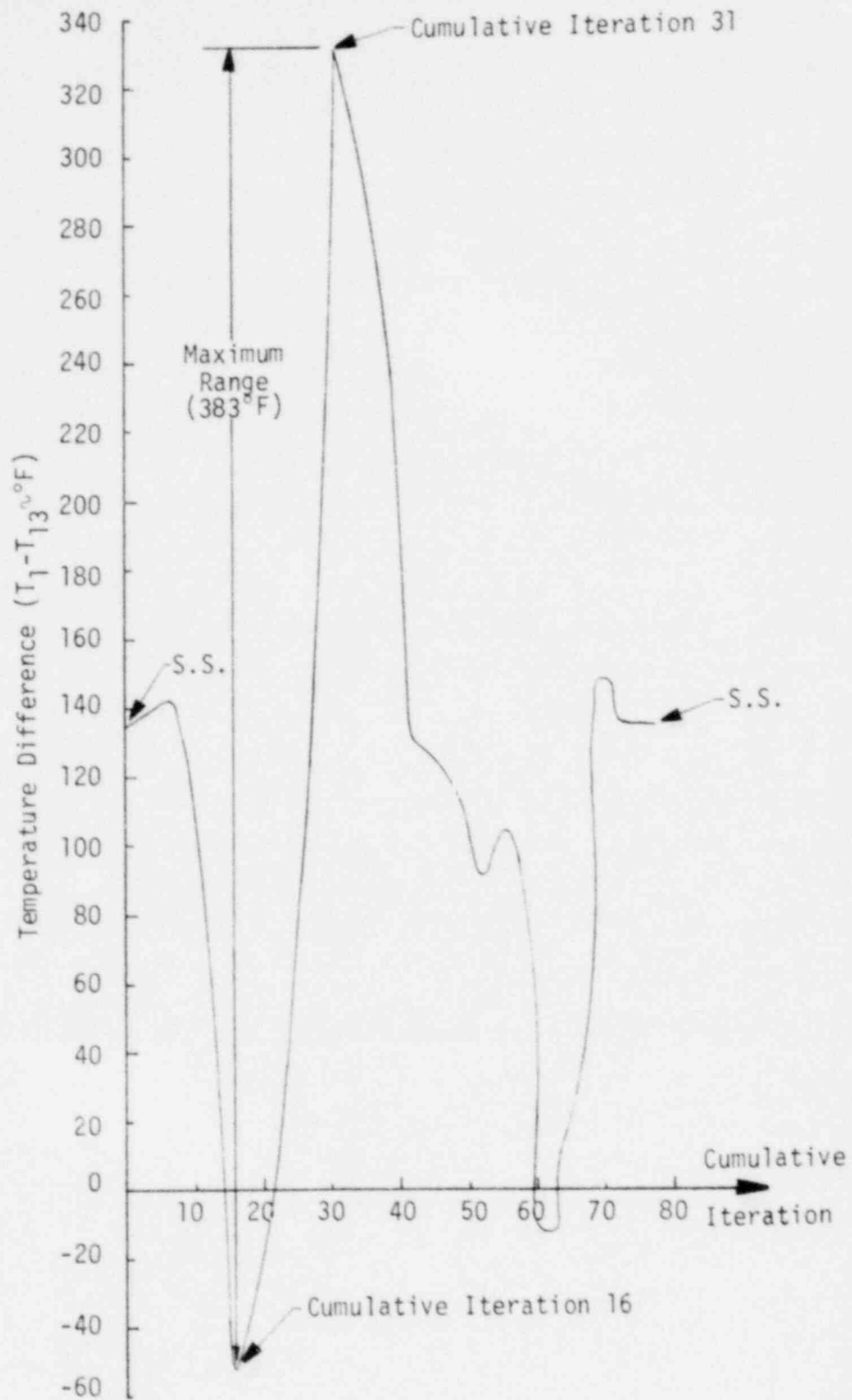


Figure 7.1-6  
 F/A Outlet Nozzle  
 E-16 Transient  
 Temperature Difference vs. Cumulative Iterations



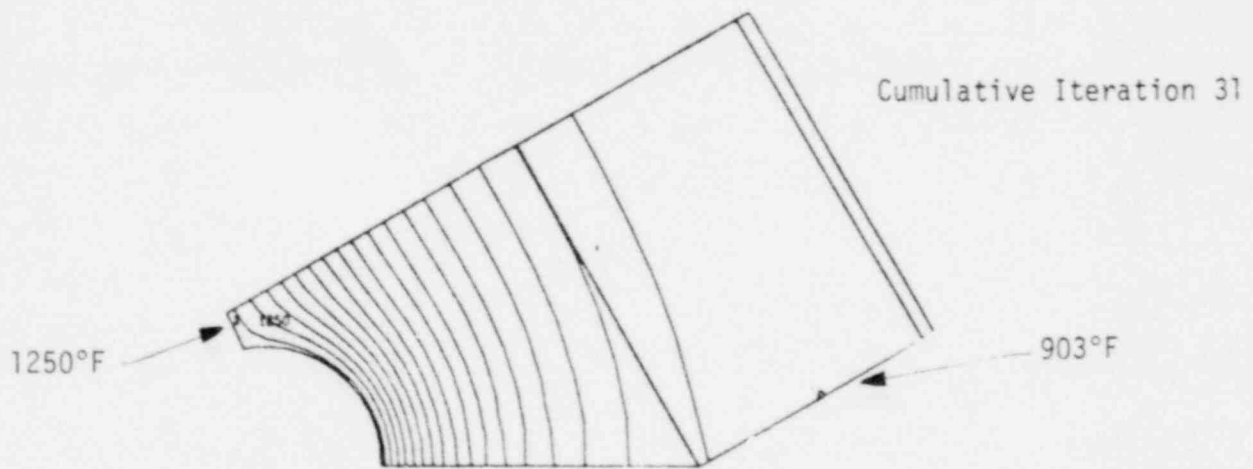
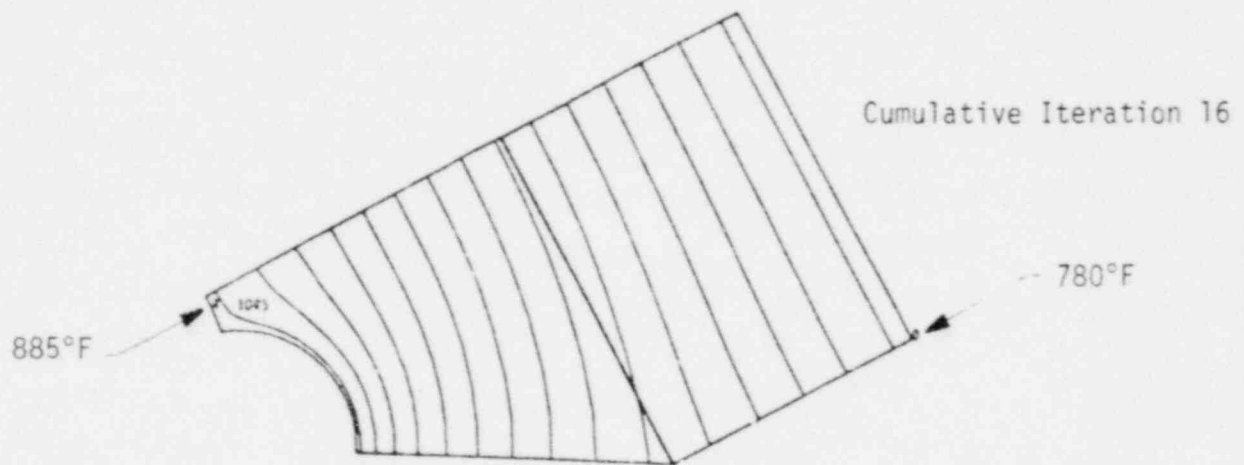
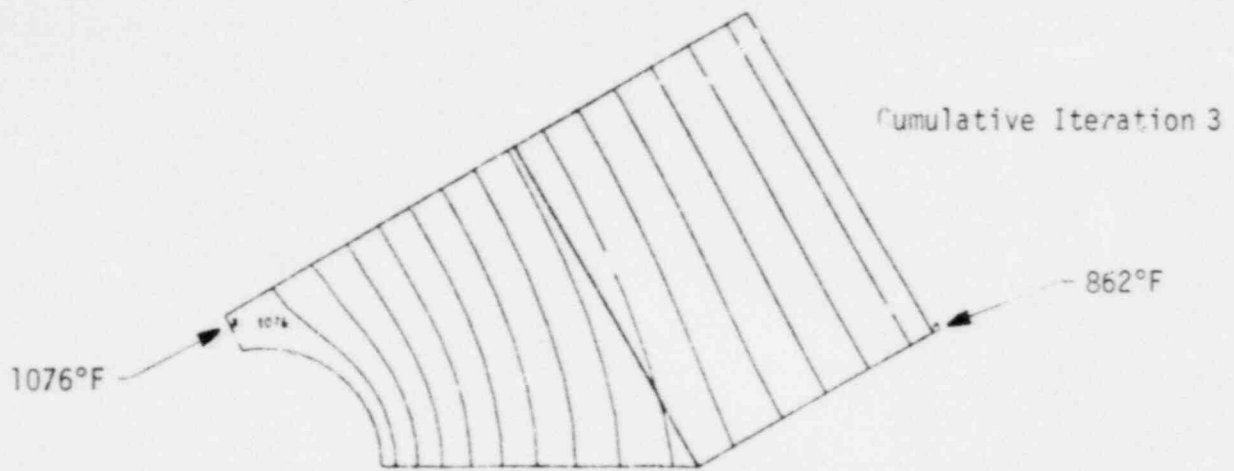


Figure 7.1-7  
F/A Outlet Nozzle  
E-16 Transient  
Cumulative Iteration 3, 16, and 31 Temperature Distributions

### 7.1.3 Worst Case Duty Cycle

The conclusions based on the F/A outlet nozzle loading analysis in relation to establishing the worst case duty cycle were as follows:

- Mechanical loads comprising OBE and SSE seismic, core restraint internal pressure, and dead weight are unimportant in establishing the worst case F/A outlet nozzle duty cycle.
- Thermal loads comprising temperature distributions associated with steady state, the E-16 transient, return to steady state, and the hold-time prior to the initiation of the next E-16 transient were considered most important in establishing the worst case F/A outlet nozzle duty cycle.

The recommendations for the specific F/A outlet nozzle loading in relation to the worst case duty cycle were based solely on time independent and dependent thermal loadings. The following sequence for the worst case F/A outlet nozzle duty cycle was recommended to be repeated 39 times so as to provide an upper bound to the 39 Upset events, and the Emergency or Faulted event.

#### Time Independent

- Select a uniform temperature equal to the reference temperature at cumulative iteration 3. Load sequentially to cumulative iteration 3 and 6 temperature distributions. Unload to uniform temperature.
- Select a uniform temperature equal to the reference temperature at cumulative iteration 16. Load to the cumulative iteration 16 temperature distribution and unload to uniform temperature.
- Select a uniform temperature equal to the reference temperature at cumulative iteration 31. Load to the cumulative iteration 31 temperature distribution and unload to uniform temperature.
- Select a uniform temperature equal to the reference temperature at cumulative iteration 3. Load to the cumulative iteration 3 temperature distribution.

#### Time Dependent

- Hold the cumulative iteration 3 temperature distribution for 10 days.

## 7.2 Structural Analysis

The F/A outlet nozzle structural analysis was directed to deriving the stresses, strains, and dimensional changes which occur during the worst case duty cycle from which subsequent structural evaluations were made. In the following, the F/A outlet nozzle structural model, geometry, and boundary conditions are described. Next, linear and non-linear material properties including the effects of irradiation on stress-strain curves and simplifications made in the thermal creep equations are presented. Further, reference temperature selection for thermal expansions in relation to axial constraints is described. Finally, the time independent and dependent inelastic analysis and results for the F/A outlet nozzle are presented in preparation for subsequent structural evaluation.

### 7.2.1 Model, Geometry, and Boundary Conditions

The F/A outlet nozzle structural model was formulated in the ANSYS finite element program so as to be compatible with the temperature distributions of the thermal model. The F/A outlet nozzle geometry was taken to be identical to that used for the thermal analysis, except that the slab simulating the RB/A was deleted.

In formulating the F/A outlet nozzle model, the ANSYS constant strain (STIF 2) structural element was used to replace the linear temperature (STIF 35) thermal element. The boundary conditions along the lateral surfaces of the 30° sector, in the manner of the conventional roller support, were taken to have zero normally disposed displacements, but free to move radially. Along the surface parallel to the global X-Axis, the UY displacements at Nodes 1 through 13 were set equal to zero. For the inclined surface, the UY displacements, after a 30° rotation to obtain normally disposed directions, were set equal to zero at Nodes 130, 131, 132, 133, 149, 150, 166, 167, 168, 205, 224 and 244. The F/A outlet nozzle structural model is illustrated in Figure 7.2-1.

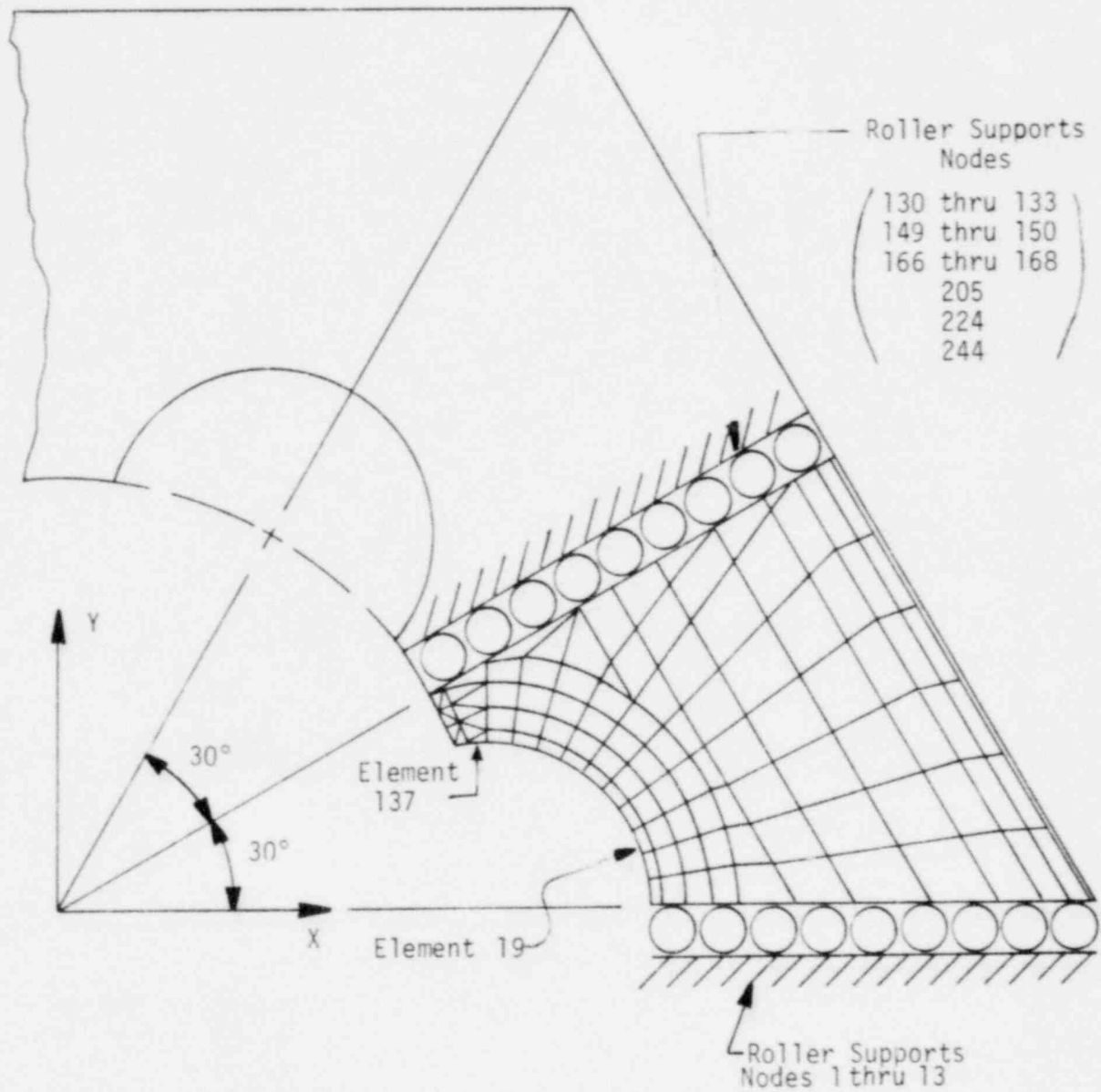


Figure 7.2-1  
 F/A Outlet Nozzle  
 Structural Model, Geometry and Boundary Conditions

## 7.2.2 Properties

The F/A outlet nozzle as constructed from SA-316-SS and initially unirradiated at BOL is irradiated to a fluence ( $E > 0.1$  Mev,  $(\phi t) = 0.07 \times 10^{22}$  N/cm<sup>2</sup>) at EOL. The linear and non-linear properties of SA-316-SS under fluence and temperature used in the F/A outlet nozzle structural analysis are described as follows.

### 7.2.2.1 Linear

The linear SA-316-SS material properties are the Young's Modulus (E), Poisson's ratio ( $\nu$ ), and coefficient of thermal expansion ( $\alpha$ ). Simplifications of the properties in terms of constant conservative values over the 700 to 1250°F range of operational temperature used in the F/A shield block structural analysis, were not made in the F/A outlet nozzle. Instead, the material properties as a function of temperature were used directly as identified in Section 4.2.2.1.

### 7.2.2.2 Non-Linear

The non-linear SA-316-SS material property behavior required in the F/A outlet nozzle structural analysis are the time independent stress-strain, and the dependent thermal creep constitutive relations. The constitutive relations with attendant simplifications used in the F/A outlet nozzle are as follows.

#### 7.2.2.2.1 Stress-Strain Curves

The true average stress-strain curves for SA-316-SS given in the NSM Handbook [6] were reviewed in relation to the F/A outlet nozzle EOL fluence ( $E > 0.1$  Mev,  $(\phi t) = 0.07 \times 10^{22}$  N/cm<sup>2</sup>) and the operational temperature range from 700 to 1250°F. Temperature effects were found to be significant, but the effect of irradiation at EOL fluence relative to unirradiated BOL values was found to be insignificant. Accordingly, the true average EOL and BOL stress-strain curves for SA-316-SS were considered identical to each other for the F/A outlet nozzle.

In the F/A outlet nozzle structural analysis, true minimum BOL and EOL stress-strain curves are required because the thermal loads which occur during the worst case duty cycle are slow acting and are basically statically applied. The true minimum BOL and EOL stress-strain curves as a function of temperature, taken as 90% of the true values given in the NSM Handbook [6], are illustrated in Figure 7.2-2 with corresponding numerical values summarized in Table 7.2-1.

TABLE 7.2-1  
F/A OUTLET NOZZLE  
TRUE MINIMUM BOL AND EOL STRESS-STRAIN DATA  
SA-316-SS

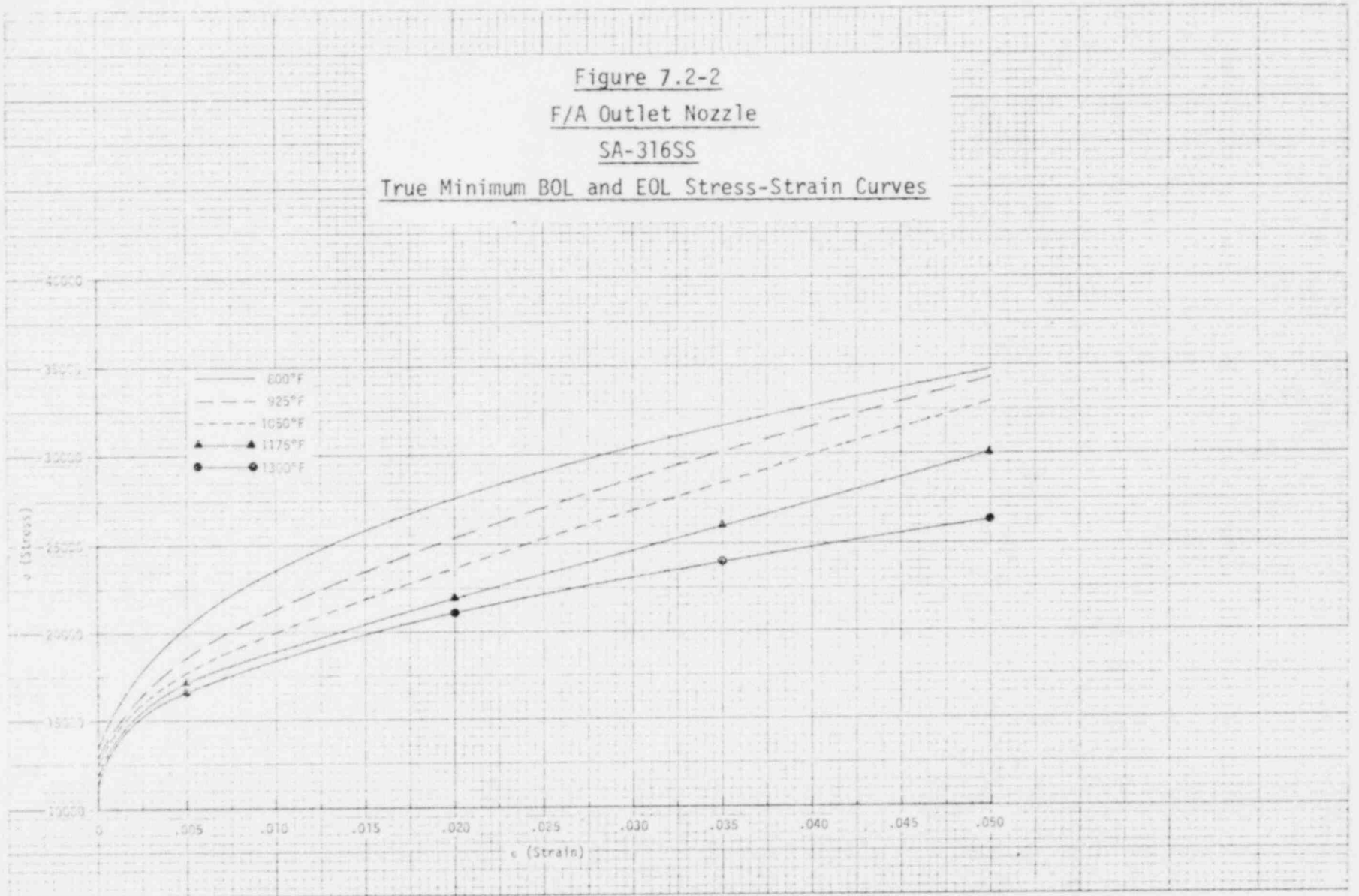
Temp. (°F)	E (10 <sup>6</sup> PSI)	Stress (KSI) at Total Strain				
		.0005617	.002	.006	.010	.050
800	24.06	13514.	17100	21240.	23490.	34740.
925	23.12	12985.	16086	19395	21211	34443
1050	22.13	12429.	15511	18236	19756	32971
1175	21.10	11851	15131	17499	18858	30048
1300	20.03	11250	15030	16920	18360	26280

#### 7.2.2.2.2 Thermal Creep Equations

The thermal creep equations for unirradiated SA-316-SS as a function of stress and temperature are identified in the NSM Handbook [6]. Thermal creep equations for irradiated SA-316-SS are not identified as the combined irradiation-thermal creep effects are included in the irradiation creep equations.

In relation to the F/A outlet nozzle with an EOL fluence ( $E > 0.1$  Mev,  $(\phi t) = 0.07 \times 10^{22}$  N/cm<sup>2</sup>) operating over a steady state temperature range of 950 to 1075°F, the effects of irradiation on thermal creep were considered insignificant, with temperature alone controlling creep rate. As such, the unirradiated SA-316-SS thermal creep equations as a function

Figure 7.2-2  
F/A Outlet Nozzle  
SA-316SS  
True Minimum BOL and EOL Stress-Strain Curves





of temperature were selected to simulate the time dependent relaxation of stresses in the F/A outlet nozzle analysis.

A review of the unirradiated SA-316-SS thermal creep equations given in the NSM Handbook [6] was made for the purposes of simplification. Over a temperature range of 800 to 1000°F, which is a reasonable approximation to the actual steady state F/A outlet nozzle temperatures, the thermal creep equation is given by:

$$\epsilon = \epsilon_L + \epsilon_t (1 - e^{-rt}) + \epsilon_m^{\circ} t$$

where,

$$\begin{aligned} \epsilon &= \text{Total Strain} \\ \epsilon_L &= \text{Loading Strain} \\ \epsilon_t (1 - e^{-rt}) &= \text{Primary Creep-Strain} \\ \epsilon_m^{\circ} &= \text{Secondary Creep Strain} \end{aligned}$$

In order to simplify the thermal creep equation, the primary creep strain was neglected. Accordingly, stress relaxation during the time dependent 10 day hold time would be minimum, with subsequent structural evaluations of creep damage conservative. Although structural evaluations of accumulated deformation would be non-conservative, the degree of non-conservatism was not considered significant.

Expressing the secondary creep strain in terms of the secondary creep strain rate ( $\epsilon_{sc}^{\circ}$ ), the thermal creep equation for SA-316-SS used in the F/A outlet nozzle time dependent analysis was:

$$\epsilon_{sc}^{\circ} = A \left[ \sinh\left(\frac{\beta\sigma}{n}\right) \right]^n e^{-\frac{Q}{RT}}$$

where,

$$\begin{aligned} \dot{\epsilon} &= \text{in/in-Hour} \\ \sigma &= \text{Stress (PSI)} \\ T &= \text{Absolute Temperature (}^{\circ}\text{R)} \end{aligned}$$



The numerical values of the secondary creep constraints used in the F/A outlet nozzle time dependent analysis are identified as follows.

$$\begin{aligned}A &= 5.6229 \times 10^{10} / \text{Hour} \\ \beta &= 2.015 \times 10^{-4} / \text{PSI} \\ n &= 4.6 \\ Q &= 67000 \text{ cal/mol} \\ R &= 1.10389 \text{ cal/mol-}^\circ\text{R}\end{aligned}$$

Thus,

$$\epsilon_{sc}^{\circ} = (5.6229 \times 10^{10}) \left[ \text{Sinh} (4.38 \times 10^{-5} \sigma) \right]^{4.6} \left[ e^{-\frac{60694}{T}} \right]$$

The secondary thermal creep rate used in the F/A outlet nozzle time independent analysis as a function of stress and temperature are illustrated in Figure 7.2-3.

### 7.2.3 Worst Case Duty Cycle Response

The structural response of the F/A outlet nozzle to the worst case duty cycle loading required the selection of reference temperatures compatible with the temperature distributions at the worst case through the wall temperature differences and axial constraints prior to deriving the time independent and dependent solutions. A description of the analysis and solutions which are required in subsequent structural evaluation is as follows.

#### 7.2.3.1 Constraints and Reference Temperature Selection

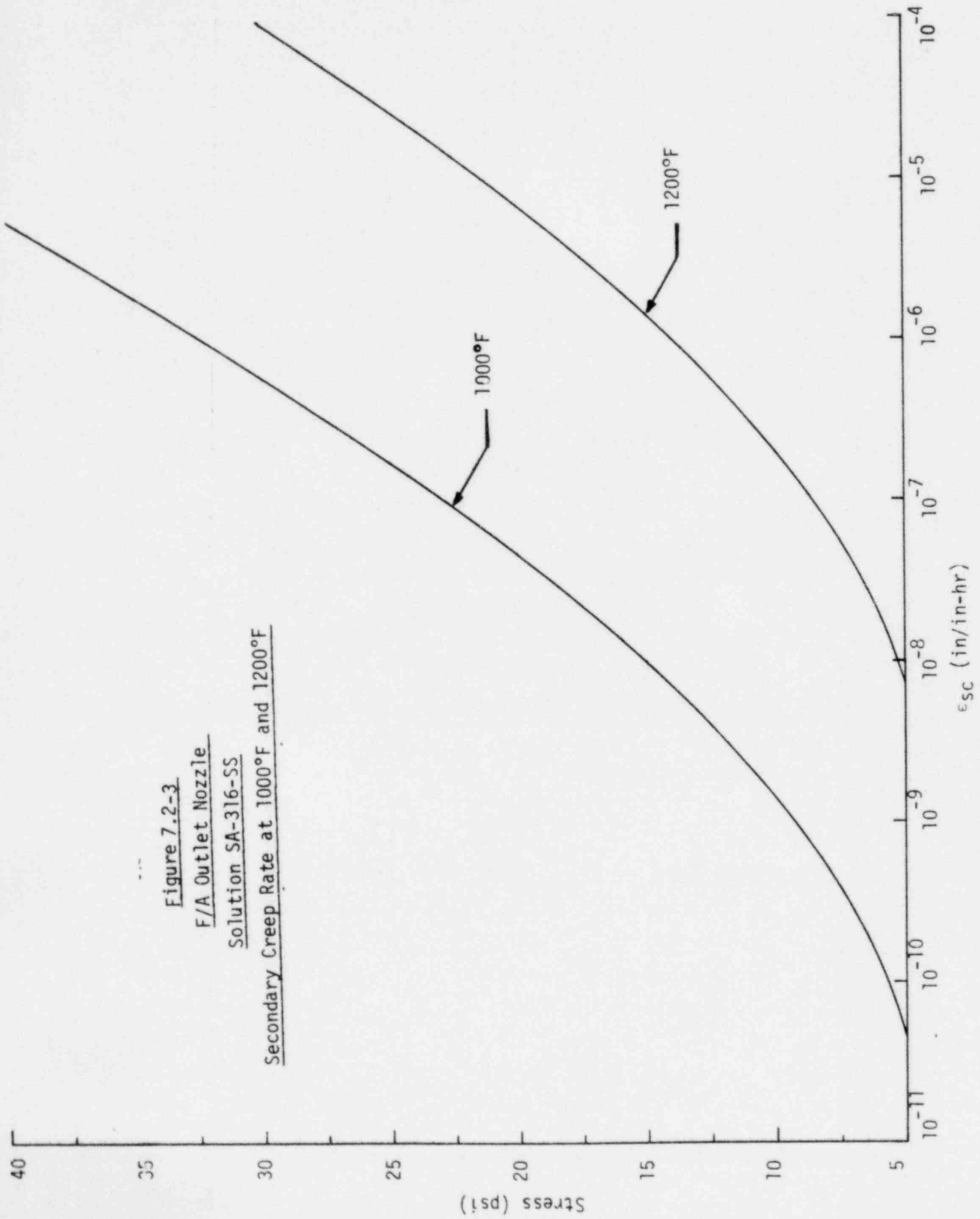
The F/A outlet nozzle structural model corresponds to a 30° sector of a lateral slice taken through the length of the outlet nozzle. Axial constraints normal to the 2 dimensional 30° sector closely simulate a plane strain condition as the length of the outlet nozzle is significantly greater than corresponding cross-sectional dimensions. Accordingly, the F/A outlet nozzle was considered to be in a plane strain condition for the purposes of analysis.

Figure 7.2-3

F/A Outlet Nozzle

Solution SA-316-SS

Secondary Creep Rate at 1000°F and 1200°F



The method of selecting a reference temperature in relation to an arbitrary temperature distribution imposed in an ANSYS plane strain model was described for the F/A shield block in Section 4.2.3.1. Using the same method as for the F/A outlet nozzle, the reference temperatures for the recommended cumulative iterations in the worst case duty cycle are summarized in Table 7.2-2.

TABLE 7.2-2  
F/A OUTLET NOZZLE  
REFERENCE TEMPERATURES

Temperature Distribution (Cum. Iter.)	Reference Temperature ( $T_R \sim ^\circ F$ )
3	1003.5
6	1003.5
16	977.2
31	1030.7

#### 7.2.3.2 Analysis and Results

The ANSYS inelastic analysis of the F/A outlet nozzle structural model under the worst case duty cycle was arranged in time-independent plastic analysis associated with the short term E-16 transient followed by time-dependent creep analysis corresponding to steady state temperatures over the 10 day hold-time. The time independent and dependent analysis provide the structural response from which evaluations of crack initiation in terms of local ductile rupture and creep-fatigue damage are made. With regard to dimensional changes that can exceed functional limits, the peak + accumulated deformations during the duty cycle and the residual deformations following the duty cycle are required.

In order to obtain the desired results in an efficient manner, the ANSYS restart option was used to follow the loading sequence within, between and after the time independent and dependent loadings. As elastic/plastic/creep instability would not be expected for the F/A outlet nozzle under the deformation controlled thermal loadings, the ANSYS small strain-small deformation option was used in the inelastic analysis. A description of the time independent and dependent analysis and results is as follows.

#### 7.2.3.2.1 Time Independent

The time independent ANSYS analysis of the F/A outlet nozzle was directed to deriving the peak plus accumulated strains and deformations associated with following the path dependent thermal loadings from initial steady state through the E-16 transient followed by the return to final steady state, but excluding the 10 day hold-time. The time independent loadings were considered as static loadings applied at zero time. A total of 18 sequential ANSYS load steps in combination with the restart option were used to obtain the time independent structural response of the F/A outlet nozzle. A summary of the F/A time independent analysis procedure is presented in Table 7.2-3.

TABLE 7.2-3  
F/A OUTLET NOZZLE  
TIME INDEPENDENT ANALYSIS SUMMARY  
INITIAL STEADY STATE, E-16 TRANSIENT, AND FINAL STEADY STATE

Load Step	Iterations	Temperature Distribution (°F)	Reference Temperature (°F)	Description
1	25	Cum. Iter. 3	1003.5	Initial Steady State Time = 0.0 Sec.
2	4	Cum. Iter. 3	1003.5	
3	5	Cum. Iter. 6	1003.5	1st E-16 Transient Loading and Unloading Time = 2.0 Sec.
4	12	1003.5	1003.5	
5	7	1003.5	1003.5	
6	1	977.3	977.3	2nd E-16 Transient Loading and Unloading Time = 9.5 Sec.
7	28	Cum. Iter. 16	977.3	
8	6	Cum. Iter. 16	977.3	
9	28	977.3	977.3	
10	5	977.3	977.3	
11	1	1030.7	1030.7	3rd E-16 Transient Loading and Unloading Time = 90 Sec.
12	68	Cum. Iter. 31	1030.7	
13	6	Cum. Iter. 31	1030.7	
14	68	1030.7	1030.7	
15	11	1030.7	1030.7	
16	25	1003.5	1003.5	Final Steady State Time = 900000 Sec.
17	1	Cum. Iter. 3	1003.5	
18	3	Cum. Iter. 3	1003.5	

The F/A outlet nozzle structural response to the time independent loadings was obtained with a plastic convergence ratio of 0.01. The detailed stress-strain response at each of the converged **solutions** was saved on ANSYS Tape 10 for subsequent recall in structural evaluations. The initial and final time independent steady state maximum equivalent stresses were found to be 14,900 and 13,157 psi respectively. During the E-16 transient, the maximum equivalent stress was 16,846 psi at cumulative iteration 31. The peak non-uniform deformation was found to be 0.00149 in. at cumulative iteration 31. The initial steady state non-uniform deformation was 0.00041 in. Computer plots of time independent equivalent stress and peak non-uniform deformation are presented in Figures 7.2-4 through -6.

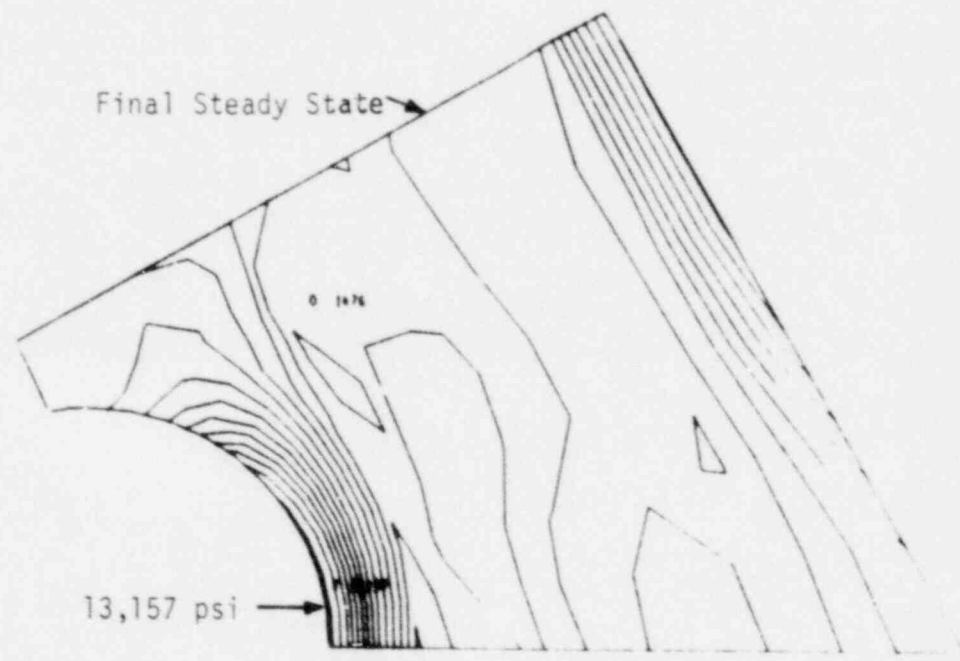
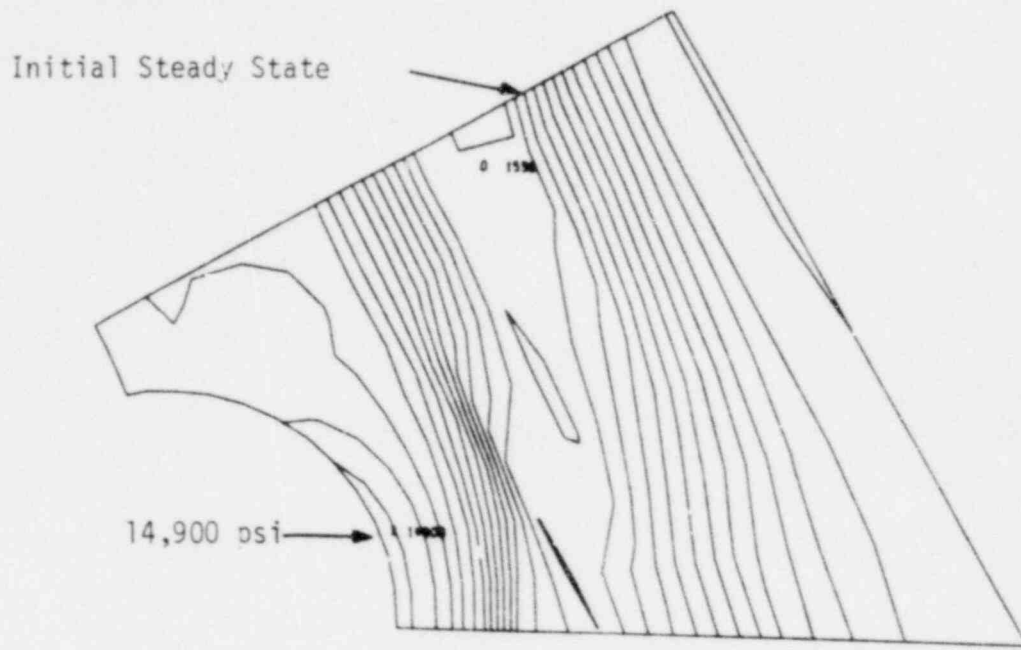


Figure 7.2-4  
F/A Outlet Nozzle  
Initial and Final Steady State  
Equivalent Stress  
Time Independent

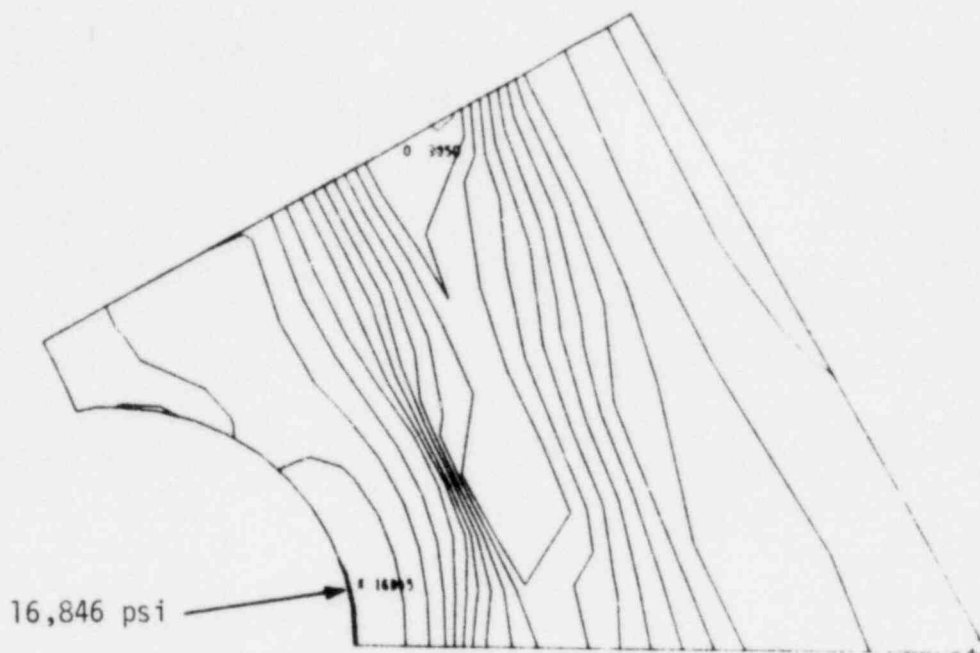


Figure 7.2-5  
F/A Outlet Nozzle  
E-16 Transient Cumulative Iteration 31  
Equivalent Stress  
Time Independent



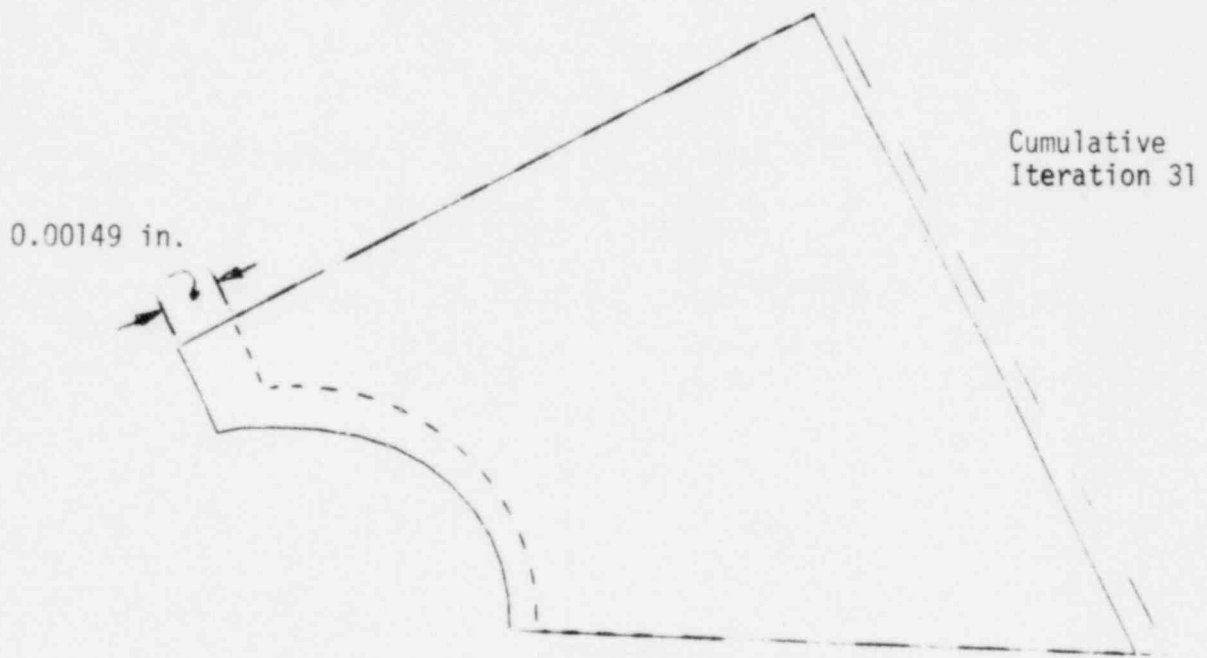
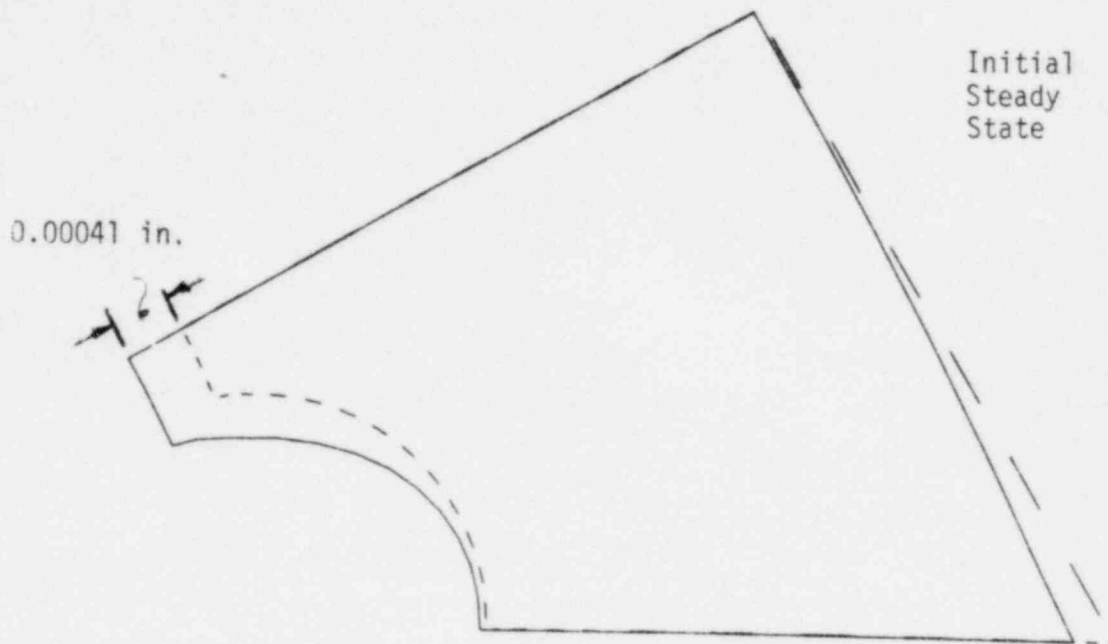


Figure 7.2-6  
 F/A Outlet Nozzle  
 Initial Steady State and E-16 Transient Cumulative Iteration 31  
 Non-Uniform Deformation  
 Time Independent

#### 7.2.3.2.2 Time Dependent

The time dependent ANSYS analysis of the F/A outlet nozzle was directed to deriving the residual strains and deformations associated with the 10 day hold-time following the final time dependent steady state condition. The time dependent analysis was performed in 3 load steps using an ANSYS restart from Load Step 18 of the time independent analysis corresponding to the cumulative iteration 3 temperature distribution. Load Steps 19 and 20 were used to stabilize the time independent final steady state condition. The time dependent relaxation of stress in relation to secondary thermal creep rate was obtained in load step 21. A total of 24 iterations at a 10 hour creep time step were used to obtain the time dependent solution over the 10 day or 240 hour hold-time. A subsequent ANSYS restart for 2 load steps was made in unloading the F/A outlet nozzle to a uniform temperature so as to obtain the residual deformation after one worst case duty cycle. A summary of the F/A outlet nozzle time dependent analysis procedure for the 10 day hold-time and unloading to a uniform temperature is presented in Table 7.2-4.

TABLE 7.2-4  
F/A OUTLET NOZZLE  
TIME DEPENDENT ANALYSIS SUMMARY  
10 DAY HOLD-TIME AND UNLOADING

Load Step	Iterations	Temperature Distribution (°F)	Reference Temperature (°F)	Description
19	1	Cum. Iter. 3	1003.5	10 day Hold-Time
20	3	Cum. Iter. 3	1003.5	
21	24	Cum. Iter. 3	1003.5	
22	1	1003.5	1003.5	Unloading for Residual Deformations
23	3	1003.5	1003.5	

The F/A outlet nozzle structural response to the time dependent loading was obtained with a creep convergence ratio of 0.25. The detailed stress-strain response was saved on ANSYS Tape 10 for subsequent recall in structural evaluations. The F/A outlet nozzle structural response at the end of the 10 day hold-time, designated as the time dependent final steady state condition, was not found to significantly differ from the time independent final steady state response because of negligible relaxation of stresses and deformations under the secondary thermal creep rate. The maximum equivalent stress and peak non-uniform deformation in the F/A outlet nozzle at the time dependent final steady state condition were found to be 13,058 psi and 0.00049 in. as illustrated in Figure 7.2-7.

With regard to the residual deformations of the F/A outlet nozzle, a maximum value of 0.00018 in. was found over the worst case duty cycle as illustrated in Figure 7.2-8.

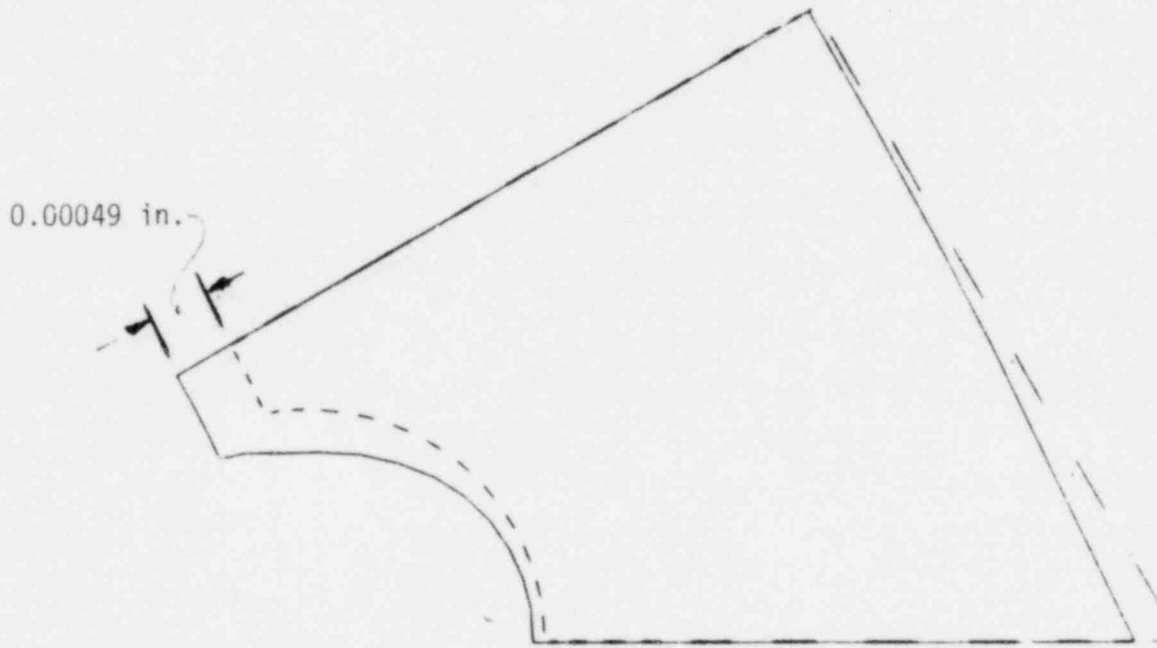
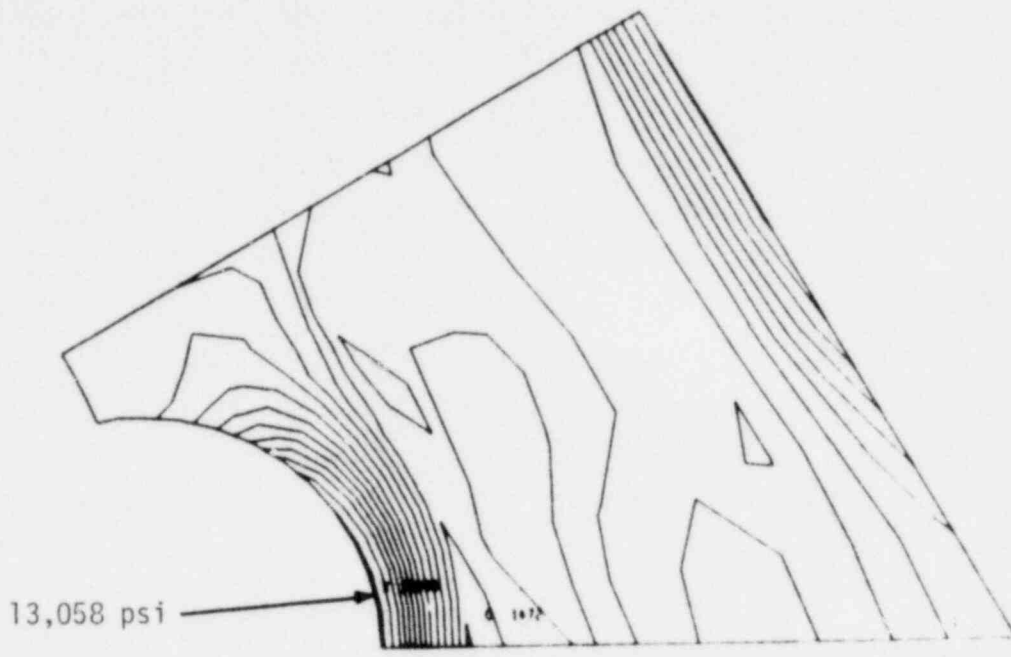


Figure 7.2-7  
F/A Outlet Nozzle  
Final Steady State Equivalent Stress and Non-Uniform Deformation  
Time Dependent

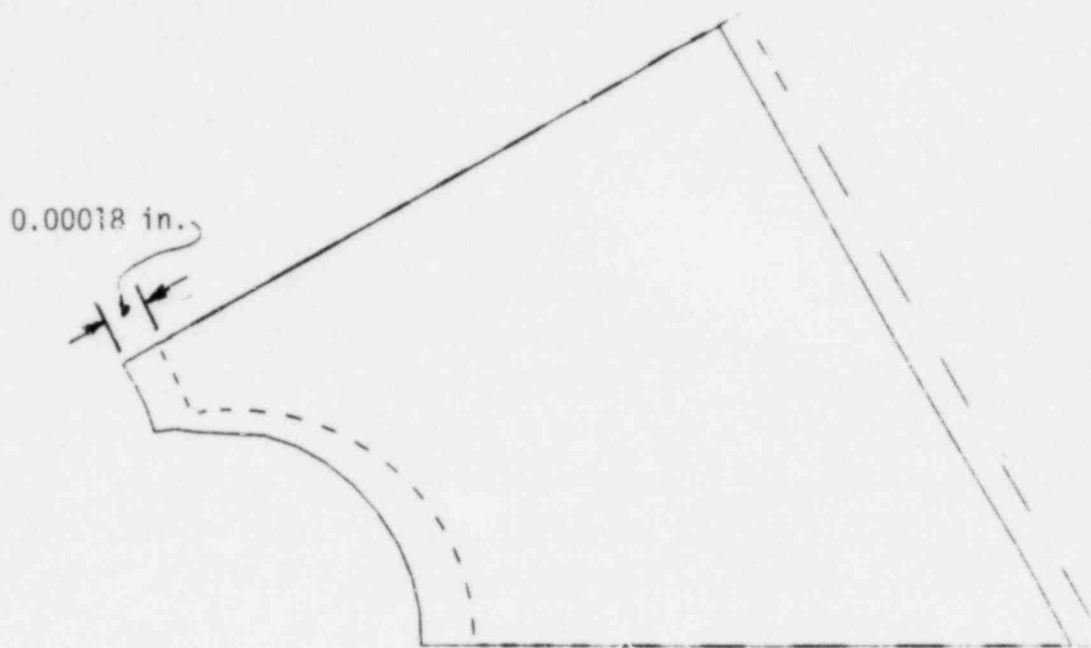


Figure 7.2-8  
F/A Outlet Nozzle  
Residual Deformation

### 7.3 Structural Evaluation

The F/A outlet nozzle structural evaluation was arranged to provide a comparison of the structural response for the 39 worst case duty cycles in relation to criteria which protect against crack initiation and excessive deformation failure modes and thereby assure F/A outlet nozzle function over the first and second reactor cycles.

The procedure for performing the F/A outlet nozzle structural evaluations in relation to crack initiation and excessive deformation criteria was identical to that for the F/A shield block presented in Section 4.3. The damage processor was used to screen the F/A outlet nozzle elements for the worst location for the ductile rupture and combined creep-fatigue factors over the 39 worst case duty cycles while attendant deformations were compared with peak + accumulated and residual deformation limits. A description of the F/A outlet nozzle structural evaluation and summary of results is presented as follows.

#### 7.3.1 Crack Initiation

The F/A outlet nozzle structural evaluation of crack initiation in relation to local ductile rupture and combined creep-fatigue damage criteria over the 39 worst case duty cycles is presented in the following subsections.

##### 7.3.1.1 Local Ductile Rupture

The local ductile rupture criterion in protecting against crack initiation requires that the ductile rupture factor ( $F_{DR}$ ) be less than unity at each point in the F/A outlet nozzle.

$$F_{DR} = \text{Maximum of } \left\{ \begin{array}{l} \bullet \frac{(\epsilon_{\text{max principal}})^{TF}}{0.3 \epsilon_{f,\text{min}}} \\ \bullet \frac{(\epsilon_{\text{max principal}})^{TF}}{\epsilon_{u,\text{min}}} \end{array} \right\}$$

In the following, the allowable uniaxial strains used in the F/A outlet nozzle structural evaluation and comparison of results with the local ductile rupture factor criterion are presented.

#### 7.3.1.1.1 Allowable Uniaxial Strains

The F/A outlet nozzle as constructed from SA-316-SS is unirradiated at BOL. The EOL fluence ( $E > 0.1$  Mev) is  $0.07 \times 10^{22}$  n/cm<sup>2</sup>. In addition, the F/A outlet nozzle temperatures range from 700 to 1250°F. The true uniaxial uniform elongation ( $\epsilon_{u, \min}$ ) and fracture ( $\epsilon_{f, \min}$ ) for unirradiated and irradiated SA-316-SS used in the F/A outlet nozzle structural evaluation were taken from the recommendations in the trial applications of the RDT Draft for Breeder Reactor Core Components [15-23] and are identical to those taken for the F/A shield block structural evaluation presented in Section 4.3.1.1.1.

#### 7.3.1.1.2 Comparison with Criterion

The F/A outlet nozzle structural evaluation in relation to the worst case location for local ductile rupture was made by screening each of the finite elements over the 39 worst case duty cycles with the damage processor. The maximum local ductile rupture factor ( $F_{DR} \max$ ) for the F/A outlet nozzle was found to occur at element 127, as identified in Figure 7.2-1.

The peak BOL strain components occurred at the cumulative iteration 31 temperature distribution in the E-16 transient where the local metal temperature was 1242°F. Accumulated BOL strain components were based on the difference between final time dependent steady state conditions and initial time independent steady state conditions in the worst case cycle. The EOL maximum principal strain for the peak BOL and accumulated BOL strain components over 39 worst case F/A outlet nozzle duty cycles was 0.03 in/in. The triaxiality factor for the local stress state was -1.868, but was taken as unity for conservatism in the structural evaluation. The true minimum irradiated uniform elongation and fracture strains at EOL fluence ( $E > 0.1$  Mev,  $\phi t = 0.07 \times 10^{22}$  N/cm<sup>2</sup>) were 0.227 and 0.137 in/in respectively.

In this arrangement, the maximum local ductile rupture ( $F_{DR}$ ) for the F/A outlet nozzle was found to be controlled by the fracture strain with a value:

$$(F_{DR})_{\max} = 0.732$$

As  $(F_{DR})_{\max} < 1.0$ , the F/A outlet nozzle is not expected to experience crack initiation over the 39 worst case duty cycles based on the local ductile rupture criterion.

#### 7.3.1.2 Creep-Fatigue Damage

The creep-fatigue damage criterion in protecting against crack initiation requires that the combined creep-fatigue damage factor ( $F_{CFD}$ ) be less than unity at each point in the F/A outlet nozzle.

$$F_{CFD} = a/b = \text{Minimum of } \left\{ \begin{array}{l} \bullet 7/3 D^C + D^f \\ \bullet D^C + 7/3 D^f \end{array} \right\}$$

In the following, the allowable limits for fatigue life and creep-rupture times used in the F/A outlet nozzle structural evaluation and a comparison of the results with the combined creep-fatigue damage factor criterion are presented.

##### 7.3.1.2.1 Allowable Limits

The F/A outlet nozzle as constructed from SA-316-SS is unirradiated at BOL. The EOL fluence ( $E > 0.1$  Mev) is  $0.07 \times 10^{22}$  N/cm<sup>2</sup>. In addition, the F/A outlet nozzle temperatures range from 700 to 1250°F. The fatigue life and creep rupture time relations used in the F/A outlet nozzle structural evaluation were identical to those used in the F/A shield block structural evaluation presented in Section 4.3.1.1.1. The fatigue life and creep rupture time relations representative of F/A outlet nozzle peak and steady state metal temperatures at EOL fluence are illustrated in Figures 7.3-1 and -2 respectively.



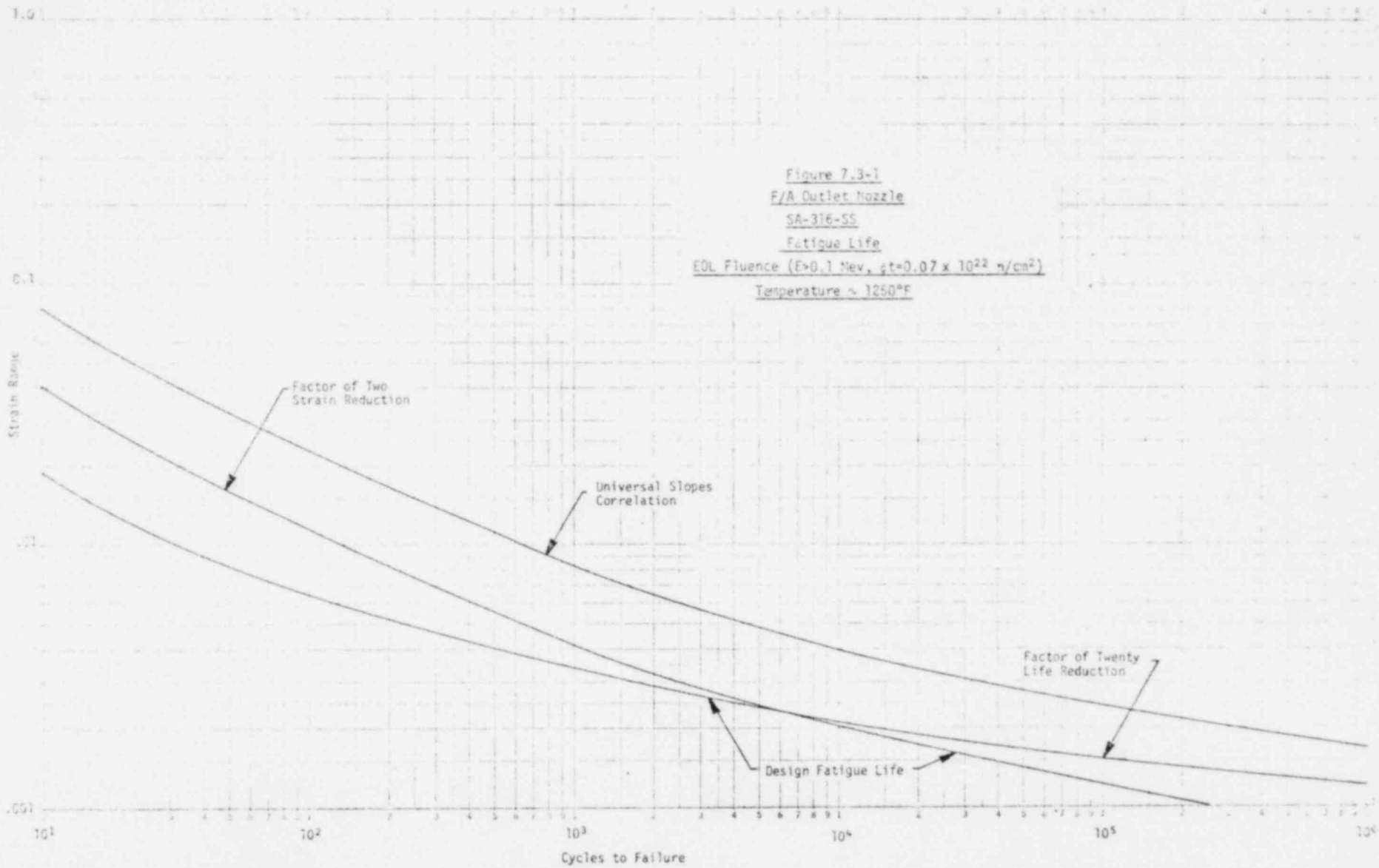


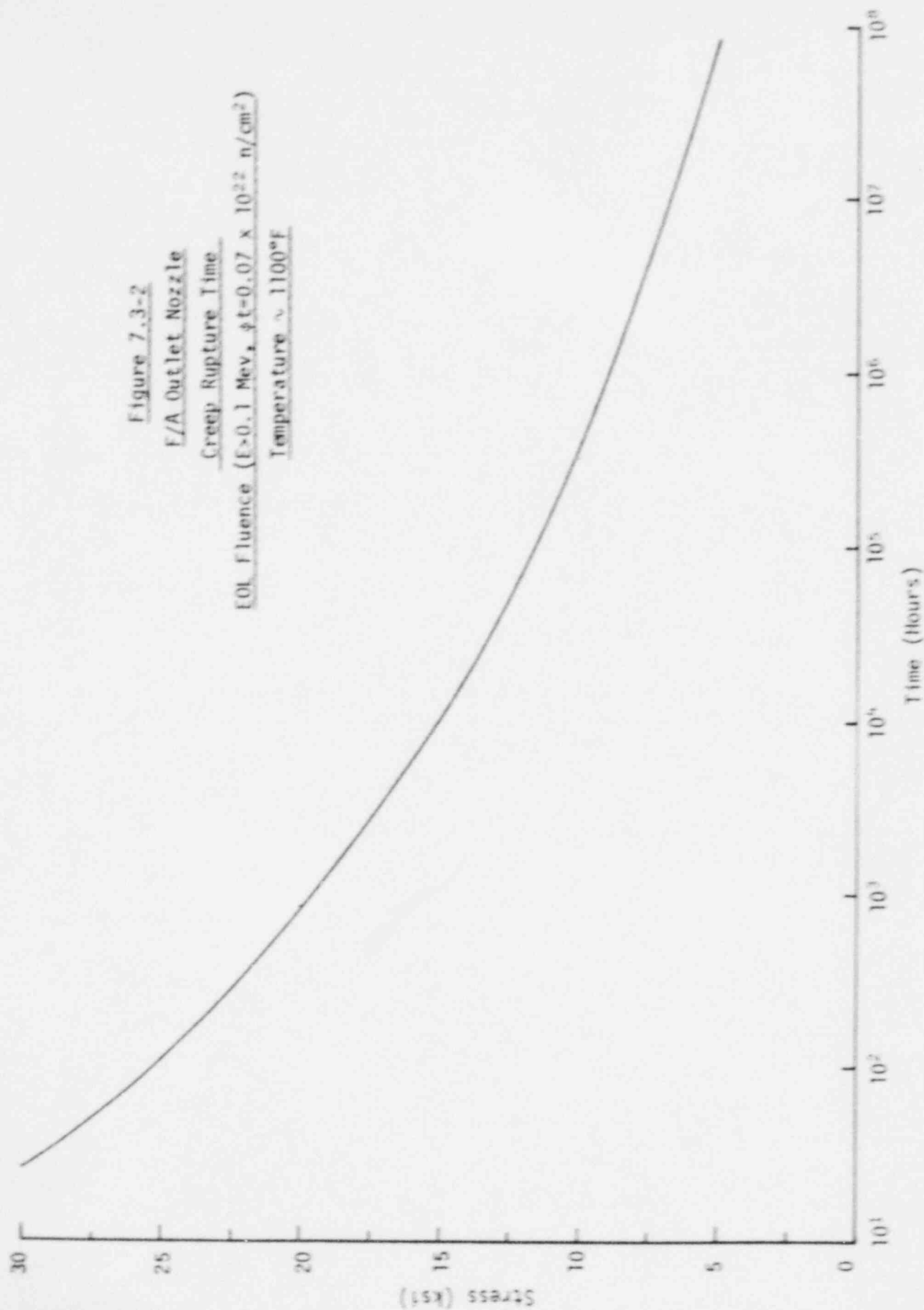
Figure 7.3-2

F/A Outlet Nozzle

Creep Rupture Time

EOL Fluence ( $E > 0.1$  MeV,  $\phi t = 0.07 \times 10^{22}$  n/cm<sup>2</sup>)

Temperature  $\sim 1100^\circ\text{F}$



### 7.3.1.2.2 Comparison with Criterion

The F/A outlet nozzle structural evaluation in relation to the worst case location for combined creep-fatigue damage was made by screening each of the finite elements over the 39 worst case duty cycles with the damage processor. The maximum combined creep-fatigue damage factor  $(F_{CFD})_{max}$  for the F/A outlet nozzle was found to occur at element 19, as identified in Figure 7.2-1.

The fatigue damage factor  $(D^f)$  was found to be 0.547 for 39 worst case duty cycles. The equivalent strain range was found to be critical and occurred between cumulative iteration 16 and 31 temperature distributions during the E-16 transient with a value of 0.0075 in/in. The peak metal temperature over the fatigue cycle was 1237°F. The fatigue life for the equivalent strain range was 71 cycles based on the EOL fluence ( $E > 0.1$  Mev,  $(\phi t) = 0.07 \times 10^{22}$  N/cm<sup>2</sup>).

The creep damage factor  $(D^c)$  was found to be 0.0966 for the 39 worst case duty cycles. The equivalent stress was found to be critical in the determination of minimum rupture times. As stress relaxation was negligible, the equivalent stress of 13,166 PSI at the beginning of the 10 day hold-time controlled the creep-damage. The mean minimum rupture time for EOL fluence ( $E > 0.1$  Mev,  $(\phi t) = 0.07 \times 10^{22}$  N/cm<sup>2</sup>) at a metal temperature of 1073°F was  $9.69 \times 10^4$  hours.

In this arrangement, the maximum combined creep-fatigue damage factor  $(F_{CFD})_{max}$  for the F/A outlet nozzle was dominated by fatigue damage while creep damage was small.

$$(F_{CFD})_{max} = 0.773$$

As  $(F_{CFD})_{max} = 0.773 < 1.0$ , the F/A outlet nozzle is not expected to experience crack initiation over the 39 worst case duty cycles based on the creep-fatigue damage criterion.

### 7.3.2 Excessive Deformation

The F/A outlet nozzle structural evaluation of peak plus accumulated, and residual deformations in relation to functional limits over the 39 worst case duty cycles is presented in the following subsections.

#### 7.3.2.1 Peak + Accumulated Deformations

The peak plus accumulated deformation criterion in protecting against excessive deformations requires that peak plus accumulated deformations ( $\delta^{P+A}$ ) be less than the peak plus accumulated deformation limit (PADL).

$$\delta^{P+A} \leq \text{PADL}$$

The peak deformation ( $\delta^P$ ) of the F/A outlet nozzle during the worst case duty cycle at BOL was found to occur at the fluted surface at the cumulative iteration 31 temperature distribution of the E-16 transient with a value of 0.00149 in. The initial time independent and final time dependent steady state non-uniform deformations were found to be 0.00041 and 0.00049 in, respectively. Accordingly, the accumulated deformation ( $\delta^A$ ) between initial time independent and final time dependent steady state conditions for one duty cycle at BOL was 0.00009 in. For 39 worst case duty cycles, the peak plus accumulated ( $\delta^{P+A}$ ) deformation at EOL is

$$(\delta^{P+A})_{\text{EOL}} = (\delta^P)_{\text{BOL}} + (N-1) (\Delta\delta^{\text{SS}})_{\text{BOL}}$$

$$(\delta^{P+A})_{\text{EOL}} = 0.00149 + (38) (0.00009)$$

$$(\delta^{P+A})_{\text{EOL}} = 0.0049 \text{ in.}$$

For the F/A outlet nozzle, the peak plus accumulated deformation limit (PADL) is

$$\text{PADL} = 0.020 \text{ in.}$$

As  $\delta^{P+A} < \text{PADL}$ , the F/A outlet nozzle is not expected to experience excessive peak deformation over the 39 worst case duty cycles.

#### 7.3.2.2 Residual Deformations

The residual deformation limit in protecting against excessive deformation requires that the residual deformation ( $\delta^R$ ) be less than the residual deformation limit (RDL).

$$\delta^R \leq \text{RDL}$$

The accumulated deformation ( $\delta^A$ ) between the initial and final uniform conditions for one worst case duty cycle at BOL was found to be 0.000180 in. For 39 duty cycles, the residual deformation ( $\delta^R$ ) at EOL.

$$(\delta^R)_{\text{EOL}} = N (\delta^A)_{\text{BOL}}$$

$$(\delta^R)_{\text{EOL}} = 0.007 \text{ in.}$$

For the F/A outlet nozzle, the residual deformation limit (RDL)

$$\text{RDL} = 0.020 \text{ in.}$$

As  $\delta^R < \text{RDL}$ , the F/A outlet nozzle is not expected to be experience excessive residual deformation over the 39 worst case duty cycles.

#### 7.3.3 Summary

The F/A outlet nozzle was found to satisfy the crack initiation and excessive deformation criteria. A summary of the F/A outlet nozzle structural evaluation is presented in Table 7.3-1.

TABLE 7.3-1  
F/A OUTLET NOZZLE  
STRUCTURAL EVALUATION SUMMARY

Criteria		Allowable Value	Calculated Value	Margin of Safety*
Crack Initiation	Ductile Rupture Factor	1	0.732	0.37
	Combined Creep-Fatigue Damage Factor	1	0.773	0.29
Excessive Deformation	Peak + Accumulated	0.020 in	0.005	3.0
	Residual	0.020 in	0.007	1.86

\* Margin of Safety =  $\frac{\text{Allowable Value}}{\text{Calculated Value}} - 1$

## 8.0 ATTACHMENT ASSEMBLY ANALYSIS AND EVALUATION

In the F/A attachment assembly analysis and evaluation, a loading analysis was made that considered mechanical seismic, pressure and deadweight loads, and thermal steady state and transient loads in establishing the number and characteristics of a worst case duty cycle that umbrellas all expected duty cycles for the attachment assembly in the first and second reactor cycles. Next, an inelastic structural analysis of the attachment was made for a single worst case BOL duty cycle to calculate the strains and dimensional changes from which EOL values were approximated. Finally, a structural evaluation of EOL strains and dimensional changes was made in relation to criteria which protect against crack initiation and excessive deformation. A summary of the loading and structural analysis and structural evaluation is presented as follows.

### 8.1 Loading Analysis

The F/A attachment assembly loading analysis was directed to establishing the number and characteristics of a worst case duty cycle that umbrellas both the number and characteristics of Upset, Emergency, and Faulted Events specified over the first and second reactor cycles. The number and characteristics of these events are specified in the Equipment Specification [1].

It is important to note that the worst case F/A attachment assembly duty cycle is, in itself, hypothetical, but permits a conservative structural evaluation to be performed on a single duty cycle instead on each of the individual events specified. In the following, the F/A attachment assembly mechanical and thermal loads are assessed individually and in relation to each other prior to establishing the worst case duty cycle which was used in structural evaluation.

#### 8.1.1 Mechanical

The F/A attachment assembly mechanical loads of significance in relation to subsequent structural evaluations are due to deadweight, flow pressure drop, and seismic excitation. A description of the mechanical loads is presented in the following subsections.

### 8.1.1.1 Deadweight

The F/A attachment assembly supports the deadweight of the fuel rod bundle. The total deadweight  $(F_{DW})_T$  of the rod bundle including a total number  $(N_T)$  of 217 rods is:

$$(F_{DW})_T = 235 \text{ LBS.}$$

Neglecting the buoyancy effects of rod bundle immersed in sodium and assuming the total deadweight  $(F_{DW})_T$  equally distributed between both support bars, the deadweight  $(F_{DW})$  suspended by a single support bar,

$$F_{DW} = \frac{(F_{DW})_T}{2}$$

$$F_{DW} = 117.5 \text{ LBS.}$$

Alternately, the deadweight  $(f_{DW})$  of a single rod, in terms of the deadweight  $(F_{DW})$  and total number  $(N_T)$  of rods, is as follows.

$$f_{DW} = \frac{F_{DW}}{(N_T/2)}$$

$$f_{DW} = 1.083 \text{ LBS.}$$

With regard to the distribution of the deadweight load  $(F_{DW})$  along the single support bar, a trapezoidal distribution consistent with the distribution of the rods in the hexagonal F/A duct was assumed. The hexagonal distribution of F/A rods supported by a symmetrical half of a single support bar is illustrated in Figure 8.1-1.



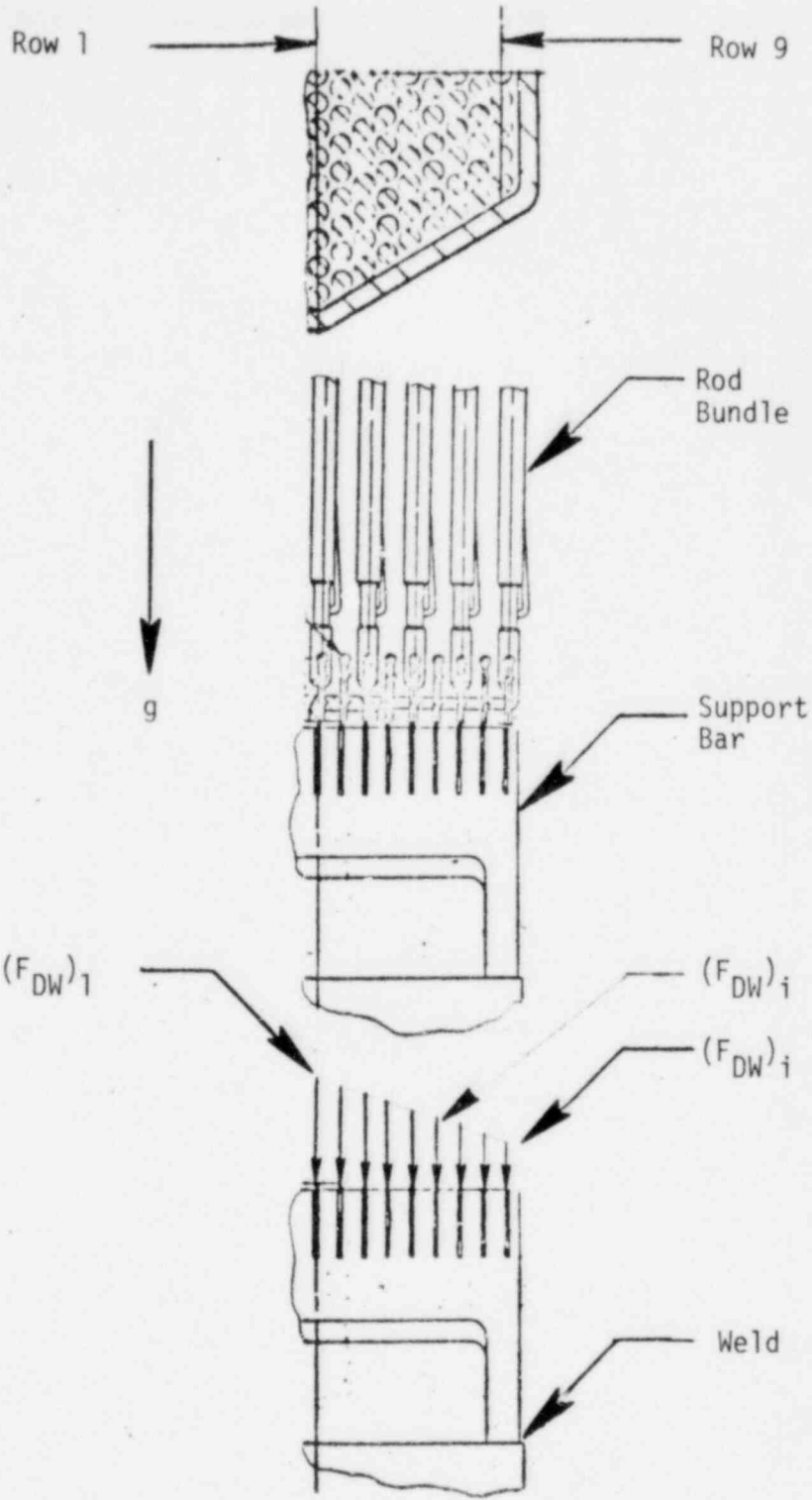


Figure 8.1-1  
 F/A Attachment Assembly  
 Deadweight Load Distribution

In the F/A rod bundle plan view, the number of rods varies over nine rows, designated by a row 1 through 9 notation. The deadweight  $(F_{DW})_i$  row distribution in terms of the number  $(N_i)$  of rods in a row and the single rod weight  $(f_{DW})$  was taken according to the relation.

$$(F_{DW})_i = N_i \cdot f_{DW}, i = 1, 9.$$

The trapezoidal row distribution of deadweight loads  $(F_{DW})_i$  for the number  $(N_i)$  of rods in each of the 9 rows is summarized in Table 8.1-1.

TABLE 8.1-1  
F/A ATTACHMENT ASSEMBLY SUPPORT BAR  
DEADWEIGHT DISTRIBUTION BY ROWS

Row	Number of Rods $(N_i)$	Row Load $(F_{DW})_i \sim$ LBS.
1	8.5	9.206
2	8.0	8.664
3	7.5	8.123
4	7.0	7.581
5	6.5	7.040
6	6.0	6.498
7	5.5	5.957
8	5.0	5.415
9	4.5	4.874

### 8.1.1.2 Pressure Drop

The F/A attachment assembly secures the rod bundle to the shield block during steady state sodium flow. Consideration was given to steady state pressure drop across the tube bundle for the CRBRP core flow zones. For the five CRBRP core flow zones, designated as flow zones 1 through 5, the total nominal pressure drops across the tube bundles are 42.66, 40.41, 37.37, 34.98, and 32.12 psi, respectively. Of these, the worst case steady state pressure drop  $(\Delta p)_{SS}$  occurs in flow zone 1. Including the additional pressure drop of 1.09 psi for the rod bundle inlet and outlet, the total worst case steady state pressure drop  $(\Delta p)_{SS}$ ,

$$(\Delta p)_{SS} = 43.75 \text{ PSI}$$

In obtaining the total load  $(F_p)_T$  acting on both support bars caused by the upward steady state sodium flow, it was decided that the full cross-sectional area (A) should be used for the worst case pressure drop  $(\Delta p)_{SS}$ .

$$(F_p)_T = A (\Delta p)_{SS}$$

The area (A) based on the F/A hex duct inside surface flat-to-flat Dimensions of 4.320 in is  $16.16 \text{ in}^2$ . Accordingly, the total upward worst case pressure drop force  $(F_p)_T$  acting on both support bars,

$$(F_p)_T = (16.16 \text{ in}^2) (43.75 \text{ PSI})$$

$$(F_p)_T = 707 \text{ LBS.}$$

Neglecting the effective pressure drop force applied to the inside surface of the F/A hex duct, and assuming the full pressure drop force  $(F_p)_T$  is equally distributed between both support bars, the worst case pressure drop load  $(F_p)$  supported by a single support bar,

$$F_p = \frac{(F_p)_T}{2}$$

$$F_p = 353.5 \text{ LBS.}$$

Alternately, the pressure drop load  $(f_p)$  for a single rod, in terms of the total load  $(F_p)$  and number of rods  $(N_T)$ , is given by the relation.

$$f_p = \frac{F_p}{N_T}$$

$$f_p = \frac{353.5}{(217/2)}$$

$$f_p = 3.258 \text{ LBS.}$$

With regard to the distribution of pressure drop load  $(F_p)$  along the single support bar, a trapezoidal distribution proportional to the number of rods in a row was assumed, in the manner described for the distribution of deadweight, as illustrated in Figure 8.1-2.

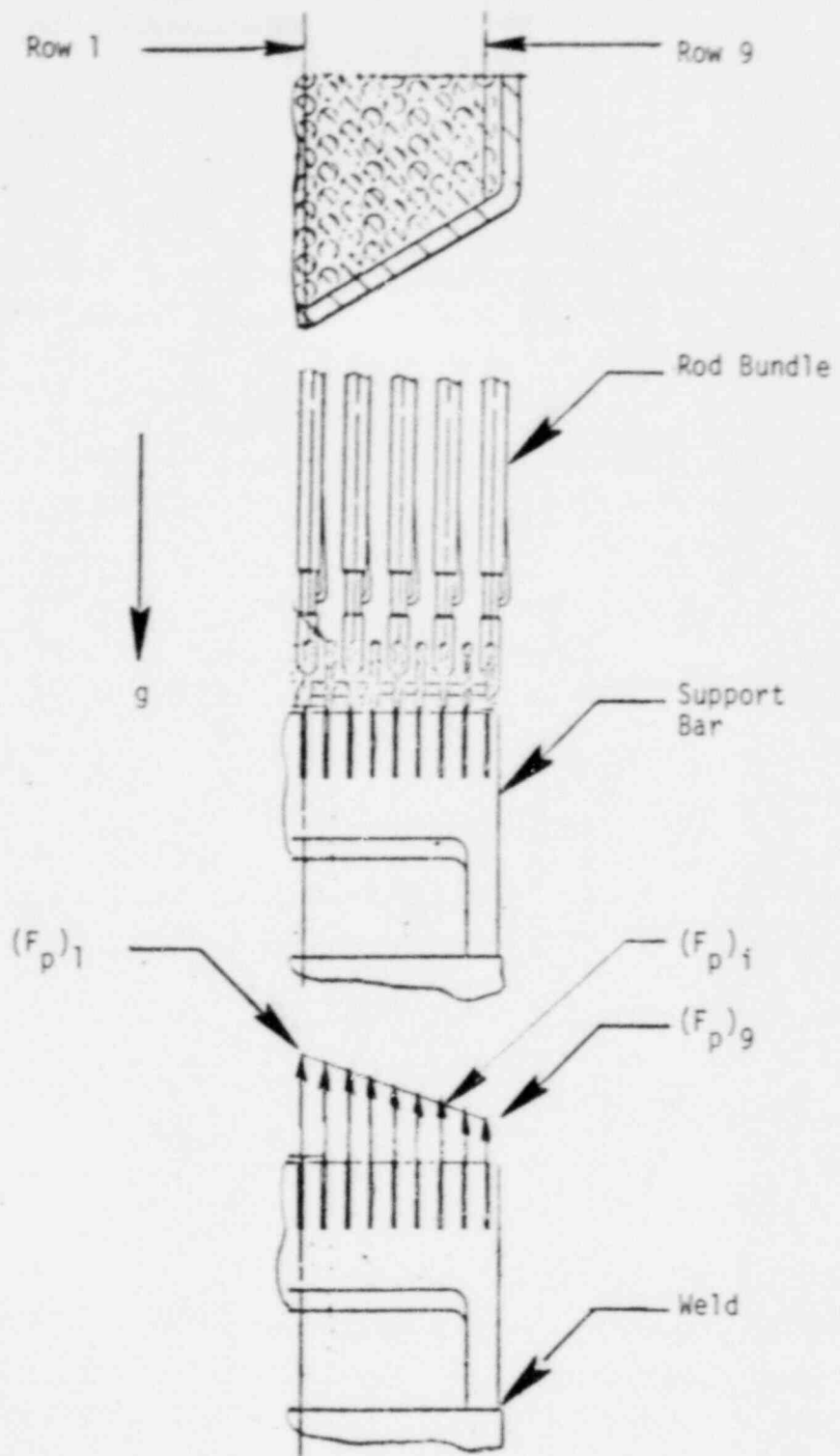


Figure 8.1-2  
 F/A Attachment Assembly  
 Pressure Drop Load Distribution

The pressure drop load  $(F_p)_i$  row distribution in terms of the number  $(N_i)$  of rods in a row and the single rod pressure drop load  $(f_p)$  was taken according to the relation.

$$(F_p)_i = N_i \cdot f_p, i = 1, 9$$

The trapezoidal row distribution of pressure drop loads  $(F_p)_i$  for the number of rods in each of the 9 rows is summarized in Table 8.1-2.

TABLE 8.1-2  
F/A ATTACHMENT ASSEMBLY SUPPORT BAR  
PRESSURE DROP DISTRIBUTION BY ROWS

Row	Number of Rods (NI)	Row Load $(F_p)_i \sim$ LBS
1	8.5	27.693
2	8.0	26.064
3	7.5	24.435
4	7.0	22.806
5	6.5	21.177
6	6.0	19.548
7	5.5	17.919
8	5.0	16.290
9	4.5	14.661

### 8.1.1.3 Seismic

The F/A attachment assembly experiences both horizontal and vertical dynamic loads during the OBE and SSE seismic events. The horizontal and vertical seismic loads applied to a single support are illustrated in Figure 8.1-3.

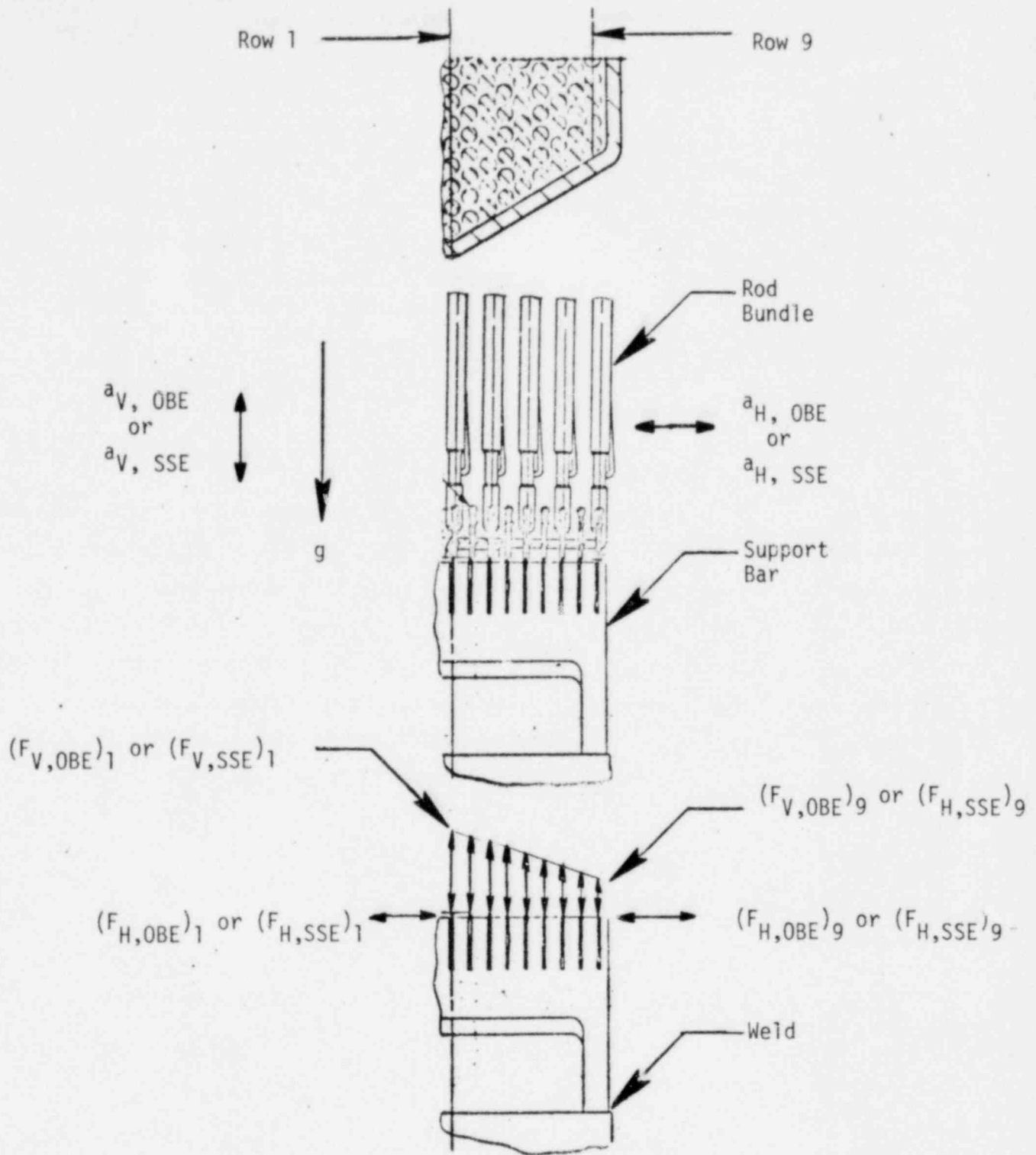


Figure 8.1-3  
 F/A Attachment Assembly  
 Seismic Load Distribution

#### 8.1.1.3.1 Horizontal

The OBE and SSE horizontal accelerations in the N-S and E-W direction at the ACLP, TLP, and CSP elevations were considered. As the rod bundle is disposed along a significant portion of the elevational extent between the TLP and CSP, the horizontal OBE and SSE accelerations ( $a_H$ ) applied to the rod bundle were taken to be the average of the N-S or E-W accelerations at the ACLP, TLP and CSP locations.

$$a_{H, OBE} = 1.62g$$

$$a_{H, SSE} = 2.26g$$

In the definition of the OBE and SSE loads transferred horizontally to the support bars, the weight of the rod bundle was assumed to be simply supported at the top of the rod bundle and at the support bars. Accordingly, the lateral support of the rod assembly by the F/A hex duct at points intermediate to the top of the rod bundle and the support bars was conservatively neglected. Thus, the static 1g horizontal load ( $F_{H,S}$ ) of the rods supported by a single support bar, in the manner of a simply supported beam, was taken as half of the corresponding deadweight load ( $F_{DW}$ ).

$$F_{H,S} = \frac{F_{DW}}{2}$$

Expressing the total OBE dynamic horizontal load ( $F_{H,OBE}$ ) applied to a single bar in terms of the static 1-g load ( $F_{H,S}$ ) and acceleration ( $a_{OBE}$ ),

$$F_{H,OBE} = [F_{H,S}] a_{H,OBE}$$

or

$$F_{H,OBE} = \frac{[F_{DW}]}{2} a_{H,OBE}$$



Similarly, for the SSE dynamic horizontal load ( $F_H, SSE$ ),

$$F_{H, SSE} = [F_{H,S}] a_{H,SSE}$$

$$F_{H, SSE} = \frac{F_{DW}}{2} a_{H,SSE}$$

With regard to the row distribution of the horizontal OBE load ( $F_{H,OBE}$ )<sub>i</sub> and SSE load ( $F_{H,SSE}$ )<sub>i</sub> along the length of the single support bar, a trapezoidal distribution consistent with the number ( $N_i$ ) of rods in a row and the weight ( $f_{DW}$ ) of a single rod was assumed as described in Section 8.1.1.1.

$$(F_{DW})_i = N_i \bullet f_{DW}, i = 1, 9$$

$$\text{Thus, } (F_{H,OBE})_i = \frac{N_i \bullet f_{DW}}{2} a_{H,OBE}$$

$$\text{and, } (F_{H,SSE})_i = \frac{N_i \bullet f_{DW}}{2} a_{H,SSE}$$

The trapezoidal row distribution of horizontal OBE and SSE seismic loads ( $F_{H,OBE}$ ) and ( $F_{H,SSE}$ ) for the number of rods in each of the 9 rows is summarized in Table 8.1-3.

TABLE 8.1-3  
F/A ATTACHMENT ASSEMBLY  
HORIZONTAL OBE AND SSE SEISMIC LOAD  
DISTRIBUTION BY ROWS

Row	Number of Rods ( $N_i$ )	Row Load (LBS)	
		$F_{H, OBE}$	$F_{H, SSE}$
1	8.5	7.456	10.402
2	8.0	7.018	9.790
3	7.5	6.579	9.178
4	7.0	6.141	8.567
5	6.5	5.702	7.955
6	6.0	5.263	7.343
7	5.5	4.825	6.731
8	5.0	4.386	6.119
9	4.5	3.948	5.507

### 8.1.1.3.2 Vertical

The OBE and SSE vertical accelerations at the ACLP, TLP, and CSP elevations were considered. As the rod bundle is disposed along a significant portion of the elevational extent between the TLP and CSP, the vertical OBE and SSE accelerations ( $a_v$ ) applied to the rod bundle were taken to be the average of the accelerations at the ACLP, TLP, and CSP locations.

$$a_{v, OBE} = \pm 0.61g$$

$$a_{v, SSE} = \pm 0.96g$$

In the definition of the OBE and SSE loads transferred vertically to the support bars, the full weight of the rod bundle was assumed to be suspended by the support bars. Accordingly, the static 1 g vertical load ( $F_{v,s}$ ) of the rods supported by a single support bar was taken as the corresponding deadweight ( $F_{DW}$ ).

$$F_{v,s} = F_{DW}$$

A distinction was made as to whether the vertical acceleration was upward or downward.

For upward OBE acceleration ( $a_{v, OBE}$ ), the downward load ( $F_{v, OBE, D}$ ) acting on a single support bar is increased over the static 1g vertical load ( $F_{v,s}$ ).

$$F_{v, OBE, D} = [F_{v,s}] (a_{v, OBE} + 1)$$

$$\text{or, } F_{v, OBE, D} = [F_{DW}] (a_{v, OBE} + 1)$$

Similarly, for upward SSE acceleration,

$$F_{v, SSE, D} = [F_{DW}] (a_{v, SSE} + 1)$$

With downward OBE acceleration ( $a_{V, OBE}$ ) the upward load ( $F_{V, OBE, U}$ ) acting on a single support bar is proportional to the difference between actual and 1g accelerations.

$$F_{V, OBE, U} = [F_{V, S}] [a_{V, OBE}^{-1}]$$

$$\text{or, } F_{V, OBE, U} = [F_{DW}] [a_{V, OBE}^{-1}]$$

Similarly, for downward SSE acceleration,

$$F_{V, SSE, U} = [F_{DW}] [a_{V, SSE}^{-1}]$$

With regard to the row distribution of the vertical OBE loads ( $F_{V, OBE, U}$ )<sub>i</sub> and ( $F_{V, OBE, D}$ )<sub>i</sub>, and vertical SSE loads ( $F_{V, SSE, U}$ )<sub>i</sub> and ( $F_{V, SSE, D}$ )<sub>i</sub> along the length of the single support bar, a trapezoidal distribution consistent with the number ( $N_i$ ) of rods in a row and the weight ( $f_{DW}$ ) of a single rod was assumed as described in Section 8.1.1.1.

$$(F_{DW})_i = N_i \bullet f_{DW}, i = 1, 9$$

$$\text{Thus, } (F_{V, OBE, D})_i = [N_i \bullet f_{DW}] (a_{V, OBE} + 1)$$

$$(F_{V, SSE, D})_i = [N_i \bullet f_{DW}] (a_{V, SSE} + 1)$$

$$\text{and, } (F_{V, OBE, U})_i = [N_i \bullet f_{DW}] [a_{V, OBE}^{-1}]$$

$$(F_{V, SSE, U})_i = [N_i \bullet f_{DW}] [a_{V, SSE}^{-1}]$$

The trapezoidal row distribution of vertical OBE and SSE seismic loads ( $F_{V, OBE}$ ) and ( $F_{V, SSE}$ ) in the upward and downward directions for the number of rods in each of the 9 rows is summarized in Table 8.1-4.

TABLE 8.1-4  
F/A ATTACHMENT ASSEMBLY SUPPORT BAR  
VERTICAL OBE AND SSE SEISMIC LOADS  
DISTRIBUTION BY ROWS

Row	Number of Rods (N <sub>i</sub> )	Row Load (LBS)			
		F <sub>V</sub> , OBE, D	F <sub>V</sub> , OBE, U <sup>*</sup>	F <sub>V</sub> , SSE, D	F <sub>V</sub> , SSE, U <sup>*</sup>
1	8.5	14.821	-3.590	18.043	-0.368
2	8.0	13.949	-3.379	16.981	-0.346
3	7.5	13.077	-3.168	15.920	-0.325
4	7.0	12.205	-2.957	14.859	-0.303
5	6.5	11.334	-2.745	13.797	-0.282
6	6.0	10.462	-2.534	12.736	-0.260
7	5.5	9.590	-2.323	11.675	-0.238
8	5.0	8.718	-2.112	10.613	-0.217
9	4.5	7.846	-1.901	9.552	-0.195

\* A negative upward load is equivalent to positive downward load.

#### 8.1.1.4 Summary

The F/A attachment assembly mechanical deadweight, pressure drop, and horizontal/vertical OBE and SSE seismic loads distributed by rows is summarized in Table 8.1-5.

TABLE 8.1-5  
F/A ATTACHMENT ASSEMBLY SUPPORT BAR  
MECHANICAL LOAD SUMMARY  
DISTRIBUTION BY ROWS

Row	Row Loads (LBS)							
	Deadweight ( $F_{DW}$ ) <sub>i</sub>	Pressure Drop ( $F_p$ ) <sub>i</sub>	Horizontal Seismic		Vertical Seismic			
			( $F_{H,OBE}$ ) <sub>i</sub>	( $F_{H,SSE}$ ) <sub>i</sub>	( $F_{V,OBE,D}$ ) <sub>i</sub>	( $F_{V,OBE,U}$ ) <sub>i</sub> *	( $F_{V,SSE,D}$ ) <sub>i</sub>	( $F_{V,SSE,U}$ ) <sub>i</sub> *
1	9.206	27.693	7.456	10.402	14.821	-3.590	18.043	-0.368
2	8.664	26.064	7.018	9.790	13.949	-3.379	16.981	-0.346
3	8.123	24.435	6.579	9.178	13.077	-3.168	15.920	-0.325
4	7.581	22.806	6.141	8.567	12.205	-2.957	14.859	-0.303
5	7.040	21.177	5.702	7.955	11.334	-2.745	13.797	-0.282
6	6.498	19.548	5.263	7.343	10.462	-2.534	12.736	-0.260
7	5.957	17.919	4.825	6.731	9.590	-2.323	11.675	-0.238
8	5.415	16.290	4.386	6.119	8.718	-2.112	10.613	-0.217
9	4.874	14.661	3.948	5.507	7.846	-1.901	9.552	-0.195

\* A negative upward load is equivalent to a positive downward load.

### 8.1.2 Thermal

The F/A attachment assembly thermal loads are the steady state and transient temperature distributions that occur during the Upset, Emergency, and Faulted events over the first and second reactor cycles. In the definition of the F/A attachment assembly temperature distributions, the sodium temperatures at the reactor vessel inlet were conservatively assumed to be applied directly to the F/A attachment assembly without the mitigating effects of mixing that would normally occur in the inlet plenum. The approach adopted for the F/A attachment assembly transient thermal response is consistent with that taken for the F/A shield block. Accordingly, the selection of the E-4a transient as the umbrella to all Upset, Emergency, and Faulted transients for the F/A attachment assembly invoked the same rationale used for the F/A shield block. Further, the number and characteristics of the worst case F/A attachment assembly duty cycle are the same as that used for the F/A shield block. The F/A shield block E-4a transient and worst case duty cycle taken for the F/A attachment assembly are presented in Figures 4.1-1 and -2, respectively.

A derivation of the detailed F/A attachment assembly temperature distributions during the worst case thermal duty cycle, in the manner described for the F/A shield block, was not made. Instead, the F/A attachment assembly was assumed to instantaneously follow the reactor vessel inlet sodium temperatures while the F/A shield block was considered to lag because of its thermal inertia. Specifically, the base of the support bar legs welded to the shield block lag the response of the attachment assembly. At steady state, the differential thermal expansion across the support bar and the base of the support bar legs is small. During the E-4a transient, however, differential thermal expansion characterized by relative motion of the support bar relative the base of the support legs occurs because of the thermal lag in the shield block.

In order to define the F/A attachment assembly support bar E-4a thermal loads in terms of relative base motion, an ANSYS thermal and structural analysis was performed for a portion of the shield block adjacent to the base of the support bar legs. Descriptions of the dimensional extent and finite element detail of the shield block region selected for analysis, thermal and structural analysis and results, and conclusions on the E-4a thermal loads in terms of relative motions of the support bar leg base are presented in the following subsections.

#### 8.1.2.1 Dimensional Extent and Finite Element Detail

The F/A shield block region selected to derive the relative motions of the support bar leg base during the E-4a transient was a 2 dimensional axisymmetric cylindrical section which approximates the outer periphery of the shield block directly below the base of the support bar legs. The inner periphery of the cylindrical section was taken tangent to the six hole pattern provided for sodium flow, while the outer periphery was selected to be tangent to the hex corners of the shield block. The dimensional extent of the axisymmetric cylindrical section in relation to the geometry of the shield block, in combination with the finite element detail along the elevation extent of the cylindrical section, is illustrated in Figure 8.1-4.

It is important to note that the 2 dimensional axisymmetric cylindrical section only approximates the actual thermal and structural response of the F/A shield block adjacent to the support bar legs during the E-4a transient. The actual response is more 3 dimensional than 2 dimensional axisymmetric. However, the 2 dimensional axisymmetric thermal and structural response was considered representative of the 3 dimensional response for the following reasons.

With regard to thermal response, the 2 dimensional axisymmetric sector approximates the 3 dimensional response because the shield block region inside the inner cylinder periphery, containing the seven hole pattern of sodium flow passages, responds more rapidly to the sodium transients



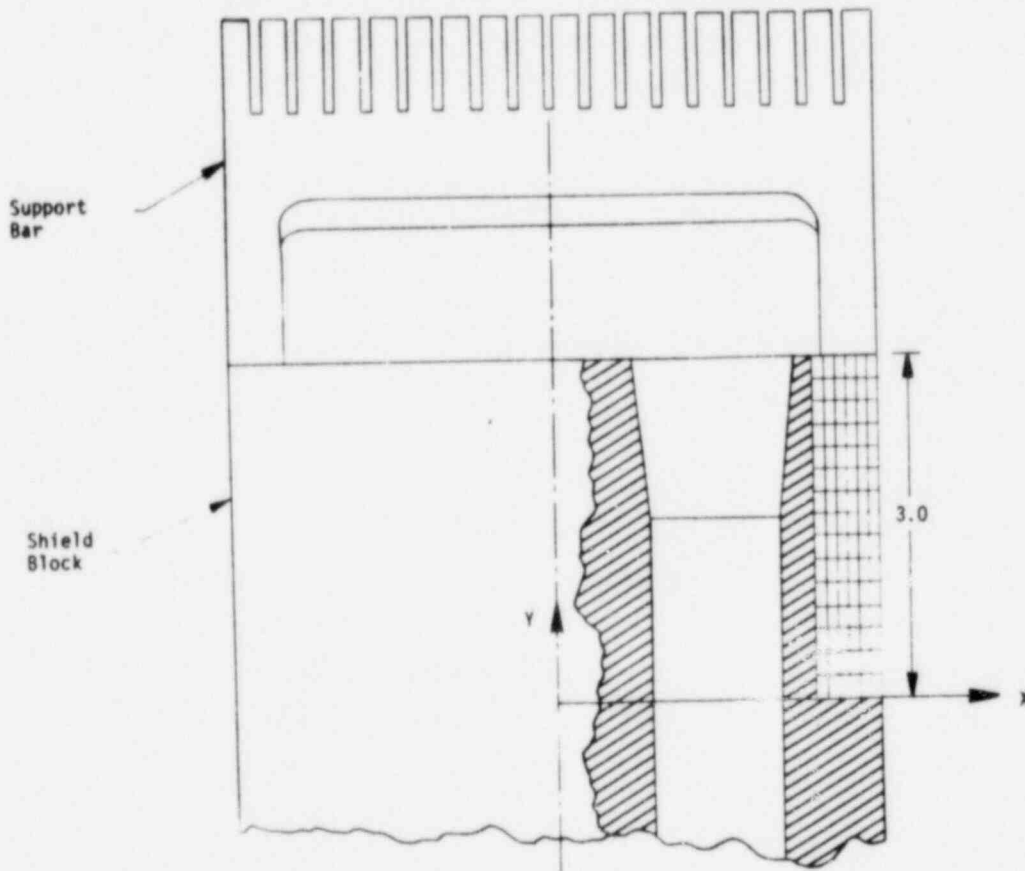
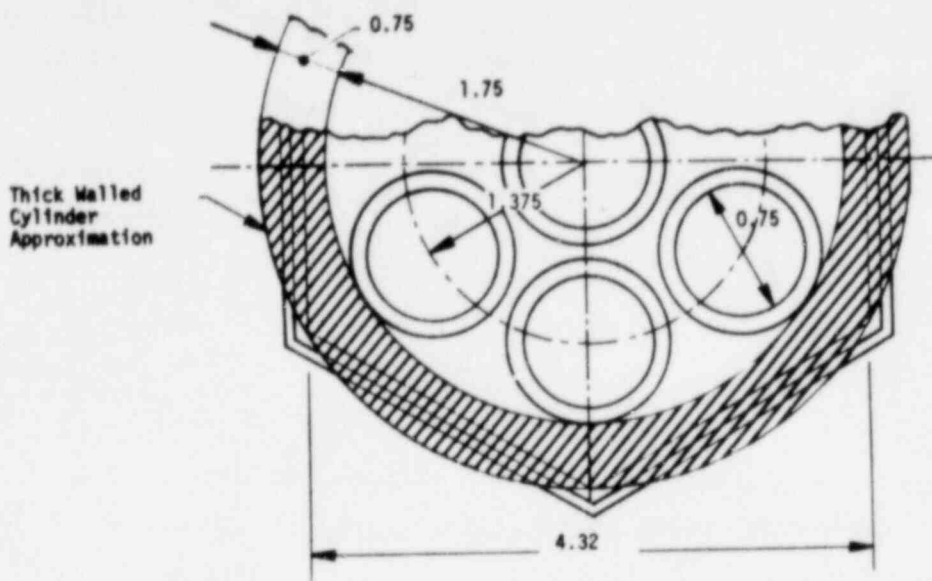


Figure 8.1-4  
 F/A Attachment Assembly Support Bar  
 Thermal Load Model  
 Dimensional Extent and Finite Element Detail

than the region exterior to the inner cylinder periphery. As such, the 3 dimensional thermal response of the shield block region between the interior and exterior peripheries of the cylindrical section can reasonably be approximated by applying the sodium transients directly to the 2 dimensional axisymmetric surface formed by the inner periphery of the cylindrical section.

In terms of structural response, the 2 dimensional axisymmetric sector provides a conservative estimate of 3 dimensional support bar base motion. With the shield block region inside the inner cylinder periphery responding rapidly to the sodium transients, attendant expansions or contractions act to force the shield block region between the interior and exterior peripheries outward and inward, respectively. As the support bar response is considered to respond instantaneously to the sodium transients, the 3 dimensional support bar base motion relative to the support bar would be diminished by the near in-phase expansions and contractions of the inner shield block region. Accordingly, the 2 dimensional axisymmetric sector, which neglects the inner shield block region, would provide an upper bound on motions of the support bar relative to the support bar leg base.

The dimensional extent of the axisymmetric section taken to approximate the outer periphery of the shield block was a cylinder with inside radius and wall thickness of 1.75 and 0.75 in., respectively. With regard to the length of the cylindrical section, a minimum length is desirable for finite element idealization. The minimum length was selected on the basis that edge effects associated with structural constraints at the lower end of the cylinder would not significantly modify the outward or inward motion of the top of the cylinder where the support bar legs are considered to be attached.

From the classical theory of cylindrical shells [14], the local effects of shear and moment are known to diminish rapidly from the point of application. For a cylinder of radius (a), wall thickness (t), and Poisson's ratio ( $\mu$ ), the distance (x) at which local effects are attenuated by approximately 95% is given by the relation

$$X = \frac{3}{\sqrt[4]{\frac{3(1-\nu^2)}{a^2 t^2}}}$$

Numerically,

$$a = 2.13 \text{ in.}$$

$$t = 0.75 \text{ in.}$$

$$\mu = 0.3$$

Thus,

$$X = \frac{3}{\sqrt[4]{\frac{3(1-.3^2)}{(2.13)^2 (0.75)^2}}}$$

$$X = 2.95 \text{ in., Say } X = 3.0 \text{ in.}$$

With regard to a finite element mesh for the 2 dimensional axisymmetric sector, a total of 90 ANSYS axisymmetric elements in a relatively uniform mesh of 136 node points was selected for the thermal and structural response analysis of the F/A support bar base motion.

### 8.1.2.2 Thermal Analysis

The thermal response of the 2 dimensional axisymmetric sector of the F/A shield block during the E-4a transient was derived with the heat transfer option of the ANSYS program. Descriptions of the model boundary conditions, wetted sodium surfaces, properties, and results are as follows.

#### 8.1.2.2.1 Model, Boundary Conditions, and Wetted Surfaces

The 2 dimensional axisymmetric thermal model of the F/A shield block including a simple representation of the support bar and boundary conditions and wetted sodium surfaces is illustrated in Figure 8.1-5.

The F/A shield block was modeled with 90 linear temperature (STIF 35) elements formulated in a condition of axisymmetry. Adiabatic conditions were selected for the bottom lateral surface and the surface forming the exterior periphery. At the top lateral surface and the surface forming the interior periphery, wetted surface conditions were taken with E-4a sodium transient temperatures directly applied to the respective surface nodes. At the top surface, the nodes 16 through 136 were coupled directly to the sodium temperature. Similarly, the interior surface nodes 1 through 16 were coupled to the sodium temperature.

The F/A support bar was modeled with a single conducting bar (STIF 32) element arranged radially from the line of axisymmetry to a point above the top surface of the cylinder representing the F/A shield block. Even though the support bar was assumed to respond instantaneously to the sodium temperature transients, the simple thermal representation permits relative displacements between the shield block and support bar to be conveniently obtained in subsequent derivations of structural response. The support bar node 156 was directly coupled to the sodium temperature and placed directly above the shield block node 96.

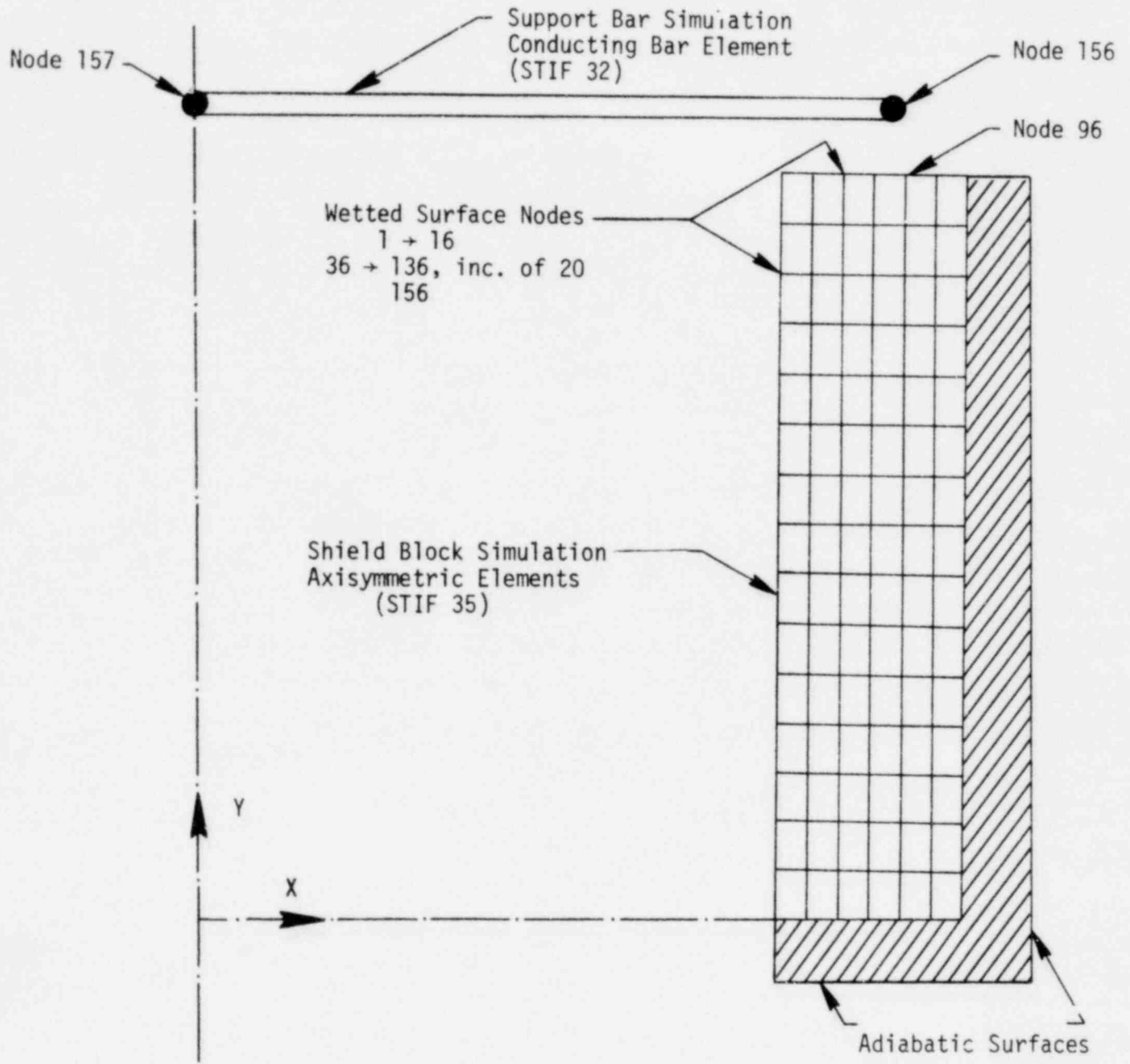


Figure 8.1-5  
F/A Attachment Assembly Support Bar  
Thermal Load Model  
Heat Transfer Boundary Conditions and Wetted Surfaces

#### 8.1.2.2.2 Properties

The F/A shield block is constructed from SA-316-SS. The thermal conductivity (K), specific heat (C), and density ( $\rho$ ) as a function of temperature (T) given in Section 4.1.2.2 were used for the 2 dimensional axisymmetric model of the F/A shield block.

The F/A support bar is also constructed from SA-316-SS. The respective thermal conductivity (K) and specific heat (C) as a function of temperature (T) were taken to be identical to those specified for the F/A shield block. However, the density ( $\rho$ ) was selected to be arbitrarily small in order to obtain a near instantaneous response of the F/A support bar to the E-4a transient.

#### 8.1.2.2.3 Results

The F/A shield block and support bar thermal response to the first 2400 seconds of the E-4a transient was derived with 14 ANSYS load steps. The sodium temperatures were directly coupled to the end of the support bar, and to the top and inside surfaces of the shield block. Heat generation rates were neglected. Prominent features of the E-4a transient are generally the same as those illustrated for the F/A shield block in Figure 4.1-5. A summary of the ANSYS input data is presented in Table 8.1-6.

TABLE 8.1-6  
F/A ATTACHMENT ASSEMBLY SUPPORT BAR  
E-4a TRANSIENT  
ANSYS INPUT DATA

<u>Load Step</u>	<u>Time (Sec)</u>	<u>Temp. (°F)</u>
1	0.0	750
2	20	750
3	80	710
4	200	675
5	260	586
6	400	915
7	760	1000
8	880	975
9	1000	800
10	1140	745
11	1260	745
12	1520	820
13	1750	735
14	2400	600

The ANSYS solution of the E-4a thermal response was obtained in 90 cumulative iterations using steady state and transient convergence criteria of 1 and 5°F, respectively. The temperature distributions in the support bar and shield block at each cumulative iteration were saved on ANSYS Tape 4 for subsequent structural response analysis.

Unlike the study of through the wall temperature differences used in structural evaluations of other F/A regions presented in this report, the temperature distributions in the F/A support bar and shield block are not of themselves significant. Accordingly, plots of temperature differences or distributions were not made. Instead, the temperature distributions at each of the 90 cumulative iterations were recommended for the derivation of relative support bar and shield block structural response motions.

#### 8.1.2.3 Structural Analysis

The structural response of the 2 dimensional axisymmetric model of the F/A shield block during the E-4a transient was derived with the static analysis option of the ANSYS program. Descriptions of the model boundary conditions, properties, and results are as follows.

##### 8.1.2.3.1 Model and Boundary Conditions

The 2 dimensional axisymmetric structural model of the F/A shield block including a simple representation of the support bar and boundary conditions is illustrated in Figure 8.1-6.

The F/A shield block was modeled with 90 constant strain (STIF 2) elements formulated in a condition of axisymmetry. In order to permit rigid body radial motion during uniform thermal expansions or contractions, roller supports were simulated by specifying the UY displacements to be zero along the bottom surface of the cylindrical surface at nodes 1 through 121, increments of 20.

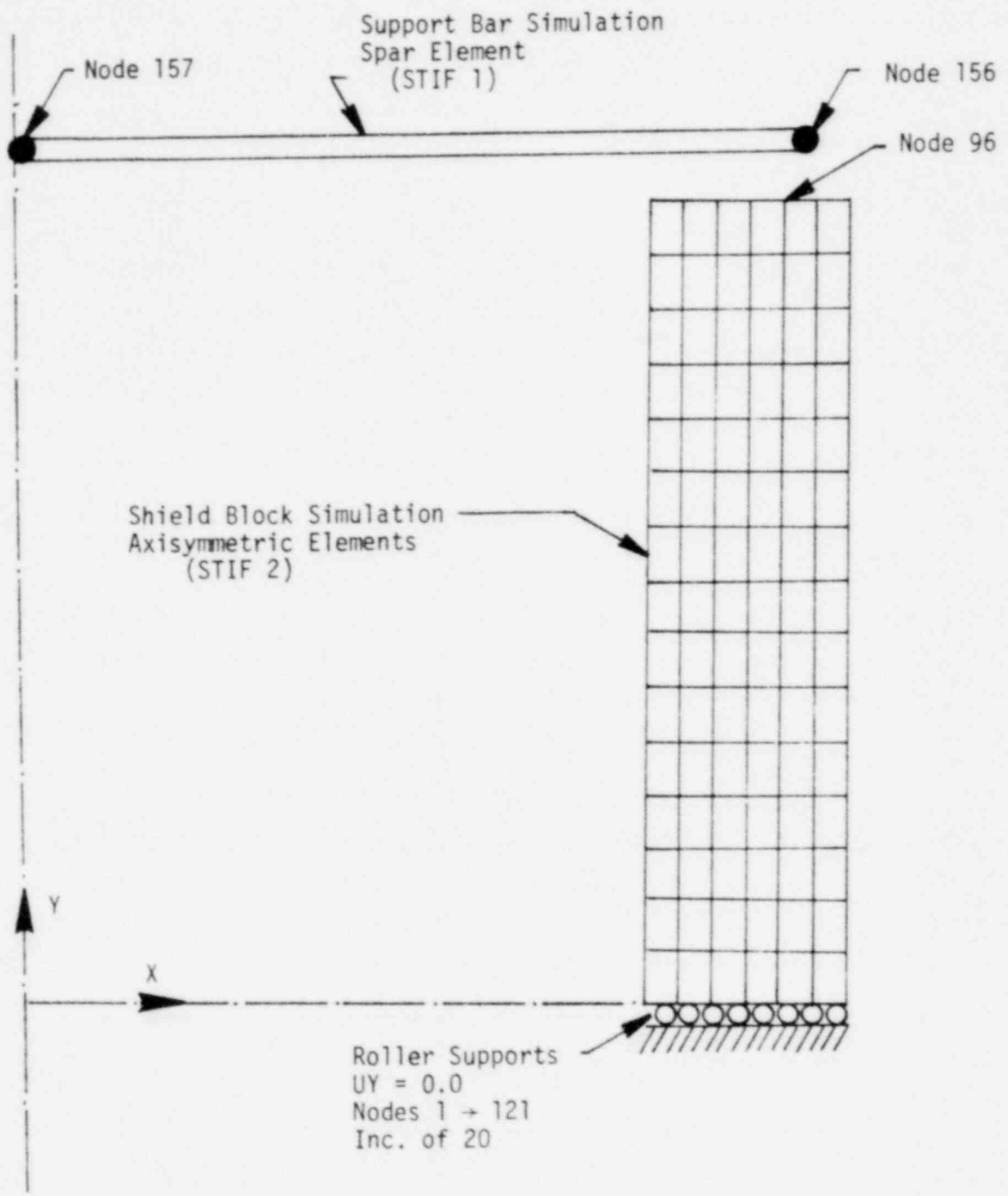


Figure 8.1-6  
F/A Attachment Assembly Support Bar  
Thermal Load Model  
Structural Boundary Conditions



The F/A support bar was modeled with a single spar (STIF 1) element arranged to be radially disposed from the line of axisymmetry to a point above the top surface of the cylinder as formulated in the thermal model. The UX displacement of Node 157 was specified to be zero.

#### 8.1.2.3.2 Properties

The F/A shield block and support bar are both constructed from SA-316-SS. The Young's modulus (E), Poisson's ratio ( $\mu$ ), and coefficient of thermal expansion ( $\alpha$ ) for SA-316-SS as a function of temperature (T) are presented in Section 4.2.2.1.

In the F/A support bar and shield block structural response, constant material properties at 1000°F were selected. Constant material properties with temperature permits the initial stiffness matrix to be used in structural response derivations of successive temperature distributions. The values taken for both support bar and shield block were:

$$E = 22.53 \times 10^6 \text{ psi}$$

$$\alpha = 11.25 \times 10^{-6} / ^\circ\text{F}$$

$$\mu = 0.305$$

#### 8.1.2.3.3 Results

The F/A shield block and support bar structural response to the first 2400 seconds of the E-4a transient was derived with 88 ANSYS load steps using the temperature distributions saved on Tape 4 at each of the cumulative iterations in the thermal solution run. The structural response assumed that the shield block remained linear elastic during the E-4a thermal loading as the effect of local inelastic behavior at the wetted sodium surfaces would not be expected to significantly alter the overall deformation pattern.

With regard to E-4a thermal loads for the F/A support bar, the lateral deformation of the top surface of the shield block relative to the end

of the support bar are of importance. A plot of the UX displacement of the shield block node 96 relative to the UX displacement of the support bar node 156 over the 2400 second duration of the E-4a transient is presented in Figure 8.1-7.

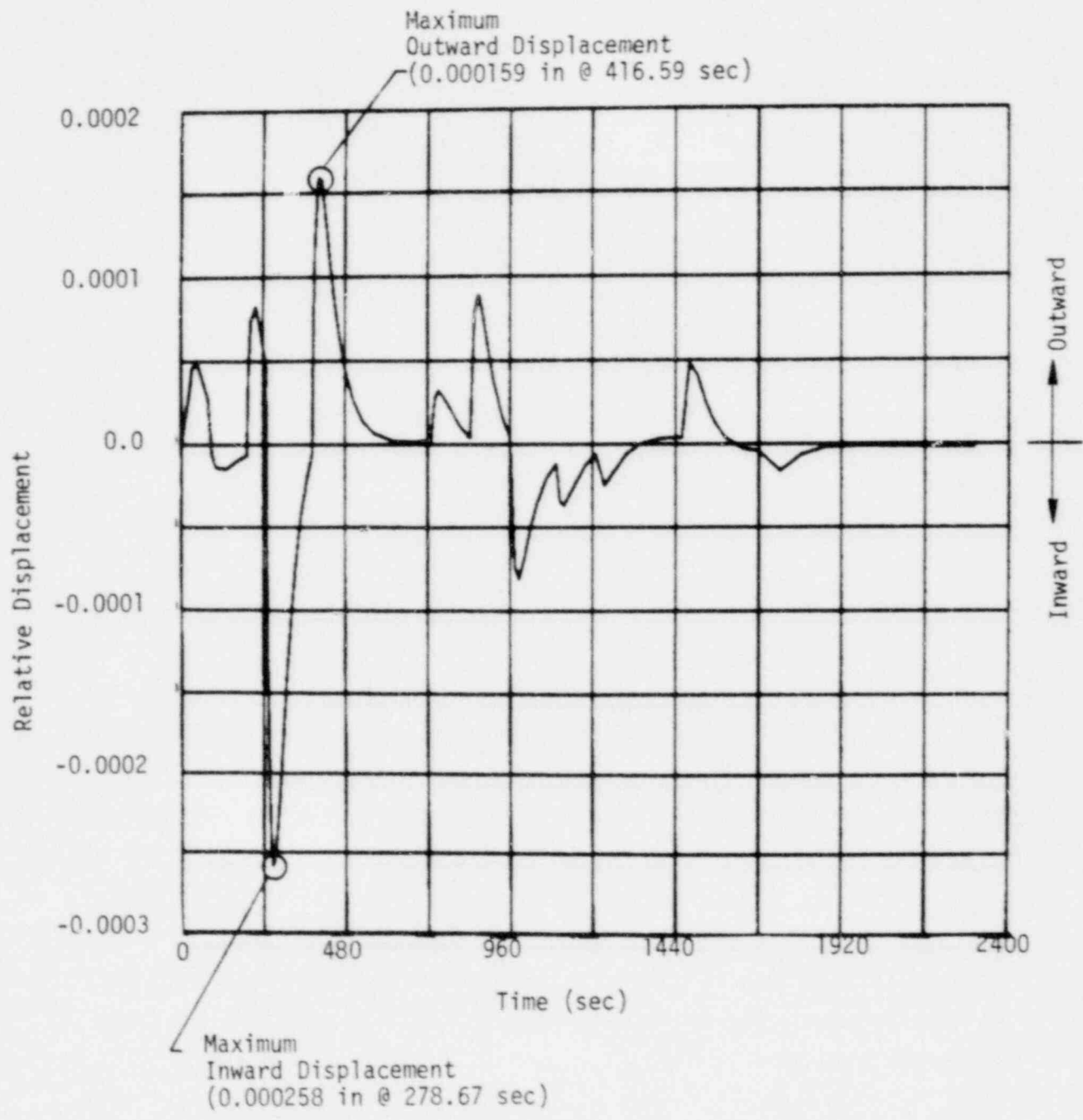


Figure 8.1-7  
F/A Attachment Assembly Support Bar  
E-4a Thermal Loads  
Relative Displacements

A review of the relative deformation plot shows a maximum inward displacement of the base of the support bar legs of 0.000258 in. at 278.67 seconds into the E-4a transient. The maximum outward displacement of the base of the support bar legs is seen to occur at 416.59 seconds with a value of 0.000159 in. At steady state, the relative displacement is zero as would be expected. The F/A support bar and block temperatures at the maximum inward and outward displacements were found to be 586 and 1000°F, respectively.

#### 8.1.2.4 Conclusions

The conclusions based on the analysis of the F/A attachment assembly support bar thermal loading were that the inward and outward lateral deformations of the support bar leg base during the E-4a transient are of most significance in establishing the worst case duty cycle.

During the E-4a transient, the F/A attachment assembly support bar thermal loads consist of lateral inward deformation  $[(\delta_L)_{TR, \text{inward}}]$  and outward deformation  $[(\delta_L)_{TR, \text{outward}}]$  applied to the base of the support bar legs.

$$(\delta_L)_{TR, \text{inward}} = 0.000258 \text{ in.}$$

$$(\delta_L)_{TR, \text{outward}} = 0.000159 \text{ in.}$$

With regard to the F/A attachment assembly support bar thermal loads during steady state conditions, the lateral deformation  $(\delta_L)_{SS}$  of the support bar leg base relative to the support bar was neglected.

$$(\delta_L)_{SS} = 0.0$$

### 8.1.3 Worst Case Duty Cycle

The conclusions based on the F/A attachment assembly support bar loading analysis in relation to recommendations for the worst case duty cycle are as follows.

- Mechanical loads comprising deadweight, pressure drop, and OBE and SSE seismic were considered important in establishing a worst case F/A attachment assembly duty cycle. SSE seismic loads were taken to conservatively bound the OBE loads.
- Thermal loads corresponding to lateral inward and outward deformations of the support bar leg base during the E-4a transient were considered important in establishing the worst case F/A attachment assembly duty cycle.

In order to establish the sequence of duty cycle loading, a worst case combination of SSE seismic loads was selected based on an assessment of the mechanical loads summarized in Table 8.1-5.

The mechanical load assessment was based on load combinations which would maximize ductile rupture and fatigue damage at the base of the support bar leg. The support bar leg base location was selected because it is representative of the weld used to join the support bar legs to the shield block. Creep damage was neglected in the load assessment as steady state temperatures are 750°F. The weld attachment location is identified in Figures 8.1-1 through -3.

With regard to steady state mechanical loads, the upward pressure drop loads are significantly higher than the downward deadweight loads and, as such, tensile strains develop in the weld at the outside surface of the support leg. Considering a SSE load combination consisting of upward vertical and left horizontal components at steady state conditions, the tensile strains would increase above steady state values. Conversely, a SSE load combination of downward vertical and right horizontal would provide the maximum compressive strains in the weld. Accordingly, the maximum fatigue damage under SSE loads would occur in the weld region for the strain range between upward vertical/left horizontal and downward vertical/right horizontal. Further, maximum ductile rupture would occur at peak tensile strain corresponding to upward vertical/left horizontal in combination with steady state upward pressure drop and downward deadweight. Other combinations of SSE seismic loads were considered less damaging.

The recommendations for the F/A attachment assembly support bar loading were directed to formulating a number of worst case duty cycles that would conservatively bound the 39 specified Upset events and the worst Emergency of Faulted event. A first and second duty cycle of time independent and dependent loading was selected. The first duty cycle, including successive applications of SSE seismic loading at steady state temperatures in combination steady state deadweight and pressure drop mechanical loads and thermal E-4a lateral deformation loads, followed by a 10 day hold-time, was considered to be applied only once. The second duty cycle comprising the steady state and E-4a transient mechanical and thermal loads followed by the 10 day hold-time, but excluding the SSE seismic loads, was considered to be repeated 38 times. The first and second cycle loading sequence is described as follows.

#### First Cycle - Time Independent (One Application)

- Apply the initial steady state upward pressure drop and downward deadweight loads at the steady state temperature of 750°F.
- At the steady state temperature of 750°F, first apply the upward vertical and left horizontal SSE seismic loads in combination with the upward pressure load. Next, apply downward vertical and right horizontal SSE seismic loads in the absence of pressure drop loads. Repeat the loading sequence until shakedown is observed.
- With deadweight acting downward, apply and then remove the inward lateral deformation of the support bar leg base during the E-4a transient at a temperature of 750°F.
- Maintaining the deadweight, apply and then remove the outward lateral deformation of the support bar leg base during the E-4a transient at a temperature of 1000°F.
- Apply the final steady state upward pressure drop and downward deadweight loads at 750°F.

#### First Cycle-Time Dependent (One Application)

- Maintain the upward pressure drop and downward deadweight loads over a 10 day hold-time at the steady state temperature of 750°F.

Second Cycle-Time Independent (Repeat 38 Times)

- Maintain the pressure drop and deadweight loads at 750°F.
- With deadweight acting downward, apply and then remove the inward lateral deformation of the support leg base during the E-4a transient at a temperature of 750°F.
- Maintaining the deadweight, apply and then remove the outward lateral deformation of the support bar leg base during the E-4a transients at a temperature of 1000°F.
- Apply the final steady state upward pressure drop and downward deadweight loads at 750°F.

Second Cycle-Time Dependent (Repeat 38 Times)

- Maintain the upward pressure drop and downward deadweight loads over a 10 day hold-time at the steady state temperature of 750°F.

## 8.2 Structural Analysis

The F/A attachment assembly structural analysis was directed to deriving the stresses, strains, and dimensional changes which occur during the first and second worst case duty cycles from which structural evaluations were made. In the following, the F/A attachment assembly support bar structural model, geometry, and boundary conditions are described. Next, linear and non-linear material properties including the effects of irradiation on stress-strain curves and the basis for neglecting thermal creep are presented. Finally, the time independent and dependent inelastic analysis and results for the first and second F/A attachment assembly duty cycles are presented in preparation for subsequent structural evaluation.

### 8.2.1 Model and Geometry

The F/A attachment assembly support bar structural model was formulated in the ANSYS finite element program. A total of 424 constant strain (STIF 2) elements formulated in a condition of plane stress with a unit thickness and arranged in mesh of 489 node points were selected to model the support bar.

The F/A attachment assembly support bar region selected for analysis included the full lateral extent of a single support including the length of the support legs above the surface of the shield block, but excluded the regions adjacent to the saw cuts provided for the attachment rails as preliminary analysis showed the effects of the local stress risers to be small. A full structural model was selected because of the non-symmetry in the support bar deformations during horizontal SSE seismic loadings. However, only one support leg, adjacent to the shield block surface, was modeled in fine detail in order to assure a proper resolution of stress and strain response which was taken to be representative of the attachment weld. Otherwise, the structural model was relatively coarse with the mesh size selected so that nodes would be provided at the locations of the attachment rails where the rod bundle row loads occur. The F/A attachment assembly support bar structural model illustrating the dimensional extent and finite element detail is presented in Figure 8.2-1.



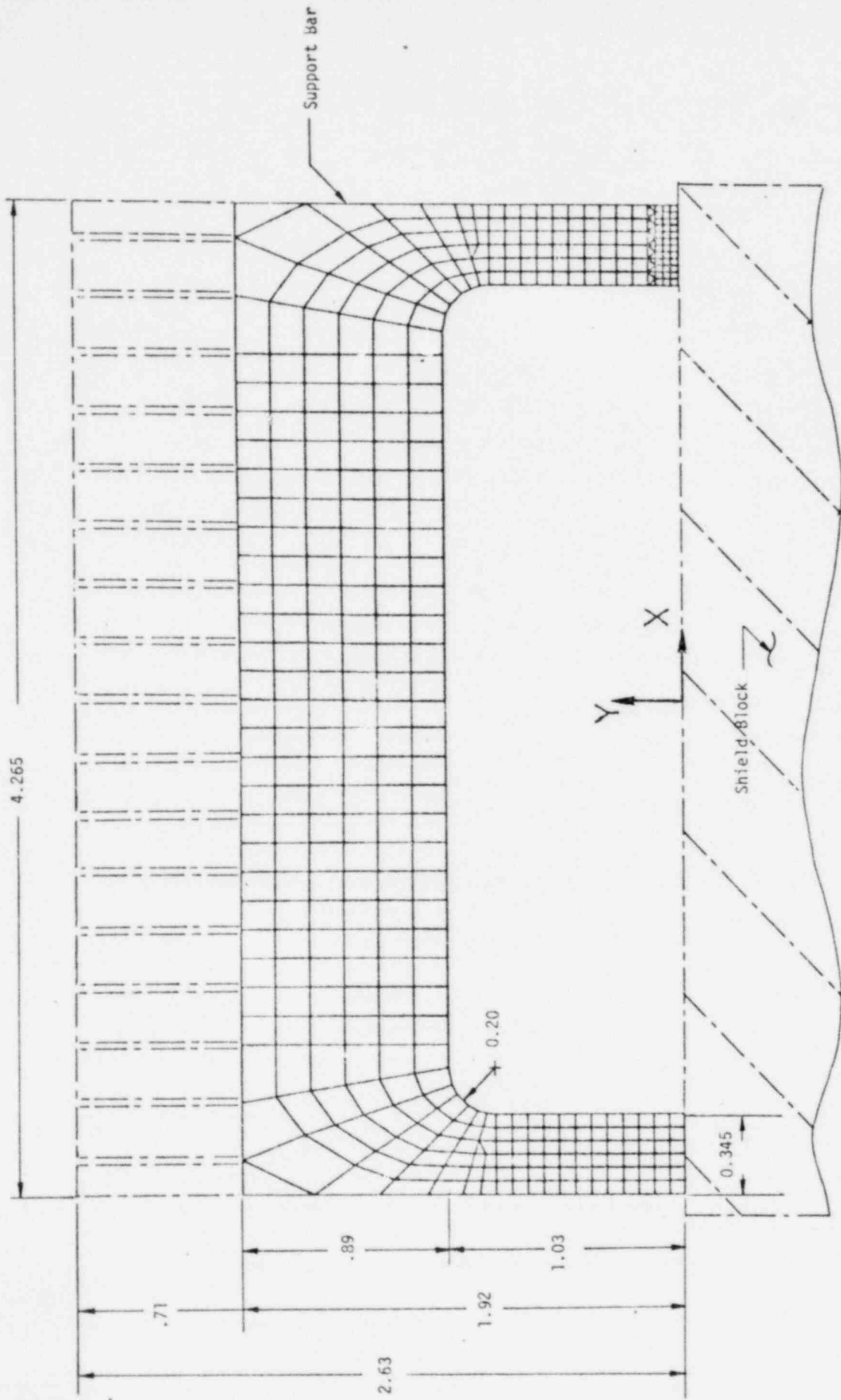


Figure 8.2-1  
 F/A Attachment Assembly Support Bar  
 Dimensional Extent and Finite Element Detail

### 8.2.2 Boundary Conditions and Loading Application

The F/A attachment assembly support bar boundary conditions and loading application are illustrated in Figure 8.2-2.

The F/A design layout drawing, included in this report as Figure 2.0-2, identifies the attachment of each support bar leg base to the shield block to be a weld located at the exterior surface of the shield block. Welds are not provided at the interfaces between the remaining sides of each support bar leg and the shield block. The boundary conditions selected for the support bar analysis consisted of fixed conditions along the side of the support bar leg adjacent to the weld provided. As the support bar is modeled in a condition of plane stress, the assumed boundary conditions are in effect totally fixed, which corresponds to fully welded support base to shield block attachment. Even though a full weld is not currently identified on the F/A design drawing, it was assumed for the purposes of analysis that a full weld would be provided prior to fabrication. The fixed boundary conditions were simulated by specifying zero UX and UY displacements at Nodes 1 through 7, and 447 through 489.

With regard to load application, mechanical row loads from the tube bundle comprising deadweight, pressure drop, and SSE seismic were assumed to be locally applied at the roots of the saw cuts, while the E-4a thermal loads were imposed by specifying lateral displacements at the weld attachments.

The mechanical load application points as related to the tube bundle row 1 through 9 designation scheme considered the center row 1 as Node 223. Row 2 nodes were 209 and 237 to the left and right of center, and so forth, for the remaining seven rows. The thermal E-4a loads were specified as equal and opposite UX displacements of Nodes 1 through 7, and 477 through 489 respectively.

Mechanical Load Points	
Row	Nodes
1	223
2	209,237
3	195,251
4	181,265
5	167,279
6	153,293
7	139,307
8	132,314
9	125,321

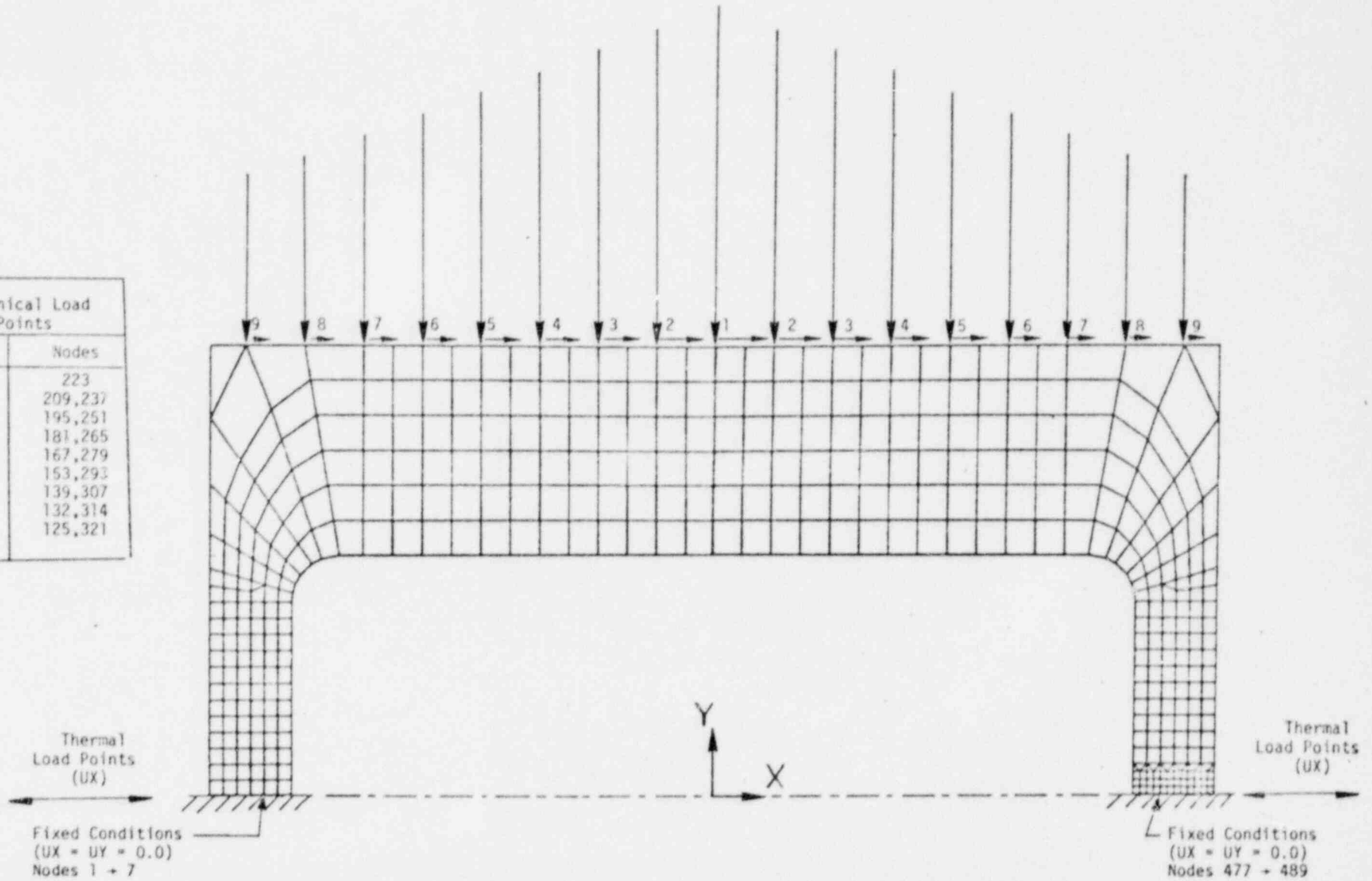


Figure 8.2-2  
F/A ATTACHMENT ASSEMBLY SUPPORT BAR  
Boundary Conditions and Load Applications

### 8.2.3 Properties

The F/A attachment assembly support bar, located at the top of the shield block, constructed from SA-316-SS and initially unirradiated at BOL is irradiated to a EOL fluence ( $E > 0.1$  Mev,  $(\phi t) = 0.31 \times 10^{22}$  N/cm<sup>2</sup>).

Operational temperatures range from 750 to 1000°F. The linear and non-linear properties of SA-316-SS at fluence and temperature selected for the F/A attachment assembly support bar analysis are as follows:

#### 8.2.3.1 Linear

The linear SA-316-SS material properties are the Young's modulus (E), Poisson's ratio ( $\nu$ ), and coefficient of thermal expansions ( $\alpha$ ). The material properties as a function of temperature ( $T \sim$  °F) used in the F/A attachment assembly support bar analysis were identical to those identified for the F/A shield block presented in Section 4.2.2.1.

#### 8.2.3.2 Non-Linear

The non-linear SA-316-SS material properties required for the F/A attachment assembly support bar structural analysis are time independent stress-strain, and the time dependent thermal creep constitutive relations. The constitutive relations with attendant simplifications used for the F/A attachment assembly support bar analysis are as follows.

##### 8.2.3.2.1 Stress-Strain Curves

The SA-316-SS stress-strain data given in the NSM Handbook [6] as a function of temperature and fluence are in terms of true average values. As the June 1977 data identifies the EOL fluence ( $E > 0.1$  Mev,  $(\phi t) = 0.31 \times 10^{22}$  N/cm<sup>2</sup>) for the F/A shield block in the vicinity of the attachment assembly support bar, the stress at a given strain increases from BOL to EOL because of time dependent hardening through irradiation embrittlement.

In the F/A shield block analysis, a mean of true minimum BOL and EOL stress-strain values was taken to represent the stress-strain curve for

the duty cycles uniformly distributed over the first and second reactor cycles. The approach was justified as the F/A shield block was essentially deformation controlled under the E-4a thermal loading. However, in the F/A attachment assembly support bar, mechanical SSE seismic loads in addition to the E-4a thermal loading occur in the first duty cycle while E-4a thermal loadings alone occur in the 38 second duty cycles. Accordingly, the approach adopted for the F/A attachment assembly support bar was to take unirradiated stress-strain data for the first duty cycle at BOL, while the mean of BOL and EOL stress strain data was used for the second duty cycle. In both first and second duty cycles, true minimum stress-strain values over the support bar operational temperature range from 750 to 1000°F were taken because of the essentially static characteristic of the mechanical and thermal loadings.

The SA-316-SS true minimum BOL stress-strain curve and data used for the F/A attachment assembly support bar in the first duty cycle analysis were identical to those used in the F/A orifice plate analysis as presented in Section 9.2.2.2.1. With regard to the mean of the true minimum BOL and EOL stress-strain curve and data used in the second duty cycles, the values were taken to be identical to those used in the F/A shield block analysis described in Section 4.2.2.2.1.

#### 8.2.3.2.2 Thermal Creep Equations

The unirradiated SA-316-SS thermal creep-time constitutive relations as a function of stress and temperature are given in the NSM Handbook [6]. The thermal creep constitutive relations for irradiated SA-316-SS are not identified as the effects of irradiation are included in the irradiation creep equations.

For the F/A attachment assembly support bar, thermal creep occurs at the steady state temperature of 750°F over the 10 day hold-times in the first and second duty cycles.

The F/A attachment assembly support bar EOL fluence ( $E > 0.1$  Mev) is  $0.31 \times 10^{22}$  N/cm<sup>2</sup>. As the EOL fluence is relatively low and steady state temperatures are below 800°F, thermal creep during both first and second F/A attachment assembly support bar duty cycles was neglected.

#### 8.2.4 Worst Case Duty Cycle Response

The structural response of the F/A attachment assembly support bar to the first and second worst case duty cycles was given a preliminary review in order to establish the severity of the mechanical and thermal loadings. The preliminary review showed that the stress, strain, and deformation response of the F/A support bar would remain linear elastic during the more severe first duty cycle. Accordingly, the recommended single first duty cycle followed by 38 of the second duty cycles was rejected in favor of applying 39 of the first duty cycles. The approach must be viewed as conservative as the SSE seismic loads are repeated in each of the 39 first duty cycles.

Even though the preliminary review indicated that the F/A attachment assembly support bar structural response would remain linear elastic, the true minimum BOL stress-strain curves for SA-316-SS at 750 and 1000°F were retained in the ANSYS analysis. In addition, the ANSYS small strain-large deformation option was used in the event that the mechanical SSE seismic loads were sufficient to initiate the collapse of the F/A attachment assembly support bar due to elastic/plastic/creep instability.

In the following, the ANSYS analysis of the first cycle time independent and dependent loading are presented. As the F/A attachment assembly support bar was modeled in a condition of plane stress, a consideration of reference temperatures and axial constraints as presented for other F/A regions modeled in a plane strain condition and presented in this report was not required.

#### 8.2.4.1 Analysis and Results

The ANSYS analysis of the F/A attachment assembly support bar for the time independent and dependent loadings of the first worst case duty cycle, including unloading for residual deformations, was obtained in a single solution run comprising 15 load steps. The time independent loading were applied at zero time, while the time dependent loading was applied over the 10 day hold-time. Thereafter, the F/A attachment assembly support bar was unloaded for residual deformations. A summary of the first cycle time independent and dependent analysis for the F/A attachment assembly support bar is presented in Table 8.2-1.

TABLE 8.2-1  
F/A ATTACHMENT ASSEMBLY SUPPORT BAR  
FIRST DUTY CYCLE  
TIME INDEPENDENT AND DEPENDENT ANALYSIS SUMMARY

Load Step	Iter.	Time (HRS)	Temp. (°F)	Description
1 2	1 3	0.0	750	Initial Steady State ( $F_{DW} + F_p$ )
3 4	1 3	0.0	750	First Seismic Loading ( $F_p + F_{SSE, U} + F_{SSE, Left}$ )
5 6	1 3	0.0	750	Second Seismic Loading ( $F_{SSE, D} + F_{SSE, Right}$ )
7 8	1 3	0.0	750	First E-4a Loading ( $F_{DW} + \delta_L, Inward$ )
9 10	1 3	0.0	1000	Second E-4a Loading ( $F_{DW} + \delta_L, Outward$ )
11 12	1 3	0.0	750	Final Steady State ( $F_{DW} + F_p$ )
13	1	240	750	10 Day Hold-Time ( $F_{DW} + F_p$ )
14 15	1 3	240	750	Unloading for Residuals (No Load)



The F/A attachment assembly support bar structural response to the first cycle of time independent and dependent loadings was saved on ANSYS Tape 10 for recall in subsequent structural evaluations. The time independent response in terms of computer plots of equivalent stress and deformations at initial steady state, first and second SSE seismic loadings, first and second E-4a thermal loadings, and final steady state are presented in Figures 8.2-3 through -8, respectively.

The time independent initial steady state maximum equivalent stress and deformations during deadweight plus pressure drop mechanical loadings were found to be 2829 psi and 0.000269 in. As the structural response remained linear elastic, the time independent final steady state maximum equivalent stress and deformations under deadweight plus pressure drop mechanical loads were identical to the respective initial steady state values. For the first application of SSE seismic loads, consisting of up vertical and left horizontal, the maximum equivalent stress and deformations were 8992 psi and 0.00045 in. With the second application of SSE seismic loads comprised of down vertical and right horizontal, the maximum equivalent stress and deformations were 7612 psi and 0.00041 in. For the E4-a thermal loads of lateral inward and outward support bar base deformations, the maximum equivalent stresses were 4314 and 1290 psi, respectively.

With regard to the structural response over the 10 day hold-time, the time dependent final steady state maximum equivalent stress and deformation are identical to the time independent final steady state response as relaxation of stresses due to thermal creep was neglected. Further, residual deformations following the removal of all loads after the 10 day hold-time were identically zero as the structural response remained linear elastic. As such, computer plots of equivalent stress and deformations for the time dependent response and unloading for residual deformations are not presented.

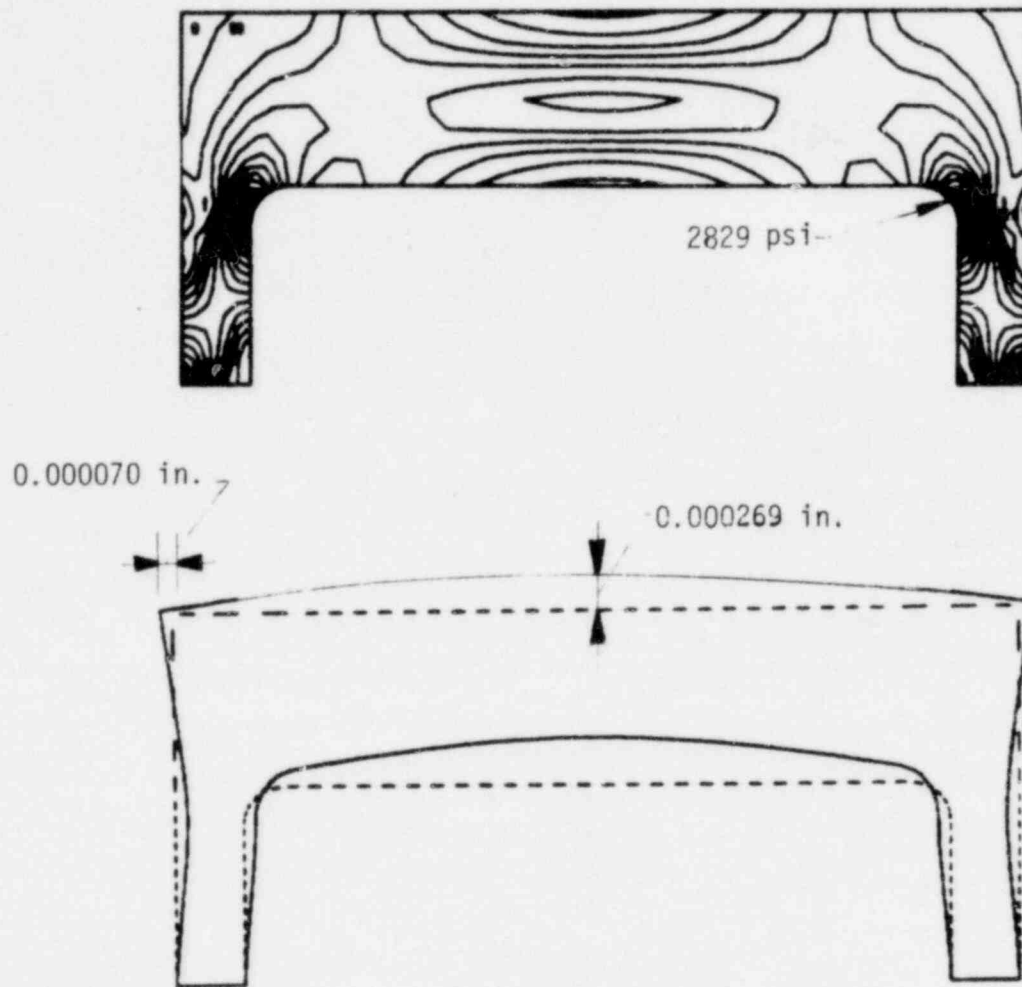


Figure 8.2-3  
F/A Attachment Assembly Support Bar  
First Cycle - Time Independent  
Initial Steady State  
Deadweight + Pressure Drop  
Equivalent Stress and Deformations

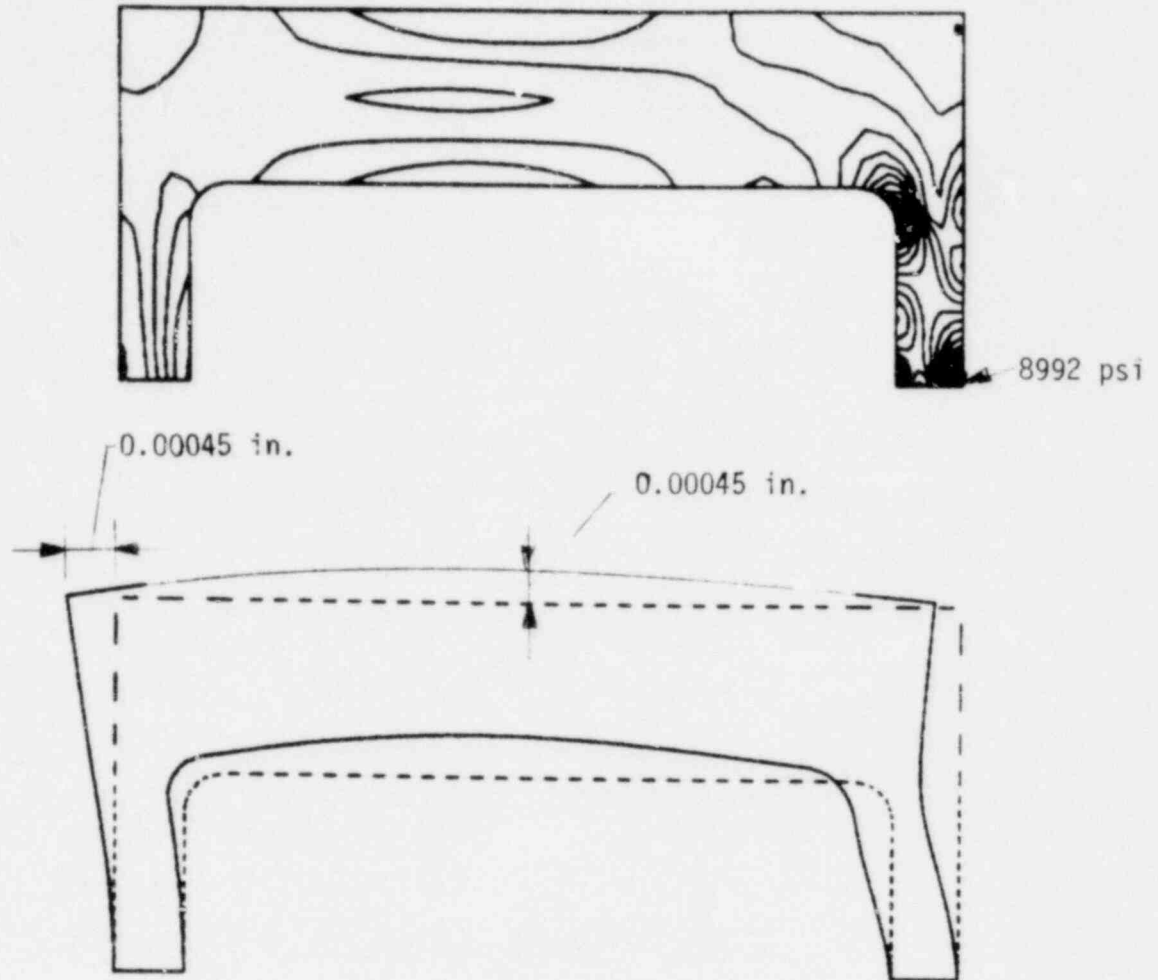


Figure 8.2-4  
F/A Attachment Assembly Support Bar  
First Cycle - Time Independent  
First SSE Seismic Loading  
Pressure Drop & + Vertical + Left Horizontal  
Equivalent Stress and Deformations

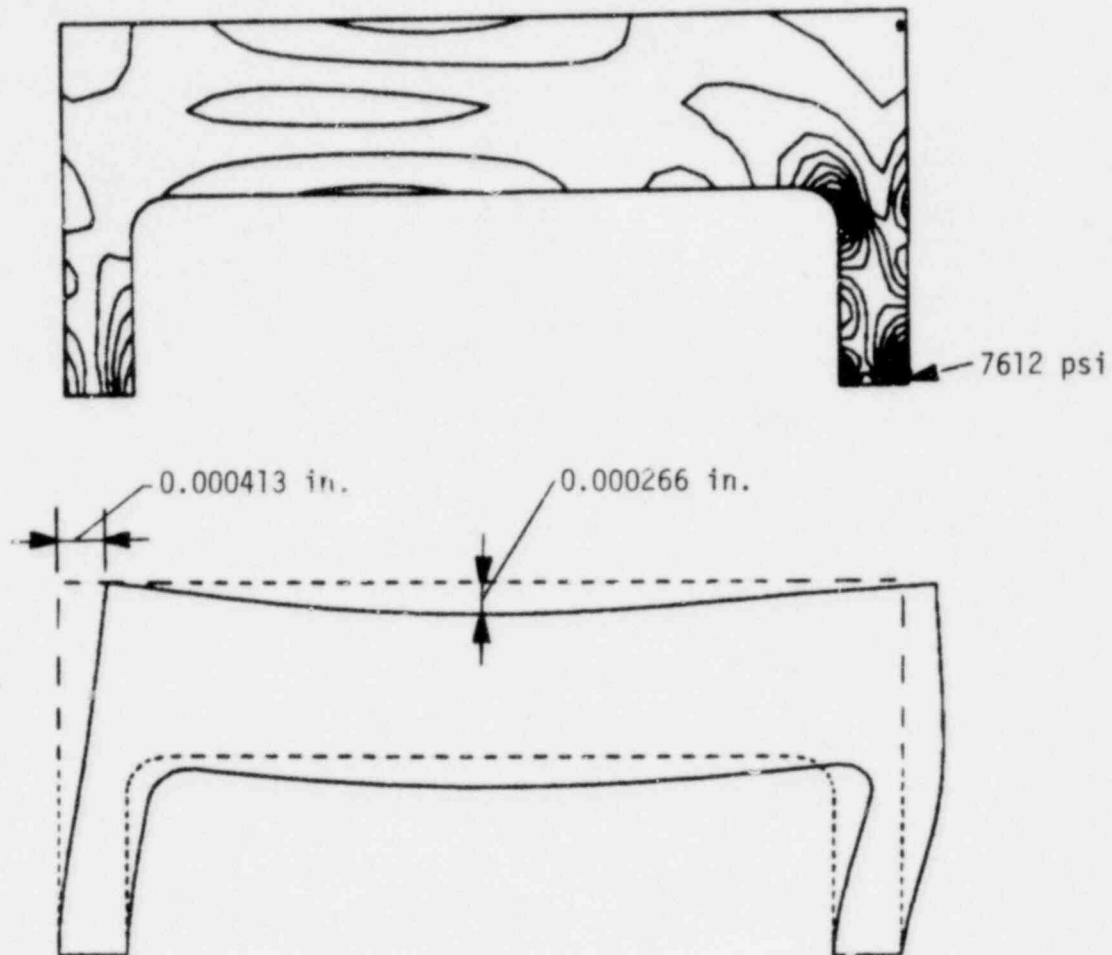


Figure 8.2-5  
F/A Attachment Assembly Support Bar  
First Cycle - Time Independent  
Second SSE Seismic Loading  
Deadweight + Down Vertical + Right Horizontal  
Equivalent Stress and Deformations

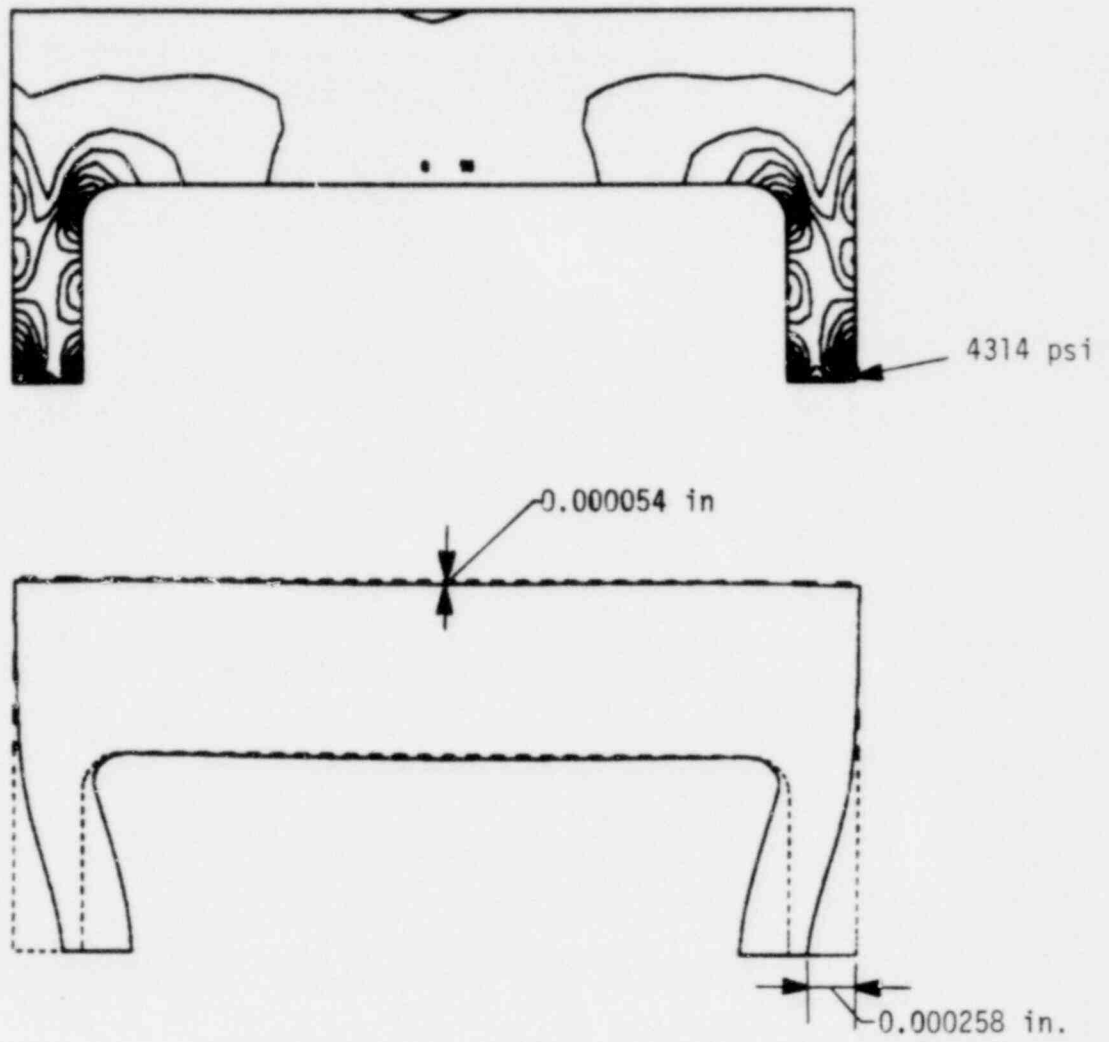


Figure 8.2-6  
F/A Attachment Assembly Support Bar  
First Cycle - Time Independent  
First E-4a Thermal Loading  
Deadweight + Inward Base Motion  
Equivalent Stress and Deformations

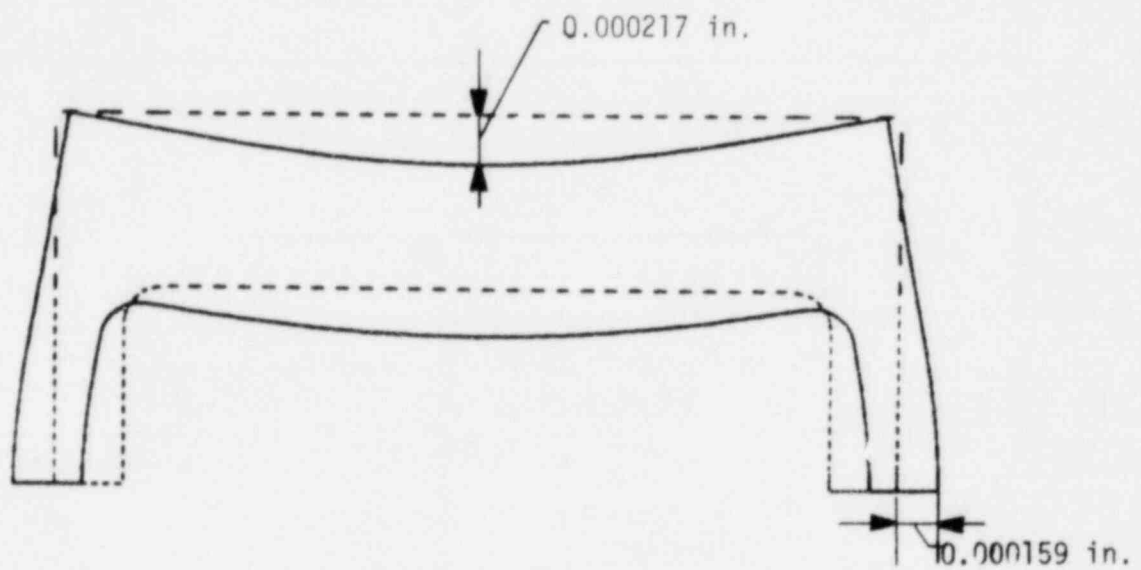
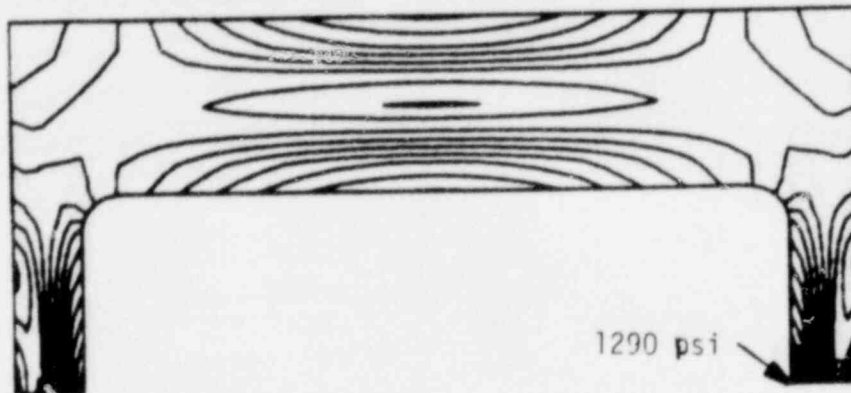


Figure 8.2-7  
F/A Attachment Assembly Support Bar  
First Cycle - Time Independent  
Second E-4a Thermal Loading  
Deadweight + Outward Base Motion  
Equivalent Stress and Deformations

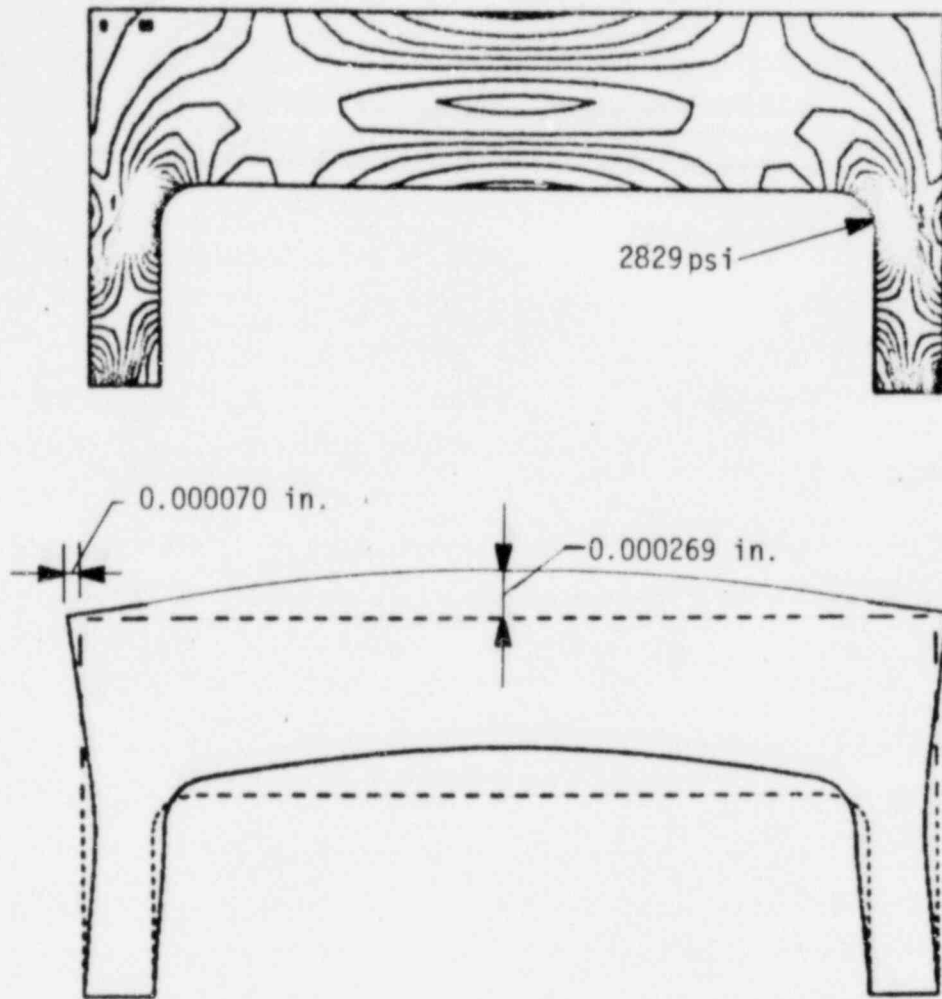


Figure 8.2-8  
F/A Attachment Assembly Support Bar  
First Cycle - Time Independent  
Final Steady State  
Deadweight + Pressure Drop  
Equivalent Stress and Deformations

### 8.3 Structural Evaluation

The F/A attachment assembly support bar structural evaluation was arranged to provide a comparison of structural response for the 39 worst case duty cycles in relation to criteria which protect against crack initiation and excessive deformation failure modes and thereby assure F/A attachment assembly support bar function over the first and second reactor cycles.

The procedure for performing the F/A attachment assembly support bar evaluation of crack initiation failure modes considered only the response to the first duty cycle in estimating the response of the 39 worst case duty cycles. The approach is conservative for creep-fatigue damage evaluations as the strain range is controlled by SSE seismic loads which occur only in the first duty cycle. Otherwise, the ductile rupture and deformation evaluations are representative as the response remained linear elastic. A description of the F/A attachment assembly support bar structural evaluation is as follows.

#### 8.3.1 Crack Initiation

The F/A attachment assembly support bar structural evaluation of crack initiation in relation to local ductile rupture and combined creep-fatigue damage criteria over the 39 worst case duty cycles is presented in the following subsections.

##### 8.3.1.1 Local Ductile Rupture

The local ductile rupture criterion for protecting against crack initiation requires that the ductile rupture factor ( $F_{DR}$ ) be less than unity at each point in the F/A attachment assembly support bar.

$$F_{DR} = \text{Maximum of} \left\{ \begin{array}{l} \bullet \frac{(\epsilon_{\text{max principal}})^{TF}}{0.3 \epsilon_{ef, \text{min}}} \\ \bullet \frac{(\epsilon_{\text{max principal}})^{TF}}{\epsilon_{u, \text{min}}} \end{array} \right\}$$



In the following, the allowable uniaxial strains used in the F/A attachment assembly support bar structural evaluation and comparison of results with the local ductile rupture factor criterion are presented.

#### 8.3.1.1.1 Allowable Uniaxial Strains

The F/A attachment assembly support bar as constructed from SA-316-SS is unirradiated at BOL. The EOL fluence ( $E > 0.1$  Mev) is  $0.31 \times 10^{22}$  n/cm<sup>2</sup>. In addition, the F/A attachment assembly support bar temperatures range from 750 to 1000°F. The true uniaxial uniform elongation ( $\epsilon_u, \min$ ) and fracture ( $\epsilon_f, \min$ ) for unirradiated and irradiated SA-316-SS used in the F/A attachment assembly support bar structural evaluation were taken from the recommendations in the trial applications of the RDT Draft for Breeder Reactor Core Components [15-23] and are identical to those taken for the F/A shield block structural evaluation presented in Section 4.3.1.1.1.

With regard to the allowable uniaxial strains of the weld material at the base of the support bar legs, true minimum uniform elongation and fracture strain data in irradiated weld materials is currently not available. Accordingly, the Code Case 1592 [4] position on reductions in parent material ductility for weld regions was adopted. Both true minimum uniform elongation and fracture strains of irradiated SA-316-SS were reduced by 50% to obtain the allowable weld strains ( $\epsilon_w$ ) used in the structural evaluation of the F/A attachment assembly support bar welds.

$$(\epsilon_w)_f, \min = 0.5 \epsilon_f, \min$$

$$(\epsilon_w)_u, \min = 0.5 \epsilon_u, \min$$

#### 8.3.1.1.2 Comparison with Criterion

The F/A attachment assembly support bar structural evaluation in relation to the worst case location for local ductile rupture was made by screening each of the finite elements over the 39 worst case duty cycles with the

damage processor. The maximum local ductile rupture factor  $(F_{DR})_{max}$  for the F/A orifice plate was found to occur at element 375, located in the support bar leg base weld and identified in Figure 8.2-2.

The peak BOL strain components occurred at the first SSE seismic loading in combination with upward pressure drop and deadweight loads where the local metal temperature was 750°F. The accumulated BOL strain components were identically zero as the structural response between the initial time independent and final time dependent steady state of the first duty cycle remained linear elastic. The EOL maximum principal strain was 0.000373 in/in at a triaxiality factor of 1.233. The true minimum irradiated uniform elongation and fracture strains in the support leg base weld region, taken as 50% of the respective SA-316-SS parent material, were 0.038 and 0.491 in/in, respectively.

In this arrangement, the maximum local ductile rupture  $(F_{DR})$  for the F/A attachment assembly support bar was controlled by the uniform elongation strain of the weld material with a value:

$$(F_{DR})_{max} = 0.012$$

As  $(F_{DR})_{max} < 1.0$ , the F/A attachment assembly support bar is not expected to experience crack initiation over the 39 worst case duty cycles based on the local ductile rupture criterion.

#### 8.3.1.2 Creep-Fatigue Damage

The creep-fatigue damage criterion in protecting against crack initiation requires that the combined creep-fatigue damage factor  $(F_{CFD})$  be less than unity at each point in the F/A attachment assembly support bar.

$$F_{CFD} = a/b = \text{Min. of } \left\{ \begin{array}{l} \bullet \frac{7}{3} D^c + D^f \\ \bullet D^c + \frac{7}{3} D^f \end{array} \right\}$$

In the following, the allowable limits for fatigue life and creep-rupture times used in the F/A attachment assembly support bar structural evaluation and a comparison of the results with the combined creep-fatigue damage factor criterion are presented.

#### 8.3.1.2.1 Allowable Limits

The F/A attachment assembly support bar as constructed from SA-316-SS is unirradiated at BOL. The EOL fluence ( $E > 0.1$  Mev) is  $0.31 \times 10^{22}$  N/cm<sup>2</sup>. In addition, the F/A attachment assembly support bar temperatures range from 750 to 1000°F. The fatigue life and creep rupture time relations used in the F/A attachment assembly support bar structural evaluation were identical to those used in the F/A shield block structural evaluation presented in Section 4.3.1.1.1. The fatigue life and creep rupture time relations representative of F/A attachment assembly support bar peak and steady state metal temperatures at EOL fluence are illustrated in Figure 4.3-1 and -2 respectively.

With regard to the allowable fatigue life and creep rupture times of the weld material at the base of the support bar legs, irradiated creep-fatigue data of weld regions is not currently available. Accordingly, the Code Case 1592 [4] position that the fatigue life and creep rupture times of weld regions be taken as the respective values of the parent material was adopted for the F/A attachment assembly support bar welds.

#### 8.3.1.2.2 Comparison with Criterion

The F/A attachment assembly support bar structural evaluation in relation to the worst case location for combined creep-fatigue damage was made by screening each of the finite elements over the 39 worst case duty cycles with the damage processor. The maximum combined creep-fatigue damage factor ( $F_{CFD}$ )<sub>max</sub> for the F/A attachment assembly support bar was found to occur at element 375, located in the support bar base weld and identified in Figure 8.2-2.

The fatigue damage factor ( $D^f$ ) was found to be  $0.108 \times 10^{-5}$  for 39 worst case duty cycles. The principal strain range was found to be critical and occurred between the first and second SSE seismic loadings with a value of 0.000696 in/in. The peak metal temperature over the fatigue cycle was 750°F. The fatigue life for the equivalent strain range was  $36.1 \times 10^6$  cycles based on the EOL fluence ( $E > 0.1$  Mev,  $(\phi t) = 0.31 \times 10^{22}$  n/cm<sup>2</sup>).

The creep damage factor ( $D^c$ ) was found to be  $0.47 \times 10^{-12}$  for the 39 worst case duty cycles. The principal stress was found to be critical with a value of 2,956 psi corresponding to the steady state temperature conditions at the beginning of the 10 day hold time. For the EOL fluence ( $E > 0.1$  Mev,  $(\phi t) = 0.31 \times 10^{22}$  n/cm<sup>2</sup>) at a metal temperature of 750°F, the minimum rupture time was  $20.98 \times 10^{15}$ .

In this arrangement, the maximum combined creep-fatigue damage factor ( $F_{CFD}$ )<sub>max</sub> for the F/A attachment assembly support bar was found to be dominated by fatigue damage while creep damage was negligible.

$$(F_{CFD})_{\max} = 0.108 \times 10^{-5}$$

As  $(F_{CFD})_{\max} < 1.0$ , the F/A attachment assembly support bar is not expected to experience crack initiation over the 39 worst case duty cycles based on the creep-fatigue damage criterion.

### 8.3.2 Excessive Deformation

The F/A attachment assembly support bar structural evaluation of peak plus accumulated, and residual deformations in relation to functional limits over the 39 worst case duty cycles is presented in the following subsections.

#### 8.3.2.1 Peak Plus Accumulated Deformation

The peak plus accumulated deformation criterion in protecting against excessive peak deformations requires that peak plus accumulated deformations ( $\delta^{P+A}$ ) be less than the peak plus accumulated deformation limit (PADL).

$$\delta^{P+A} \leq \text{PADL}$$

The F/A attachment assembly support bar peak deformation ( $\delta^P$ ) during the first duty cycle occurred at the first SSE seismic loading with a value of 0.00045 in. The accumulated deformation ( $\Delta \delta^{SS}$ ) between the initial time independent and final time dependent steady state conditions was identically zero as the structural response remained linear elastic throughout the first duty cycle. For the 39 worst case duty cycles, the EOL peak plus accumulated ( $\delta^{P+A}$ ) deformation is given by the relation.

$$(\delta^{P+A})_{EOL} = (\delta^P)_{BOL} + (N-1) (\Delta \delta^{SS})_{BOL}$$

$$(\delta^{P+A})_{EOL} = 0.00045 + 38(0.0)$$

$$(\delta^{P+A})_{EOL} = 0.00045 \text{ in.}$$

For the F/A attachment assembly support bar, the specified peak plus accumulated deformation limit (PADL) is 0.005 in. As  $\delta^{P+A} < \text{PADL}$ , the F/A attachment assembly support bar is not expected to experience failure by excessive deformation during the 39 worst case duty cycles.

#### 8.3.2.2 Residual Deformations

The residual deformation limit in protecting against excessive residual deformations requires that the residual deformation ( $\delta^R$ ) be less than the residual deformation limit (RDL).

$$\delta^R \leq \text{RDL}$$

The F/A attachment assembly support bar residual deformation ( $\delta^R$ ) after the first duty cycle at BOL was identically zero as the structural response remained linear elastic. Accordingly, the EOL residual deformation ( $\delta^R$ ) EOL after 39 worst case duty cycles,

$$(\delta^R)_{EOL} = N(\delta^R)_{BOL}$$

$$(\delta^R)_{EOL} = 39 (0.0)$$

$$(\delta^R)_{EOL} = 0.0$$

For the F/A attachment assembly support bar, the specified residual deformation limit (RDL) is 0.005 in. As  $\delta^R < \text{RDL}$ , the F/A attachment assembly support bar is not expected to experience excessive residual deformation during the 39 worst case duty cycles.

### 8.3.3 Summary

The F/A attachment assembly support bar was found to satisfy the crack initiation and excessive deformation criteria for a total of 39 worst case duty cycles. A summary of the F/A attachment assembly support bar structural evaluation is presented in Table 8.3-1.

TABLE 8.3-1

F/A ATTACHMENT ASSEMBLY SUPPORT BAR  
STRUCTURAL EVALUATION SUMMARY

Criteria		Allowable Value	Calculated Value	Margin of Safety*
Crack Initiation	Ductile Rupture Factor	1	0.012	82.33
	Combined Creep-Fatigue Damage Factor	1	$0.108 \times 10^{-5}$	925,925
Excessive Deformation	Peak + Accumulated	0.005 in.	0.00045	10.11
	Residual	0.005 in	0.0	$\infty$

$$* \text{ Margin of Safety} = \frac{\text{Allowable Value}}{\text{Calculated Value}} - 1$$

## 9.0 ORIFICE PLATE ANALYSIS AND EVALUATION

In the F/A orifice plate analysis and evaluation, a loading analysis was made that considered mechanical pressure drop, and thermal steady state and transient loads in establishing the number and characteristics of a worst case duty cycle that umbrellas all expected duty cycles for the orifice plate region in the first and second reactor cycles. Next, an inelastic structural analysis of the orifice plate region was made for a single worst case BOL duty cycle to calculate the strains and dimensional changes from which EOL values were approximated. Finally, a structural evaluation of EOL strains and dimensional changes was made in relation to criteria which protect against crack initiation and excessive deformation. A summary of the loading, structural analysis, and structural evaluation is presented as follows.

### 9.1 Loading Analysis

The F/A orifice plate loading analysis was directed to establishing the number and characteristics of a worst case duty cycle that umbrellas both the number and characteristics of Upset, Emergency, and Faulted Events specified over the first and second reactor cycles. The number and characteristics of these events are specified in the Equipment Specification [1].

It is important to note that the worst case F/A orifice plate duty cycle is, in itself, hypothetical, but permits a conservative structural evaluation to be performed on a single duty cycle instead on each of the individual events specified. In the following, the F/A orifice plate mechanical and thermal loads are assessed individually and in relation to each other prior to establishing the worst case duty cycle which was used in structural evaluation.

#### 9.1.1 Mechanical

The F/A orifice plate mechanical load of any significance in relation to subsequent structural evaluations is the pressure drop under sodium flow, as deadweight and OBE/SSE seismic and core restraint loads are relatively insignificant.



In order to establish the worst case F/A orifice plate pressure drop loading, the CRBRP core was reviewed in relation to flow zones, the number of orifice plates in each F/A of a particular flow zone, and the total pressure drop across the full number of orifice plates in a F/A of a flow zone.

For the CRBRP core design, a total of five flow zones, designated as flow zones 1 through 5, are provided. The F/A in flow zones 1 and 2 contain 2 orifice plates. In flow zone 3, each F/A is provided with 3 orifice plates. Each F/A in flow zones 4 and 5 include 4 orifice plates.

With regard to the F/A orifice plate pressure drop under steady state flow conditions, consideration was given to the total pressure drop across the full number of orifice plates in a F/A according to the flow zone. For the flow zones 1 through 5, the total pressure drops were 26.75, 29.84, 33.94, 37.58, and 41.63 psi, respectively.

The average steady state pressure drop  $(\Delta p)_{av}$  was calculated from the total pressure drop  $(\Delta p)_{TOT}$  and the number (N) of orifice plate using the relation.

$$(\Delta p)_{av} = \frac{(\Delta p)_{TOT}}{N}$$

A summary of the average steady state pressure drop for the number of F/A orifice plates in the CRBR core flow zones is presented in Table 9.1-1.

TABLE 9.1-1  
F/A ORIFICE PLATE  
AVERAGE STEADY STATE PRESSURE DROPS

Flow Zone	Total Pressure Drop (PSI)	Number of Orifice Plates	Average Pressure Drop (PSI)
1	26.75	2	13.38
2	29.84	2	14.90
3	33.94	3	11.31
4	37.58	4	9.39
5	41.63	4	10.41

A review of the average F/A orifice plate pressure drops shows that the worst case steady state loading occurs in flow zone 2 containing 2 orifice plates where the average pressure drop is 14.90 psi. However, the actual pressure distribution over a series arrangement of orifice plate is not uniform, but is greater for the leading orifice plate. An estimate of the actual pressure drop in the leading orifice plates is 50% greater than the average pressure drop. Accordingly, the worst case F/A orifice plate steady state pressure drop  $(\Delta p)_{SS}$  was taken according to the relation.

$$(\Delta p)_{SS} = 1.5 (\Delta p)_{av}$$

$$(\Delta p)_{SS} = 1.5 (14.9 \text{ psi})$$

$$(\Delta p)_{SS} = 22.35 \text{ psi.}$$

With regard to the variation in pressure drop across the F/A orifice plates during the Upset, Emergency, and Faulted Transients, sodium flows at steady state conditions decrease to 7.5% of nominal conditions immediately after the transients are initiated and return to 100% of nominal conditions upon the return to steady state conditions. Accordingly, the maximum F/A orifice plate pressure drop occurs during steady state flow conditions while the pressure drop during the transients are negligible. For the purposes of the F/A orifice plate structural evaluation, the transient pressure drop  $(\Delta p)_{TR}$  was taken to be zero.

$$(\Delta p)_{TR} \approx 0.0$$

### 9.1.2 Thermal

The F/A orifice plate thermal loads are the steady state and transient temperature distributions that occur during the Upset, Emergency, and Faulted Events over the first and second reactor cycles. In the definition of the F/A orifice plate temperature distributions, the sodium temperatures at the reactor vessel inlet were conservatively assumed to be applied directly to the F/A orifice plate without the mitigating effects of mixing that would normally occur in the inlet plenum. The approach adopted for the F/A orifice plate transient thermal response is consistent with that taken for the F/A shield block. Accordingly, the selection of the E-4a transient as the umbrella to all Upset, Emergency, and Faulted transients for the F/A orifice plate invoked the same rationale used for the F/A shield block. Further, the number and characteristics of the worst case F/A orifice plate duty cycle are the same as that used for the F/A shield block. The F/A shield block E-4a transient and worst case duty cycle taken for the F/A orifice plate are presented in Figures 4.1-1 and -2, respectively.

A derivation of the detailed F/A orifice plate temperature distributions during the worst case thermal duty cycle, in the manner described for the F/A shield block, was not made. Instead, the F/A orifice plate was assumed to instantaneously follow the reactor vessel inlet sodium temperatures while the mating F/A inlet nozzle housing was considered to lag the F/A orifice plate response because of its thermal inertia. The thermal response assumption is conservative in relation to the subsequent structural evaluation of the F/A orifice plate under thermal loads. For the F/A orifice plate responding instantaneously to the sodium temperatures, the radial gap between the periphery of the orifice plate and the inlet nozzle housing are closed and interfere to a greater amount than if the thermal inertia of the orifice plate were considered.

In order to define the F/A orifice plate thermal loads induced by in-plane radial interference, the temperature difference ( $\bar{\Delta T}$ ) between the orifice plate or sodium and the inlet nozzle housing during the E-4a transient is required. An estimate of the temperature difference ( $\bar{\Delta T}$ ) is to use the plot of the temperature difference ( $\Delta T$ ) between Nodes 1 and 237,  $\Delta T = T_{237} - T_1$ , in the F/A shield block thermal model during the E-4a transient as illustrated in Figure 4.1-6.

$$\bar{\Delta T} = \Delta T$$

The estimate of the temperature difference ( $\bar{\Delta T}$ ) is conservative because the F/A shield block region is thick-walled with greater thermal inertia than the relatively thin-walled inlet nozzle mating housing.

A review of the F/A shield block temperature difference ( $\Delta T$ ) plot shows both positive and negative values during the E-4a transient. As applied to the F/A orifice, positive temperature differences tend to open the gap at the orifice plate periphery while negative values cause the gap to close and cause interference. With regard to structurally damaging in-plane thermal loads, only the negative temperature differences which place the orifice plate in in-plane compression due to radial interference are of significance. Positive temperature differences do not place the orifice plate in in-plane tension because the orifice plate is free to slide inward on the locating pins. The maximum negative temperature difference ( $\bar{\Delta T}_{\max}$ ) for the F/A orifice plate is:

$$(\bar{\Delta T})_{\max} = 170^{\circ}\text{F}$$

In order to establish the maximum amount of radial interference ( $\delta_r$ ) at the outer orifice plate periphery during the E-4a transient the following relation was used.

$$(\delta_r)_{TR} = \alpha R_o (\Delta T)_{max} - G$$

Where,

$\alpha$  = Coefficient of thermal expansion (1/°F)

$R_o$  = Nominal outer radius (in)

$G$  = Nominal gap (in)

Numerically, the F/A orifice plate nominal outer, radius ( $R_o$ ) and gap ( $G$ ) are 1.87 and 0.0025 in. respectively. For the F/A orifice plate constructed from SA-316-SS, the coefficient of thermal expansion ( $\alpha$ ) as a function of temperature ( $T \sim ^\circ F$ ) is given in the F/A shield block analysis described in Section 4.2.2.1. During the E-4a transient, the peak F/A orifice plate temperature is 1000°F. The corresponding coefficient of thermal expansion ( $\alpha$ ) is  $11.25 \times 10^{-6}/^\circ F$ . Accordingly, the worst case F/A orifice plate E-4a transient radial interference ( $\delta_r$ )<sub>TR</sub> taken for the thermal loads.

$$(\delta_r)_{TR} = (11.25 \times 10^{-6}/^\circ F) (1.87) (170) - 0.0025$$

$$(\delta_r)_{TR} = 0.00108 \text{ in.}$$

With regard to the F/A orifice plate thermal loads during steady state conditions, the radial interference ( $\delta_r$ ) does not exist and was neglected in the structural evaluation.

$$(\delta_r)_{SS} = 0.0$$

### 9.1.3 Worst Case Duty Cycle

The conclusions based on the F/A orifice plate loading analysis in relation to recommendations for the worst case duty cycle are as follows.

- Mechanical loads comprising OBE and SSE seismic, and core restraint, internal pressure, and deadweight are negligible. Only the steady state pressure drop is of relative significance in establishing the worst case F/A orifice plate duty cycle.
- Thermal loads corresponding to in-plane radial interference at the outer orifice plate periphery during the E-4a transient was considered most important in establishing the worst case F/A orifice plate duty cycle.

The recommendations for the F/A orifice plate loading were to apply a single worst case duty cycle of the time independent mechanical loads combined with time dependent thermal loads. The worst case duty cycle was recommended to be repeated 39 times so as to umbrella the 39 Upset and worst Emergency or Faulted events specified for the F/A orifice plate. The single cycle loading sequence is as follows.

#### Time Independent

- Apply the worst case pressure drop at the initial steady state temperature of 750°F.
- Reduce the pressure drop to zero at the start of the E-4a transient while maintaining the 750°F steady state temperature.
- With the pressure drop removed, apply the worst case radial interference at the peak E-4a transient temperature of 1000°F.
- Remove the radial interference and apply the worst case pressure drop at the final steady state temperature of 750°F.

#### Time Dependent

- Maintain the worst case pressure drop over a 10 day hold-time at the 750°F steady state temperature.

## 9.2 Structural Analysis

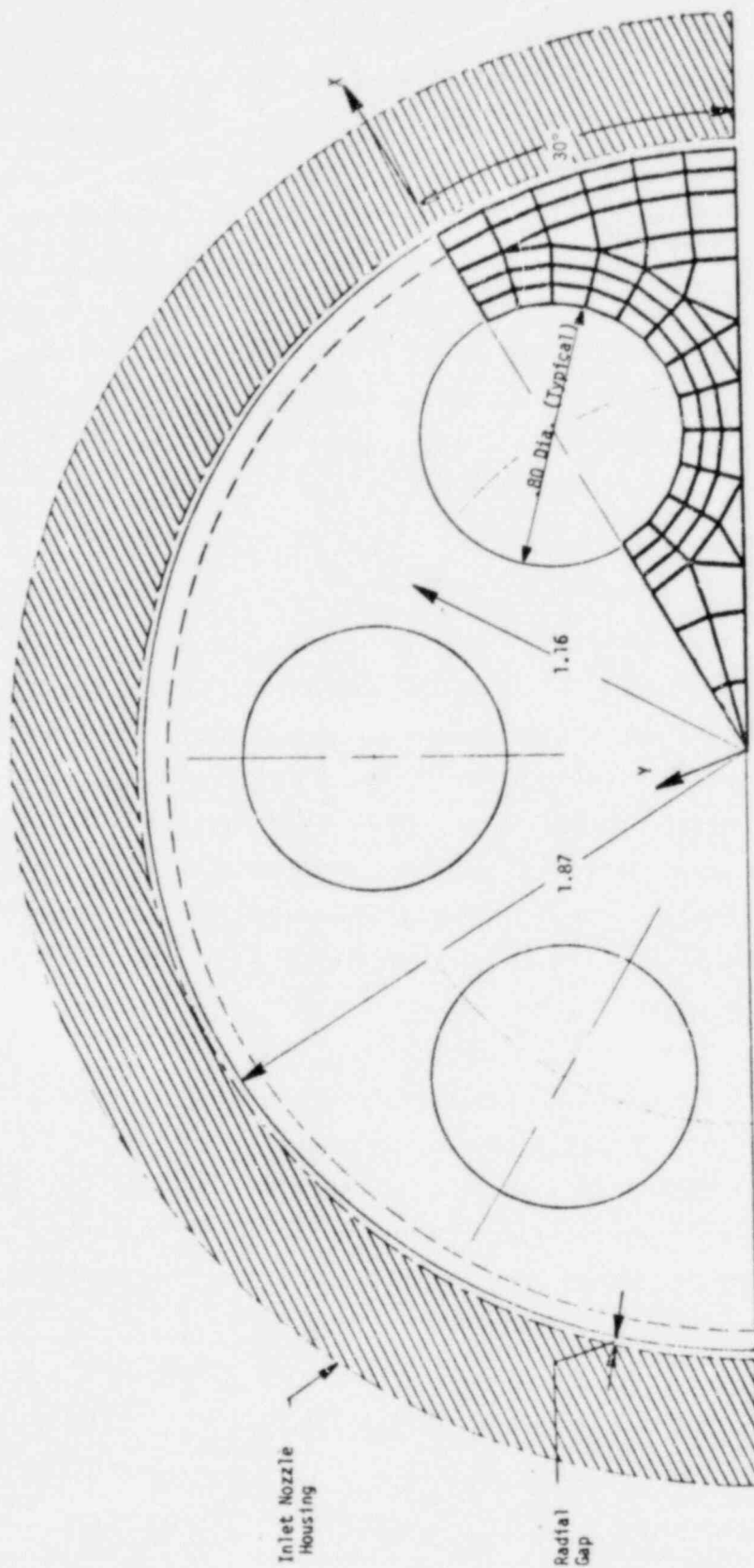
The F/A orifice plate structural analysis was directed to deriving the stresses, strains, and dimensional changes which occur during the worst case duty cycle from which structural evaluations were made. In the following, the F/A orifice plate structural model and geometry are described. Next, linear and nonlinear material properties including the effects of irradiation on stress-strain curves and the basis for neglecting thermal creep are presented. Elastic analysis is presented to establish that mechanical pressure drop loading is negligible in relation to thermal loading induced by radial interference at the orifice plate periphery. Finally, the time independent and dependent inelastic analysis and results for the worst case F/A orifice plate duty, cycle are presented in preparation for subsequent structural evaluation.

### 9.2.1 Model and Geometry

The F/A orifice plate structural model was formulated in the ANSYS finite element program. In the pressure drop analysis, the triangular plate (STIF 13) and quadrilateral plate (STIF 63) elements were used to derive the out-of-plane bending stresses and strains. For the analysis of in-plane response to radial interference loadings, the constant strain (STIF 2) element in a condition of plane stress with a constant thickness was used. In both the pressure drop and inplane response ANSYS analysis, the geometry and finite element mesh were identical in deriving the structural response.

The F/A orifice plate region selected for analysis corresponds to a symmetrical  $30^\circ$  sector taken through the 6 hole flow pattern. The  $30^\circ$  symmetrical sector is justified as pressure drop and radial interference loadings are essentially uniform. The F/A orifice plate structural model illustrating the dimensional extent and finite element detail of the  $30^\circ$  sector is presented in Figure 9.2-1.

Figure 9.2-1  
F/A Orifice Plate  
Dimensional Extent and Finite Element Detail





### 9.2.2 Properties

The F/A orifice plate as constructed from SA-316-SS and initially unirradiated at BOL is irradiated to a fluence ( $E > 0.1$  Mev,  $(\phi t) = 0.0066 \times 10^{22}$  n/cm<sup>2</sup>) at EOL. Operational temperatures range from 750 to 1000°F. The linear and non-linear properties of SA-316-SS at fluence and temperature selected for the F/A orifice plate analysis are described as follows.

#### 9.2.2.1 Linear

The linear SA-316-SS material properties are the Young's modulus (E), Poisson's ratio ( $\mu$ ), and coefficient of thermal expansion ( $\alpha$ ). The material properties as a function of temperature ( $T \sim$  °F) used in the F/A orifice plate structural analysis were identical to those identified for the F/A shield block presented in Section 4.2.2.1.

#### 9.2.2.2 Non-Linear

The non-linear SA-316-SS material property behavior required in the F/A orifice plate structural analysis are the time independent stress-strain, and the time dependent thermal creep constitutive relations. The constitutive relations with attendant simplifications used in the F/A orifice plate analysis are as follows.

##### 9.2.2.2.1 Stress-Strain Curves

The true average stress-strain curves for SA-316-SS given in the NSM Handbook [6] were reviewed in relation to the F/A orifice plate EOL fluence ( $E > 0.1$  Mev,  $(\phi t) = 0.0066 \times 10^{22}$  N/cm<sup>2</sup>) and the operational temperature range from 750 to 1000°F. Temperature effects were found to be significant, but the effect of irradiation at EOL fluence relative to unirradiated BOL values was found to be insignificant. Accordingly, the true average EOL and BOL stress-strain curves for SA-316-SS were considered identical to each other for the F/A orifice plate.

In the F/A orifice plate structural analysis, true minimum BOL and EOL stress-strain curves are required because the mechanical and thermal loads which occur during the worst case duty cycle are slow acting and are basically statically applied. The true minimum BOL and EOL stress-strain curves as a function of temperature, taken as 90% of the true values given in the NSM Handbook [6], are illustrated in Figure 9.2-2 with corresponding numerical values summarized in Table 9.2-1.

TABLE 9.2-1  
F/A ORIFICE PLATE  
TRUE MINIMUM BOL AND EOL STRESS-STRAIN DATA  
SA-316-SS

Temp (°F)	F. (10 <sup>6</sup> PSI)	Stress (PSI) at Total Strain				
		0.00049	0.00249	0.0105	0.0205	0.0505
750	24.77	12,370	17,100	23,490	26,100	34,740
1000	22.53	11,250	15,750	20,250	24,930	33,750

#### 9.2.2.2.2 Thermal Creep Equations

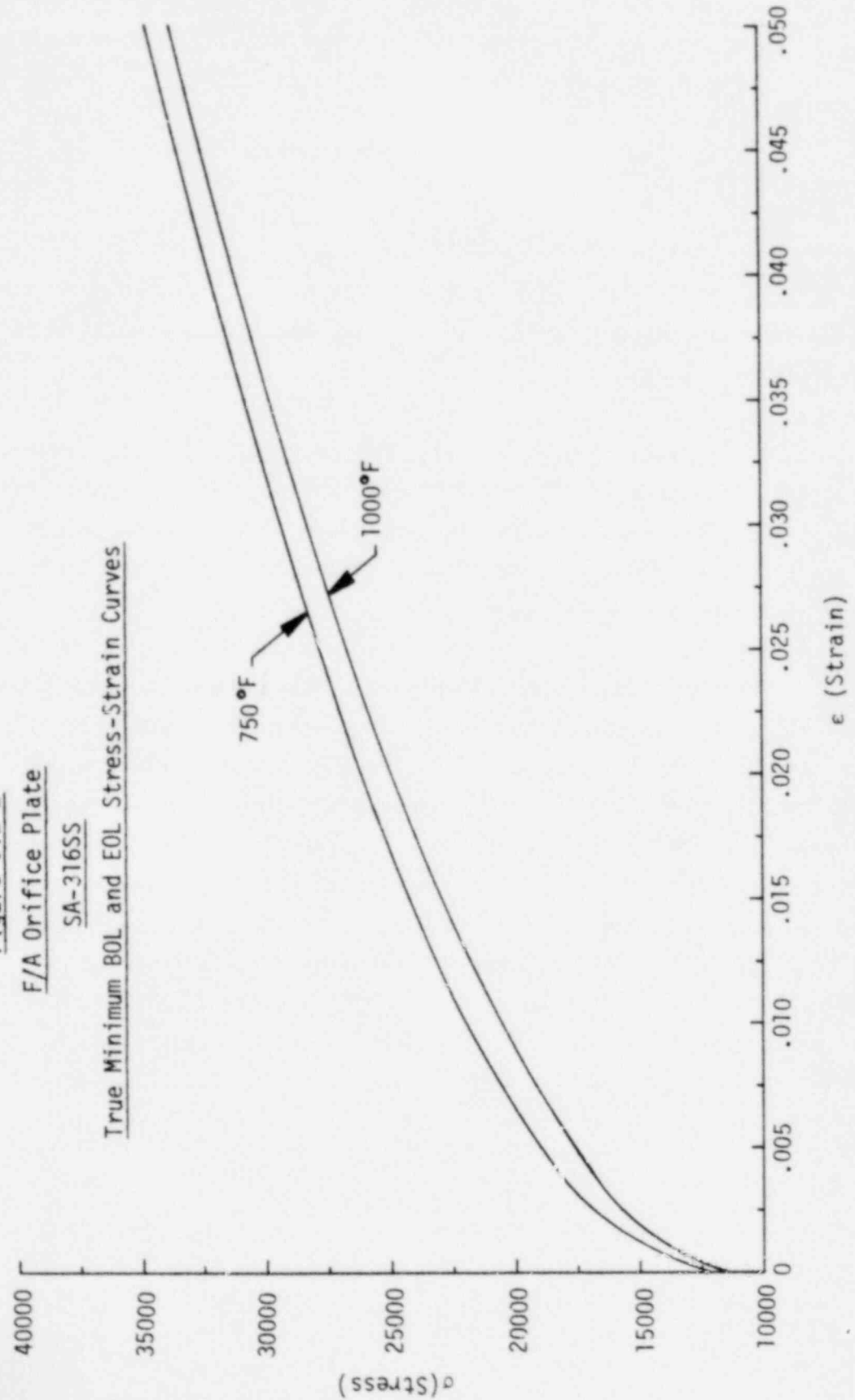
The unirradiated SA-316-SS thermal creep-time constitutive relations as a function of stress and temperature are given in the NSM Handbook [6]. The thermal creep constitutive relations for irradiated SA-316-SS are not identified as the effects of irradiation are included in the irradiation creep equations.

For the F/A orifice plate, the EOL fluence is  $0.0066 \times 10^{22}$  n/cm<sup>2</sup> with thermal creep occurring at a steady state temperature of approximately 750°F over the 10 day hold time of the worst case duty cycle. As the EOL fluence is relatively low and steady state temperatures are below 800°F, thermal creep over the worst case F/A orifice plate duty cycle was neglected.

Figure 9.2-2  
F/A Orifice Plate

SA-316SS

True Minimum BOL and EOL Stress-Strain Curves



### 9.2.3 Elastic Response

The F/A orifice plate elastic structural response to the pressure drop and radial interference loading was obtained in order to determine their relative importance in the worst case duty cycle. The ANSYS analysis and results are described as follows.

#### 9.2.3.1 Pressure Drop

##### 9.2.3.1.1 Model and Boundary Conditions

The ANSYS elastic structural response of the F/A orifice plate to pressure drop loading was obtained using the geometry and finite element mesh identified in Figure 9.2-1.

The F/A orifice plate structural model for pressure drop analysis included 9 elastic triangular (STIF 13) and 59 elastic quadrilateral (STIF 63) flat plate elements arranged in a finite element mesh of 252 node points. The F/A orifice plate pressure drop structural model illustrating the boundary conditions is presented in Figure 9.2-3.

Simply supported boundary conditions were simulated at the outer periphery of the 30° sector by specifying the UZ displacements, normal to X-Y plane, to be zero at nodes 113 through 119. The boundary conditions along the lateral surfaces of the 30° sector were selected to maintain the symmetry of the deformations under the pressure drop loading. Along the lateral surface coincident with the Global X-Axis, the UY displacements and RØTX rotations were set equal to zero at Nodes 1, 2, 5, 201 through 204, 249 through 252, 106, and 113. For the lateral surface inclined to the Global X-Axis, the UY displacements and RØTX rotations, after a -30° rotation to obtain normally disposed directions, were set equal to zero at Nodes 1, 4, 7, 8, 216, 220, 224, 9, 11, 14, 105, 112 and 119.

— Symmetry Conditions ( $U_Y = ROTX = 0.0$ )  
Nodes (1, 2, 5, 201 thru 204, 249 thru 252, 106, 113)

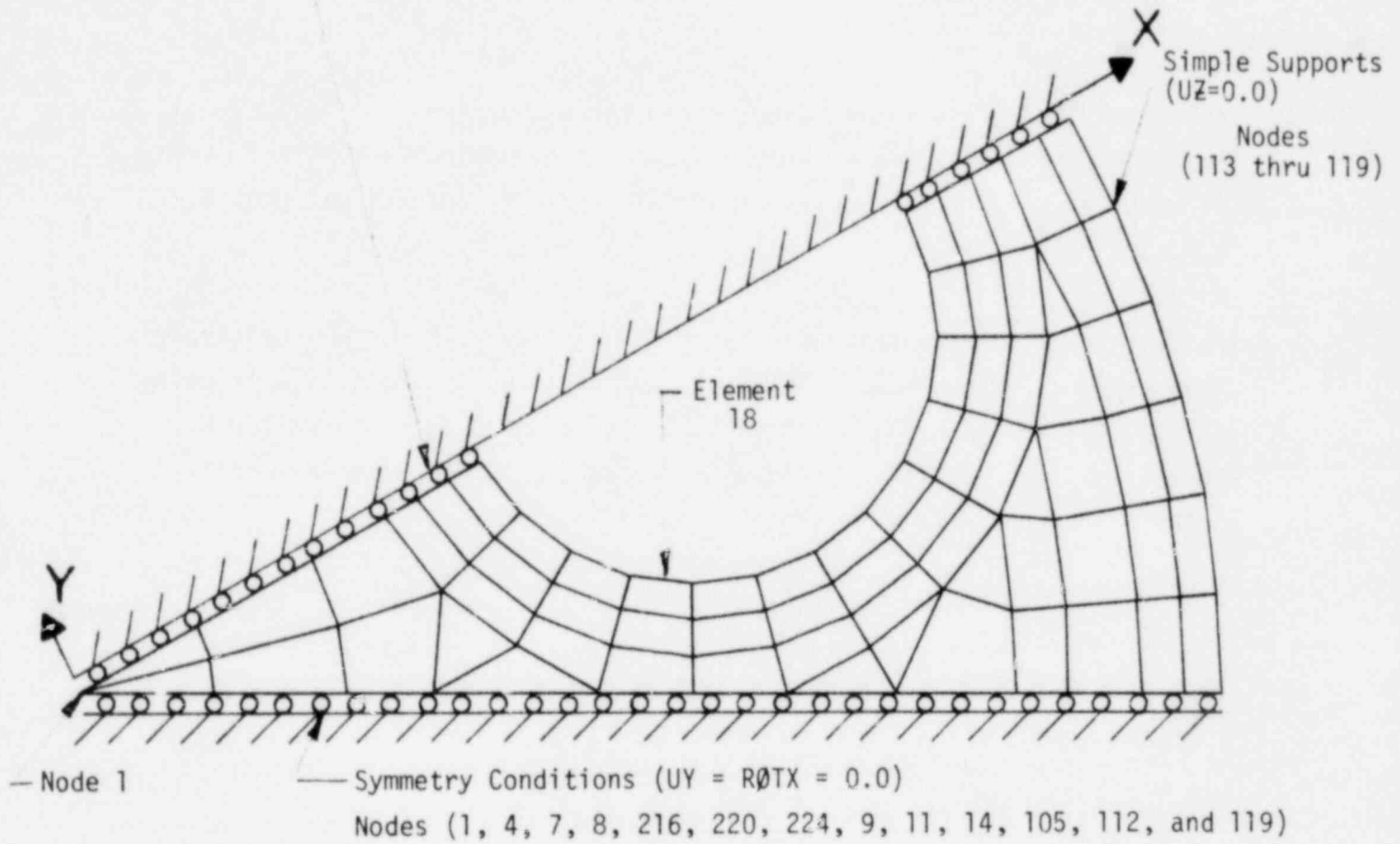


Figure 9.2-3  
F/A Orifice Plate  
Pressure Drop Structural Model

#### 9.2.3.1.2 Analysis and Results

The F/A orifice plate elastic response to the pressure drop loading was obtained in a single ANSYS solution run. The orifice plate minimum thickness of 0.240 in. was taken in the analysis. The steady state pressure drop  $(\Delta p)_{SS}$  of 22.35 psi was applied to the lateral face of each element. The SA-316-SS material properties of Young's modulus (E) and Poisson's ratio ( $\nu$ ) were taken at 750°F.

The F/A orifice plate maximum equivalent stress was found to be 2284 psi. The maximum UZ displacement was 0.00075 in. The maximum equivalent stress and UZ displacement occurred at element 18 and node point 1 as identified in Figure 9.2-3.

The elastic structural response of the F/A orifice plate under the steady state pressure drop shows that the maximum equivalent stress is well below the SA-316-SS proportional elastic limit stress of 12,370 psi at 750°F. Plots of maximum equivalent stress and perpendicular UZ displacement contours are presented in Figure 9.2-4.

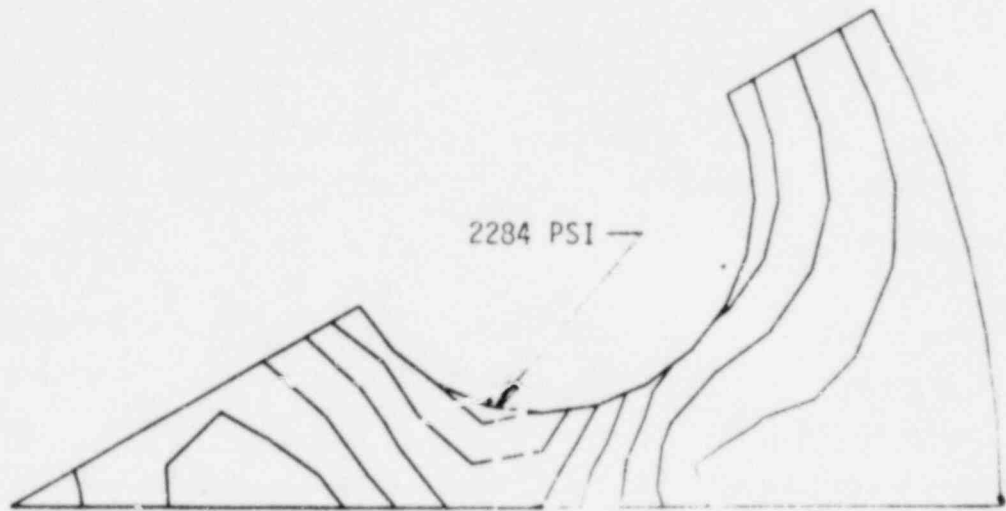


Figure 9.2-4  
F/A Orifice Plate  
Pressure Drop Elastic Response  
Equivalent Stress and Perpendicular Displacements

### 9.2.3.2 Radial Interference

#### 9.2.3.2.1 Model and Boundary Conditions

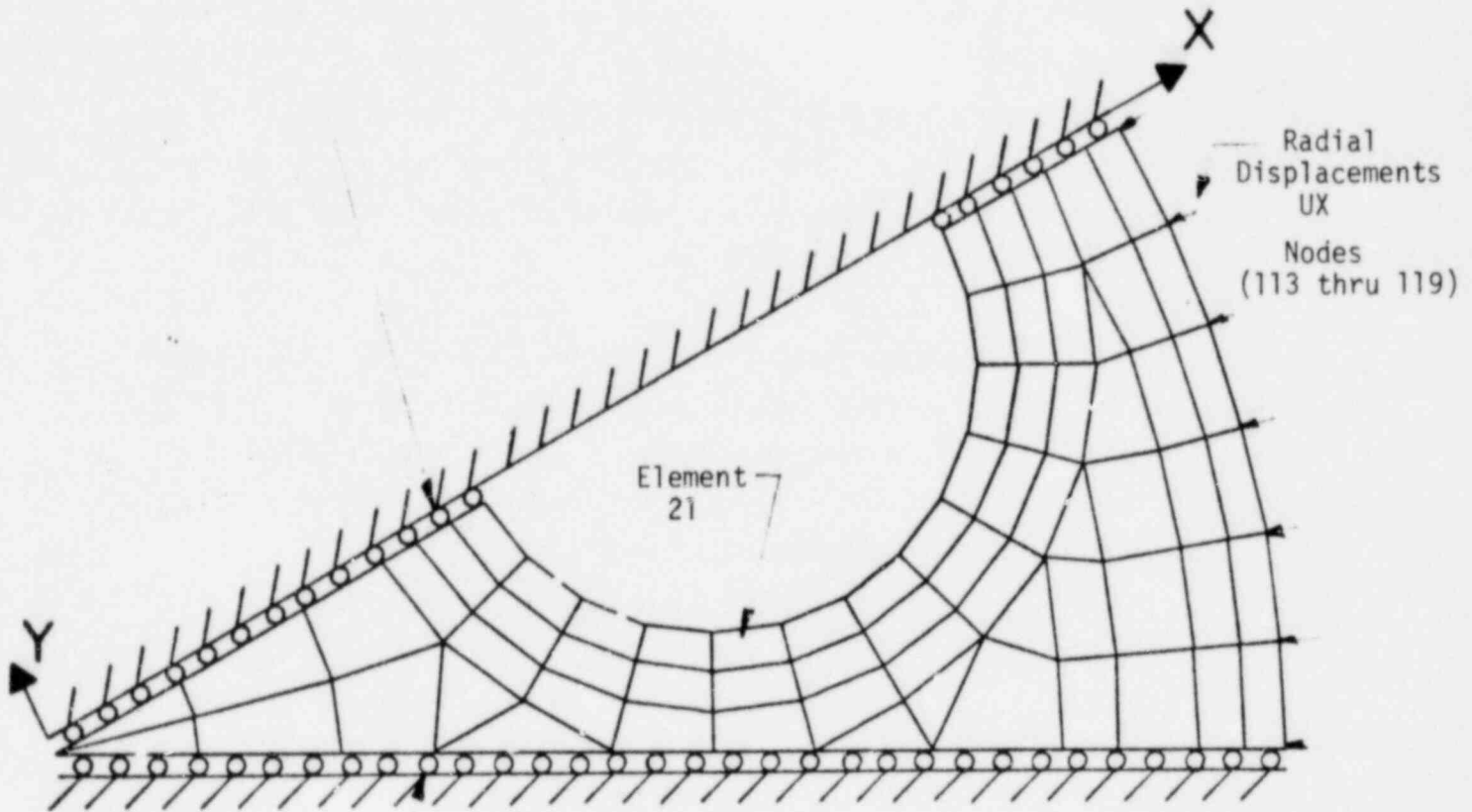
The ANSYS elastic structural response of the F/A orifice plate to radial interference loading was obtained using the geometry and finite element mesh identified in Figure 9.2-1.

The F/A orifice plate structural model for radial interference analysis included 68 constant strain (STIF 2) elements formulated in a condition of plane stress with a constant thickness and arranged in a finite element mesh of 252 node points. The F/A orifice plate radial interference structural model illustrating the boundary conditions is presented in Figure 9.2-5.

The radial interference ( $\delta r$ ) deformations at the outer periphery of the 30° sector were specified as the in-plane UX displacements after rotating the local coordinates of the node points on the periphery to obtain radially disposed directions. For node points 113 through 119, arranged counter-clockwise from the Global X-axis, the rotations of the local coordinates were 0 to 30°, in increments of 5°. The boundary conditions along the lateral surfaces of the 30° sector were selected to maintain the symmetry of the deformations under radial interference loading. Along the lateral surface coincident with the Global X-Axis, the UY displacements were set equal to zero at Nodes 1, 2, 5, 201 through 204, 249 through 252, 106 and 113. For the lateral surface inclined to the Global X-Axis, the UY displacements, after a -30° rotation to obtain normally disposed directions, were set equal to zero at Nodes 1, 4, 7, 8, 216, 220, 224, 9, 11, 14, 105, 112, and 119.



— Symmetry Conditions ( $U_Y = 0.0$ )  
Nodes (1, 2, 5, 201 thru 204, 249 thru 252, 106, 113)



— Symmetry Conditions ( $U_Y = 0.0$ )  
Nodes (1, 4, 7, 8, 216, 220, 224, 9, 11, 14, 105, 112 and 119)

Figure 9.2-5  
F/A ORIFICE PLATE  
RADIAL INTERFERENCE STRUCTURAL MODEL

#### 9.2.3.2.2 Analysis and Results

The F/A orifice plate elastic response to the radial interference loading was obtained in a single ANSYS solution run. The orifice plate minimum thickness of 0.240 in. was taken in the analysis. The radial interference ( $\delta r$ ) at the maximum E-4a transient value of 0.00108 in. was applied to the outer orifice plate periphery. Values of Young's modulus (E) and Poisson's ratio ( $\mu$ ) material properties were taken at 1000°F.

The elastically calculated F/A orifice plate maximum equivalent stress was found to be 28,383 psi. The maximum equivalent stress and attendant in-plane deformation occur at element 21 and outer periphery Nodes 113 through 119 as identified in Figure 9.2-5.

The elastic structural response of the F/A orifice plate under the maximum E-4a radial interference shows that the maximum elastically calculated equivalent stress is well beyond the SA-316-SS proportional elastic limit stress of 11,250 psi at 1000°F. Plots of the maximum equivalent stress and in-plane displacements are presented in Figure 9.2-6.

#### 9.2.3.3 Conclusions

The conclusions based on the elastic analysis of the F/A orifice plate under pressure drop and radial interference loading are as follows.

- Pressure drop loadings produce stresses within the F/A orifice plate which are well below the proportional elastic limit.
- Radial interference loadings cause elastically stresses within the F/A orifice plate which are well above the proportional elastic limit.
- Only radial interference loadings are of significance in the worst case F/A orifice plate duty cycle. Pressure drop loadings can be neglected without a significant loss of accuracy in overall structural response.

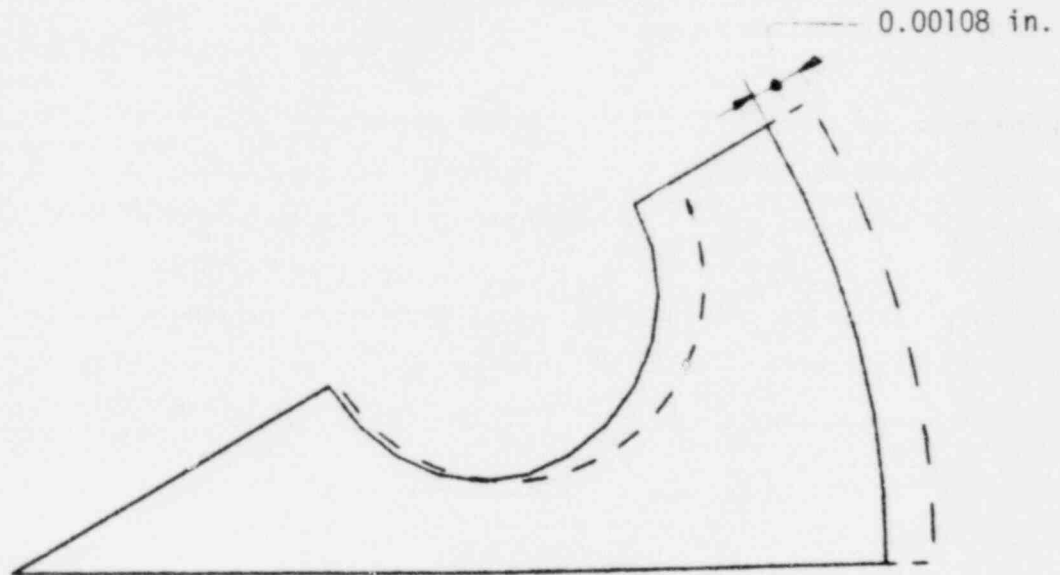
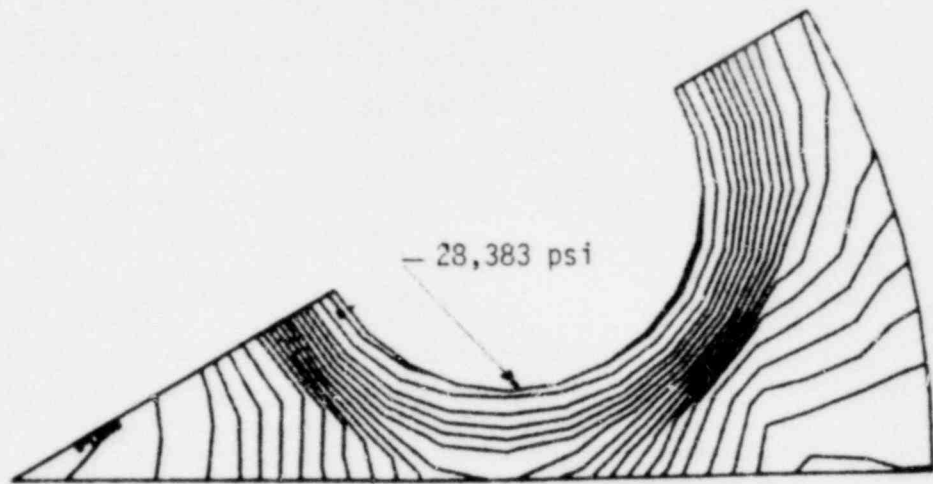


FIGURE 9.2-6  
F/A ORIFICE PLATE  
RADIAL INTERFERENCE ELASTIC RESPONSE  
EQUIVALENT STRESS AND IN-PLANE DEFORMATIONS

#### 9.2.4 Worst Case Duty Cycle Response

The F/A orifice plate structural response to the worst case duty cycle included only the thermal loads caused by radial interference as the mechanical loads caused by pressure drop were shown to be negligible. Further, the response to both first and second duty cycles was used to approximate the response to the 39 worst case duty cycles. The first cycle was considered to be applied once, while the second cycle was repeated 38 times. The F/A orifice plate structural response to the time independent and dependent loadings of the first cycle provides the basis from which evaluations of crack initiation in terms of local ductile rupture and creep-fatigue damage are made. For the evaluation of peak plus accumulated and residual deformation over the 39 worst case duty cycles in relation to deformation limits, the response of both first and second duty cycles were used.

In order to obtain the first and second cycle response in an efficient manner, the ANSYS restart option was used to provide the loading sequence within, between and after the time independent and time dependent solutions. As elastic/plastic/creep instability would not be expected for the F/A orifice plate under the deformation controlled radial interference loadings, the ANSYS small strain-small deformation option was used in the inelastic analysis. Descriptions of the first and second cycle time independent and dependent analysis and results are as follows.

##### 9.2.4.1 First Cycle-Time Independent

The first cycle time independent ANSYS analysis of the F/A orifice plate was directed to deriving the peak plus accumulated strains and deformations associated with following the path dependent radial interference loadings from initial steady state conditions through the E-4a transient followed by the return to final steady state conditions, but excluding the 10-day hold-time. The time independent loadings were considered as static loadings applied at zero time. A total of 5 load steps were used to derive the first cycle-time independent F/A orifice plate response from initial to final steady state conditions as summarized in Table 9.2-2.

TABLE 9.2-2  
 F/A ORIFICE PLATE  
 FIRST CYCLE-TIME INDEPENDENT ANALYSIS SUMMARY

Load Steps	Iterations	Temperature Distribution (°F)	Radial Deformation ( $\delta_r \sim$ in)	Description
1	1	750	None	Initial Steady State
2	1	1000	None	Peak E-4a Loading and Unloading
3	12	1000	0.00108	
4	1	1000	None	
5	1	750	None	Final Steady State

The F/A orifice plate structural response to the first cycle time independent loading was obtained with a plastic convergence ratio of 0.01. The detailed stress-strain response at each of the converged solutions was saved on ANSYS Tape 10 for subsequent recall in structural evaluations. The initial and final time independent maximum equivalent stresses were zero and 3449 psi. During the E-4a transient, the maximum equivalent stress and non-uniform deformation at the maximum radial interference were found to be 14,305 psi and 0.0011 in. The initial and final time independent steady state non-uniform deformations were zero and 0.0004662 in. Computer plots of first cycle time independent peak and final steady state response are presented in Figures 9.2-7 and -8.

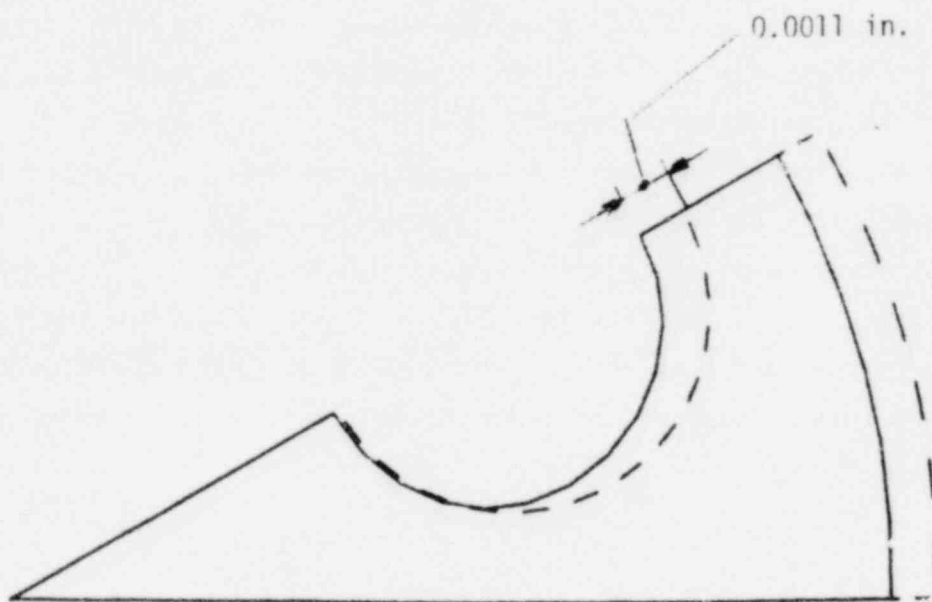
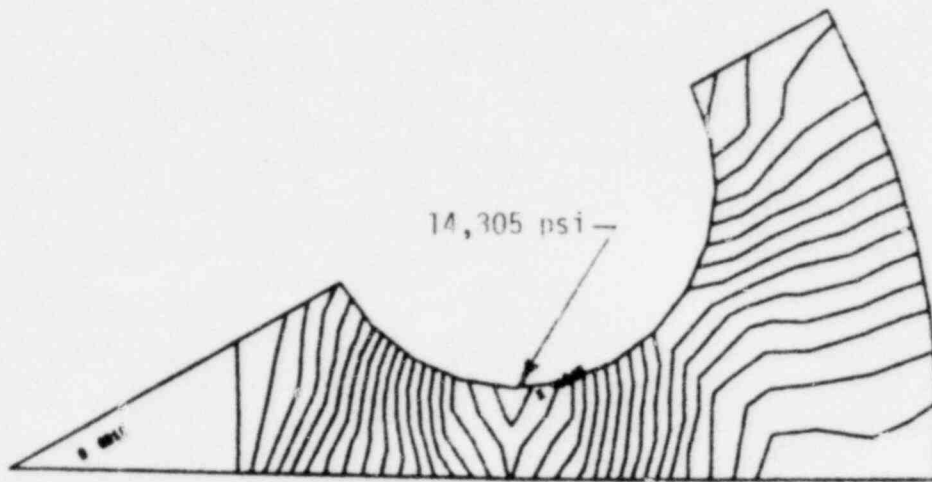


Figure 9.2-7  
 F/A Orifice Plate  
 First Cycle - Time Independency  
 Peak E-4a Radial Interference  
 Equivalent Stress and Non-Uniform Deformation

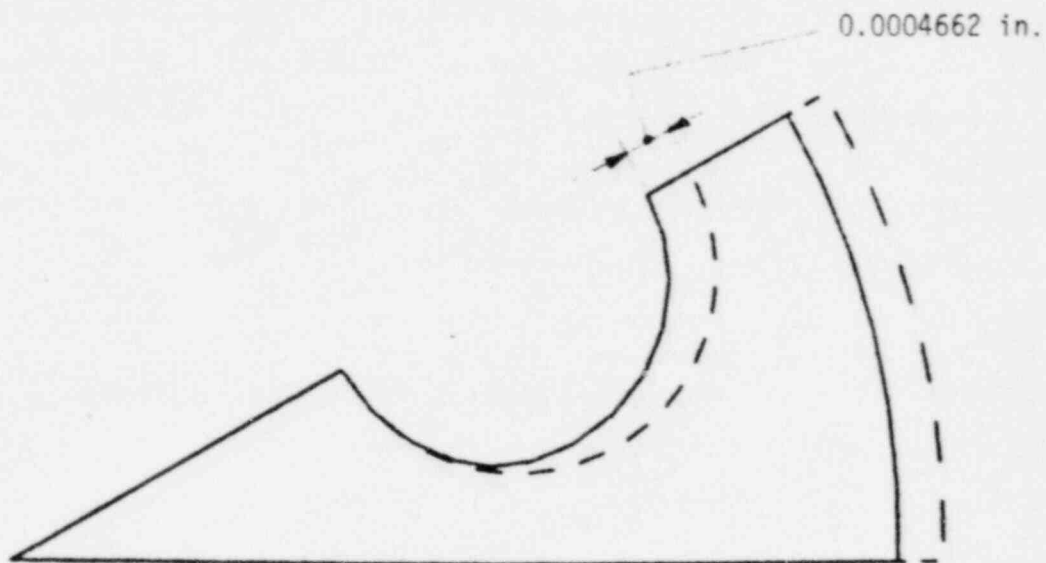
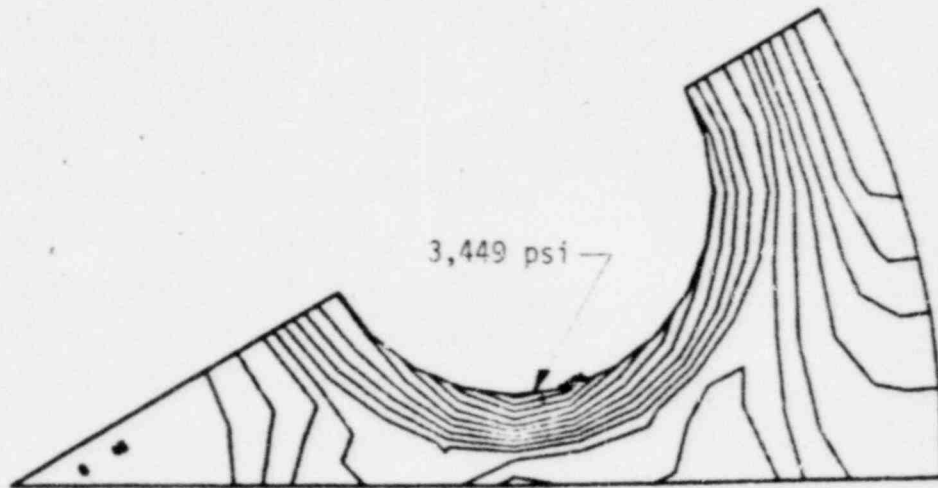


Figure 9.2-8  
F/A Orifice Plate  
First Cycle - Time Independent  
Final Steady State  
Equivalent Stress and Non-Uniform Deformation

#### 9.2.4.2 First Cycle-Time Dependent

The first cycle time dependent ANSYS analysis of the F/A orifice plate was directed to deriving the final steady state strains and deformations associated with the 10 day hold-time. As thermal creep was neglected for the F/A orifice plate, the final time dependent steady state response was identical to the time independent final steady state response. Nevertheless, a time dependent solution was still derived in order to initialize the second duty cycle. The first cycle time dependent solution was obtained in load step 6 for 1 iteration over the 240 hour hold-time with an ANSYS restart from load step 5 of the first cycle time independent analysis.

#### 9.2.4.3 Second Cycle-Time Independent

The second cycle time independent ANSYS analysis of the F/A orifice plate was directed to deriving the peak and final steady state response associated with the second application of the radial interference loading at 240 hours. Using an ANSYS restart from load step 6 of the first cycle time dependent solution, a total of 3 additional load steps were used to derive the second cycle time independent response as summarized in Table 9.2-3.

TABLE 9.2-3  
F/A ORIFICE PLATE  
SECOND CYCLE-TIME INDEPENDENT ANALYSIS SUMMARY

Load Steps	Iterations	Temperature Distribution (°F)	Radial Deformation ( $\delta_r \sim$ in.)	Description
7	1	750	None	Initial Steady State
8	12	1000	0.00108	Peak E-4a Loading
9	1	750	None	Final Steady-State



During the E-4a transient, the maximum equivalent stress and peak non-uniform deformation was found to be 14,799 psi and 0.0011 in. The final steady state maximum equivalent stress and peak non-uniform deformation were 3055 psi and 0.0004748 in. Corresponding computer plots are presented in Figures 9.2-9 and -10.

#### 9.2.4.4 Second Cycle-Time Dependent

The second cycle time dependent ANSYS analysis of the F/A orifice plate was obtained in load step 10 for 1 iteration at 480 hours using a restart from load step 9 of the second cycle time independent analysis. As thermal creep was neglected, the time dependent stress and deformation response was identical to the second cycle time independent final steady state response.

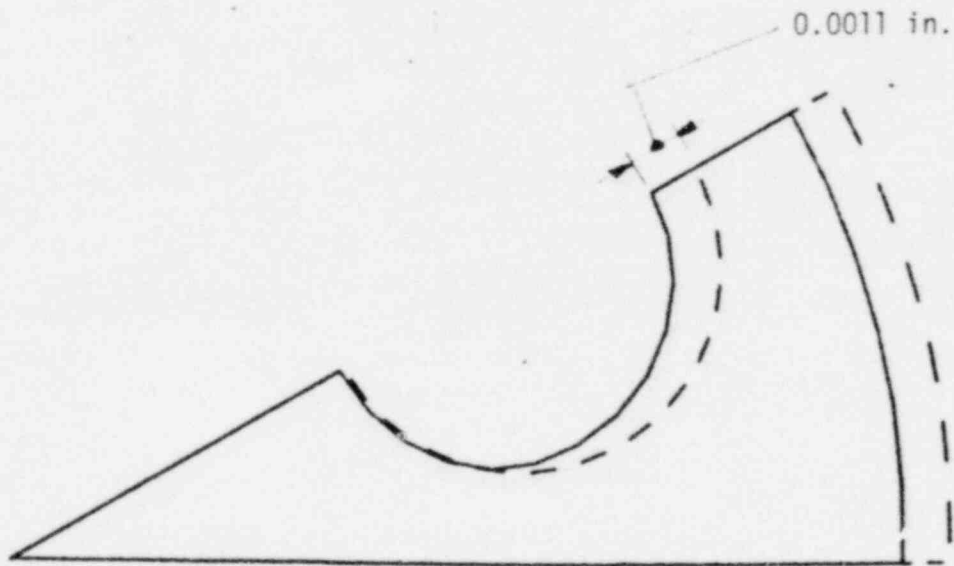
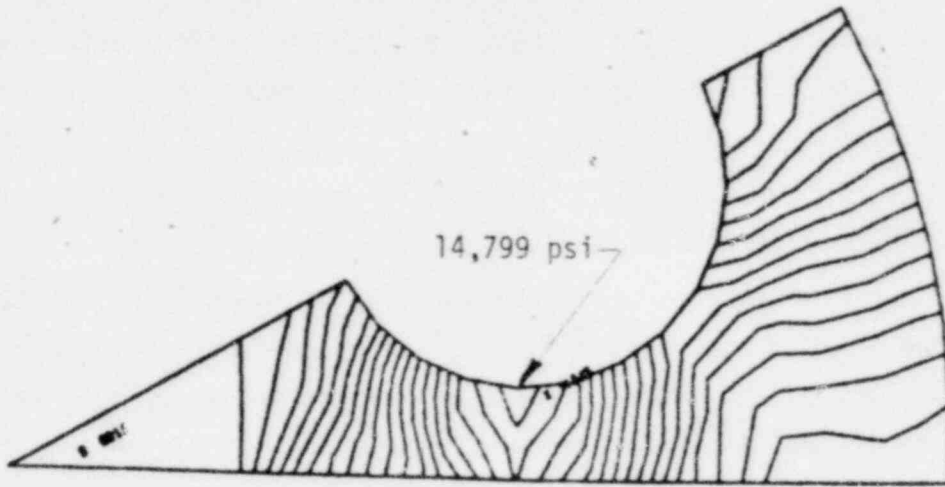


Figure 9.2-9  
 F/A Orifice Plate  
 Second Cycle - Time Independent  
 Peak E-4a Radial Interference  
 Equivalent Stress and Non-Uniform Deformation

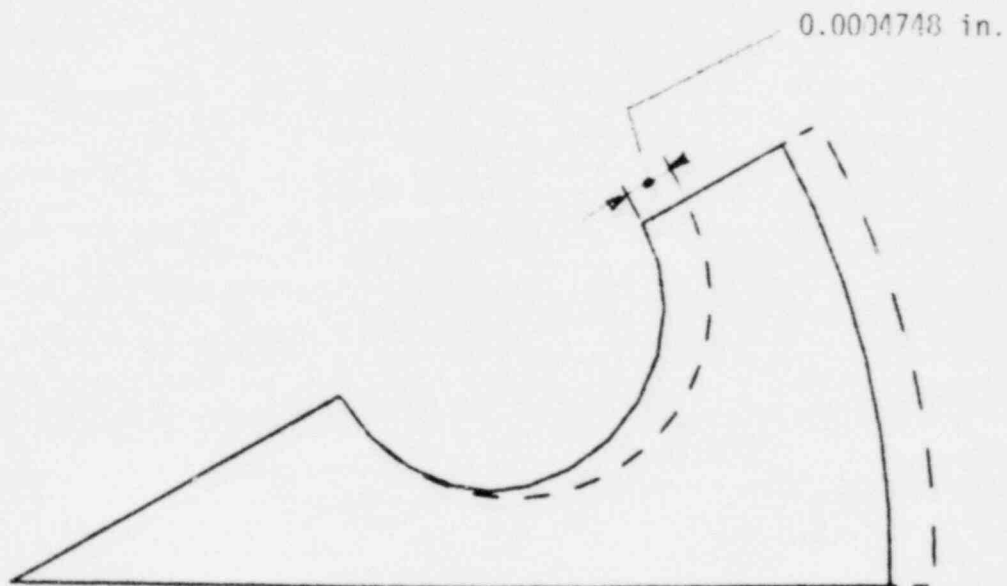
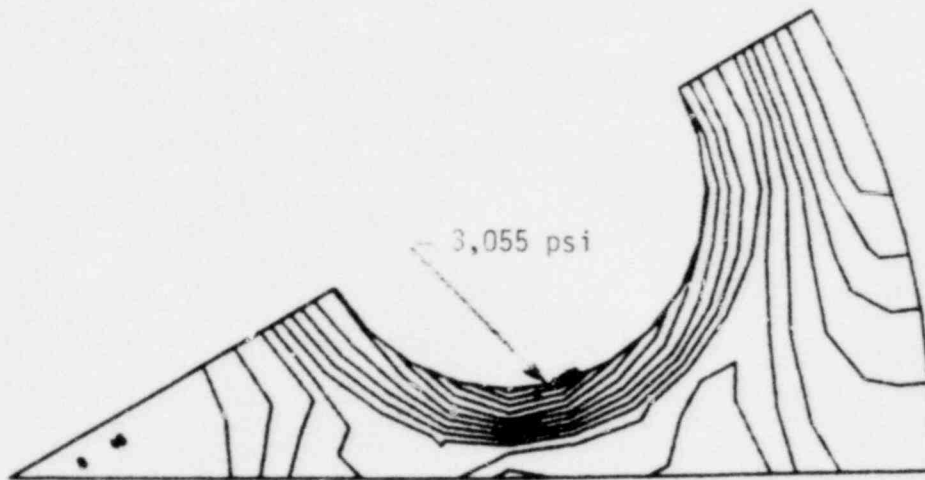


Figure 9.2-10  
F/A Orifice Plate  
Second Cycle - Time Independent  
Final Steady State  
Equivalent Stress and Non-Uniform Deformation

### 9.3 Structural Evaluation

The F/A orifice plate structural evaluation was arranged to provide a comparison of the structural response for the 39 worst case duty cycles in relation to criteria which protect against crack initiation and excessive deformation failure modes and thereby assure F/A orifice plate function in the first and second reactor cycles.

The procedure for performing the F/A orifice plate evaluation of crack initiation failure modes considered only the response to the first duty cycle in estimating the response of the 39 worst case duty cycles. The approach is representative for creep fatigue damage evaluations as strain range and residual stresses do not change appreciably during successive duty cycles. However, the ductile rupture evaluation based on the first duty cycle is conservative because the difference in strain components between initial and final steady state conditions are reduced significantly in successive duty cycles. Nevertheless, only the first duty cycle response was used because the local ductile rupture criterion could be satisfied even though the evaluation was conservative. For evaluations of peak plus accumulated and residual deformations, the conservatism in using the first duty cycle alone could not be invoked and still establish acceptability. Accordingly, both first and second duty cycle deformation response were used in establishing the F/A orifice plate acceptability in relation to excessive deformation. A description of the F/A orifice plate structural evaluation is presented as follows.

#### 9.3.1 Crack Initiation

The F/A orifice plate structural evaluation of crack initiation in relation to local ductile rupture and combined creep-fatigue damage criteria over the 39 worst case duty cycles is presented in the following subsections.

### 9.3.1.1 Local Ductile Rupture

The local ductile rupture criterion for protecting against crack initiation requires that the ductile rupture factor ( $F_{DR}$ ) be less than unity at each point in the F/A orifice plate.

$$F_{DR} = \text{Maximum of } \left\{ \begin{array}{l} \bullet \frac{(\epsilon_{\text{max principal}})^{TF}}{0.3 \epsilon_{f, \text{min}}} \\ \bullet \frac{(\epsilon_{\text{max principal}})^{TF}}{\epsilon_{u, \text{min}}} \end{array} \right\}$$

In the following, the allowable uniaxial strains used in the F/A orifice plate structural evaluation and comparison of results with the local ductile rupture factor criterion are presented.

#### 9.3.1.1.1 Allowable Uniaxial Strains

The F/A orifice plate as constructed from SA-316-SS is unirradiated at BOL. The EOL fluence ( $E > 0.1$  Mev) is  $0.0066 \times 10^{22}$  n/cm<sup>2</sup>. In addition, the F/A outlet nozzle temperatures range from 750 to 1000°F. The true uniaxial uniform elongation ( $\epsilon_{u, \text{min}}$ ) and fracture ( $\epsilon_{f, \text{min}}$ ) for unirradiated and irradiated SA-316-SS used in the F/A orifice plate structural evaluation were taken from the recommendations in the trial applications of the RDT Draft for Breeder Reactor Core Components [15-23] and are identical to those taken for the F/A shield block structural evaluation presented in Section 4.3.1.1.1.

#### 9.3.1.1.2 Comparison with Criterion

The F/A orifice plate structural evaluation in relation to the worst case location for local ductile rupture was made by screening each of the finite elements over the 39 worst case duty cycles with the damage processor. The maximum local ductile rupture factor ( $F_{DR} \text{ max}$ ) for the F/A orifice plate was found to occur at element 21, as identified in Figure 9.2-5.

The peak BOL strain components occurred at the maximum radial interference in the E-4a transient where the local metal temperature was 1000°F. Accumulated BOL strain components were based on the difference between final time dependent steady state conditions and initial time independent steady state conditions in the first duty cycle. The EOL maximum principal strain for the peak BOL and accumulated BOL strain components over 39 worst case F/A orifice plate duty cycles was 0.027 in/in. The triaxiality factor for the local stress state was -1.244, but was taken as unity for conservatism in the structural evaluation. The true minimum irradiated uniform elongation and fracture strains at EOL fluence ( $E > 0.1$  Mev,  $\phi t = 0.0066 \times 10^{22}$  N/cm<sup>2</sup>) were 0.223 and 0.450 in/in respectively.

In this arrangement, the maximum local ductile rupture ( $F_{DR}$ ) for the F/A orifice plate was controlled by the fracture strain with a value.

$$(F_{DR})_{max} = 0.199$$

As  $(F_{DR})_{max} < 1.0$ , the F/A orifice plate is not expected to experience crack initiation over the 39 worst case duty cycles based on the local ductile rupture criterion.

### 9.3.1.2 Creep-Fatigue Damage

The creep-fatigue damage criterion in protecting against crack initiation requires that the combined creep-fatigue damage factor ( $F_{CFD}$ ) be less than unity at each point in the F/A orifice plate.

$$F_{CFD} = a/b = \text{Minimum of } \left\{ \begin{array}{l} \bullet \frac{7}{3} D^c + D^f \\ \bullet D^c + \frac{7}{3} D^f \end{array} \right\}$$

In the following, the allowable limits for fatigue life and creep-rupture times used in the F/A orifice plate structural evaluation and a comparison of the results with the combined creep-fatigue damage factor criterion are presented.

#### 9.3.1.2.1 Allowable Limits

The F/A orifice plate as constructed from SA-316-SS is unirradiated at BOL. The EOL fluence ( $E > 0.1$  Mev) is  $0.0066 \times 10^{22}$  N/cm<sup>2</sup>. In addition, the F/A orifice plate temperatures range from 750 to 1000°F. The fatigue life and creep rupture time relations used in the F/A orifice plate structural evaluation were identical to those used in the F/A shield block structural evaluation presented in Section 4.3.1.1.1. The fatigue life and creep rupture time relations representative of F/A orifice plate peak and steady state metal temperatures at EOL fluence are illustrated in Figure 4.3-1 & 2, respectively.

### 9.3.1.2.2 Comparison with Criterion

The F/A orifice plate structural evaluation in relation to the worst case location for combined creep-fatigue damage was made by screening each of the finite elements over the 39 worst case duty cycles with the damage processor. The maximum combined creep-fatigue damage factor  $(F_{CFD})_{max}$  for the F/A orifice plate was found to occur at element 21 as identified in Figure 9.2-5.

The fatigue damage factor  $(D^f)$  was found to be  $0.343 \times 10^{-5}$  for 39 worst case duty cycles. The principal strain range was found to be critical and occurred between the final steady state and maximum radial interference during the E-4a transient with a value of 0.00077 in/in. The peak metal temperature over the fatigue cycle was 1000°F. The fatigue life for the equivalent strain range was  $11.4 \times 10^6$  cycles based on the EOL fluence ( $E > 0.1$  Mev,  $(\phi t) = 0.0066 \times 10^{22}$  n/cm<sup>2</sup>).

The creep damage factor  $(D^c)$  was found to be  $0.12 \times 10^{-11}$  for the 39 worst case duty cycles. The equivalent stress was found to be critical with a value of 3,348 psi corresponding to the steady state temperature conditions at the beginning of the 10 day hold time. For the EOL fluence ( $E > 0.1$  Mev,  $(\phi t) = 0.0066 \times 10^{22}$  n/cm<sup>2</sup>) at a metal temperature of 750°F, the minimum rupture time was  $7.61 \times 10^{15}$ .

In this arrangement, the maximum combined creep-fatigue damage factor  $(F_{CFD})_{max}$  for the F/A orifice plate was found to be dominated by fatigue damage while creep damage was negligible.

$$(F_{CFD})_{max} = 0.343 \times 10^{-5}$$

As  $(F_{CFD})_{max} < 1.0$ , the F/A orifice plate is not expected to experience crack initiation over the 39 worst case duty cycles based on the creep-fatigue damage criterion.



### 9.3.2 Excessive Deformation

The F/A orifice plate structural evaluation of peak plus accumulated, and residual deformations in relation to functional limits over the 39 worst case duty cycles is presented in the following subsections.

#### 9.3.2.1 Peak Plus Accumulated Deformations

The peak plus accumulated deformation criterion in protecting against excessive peak deformations requires that peak plus accumulated deformations ( $\delta^{P+A}$ ) be less than the peak plus accumulated deformation limit (PADL).

$$\delta^{P+A} \leq \text{PADL}$$

The peak deformation ( $\delta^P$ ) of the F/A orifice plate during the first duty cycle of radial interference loading occurs at the orifice holes with a value of 0.0011 in. In the second duty cycle, the initial time independent and the final time dependent steady state deformations were 0.0004662 and 0.0004748 in. Accordingly, the accumulated deformation ( $\Delta \delta^{SS}$ ) between the initial and final steady state conditions of the second duty cycle at BOL was 0.0000086 in. For 39 worst case duty cycles, the EOL peak plus accumulated ( $\delta^{P+A}$ ) deformation is given by the relation.

$$(\delta^{P+A})_{\text{EOL}} = (\delta^P)_{\text{BOL}} + (N-1) (\Delta \delta^{SS})_{\text{BOL}}$$

$$(\delta^{P+A})_{\text{EOL}} = 0.0011 + 38 (0.0000086)$$

$$(\delta^{P+A})_{\text{EOL}} = 0.0014 \text{ in.}$$

For the F/A orifice plate, the specified nominal peak plus accumulated deformation limit (PADL) is 0.005 in. However, the tolerance on the orifice holes of 0.002 in. is more restrictive and was used as the PADL.

$$\text{PADL} = 0.002 \text{ in.}$$

As  $\delta^{P+A} < \text{PADL}$ , the F/A orifice plate is not expected to experience excessive peak deformation during the 39 worst case duty cycles.

### 9.3.2.2 Residual Deformations

The residual deformation limit in protecting against excessive residual deformations requires that the residual deformation ( $\delta^R$ ) be less than the residual deformation limit (RDL).

$$\delta^R \leq \text{RDL}$$

The residual deformation ( $\delta_1^R$ ) at the F/A orifice plate holes after the first duty cycle at BOL was 0.0004662 in. After the second duty cycle at BOL, the residual deformation ( $\delta_2^R$ ) was 0.0004748 in. Accordingly, the EOL residual deformation ( $\delta^R$ ) EOL after 39 worst case duty cycles is given by the relation.

$$(\delta^R)_{\text{EOL}} = (\delta_1^R)_{\text{BOL}} + (N-1) (\delta_2^R - \delta_1^R)_{\text{BOL}}$$

$$(\delta^R)_{\text{EOL}} = 0.0004662 + (38) (0.0000086)$$

$$(\delta^R)_{\text{EOL}} = 0.000793 \text{ in.}$$

For the F/A orifice plate, the specified nominal residual deformation limit (RDL) is 0.005 in. However, the tolerance of the orifice holes of 0.002 in. is more restrictive and was used as the RDL.

$$\text{RDL} = 0.002 \text{ in.}$$

As  $\delta^R < \text{RDL}$ , the F/A orifice plate is not expected to experience excessive residual deformation during the 39 worst case duty cycles.

### 9.3.3 Summary

The F/A orifice plate was found to satisfy the crack initiation and excessive deformation criteria for a total of 39 worst case duty cycles. A summary of the F/A orifice plate structural evaluation is presented in Table 9.3-1.

TABLE 9.3-1  
F/A ORFICE PLATE  
STRUCTURAL EVALUATION SUMMARY

Criteria		Allowable Value	Calculated Value	Margin of Safety*
Crack Initiation	Ductile Rupture Factor	1	0.199	4.03
	Combined Creep-Fatigue Damage Factor	1	$0.343 \times 10^{-5}$	291,544
Excessive Deformation	Peak + Accumulated	0.002 in.	0.0014	0.43
	Residual	0.002 in	0.000793	1.52

\* Margin of Safety =  $\frac{\text{Allowable Value}}{\text{Calculated Value}} - 1$

## 10.0 REFERENCES

- (1) E-953015, Revision 9, CRBRP Equipment Specification, First Core Fuel Assembly, Westinghouse Electric Corporation, Advanced Reactors Division, November 1977.
- (2) G. J. DeSalvo and J. A. Swanson, ANSYS - Engineering Analysis User's Manual, Swanson Analysis Systems, Inc., Elizabeth, PA., 1975.
- (3) ASME Boiler and Pressure Vessel Code, Section III, Division 1 - Subsection NB, - "Class 1 Components," Rules for Construction of Nuclear Power Plant Components, American Society of Mechanical Engineers, New York, 1977.
- (4) ASME Boiler and Pressure Vessel Code Case N-47 (1592-10), "Components in Elevated Temperature Service, Section III, Division A," in "Nuclear Components," American Society of Mechanical Engineers, New York, 1977.
- (5) Draft RDT Design Guideline/Criteria for FBR Core Components, Vol. I, Structural Design Criteria, June 1976.
- (6) "Nuclear Systems Materials Handbook," TID-26666, Hanford Engineering Development Laboratory, Richland, Washington
- (7) S. S. Manson, "Fatigue: A Complex Subject-Some Simple Approximations", Exp. Mech. 5, pp 193-226 (1965).
- (8) "Oxide Fuel Element Development", Quarterly Progress Report for Period Ending September 30, 1974," January 1975. (Availability: US DOE Technical Information Center).
- (9) E953019, CRBRP, Core Former Equipment Specification, Appendix B, Environmental Effects on Material Properties.

- (10) H. D. Garkisch, et al., "Clinch River Breeder Reactor Plant, Irradiated EBR-II Duct Crushing Tests and Analysis," CRBRP-ARD-0164, April 1977. (Availability: US DOE Technical Information Center).
- (11) D. R. Duncan, M. M. Paxton and J. L. Straalsund, "Postirradiation Tensile Properties of an FTR Fuel Duct Produced from FTR Core 1-2 Steel" in "Cladding and Structural Materials. Semi-Annual Progress Report, July 1975 to January 1976", HEDL-TME-76-13, pp 181-182, April 1976.
- (12) D. C. Jacobs, "CRBRP, the Development and Application of a Cumulative Mechanical Damage Function for Fuel Pin Failure Analysis in LMRBR Systems," CRBRP-ARD-0115, May 1976. (Availability: US DOE Technical Information Center).
- (13) "CRBRP Core Inter-Duct Force Analyses for Unit Gravitational Loading," Westinghouse Electric Corporation, WARD-D-0208, Advanced Reactors Division, January 1978.
- (14) S. Timoshenko, Theory of Plates and Shells, McGraw-Hill, New York, 1940.
- (15) T. T. Claudson, "Irradiation Effects on Reactor Structural Materials: Quarterly Progress Report, February, March, April 1973," HEDL-TME-73-47, May 1973. (Availability: US DOE Technical Information Center).
- (16) T. T. Claudson, "Quarterly Progress Report Irradiation Effects on Reactor Structural Materials - August, September, October, 1972," HEDL-TME-72-144, December 1972.
- (17) T. T. Claudson, "Quarterly Progress Report Irradiation Effects on Reactor Structural Materials - May, June, July 1972," HEDL-TME-72-105, August 1972.

- (18) T. T. Claudson, "Irradiation Effects on Reactor Structural Materials Quarterly Progress Report, February-April, 1972," HEDL-TME-72-64, June 1972.
- (19) T. T. Claudson, "Irradiation Effects on Reactor Structural Materials Quarterly Progress Report, August-October 1970," WHAN-FR-40-1, January 1971.
- (20) R. Carlender, S. D. Harkness and F. L. Yaggee, "Fast-Neutron Effects on Type-304 Stainless Steel," Nucl. Appl. & Tech. 7, pp. 67-75 (1969).
- (21) H. J. Busboom and R. R. Asamoto, "Evaluation of Physical and Mechanical Properties of Type-304 Stainless Steel After Irradiation to  $3.9 \times 10^{22} \text{ n/cm}^2$  Total Fluence," GEAP-13571, February 1970.
- (22) T. Lauritzen, A. Withop and G. P. Ferguson, "Mechanical Properties Evaluation of Austenitic Stainless Steels Irradiated in EBR-II," GEAP-10066, July 1969.
- (23) L. D. Blackburn, A. L. WARD and J. M. Steichen, "Ductility of Irradiated Type 304 and 316 Stainless Steels," Presented at the International Conferences on Radiation Effects in Breeder Reactor Structural Materials, Scottsdale, Arizona, June 1977.
- (24) E. R. Gilbert and L. D. Blackburn, "Creep Deformation of 20 Percent Cold Worked Type 316 Stainless Steel", Trans. ASME 99 p. 168 (1977).

## 11.0 ACKNOWLEDGMENTS

The objective of the F/A structural evaluation presented in this document was to provide an analytical assessment of the functional adequacy of the F/A in the CRBRP core over the first and second reactor cycles. The scope of effort associated with accomplishing this objective was significant and required the contributions of many individuals in the areas of criteria formulation, development of analytical methods, and the implementation of the criteria and analytical methods in the structural evaluations. Acknowledgments of individuals most directly involved in accomplishing the objective of this document are as follows.

In the area of F/A criteria development, the guidance provided by J. L. Bitner, B. A. Bishop, H. D. Garkisch, V. J. Sazawal, and A. F. Snow of W-ARD was greatly appreciated. In addition, the guidelines provided by the National Working Group on FBR code components criteria under the direction of R. G. Sim, Chairman, and the General Electric FBR Department members, in particular, was appreciated.

With regard to the development analytical methods, recognition is given to the Swanson Analysis System personnel who provided guidance on the use of the ANSYS code. In the area of implementing an automated procedure for assessing crack initiation failure modes, special acknowledgment is given to M. A. Todd of W-ARD for developing the damage processor.

In the area of implementing the criteria through analytical methods, special recognition is given to A. D. Sane and M. A. Todd of W-ARD for their invaluable assistance in completing the structural evaluations within schedular constraints.

APPENDIX A  
DAMAGE PROCESSOR

Since the CRBRP First-Core Fuel Assembly is designed for a service life of two years and is subjected to various thermal transients and mechanical loads during this period, there exists a possibility of crack initiation at one or more critical locations during the two-year period. The identified mechanisms of crack initiation for the Fuel Assembly are local accumulation of creep-fatigue damage and local accumulation of inelastic strain (ratchetting). Criteria have been established to limit creep-fatigue damage and local strain accumulation to safe levels. Because the application of these criteria requires careful screening of the stress-strain history for the Fuel Assembly, with extensive calculation involved, the crack initiation assessment procedure was automated, a damage processor being prepared for use on the W-NES CDC 7600 computer system. This appendix describes the damage processor and illustrates the results obtained from its use.

The sequence of calculations and comparisons comprising a damage assessment are illustrated in the Damage Assessment Flow Chart, Figure A-1. As may be seen from the figure, the damage assessment procedure consists of two steps, stress analysis and damage calculation. The stress analysis, which is described elsewhere, supplies the stress-strain history for one duty cycle. This history then becomes the input to the damage processor. The stress-strain history supplied to the processor is not a complete time history. For purposes of calculating strain range for fatigue, only peak values are needed and are supplied. Creep calculations require a detailed stress-time history only if relaxation is occurring with time. In practice, the stress-strain history used by the damage processor is an edited one. Since the processor was written to make use of data generated by the ANSYS finite element computer program, it was possible to edit and combine the permanent files containing the stress-strain histories for the Fuel Assembly by means of a file combination option available with ANSYS.



The damage processor functions by calculating stress and strain parameters identified in the criteria as critical, calculating the damage factors associated with these parameters and screening the values obtained to determine peak damage factors and critical locations. The processor then prints an element-by-element list of the stress and strain parameters, damage factors and stress-strain-temperature-time data for the particular element, followed by a list of the peak damage factors and the numbers of the critical elements. Typical output data from the damage processor are reproduced in Tables A.1 and A.2. A listing of the damage processor source deck is in Table A.3.

Since it was intended to use the processor to supplement several analyses, involving different materials, the computer code was written so that necessary materials data would be obtained from separate subprograms. This arrangement allowed quick conversion when different materials were involved. Separate materials data packages, containing the necessary subprograms, were written for solution annealed and 20% cold-worked 316 stainless steels. Source deck listings for these two data packages are shown in Tables A.4 and A.5, respectively.

FIGURE A-1  
DAMAGE ASSESSMENT  
FLOW CHART

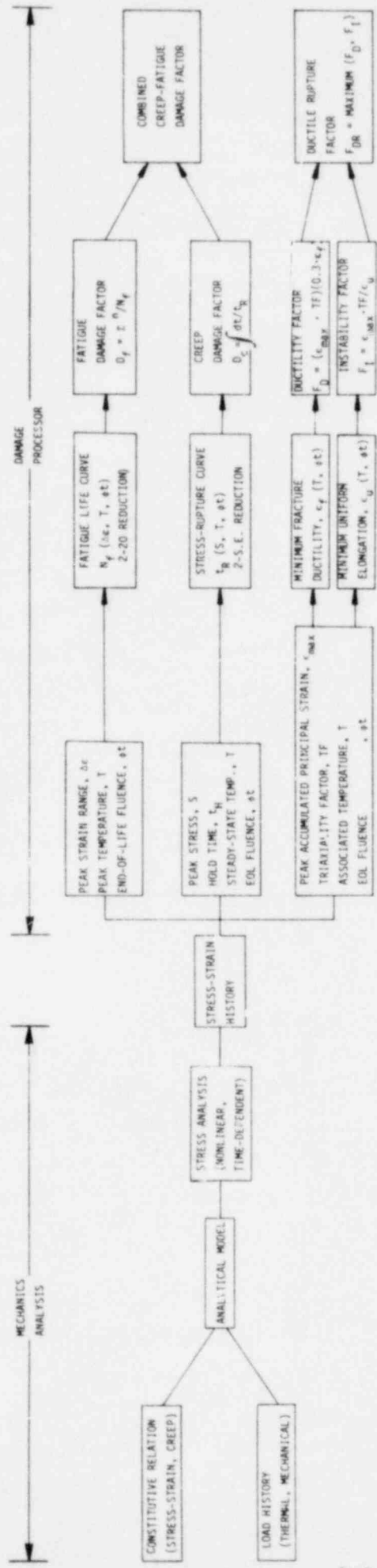


TABLE A.1  
DAMAGE PROCESSOR  
TYPICAL OUTPUT FOR ONE ELEMENT

DAMAGE ASSESSMENT FOR CRBR FIRST-CORE FUEL ASSEMBLY SHIELD BLOCK

DAMAGE AND STRAIN LIMIT ASSESSMENT FOR ELEMENT 98

FATIGUE DAMAGE

EQUIVALENT STRAIN IS CRITICAL  
 BETWEEN LOAD STEPS 3 AND 4  
 EQUIVALENT STRAIN RANGE = .4117E-02  
 PEAK TEMPERATURE = 911.2 DEG. F.  
 FATIGUE LIFE = .2505E+04 CYCLES  
 DAMAGE PER CYCLE = .39915E-03  
 DAMAGE FOR 40 CYCLES = .15966E-01

CREEP DAMAGE

PRINCIPAL STRESS IS CRITICAL  
 PEAK STRESS = .12579E+05 PSI  
 PEAK TEMPERATURE = 751.5 DEG. F.  
 MEAN RUPTURE TIME = .1437E+11 HRS.  
 HOLD TIME PER CYCLE = 240.0 HRS.  
 DAMAGE PER CYCLE = .16707E-07  
 DAMAGE FOR 40 CYCLES = .66827E-06

ACCUMULATED STRAIN LIMITS

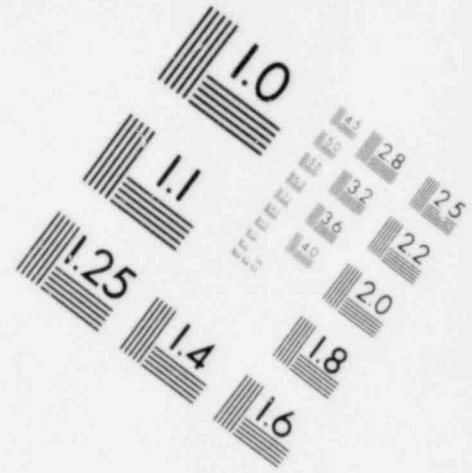
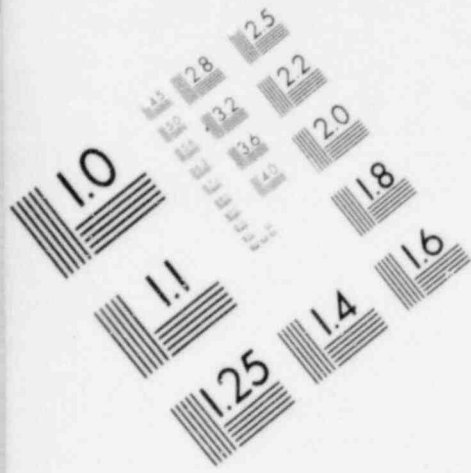
QUANTITY	DUCTILE RUPTURE CRITERION	GARKISCH CRITERION
CRITICAL LOAD STEP	4	4
MAXIMUM PRINCIPAL STRAIN	.9454E-02	.9454E-02
TRIAXIALITY FACTOR	2.099	2.099
METAL TEMPERATURE	802.4	802.4
FRACTURE DUCTILITY	.9723E+00	
UNIFORM ELONGATION		.7644E-01

COMBINED CREEP-FATIGUE DAMAGE FACTOR PER CYCLE = .39918E-03

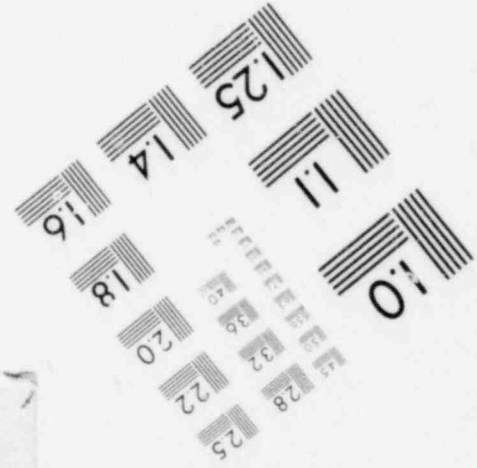
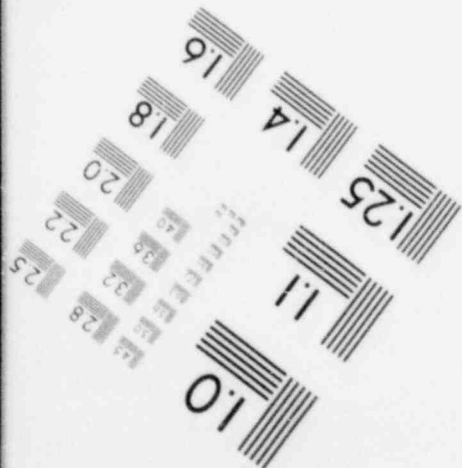
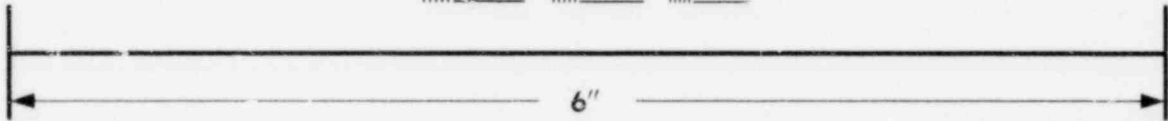
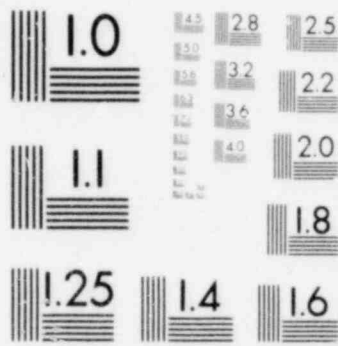
COMBINED CREEP-FATIGUE DAMAGE FACTOR FOR 40 CYCLES = .15967E-01

DUCTILE RUPTURE FACTOR = .68041E-01

GARKISCH FACTOR = .25962E+00



**IMAGE EVALUATION  
TEST TARGET (MT-3)**



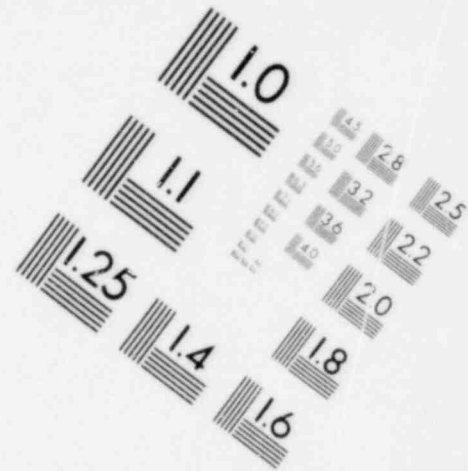
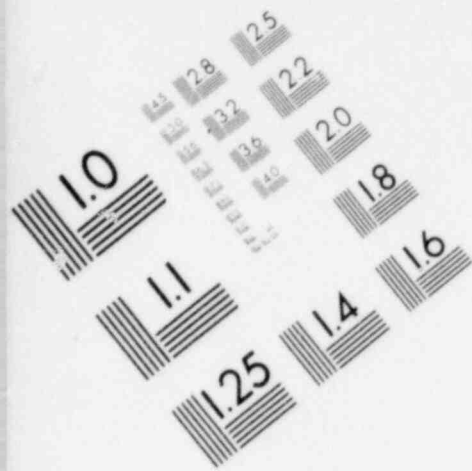


**IMAGE EVALUATION  
TEST TARGET (MT-3)**

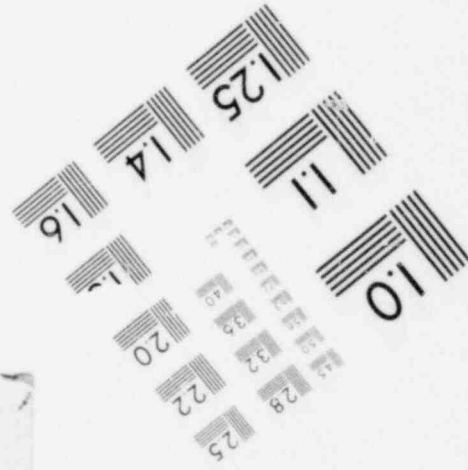
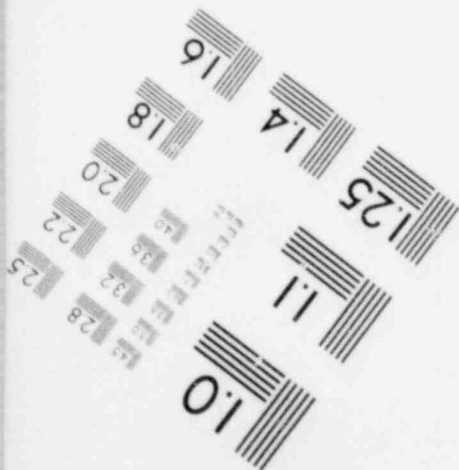
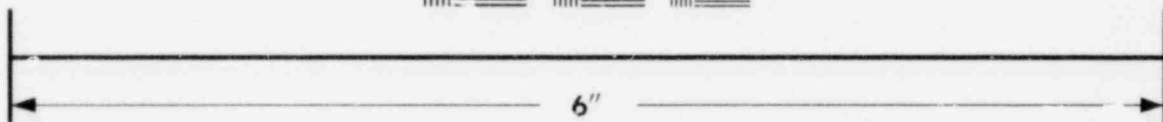
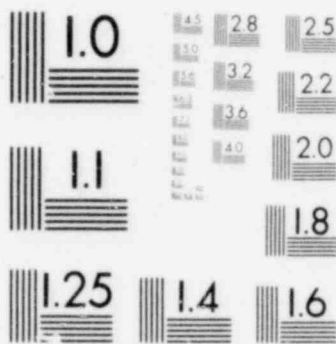


TABLE A.1  
(continued)

DAMAGE ASSESSMENT FOR CRBR FIRST-CORE FUEL ASSEMBLY SHIELD BLOCK

STRESS AND STRAIN COMPONENTS FOR ELEMENT 96

LOAD STEP	TIME/TEMP	STRESS/STRAIN COMPONENTS			
		XX	YY	XY	ZZ
1	0.00	.191440E+05	.254403E+04	-.582659E+04	.161040E+05
	751.51	.606958E-03	-.391966E-03	-.701344E-03	.423985E-03
2	0.00	.203789E+05	.275099E+04	-.618585E+04	.174530E+05
	588.11	.785838E-03	-.648861E-03	-.100713E-02	.549186E-03
3	0.00	-.252448E+05	-.366867E+04	.758769E+04	-.213185E+05
	911.23	-.164730E-02	.181938E-02	.243819E-02	-.102138E-02
4	0.00	.213205E+05	.310456E+04	-.639498E+04	.175705E+05
	802.43	.109082E-02	-.104301E-02	-.148965E-02	.662240E-03
5	0.00	-.163975E+05	-.193850E+04	.507721E+04	-.142120E+05
	819.43	-.706591E-04	-.318679E-03	-.165246E-03	-.160974E-03
6	0.00	.114780E+05	.163143E+04	-.347145E+04	.918887E+04
	751.51	.755441E-03	-.802412E-03	-.108663E-02	.423985E-03
7	0.00	.114780E+05	.163143E+04	-.347145E+04	.918887E+04
	751.51	.755441E-03	-.802412E-03	-.108663E-02	.423985E-03
8	240.00	.114780E+05	.163143E+04	-.347145E+04	.918887E+04
	751.51	.755441E-03	-.802412E-03	-.108663E-02	.423985E-03

TABLE A.2  
DAMAGE PROCESSOR  
MAXIMUM DAMAGE FACTORS  
TYPICAL OUTPUT

DAMAGE ASSESSMENT FOR CRBR FIRST-CORE FUEL ASSEMBLY SHIP

MAXIMUM DAMAGE FACTORS AND LOCATIONS

MAXIMUM FATIGUE DAMAGE FACTOR IS .15966E-01 AT ELEMENT 98  
MAXIMUM CREEP DAMAGE FACTOR IS .11442E-04 AT ELEMENT 106  
MAXIMUM COMBINED CREEP-FATIGUE DAMAGE FACTOR IS .15967E-01 AT ELEMENT 98  
MAXIMUM DUCTILE RUPTURE FACTOR IS .69172E-01 AT ELEMENT 98  
MAXIMUM GARYSCH FACTOR IS .26383E+01 AT ELEMENT 106





TABLE A.3  
(continued)

\*\*\*\* INPUT DATA REQUIREMENTS \*\*\*\*

INPUT TO THIS PROGRAM CONSISTS OF A PERMANENT FILE CONTAINING THE FINITE ELEMENT SOLUTION DATA SETS AND A DATA DECK OF TWO OR MORE CARDS CONTAINING INTEGER AND REAL VARIABLES DESCRIBING THE MODEL AND SOLUTION DATA.

THE PERMANENT FILE MUST BE AN ANSYS STRESS FILE (TAPE10) WRITTEN DURING A STATIC OR NON-LINEAR TRANSIENT DYNAMIC SOLUTION RUN, WITH A POST-PROCESSING OPTION OTHER THAN POST7 SPECIFIED. THIS FILE MUST BE ATTACHED AS TAPE10 FOR THE TOTDMG COMPUTATION. THE CONTENTS OF TAPE10 MUST BE AS FOLLOWS.

1. THE FIRST DATA SET MUST DESCRIBE THE INITIAL STEADY STATE OF THE MODEL OR THE STEADY STATE AT THE BEGINNING OF A NEW DUTY CYCLE.
2. THIS DATA SET MUST BE IMMEDIATELY FOLLOWED BY TWO OR MORE DATA SETS DESCRIBING THE FATIGUE SEQUENCE OF THE DUTY CYCLE.
3. THE FATIGUE SEQUENCE DATA SETS MUST BE FOLLOWED IMMEDIATELY BY TWO OR MORE DATA SETS DESCRIBING THE CREEP-RELAXATION SEQUENCE OF THE DUTY CYCLE.
4. THE LAST CREEP-RELAXATION DATA SET IS ASSUMED TO BE THE END-OF-CYCLE STEADY-STATE SOLUTION DATA SET FOR THE MODEL.

A FILE COPY OPERATION MAY BE NEEDED TO ACHIEVE THIS ORDERING OF DATA SETS.

NOTE THAT TOTDMG IMPLICITLY TREATS THE SOLUTION AS IF CREEP AND FATIGUE ARE OCCURRING SEPARATELY. THE FINITE ELEMENT ANALYSIS SHOULD BE PERFORMED IN A MANNER CONSISTENT WITH THIS ASSUMPTION.

THE DATA DECK CONSISTS OF TWO OR THREE CARD SETS, DESIGNATED CARD A, B, AND C. CARDS B AND C ARE REPEATED, CARD C IS OPTIONAL.

CARD A IS THE TITLE CARD. ITS CONTENTS WILL BE WRITTEN AS 80 ALPHANUMERIC CHARACTERS AT THE HEAD OF EACH PAGE OF PRINTOUT.

CARD B CONTAINS INTEGER AND REAL DATA, READ AS FOLLOWS.

COLUMNS	VARIABLE	DEFINITION
1-6	NFTG	NO. OF FATIGUE DATA SETS ON TAPE10 (INTEGER)
7-12	NCRP	NO. OF CREEP DATA SETS ON TAPE10 (INTEGER)
13-18	NEL	NO. OF ELEMENTS IN MODEL (INTEGER)
19-24	NPR	NO. OF ACTIVE ELEMENTS TO BE ASSESSED (INTEGER)
25-30	NCYC	NO. OF DUTY CYCLES CONSTITUTING THE SERVICE LIFE (INTEGER)
31-42	FLNC	IRRADIATION FLUENCE AT END OF DUTY CYCLE IN UNITS OF $1.E+22$ NEUTRONS/CM <sup>2</sup> . (REAL)
43-54	PCRP	CONFIDENCE FACTOR FOR STRESS-RUPTURE CALCULATION (DIFFERENCE BETWEEN NOMINAL AND DESIGN RUPTURE STRENGTH EXPRESSED IN STANDARD DEVIATIONS) (REAL)

CARD C IS OPTIONAL, TO BE INCLUDED ONLY IF NPR IS SMALLER THAN NEL. CARD C, WHICH MAY BE REPEATED AS NECESSARY, CONTAINS THE NUMBERS OF THE ACTIVE ELEMENTS IN ASCENDING ORDER. A TOTAL OF NPR NUMBERS MUST BE PROVIDED. THE FORMAT FOR EACH CARD IS I3I6.



TABLE A.3  
(continued)

```

SUBROUTINE FIRST (SIGMA, EPSLN, TEMP, TIME, NLIST, NSETS, NPR, NEL, NEI,
1  NCRP, NCCYC, FLNC)
C THIS SUBROUTINE READS AND STORES THE DATA ON TAPE10
DIMENSION W(34), IW(34), SIGMA(4, NSETS, NPR), EPSLN(4, NSETS, NPR),
1  TEMP(NSETS, NPR), TIME(NSETS), NLIST(NPR)
EQUIVALENCE (IW(1), W(1))
COMMON/TITLE/HEAD(8)
IF (NPR.LT.NEL) READ(5,98) (NLIST(I), I=1, NPR)
WRITE (6,96) (HEAD(I), I=1, 8)
2 WRITE (6,94) NSETS, NSETS, NCRP, NCCYC, FLNC, NPR, NEL
CALL READST (IW, 10)
N = 7
DO 4 I=1, NSETS
CALL READER (IW, N)
TIME(1) = W(1)
K = 1
DO 4 IEL=1, NEL
CALL READER (IW, N)
C STORE ONLY THE DATA FROM THE ACTIVE ELEMENTS
IF ((NPR.LT.NEL).AND.(NLIST(K).NE.IEL)) GO TO 4
TEMP(I, K) = W(10)
DO 3 J=1, 4
C MECHANICAL STRAIN = ELASTIC + PLASTIC + ORIGIN SHIFT + CREEP + SWELLING
EPSLN(J, I, K) = W(10+J) + W(14+J) + W(18+J) + W(22+J) + W(34)
3 SIGMA(J, I, K) = W(6+J)
SIGMA(4, I, K) = W(4)
EPSLN(3, I, K) = EPSLN(3, I, K) - W(34)
K = K + 1
4 CONTINUE
RETURN
94 FORMAT (////16X, 'THE DUTY CYCLE IS DEFINED BY 13, LOAD STEPS, IN
1 INCLUDING THE INITIAL STEADY STATE, //15X, 12, LOAD STEPS DEFINING THE
2 THE FATIGUE SEQUENCE, AND 13, LOAD STEPS DEFINING THE CREEP AND SWELLING
3 SEQUENCE. THIS DAMAGE ASSESSMENT IS FOR 13, SUCH DUTY CYCLES.
4 THE END-OF-LIFE //16X, 'FAST FLUENCE FOR THIS COMPONENT IS
5 6.6E+22 NEUTRONS/CM2 (E, DT, 0.1 MEV). //16X, 'DAMAGE APPROPRIATE
6 ARE PRINTED FOR 14, OF THE 14, ELEMENTS IN THE FILE
7
8
9
10
11
12
13
14
15
16
17
18
19
20
21
22
23
24
25
26
27
28
29
30
31
32
33
34
35
36
37
38
39
40
41
42
43
44
45
46
47
48
49
50
51
52
53
54
55
56
57
58
59
60
61
62
63
64
65
66
67
68
69
70
71
72
73
74
75
76
77
78
79
80
81
82
83
84
85
86
87
88
89
90
91
92
93
94
95
96
97
98
99

```

TABLE A.3  
(continued)

```

SUBROUTINE SECOND (SIGMA, EPSLN, TEMP, TIME, NI IST, IPR, NSET, NE, NCRP,
1 NFTG, NCRP, NCV, FLNC, EPRP)
C THIS SUBROUTINE PERFORMS ALL DAMAGE CALCULATIONS
DIMENSION LBLFTG(2), LBLCRP(4), SIGMA(4, NSETS, NPR), TEMP(NSET, NE),
1 EPSLN(4, NSETS, NPR), TIME(NSETS), NI IST(NPR), IPR(2, NPR), EPRP(2,
COMMON/TITLE/HEAD(8)
DATA LBLCRP/8HPRINCIPA, 8HL STRESS, 8HSTRESS 1, 8HNT-NCTY/,
1 LBLFTG/10HEQUIVALENT, 10HPRINCIPAL /
IFEN = NSETS - NCRP
IFST = IFEN - NFTG + 1
IFEN1 = IFEN - 1
ICST = IFEN + 1
C INITIALIZE PEAK DAMAGE VALUES AND LOCATION TAGS
FATDAM = 0.0
CRPDAM = 0.0
TUTDAM = 0.0
RUPDUC = 0.0
HANGAR = 0.0
IELFAT = 0
IELCRP = 0
IELTOT = 0
IELRUP = 0
IELGAR = 0
C CALCULATE DAMAGE FOR ALL ACTIVE ELEMENTS
DO 60 N=1, NPR
IEL = N
IF (NPR .LT. NE) IEL = NI IST(N)
C FATIGUE DAMAGE CALCULATION
11 CYMIN = 1.E30
EPRTG = 0.0
JFTG = 0
IFTG = 0
EFTG = 0
JFTG = 0.0
C OPEN ALL FATIGUE CYCLES TO FIND MOST DAMAGING STRAIN RANGE
DO 14 I=IFST, IFEN1
IAT = I + 1
DO 14 J=IP1, IFEN
DO 12 K=1, 4
12 EP(K) = EPCN(X(I, N) - EPCN(X(J, N)) - EPR - NCTY, I, K)
C PICK LARGER OF TWO STRAIN RANGES
EP2 = ABS(OC - R)
EP3 = ABS(EP(4))
EPPR = AMAX1(EP1, EP2, EP3)
C CALCULATE EQUIVALENT STRAIN RANGE
EPEQ = SQRT(3.*RR**2 + (OC-EP(4))**2)/1.5
C PICK LARGER OF TWO STRAIN RANGES
BIG = EPEQ
L = 1
IF (BIG .GE. EPPR) GO TO 13
BIG = EPPR
L = 2
13 TIJ = AMAX1(TEMP(I, N), TEMP(J, N))
C DESIGN FATIGUE LIFE COMES FROM FTGLIF FUNCTION
CYIJ = FTGLIF(BIG, TIJ, FLNC)
IF (CYMIN .LE. CYIJ) GO TO 14
C IF THIS IS WORST CASE SO FAR, RESET FATIGUE LIFE, STRAIN RANGE AND POINTERS.
CYMIN = CYIJ
EPRTG = BIG
IFTG = I
JFTG = J

```

TABLE A.3  
(continued)

```

LFTG = L
TFTG = TIJ
14 CONTINUE
C CALCULATE FATIGUE DAMAGE (PER CYCLE AND TOTAL) FOR THIS ELEMENT.
  FDPC = 1. / CYMIN
  FDLFTM = FDPC * FLOAT(NCYC)
  IF (FATDAM .GE. FDLFTM) GO TO 21
C IF THIS ELEMENT IS WORST SO FAR, RESET PEAK DAMAGE VALUE AND LOCATION TAG.
  FATDAM = FDLFTM
  IELFAT = IEL
C CREEP DAMAGE CALCULATION
C INITIALIZE STRESSES AND MEAN RUPTURE TIME
  21 HISI = 0.0
  HISM = 0.0
  TCRP = 0.0
  DO 22 I=ICST,NSETS
    QC = 0.5 * (SIGMA(1,I,N) + SIGMA(2,I,N))
    RR = SQRT (0.25 (SIGMA(1,I,N)-SIGMA(2,I,N))2+SIGMA(4,I,N)2)
C CALCULATE PRINCIPAL NORMAL STRESSES AND SELECT LARGEST VALUE
    S1 = ABS(QC + RR)
    S2 = ABS(QC - RR)
    S3 = ABS(SIGMA(4,I,N))
    S4 = ABS(SIGMA(3,I,N))
    SM = MAX(S1,S2,S3,S4)
C SAVE HIGHEST VALUE OF PRINCIPAL STRESS
    HISM = AMAX1(HISM,SM)
C CALCULATE PRINCIPAL STRESS DIFFERENCES AND SELECT LARGEST VALUE
    S1 = QC + RR - SIGMA(4,I,N)
    S2 = RR + RR
    S3 = ABS(S1 - S2)
    S1 = ABS(S1)
    S1 = AMAX1(S1,S2,S3)
C SAVE HIGHEST STRESS INTENSITY
    HISI = AMAX1(HISI,S1)
C SAVE HIGHEST TEMPERATURE
    TIJ = TEMP(I,N)
    TCRP = AMAX1(TIJ,TCRP)
C DAMAGE RATE IS INVERSE OF RUPTURE TIME, OBTAINED FROM RUPTIM FUNCTION
    DMG(1,I-IFEN) = 1. / RUPTIM ( SI, TIJ, FLNC, PCRP )
    22 DMG(2,I-IFEN) = 1. / RUPTIM ( SM, TIJ, FLNC, PCRP )
    DGI = 0.0
    DGM = 0.0
C INTEGRATE DAMAGE RATE BY TRAPEZOIDAL RULE TO OBTAIN DAMAGE
    DO 23 I=2,NCRP
      DELT = TIME(IFEN+I) - TIME(IFEN+I-1)
      IF (DELT .LE. 0.0) GO TO 20
      DGI = DGI + 0.5 * DELT * (DMG(1,I) + DMG(1,I-1))
    23 DGM = DGM + 0.5 * DELT * (DMG(2,I) + DMG(2,I-1))
C SELECT HIGHER OF TWO DAMAGE VALUES AND SET TAG.
    CDPC = DGM
    L = 1
    STRESS = HISM
    IF ( DGM .GE. DGI ) GO TO 24
    STRESS = HISI
    L = 3
    CDPC = DGI
  24 THOLD = TIME(NSETS) - TIME(ICST)
    TRUP = THOLD / CDPC
    CDLFTM = CDPC * FLOAT(NCYC)
    IF (CRPDAM .GE. CDLFTM) GO TO 31
C IF THIS IS WORST ELEMENT SO FAR, SAVE DAMAGE VALUE AND RESET TAG.
    CRPDAM = CDLFTM
    IELCRP = IEL

```



TABLE A.3  
(continued)

```

EPMPI = EPI
IEPPI = I
EPELNG = EPINS
TRFACI = TF
GARFAC = FHG
TMPLNG = TIJ
44 CONTINUE
C IF WORST LOCATION, RESET VALUES AND TAGS
  IF (HANGAR .GE. GARFAC) GO TO 45
  HANGAR = GARFAC
  IELGAR = IEL
45 IF (RUPDUC .GE. RUPFAC) GO TO 51
  RUPDUC = RUPFAC
  IELRUP = IEL
C PRINT CALCULATED DAMAGE FACTORS, ETC.
51 WRITE (6,96) (HEAD(I),I=1,8)
  WRITE (6,101) IEL
  WRITE (6,102) LBLFTG(LFTG),LBLCRP(L),LBLCRP(L+1),IFTG,JFTG,STRESS,
1  LBLFTG(LFTG),EPFTG,TRP,TFGT,TRUP,CYMIN,THOLD,FDPC,CDPC,NCYC,
2  FDLFTM,NCYC,CDLFTM
  WRITE (6,103) IEPFR,IEPPI,EPMPR,EPMPI,TRFACF,TRFACI,TMPRUP,TMPLNG,
1  EPFRAC,EPELNG
  WRITE (6,104) TDPG,NCYC,TDLFTM,RUPFAC,GARFAC
C PRINT STRESSES AND STRAINS
  WRITE (6,96) (HEAD(I),I=1,8)
  WRITE (6,130) IEL
  DO 60 I=1,NSETS
  WRITE (6,131) I,TIME(I),(SIGMA(J,I,N),J=1,4),TEMP(I,N),
1  (EPSLN(J,I,N),J=1,4)
60 CONTINUE
C PRINT WORST-CASE DAMAGE FACTORS AND LOCATIONS.
  WRITE (6,96) (HEAD(I),I=1,8)
  WRITE (6,110) FATDAM,IELFAT,CRPDAM,IELCRP,TOTDAM,IELTOT,RUPDUC,
1  IELRUP,HANGAR,IELGAR
  RETURN
C ERROR MESSAGE FOR ZERO OR NEGATIVE TIME INCREMENT.
70 WRITE (6,120) (TIME(J),J=ICST,NSETS)
95 FORMAT (1H0,16X,8A10)
96 FORMAT (1H1,///16X,8A10)
101 FORMAT (///31X,*DAMAGE AND STRAIN LIMIT ASSESSMENT FOR ELEMENT*,
1  I4)
102 FORMAT (/26X,*FATIGUE DAMAGE*,33X,*CREEP DAMAGE*//16X,A10,* STRAIN
1  IS CRITICAL*,17X,2A8,* IS CRITICAL*/16X,*BETWEEN LOAD STEPS*,13,*
2  AND*,13,18X,*PEAK STRESS *=,E11.5,* PSI*/16X,A10,* STRAIN RANGE =
3  *,E10.4,11X,*PEAK TEMPERATURE *=,F7.1,* DEG. F.*/16X,*PEAK TEMPERA
4  TURE *=,F7.1,* DEG. F.*/13X, EAM RUPTURE TIME =,E10.4,* HRS.*/
5  16X,*FATIGUE LIFE =,E10.4,* CYCLES*,15X,*HOLD TIME PER CYCLE =,
6  F7.1,* HRS.*/16X,*DAMAGE PER CYCLE =,E11.5,17X,*DAMAGE PER CYCLE
7  =,E11.5/16X,*DAMAGE FOR*,I4,* CYCLES =,E11.5,12X,*DAMAGE FOR*,I4
8  ,* CYCLES =,E11.5)
103 FORMAT (///43X,*ACCUMULATED STRAIN LIMITS*/56X,*DUCTILE RUPTURE*,
112X,*GARKISCH*/37X,*QUANTITY*,14X,*CRITERION*,14X,*CRITERION*/27X
2  ,*CRITICAL LOAD STEP*,2I23/21X,*MAXIMUM PRINCIPAL STRAIN*,2F23.4/
3  327X,*TRIAxIALITY FACTOR*,2F23.5/28X,*METAL TEMPERATURE*,2F23.1/27X
4  ,*FRACTURE DUCTILITY*,E23.4/27X,*UNIFORM ELONGATION*,23X,E23.4)
104 FORMAT (///29X,*COMBINED CREEP-FATIGUE DAMAGE FACTOR PER CYCLE =,
1  E,1.5//24X,*COMBINED CREEP-FATIGUE DAMAGE FACTOR FOR*,I4,* CYCLES
2  =,E11.5//53X,*DUCTILE RUPTURE FACTOR =,E11.5//60X,*GARKISCH FAC
3  TOR =,E11.5)
110 FORMAT (///38X,*MAXIMUM DAMAGE FACTORS AND LOCATIONS*///27X,*MAXIM
1  UM FATIGUE DAMAGE FACTOR IS*,E11.5,* AT ELEMENT*,I4//28X,*MAXIMUM
2  CREEP DAMAGE FACTOR IS*,E11.5,* AT ELEMENT*,I4//19X,*MAXIMUM COMBI
3  NED CREEP-FATIGUE DAMAGE FACTOR IS*,E11.5,* AT ELEMENT*,I4//26X,*M
4  AXIMUM DUCTILE RUPTURE FACTOR IS*,E11.5,* AT ELEMENT*,I4//30X,*MAX
5  SIMUM GARKISCH FACTOR IS*,E11.5,* AT ELEMENT*,I4)
120 FORMAT (///13X,*INPUT DATA ERROR--CREEP TIME STEP IS NEGATIVE--CALC
1  ULATION TERMINATED--CREEP TIMES ARE*//16X,(8F10.2))
130 FORMAT (///34X,*STRESS AND STRAIN COMPONENTS FOR ELEMENT*,I4//16X,
1  1,10A1, TIME/TEMP*,22X,*STRESS/STRAIN COMPONENTS*/16X,*STEP*,21X,
2  2,XX,3,XX,4,YY,14X,5,YY,14X,6,ZZ)
131 FORMAT (/16X,13,F13.2,4F16.6/19X,F13.2,4F16.6)
  RETURN

```



TABLE A.3 (Cont)

```
SUBROUTINE READER (LL,N)
DIMENSION LL(1),NBLOCK(600)
DATA NT,KLSIZ,NCBLK,NINBLK,NFBLK /10,600,0,0,1/
MM=NCBLK
GO TO 10
ENTRY READST
NT=IABS(N)
NINBLK=0
NFBLK=1
NCBLK=0
KLSIZ=600
RETURN
10 IF ((MM+2).LE. NINBLK) GO TO 12
   IF ((NBLOCK(MM).LT.0) .AND. (MM.GT.0)) GO TO 14
   IF (NFBLK .GT. 0) REWIND NT
   READ (NT) IX,(NBLOCK(I),I=1,IX)
   IF (EOF(NT)) 14,13
14 N= -1
   RETURN
13 NFBLK= -1
   NINBLK = IX
   MM = 0
12 MM = MM + 1
   N = NBLOCK(MM)
   DO 11 I = 1,N
   MM = MM + 1
11 LL(I) = NBLOCK(MM)
   MM = MM + 1
   NCBLK = MM
RETURN
END
```



TABLE A.4  
MATERIAL DATA PACKAGE FOR SA 316 SS  
SOURCE DECK LISTING

```

FUNCTION FTGLIF (DELEP, TEMP, FLUENC)
C
C FTGLIF CALCULATES DESIGN FATIGUE LIFE FOR SA316SS, USING UNIVERSAL SLOPES
C CORRELATION AND 2-20 REDUCTION RULE
C
C          DEFINITION OF TERMS
C DELEP = STRAIN RANGE (INPUT)
C TEMP = METAL TEMPERATURE IN DEG. F. (INPUT)
C FLUENC = FAST FLUENCE IN E22 N/CM2 (INPUT)
C FTGLIF = FATIGUE LIFE IN CYCLES (OUTPUT)
C
C FUNCTION EPFMIN (TEMP, FLUENC) IS EXTERNAL TO THIS PROGRAM AND MUST BE SUPPLIED
C AS A PART OF THE MATERIAL PROPERTY PACKAGE
C
C
C CALCULATE TRUE FRACTURE STRAINS FOR IRRADIATED AND UNIRRADIATED MATERIAL.
  EPFI = EPFMIN (TEMP, FLUENC)
  EPFU = EPFMIN (TEMP, 0.0)
C COEFFICIENT FOR PLASTIC STRAIN TERM
  A = (EPFU**(-0.4)) * EPFI
C FOR TEMPERATURES LESS THAN 800 F, USE 800 F DATA.
  T = AMAX1(TEMP, 800.)
  E = 28336690. - T * (2882.211 + T*(3.697849 - .0007709188*T))
  U = ( ( (.8634445E-07*T - .3247471E-03)*T + .3678569 ) *T
    - 161.4171 ) * T + 100220.8
C COEFFICIENT FOR ELASTIC STRAIN TERM
  B = 3.5 * U / E
C SET MINIMUM STRAIN VALUE TO AVOID OBTAINING INFINITE FATIGUE LIFE.
  Y = AMAX1(DELEP, 5.E-04)
C DEFINE COEFFICIENTS FOR NEWTON EXTRAPOLATION METHOD.
  Q = Y/B
  R = 5.*A/B
C CALCULATE INITIAL VALUE OF XI.
  XI = Q * ( 0.8 + 0.2/(R*Q**4 + 1.) )
C CALCULATE DX.
  1 DX = 0.2 * XI + (0.8*XI - Q)/(R*XI**4 + 1.)
C CALCULATE NEW VALUE OF XI.
  XI = XI - DX
C TEST FOR CONVERGENCE.
  IF ( ABS(DX/XI) .GE. 1.E-04 ) GO TO 1
C CALCULATE FATIGUE LIFE FOR LIFE FACTOR OF 20.
  FL1 = 0.05 * XI**(-8.333333333333333)
C REPEAT NEWTON EXTRAPOLATION FOR STRAIN FACTOR OF 2.
  Y = Y * Y
  Q = Q + Q
  XJ = Q * ( 0.8 + 0.2/(R*Q**4 + 1.) )
  2 DX = 0.2 * XJ + (0.8*XJ - Q)/(R*XJ**4 + 1.)
  XJ = XJ - DX
  IF ( ABS(DX/XJ) .GE. 1.E-04 ) GO TO 2
  FL2 = XJ**(-8.333333333333333)
C SELECT SMALLER VALUE OF FATIGUE LIFE AS OUTPUT VALUE.
  FTGLIF = AMIN1(FL1, FL2)
  RETURN
  END

```

TABLE A.4

(continued)

```

FUNCTION EPFMIN(T,F)
C
C EPFMIN CALCULATES MINIMUM FRACTURE DUCTILITY FOR SA316SS FROM AN EMPIRICAL
C CORRELATION DEVELOPED BY GE
C
C      DEFINITION OF TERMS
C      T = TEMPERATURE IN DEG F
C      F = IRRADIATION FLUENCE IN 1.E22 N/CM2
C      EPFMIN = MINIMUM FRACTURE DUCTILITY
C
C DIVIDE TEMPERATURE BY 1000
  TT = T * .001
C FOR TEMPERATURES LESS THAN 800 F, USE 800 F DATA
  TT = AMAX1(TT,.8)
C CALCULATE THRESHOLD FLUENCE FOR REDUCTION OF DUCTILITY
  FO = 1.4 - TT
  IF (T .GT. 1200.) FO = TT - 1.0
C CALCULATE MINIMUM DUCTILITY FOR UNIRRADIATED MATERIAL
  EPO = .45 / (SQRT(TT) * (TT**3))
  IF (T .GT. 1000.) EPO = EPO/(TT**2)
  IF (F .LE. FO) GO TO 1
C IF FLUENCE EXCEEDS THRESHOLD FLUENCE, APPLY DUCTILITY REDUCTION FACTOR
  ZZ = TT - 1.7
  EPO = EPO * ((F/FO)**ZZ)
1 EPFMIN = EPO
  RETURN
END

```

```

FUNCTION RUPTIM(SIGMA,TEMP,FLUENC,CONF)
C
C RUPTIM CALCULATES DESIGN RUPTURE TIME FOR SA316SS, USING AN EMPIRICAL FIT
C TO EXPERIMENTAL DATA FROM HEDL.
C      DEFINITION OF TERMS
C      TEMP--METAL TEMPERATURE IN DEG. F.
C      SIGMA--CRITICAL STRESS IN PSI
C      FLUENC--FLUENCE IN 1.E+22 NEUTRONS/CM2
C      CONF--CONFIDENCE FACTOR ON RUPTURE TIME
C
C CALCULATE STRENGTH REDUCTION FACTOR FOR SODIUM EXPOSURE
  ALPHA = 1270. - 0.3*TEMP
  ALPHA = AMIN1(ALPHA,1000.)
C CALCULATE AUGMENTED STRESS INCLUDING SODIUM EXPOSURE FACTOR
  S = AMAX1(SIGMA,1000.)/ALPHA
C FOR TEMPERATURES LESS THAN 800 F, USE 800 F DATA
  T = AMAX1(TEMP,800.)
  BETA = ALOG10(S)
C FIRST CALCULATE LARSON-MILLER PARAMETER FOR UNIRRADIATED MATERIAL
  Q1 = 49950. - (520.*CONF + BETA*(5270. + 2995.*BETA))
  IF (FLUENC .GT. 0.) GO TO 1
C IF FLUENCE IS ZERO, USE UNIRRADIATED DATA FOR RUPTURE TIME
  Q2 = Q1
  GO TO 2
C IF FLUENCE IS GREATER THAN ZERO, CALCULATE LMP USING IRRADIATED DATA
  Q2 = 54*(14. - (290.*CONF + 13353.*BETA + 1311.*ALOG10(FLUENC)))
C USE SMALLER VALUE OF LMP TO CALCULATE RUPTURE TIME
  Z2 = -20. + AMIN1(Q1,Q2)/(T + 460.)
  RUPTIM = 10. - Z2
  RETURN
END

```

TABLE A.4  
(continued)

```
FUNCTION ELUNIF (TEMP,FLUENC)
C
C ELUNIF CALCULATES MINIMUM TRUE UNIFORM ELONGATION FOR SA316SS, USING A
C CORRELATION DEVELOPED BY GE.
C
C          DEFINITION OF TERMS
C TEMP = TEMPERATURE IN DEG F
C FLUENC = IRRADIATION FLUENCE (FAST) IN 1.E22 N/CM2
C ELUNIF = MINIMUM TRUE UNIFORM ELONGATION
C
C FOR TEMPERATURES LESS THAN 800 F, USE 800 F DATA
  T = AMAX1(TEMP,800.)
C CALCULATE ENGINEERING UNIFORM ELONGATION FOR UNIRRADIATED MATERIAL, USING
C POLYNOMIAL CORRELATION FOR BAR STOCK FROM NSM HANDBOOK.
  EU = (((((((((0.6172085E-29*T-.6840613E-25)*T+.2987206E-21)*T -
  1 .694287E-18)*T+.960199E-15)*T-.8284638E-12)*T+.452497E-09)*T -
  2 .1554308E-06)*T+.3283548E-04)*T-.004073204)*T + .4965583
C IF FLUENCE IS ABOVE THRESHOLD VALUE OF 0.1, APPLY IRRADIATION CORRECTION.
  IF (FLUENC .LE. 0.1) GO TO 1
  EU = EU / (10. * FLUENC)
C CALCULATE TRUE STRAIN VALUE FROM ENGINEERING STRAIN VALUE.
  1 FLUNIF = ALOG(1. + EU)
  RETURN
FN:
```

TABLE A.5  
 MATERIAL DATA PACKAGE FOR CW-316-SS  
 SOURCE DECK LISTING

```

FUNCTION FTGLIF (DELEP, TEMP, FLUENC)
C
C FTGLIF CALCULATES DESIGN FATIGUE LIFE FOR CW316SS, USING UNIVERSAL SLOPES
C CORRELATION AND 2-20 REDUCTION RULE
C
C      DEFINITION OF TERMS
C      DELEP = STRAIN RANGE (INPUT )
C      TEMP = METAL TEMPERATURE IN DEG. F. (INPUT)
C      FLUENC = FAST FLUENCE IN E22 N/CM2 (INPUT)
C      FTGLIF = FATIGUE LIFE IN CYCLES (OUTPUT)
C
C FUNCTION EPFMIN (TEMP,FLUENC) IS EXTERNAL TO THIS PROGRAM AND MUST BE SUPPLIED
C AS A PART OF THE MATERIAL PROPERTY PACKAGE
C
C
C CALCULATE TRUE FRACTURE STRAINS FOR IRRADIATED AND UNIRRADIATED MATERIAL.
  EPFI = EPFMIN (TEMP,FLUENC)
  EPFU = EPFMIN (TEMP,0.0)
C COEFFICIENT FOR PLASTIC STRAIN TERM
  A = (EPFU**(-0.4)) * EPFI
C FOR TEMPERATURES LESS THAN 800 F, USE 800 F DATA.
  T = AMAX1(TEMP,800.)
  E = 29336690. - T * (2882.211 + T*(3.697849 - .0007709188*T) )
  U = 78918. + T * (36.854 - .047012 * T)
C COEFFICIENT FOR ELASTIC STRAIN TERM
  B = 3.5 * U / E
C SET MINIMUM STRAIN VALUE TO AVOID OBTAINING INFINITE FATIGUE LIFE.
  Y = AMAX1(DELEP,5.E-04)
C DEFINE COEFFICIENTS FOR NEWTON EXTRAPOLATION METHOD.
  Q = Y/B
  R = 5.*A/B
C CALCULATE INITIAL VALUE OF XI.
  XI = Q * ( 0.8 + 0.2/(R*Q**4 + 1.) )
C CALCULATE DX.
  1 DX = 0.2 * XI + (0.8*XI - Q)/(R*XI**4 + 1.)
C CALCULATE NEW VALUE OF XI.
  XI = XI - DX
C TEST FOR CONVERGENCE.
  IF ( ABS(DX/XI) .GE. 1.E-04 ) GO TO 1
C CALCULATE FATIGUE LIFE FOR LIFE FACTOR OF 20.
  FL1 = 0.05 * XI**(-8.33333333333333)
C REPEAT NEWTON EXTRAPOLATION FOR STRAIN FACTOR OF 2.
  Y = Y + Y
  Q = Q + Q
  XJ = Q * ( 0.8 + 0.2/(R*Q**4 + 1.) )
  2 DX = 0.2 * XJ + (0.8*XJ - Q)/(R*XJ**4 + 1.)
  XJ = XJ - DX
  IF ( ABS(DX/XJ) .GE. 1.E-04 ) GO TO 2
  FL2 = XJ**(-8.33333333333333)
C SELECT SMALLER VALUE OF FATIGUE LIFE AS OUTPUT VALUE.
  FTGLIF = AMIN1(FL1,FL2)
  RETURN
  END

```

TABLE A.5  
(continued)

```

FUNCTION RUPTIM (SGPRNC,TF,FLNC,DUMMY)
REAL LMP
DIMENSION XHAT(2),XBAR(2),SIGX(2),CORREL(2),A(4),B(4),C(4),
1 XBR(4),XSIG(4),N(4),STDERR(4),COR(4),TSTAT(4),TOLFACT(4),
2 AX(2),BX(2),XBR2(4),XSIG2(4),COR2(4)
DATA (A(J),J=1,4)/58826.0,35599.0,64292.0,44270.0
1 /,(B(J),J=1,4)/0.0,6.9413,0.0,2.2947
2 /,(C(J),J=1,4)/-6135.8,-2637.0,-7762.1,-3040.0
3 /,(XBR(J),J=1,4)/0.0,1760.0,0.0,1823.6
4 /,(XBR2(J),J=1,4)/3.6800,2.8154,3.9666,2.3714
5 /,(XSIG(J),J=1,4)/0.0,92.195,0.0,48.105
6 /,(XSIG2(J),J=1,4)/0.38416,0.23989,0.24960,0.37468
7 /,(N(J),J=1,4)/85,40,37,11
8 /,(STDERR(J),J=1,4)/300.84,199.28,469.89,308.97
1 /,(COR(J),J=1,4)/4*1.0/(COR2(J),J=1,4)/4*1.0
2 /,(TSTAT(J),J=1,4)/1.989,2.026,2.032,2.306
4 /,(AX(K),K=1,2)/763.959,69.405
5 /,(BX(K),K=1,2)/-1.9839E-03,-4.8595E-04 /

C
C THIS COMPUTES TIME TO RUPTURE (HR) FOR 20 PCT CW 316
C MODEL ** LMP=A+B*TR+C*LN(SIG)
C SIG=MAX PRINCIPAL STRESS (KSI) OR STRESS INTENSITY (KSI)
C TR=TEMP (DEG R)
C TRANSITION GIVEN BY ** SIGT=AX*EXP(BX/TR)
C POST TRANSITION IF SIG.LT.SIGT (BRITTLE RUPTURE)
C J=1 FOR UN-IRR,PRE-TRANSITION
C J=2 FOR UN-IRR,POST-TRANSITION
C J=3 FOR IRR,PRE-TRANSITION
C J=4 FOR IRR,POST-TRANSITION
C ENTERED WITH****
C TF=TEMPERATURE IN DEG. F.
C SGPRNC=MAX PRINCIPAL STRESS OR STRESS INTENSITY (PSI)
C ICOD = 1 FOR UN-IRR,NO SODIUM
C       =2 FOR IRR,NO SODIUM
C       =3 FOR UN-IRR,IN SODIUM
C       =4 FOR IRR, IN SODIUM
C RETURNS ****
C RUPTIM=LOWER VALUE RUPTURE TIME FOR 2-STD.DEVIATION CONFIDENCE BAND
C GET TEMP (DEG R) AND STRESS (KSI)
TR=TF+460.0
SIG = SGPRNC * 0.001
SIG = AMAX1(SIG,1.0)
C SELECT CONSTANTS
ICOND = 3
IF ( FLNC .GT. 0.0) ICOND = 4
J=1
K=1
IF (ICOND.EQ.2.OR.ICOND.EQ.4)J=3
IF (ICOND.EQ.2.OR.ICOND.EQ.4)K=2
SIGT=AX(K)*EXP(BX(K)*TR)
IF (SIG.LT.SIGT)J=J+1
LMP = A(J) + (B(J) - ALOG10(4.0))* TR + C(J) * ALOG(SIG)
XHAT(1)=TR
XBAR(1)=XBR(J)
SIGX(1)=XSIG(J)
CORREL(1)=COR(J)
XHAT(2)=ALOG(SIG)
XBAR(2)=XBR2(J)
SIGX(2)=XSIG2(J)
CORREL(2)=COR2(J)
CFACT = CNFLIM (2,N(J),XHAT,XBAR,SIGX,STDERR(J),CORREL,TSTAT(J))
RUPTIM = EXP(ALOG(10.) * ((LMP - CFACT)/TR - 20.))
RETURN
END

```

TABLE A.5  
(continued)

```

FUNCTION EPFMIN(T,F)
C
C EPFMIN CALCULATES MINIMUM FRACTURE DUCTILITY FOR CW316SS FROM AN EMPIRICAL
C CORRELATION DEVELOPED BY GE
C
C          DEFINITION OF TERMS
C      T = TEMPERATURE IN DEG F
C      F = IRRADIATION FLUENCE IN 1.E22 N/CM2
C      EPFMIN = MINIMUM FRACTURE DUCTILITY
C
C DIVIDE TEMPERATURE BY 1000
      TT = T * .001
C FOR TEMPERATURES LESS THAN 800 F, USE 800 F DATA
      TT = AMAX1(TT,.8)
C CALCULATE THRESHOLD FLUENCE FOR REDUCTION OF DUCTILITY
      FO = 1.4 - TT
      IF (T .GT. 1200.) FO = TT - 1.0
C CALCULATE MINIMUM DUCTILITY FOR UNIRRADIATED MATERIAL
      EPO = .45 / (SQRT(TT) * (TT**3))
      IF (T .GT. 1000.) EPO = EPO/(TT**2)
      IF (F .LE. FO) GO TO 1
C IF FLUENCE EXCEEDS THRESHOLD FLUENCE, APPLY DUCTILITY REDUCTION FACTOR
      ZZ = TT - 1.7
      EPO = EPO * ((F/FO)**ZZ)
1 EPFMIN = EPO
  RETURN
  END

```

```

FUNCTION ELUNIF (TEMP,FLUENC)
C
C ELUNIF CALCULATES MINIMUM TRUE UNIFORM ELONGATION FOR CW316SS, USING A
C CORRELATION DEVELOPED BY HEDL FOR FIRST-CORE STEEL.
C
C          DEFINITION OF TERMS
C      TEMP = TEMPERATURE IN DEG F
C      FLUENC = IRRADIATION FLUENCE (FAST) IN 1.E22 N/CM2
C      ELUNIF = MINIMUM TRUE UNIFORM ELONGATION
C
C FOR TEMPERATURES LESS THAN 800 F, USE 800 F DATA
      T = AMAX1(TEMP,800.)
C CALCULATE ENGINEERING UNIFORM ELONGATION, USING POLYNOMIAL CORRELATION
      EU = .12854 + T * (.00010857 + T*(.93846E-07 - .17995E-09*T) )
C CALCULATE TRUE STRAIN VALUE FROM ENGINEERING STRAIN VALUE.
1 ELUNIF = ALOG(1. + EU)
  RETURN
  END

```

TABLE A.5  
(continued)

```
FUNCTION CNFLIM (M,N,XHAT,XBAR,SIGX,SEE,CORREL,TSTAT)
DIMENSION XHAT(M),XBAR(M),SIGX(M),CORREL(M)
C THIS COMPUTES CONFIDENCE BAND AND TOLERANCE BAND ABOUT MULTI-LINEAR
C REGRESSION EQUATION
C ENTERED WITH FOLLOWING VARIABLES**
C M=NUMBER OF INDEPENDANT VARIABLES IN MODEL
C N=NUMBER OF DATA POINTS USED IN OBTAINING MODEL
C XHAT(I)=VALUE OF I-TH INDEPENDANT VARIABLE (TRANSFORMED IF APPLICABLE)
C   TO BE USED IN CALCULATION, I=1,2,3,...,M
C XBAR(I)=MEAN VALUE OF I-TH INDEPENDANT VARIABLE (FROM MELB)
C SIGX(I)=STD DEVIATION ABOUT EACH INDEPENDANT VARIABLE (FROM MELB)
C SEE=STANDARD ERROR IN ESTIMATE OF DEPENDANT VARIABLE (FROM MELB)
C CORREL(I)=CORRELATION COEF FOR I-TH IND.VARIABLE (FROM MELB)
C TSTAT=DESIRED T STATISTIC TO BE USED IN CALC OF CONF LIMIT
C TOLFACT=DESIRED TOLERANCE FACTOR USED IN CALC OF TOL. LIMIT
C THE FOLLOWING IS RETURNED ***
C CNFLIM=2- STD. DEV. CONFIDENCE BAND ABOUT DEPENDENT VARIABLE
C
SUM=0.0
DO 10000 I=1,M,1
TERM1=1.00+SQRT(1.0-CORREL(I)**2)
TERM2=(XBAR(I)-XHAT(I))**2
TERM3=FLOAT(N)*SIGX(I)**2
IF (TERM3.EQ.0.0)GO TO 10000
SUM=SUM+TERM1*TERM2/TERM3
10000 CONTINUE
CNFLIM = ABS(TSTAT * SEE * SQRT(SUM + 1.0/FLOAT(N)))
RETURN
END
```